Corrosion Forecasting and Failure Projection of Post-Tension Tendons in Deficient Cementitious Grout

PUBLICATION NO. FHWA-HRT-17-074

MAY 2018

U.S. Department of Transportation
Federal Highway Administration

Research, Development, and Technology
Turner-Fairbank Highway Research Center
6300 Georgetown Pike
McLean, VA 22101-2296

FOREWORD

The objective of this investigation was to provide bridge engineers with a practical methodology for projecting timing of corrosion-induced, post-tensioned (PT) tendon failures caused by a grout deficiency or deficiencies. Bridge tendons can be more susceptible to corrosion than conventional reinforcement with no indication that this is taking place, and failures from deficient grout–induced corrosion have been reported as soon as 2 yr post construction. Of particular concern are situations where the PT grout exhibits either chemical deficiencies (elevated chlorides beyond the allowable limit specified by the American Association of State Highway and Transportation Officials and other specifications or free sulfates, or both), physical deficiencies (soft, chalky, separated, segregated grout with air voids and free water), or a combination of these. Failure of relatively few tendons can compromise overall structural integrity.

The results of this study provide bridge owners with a practical protocol for projecting the timing of corrosion-induced tendon failures, given the extent of any grout deficiency or deficiencies, and thereby for responding to concerns arising therefrom.

Cheryl Allen Richter, Ph.D., P.E.
Director, Office of Infrastructure
Research and Development

TECHNICAL REPORT DOCUMENTATION PAGE

1. Report No. FHWA-HRT-17-074	2. Government Accession No.	3. Recipient's Catalog No.
4. Title and Subtitle Corrosion Forecasting and Failure Projection of Post-Tensioned Tendons in Deficient Cementitious Grout		5. Report Date May 2018 6. Performing Organization Code CAGE Code: 1YX01
7. Author(s) William H. Hartt and Seung-Kyoung Lee		8. Performing Organization Report No. Task Order #5009
9. Performing Organization Name and Address Engineering & Software Consultants, Inc. 14123 Robert Paris Court Chantilly, VA 20151		10. Work Unit No. 11. Contract or Grant No. DTFH61-14-D-00011
12. Sponsoring Agency Name and Address Office of Infrastructure Research and Development Federal Highway Administration 6300 Georgetown Pike McLean, VA 22101-2296		13. Type of Report and Period Covered Final Report; September 2014–January 2017 14. Sponsoring Agency Code HRDI-20
15. Supplementary Notes The Contracting Officer's Representative is Hoda Azari HRDI-20.		

16. Abstract

Post-tensioning has evolved to become the construction method of choice for many large structures, including bridges. However, instances of corrosion-induced fracture of wires and strands and resultant tendon failures have occurred as a consequence of either chemically or physically deficient grout (or a combination of these), where the former involves elevated levels of chlorides or free sulfates (or both) and the latter soft, chalky, separated, segregated grout with free water. In the extreme, there is the possibility of structure collapse. The present project builds on results from a recently completed in-house Federal Highway Administration study, termed "phase 1," which determined the extent of localized wire and strand corrosion as a function of grout chloride concentration, presence of free sulfates, and physical deficiencies.(1) The objective of the present study was twofold: first, to present results from a phase 2 experimental study that extended what was accomplished in phase 1 and, second, to develop a methodology whereby the onset and subsequent rate of wire and strand fractures and tendon failures can be forecast given information regarding the extent of grout deficiency or deficiencies.(1) The former involved stressed, single-wire specimens that were exposed to deficient grouts. The latter was accomplished by relating occurrence of fractures and failures to the extent of localized wire corrosion and to the resultant rate of wire cross-section loss with time, as affected by the severity of a grout deficiency or deficiencies. Primary inputs to the model are the mean and standard deviation of, first, localized wire corrosion rate and, second, residual wire fracture strength. Results indicate an initiation period for fractures and failures during which corrosion progresses and that, once these commence, they do so initially at a progressively increasing rate up to a point beyond which this rate moderates. Other variables that were investigated include level of prestress, wire strength, number of tendons, tendon length, and fracture and failure rates subsequent to initial occurrence. Equations are presented whereby bridge engineers can forecast the onset of fractures and failures based on either localized wire corrosion wastage statistics or grout chloride concentration, and examples are provided.

17. Key Words Post-tension tendons, bridges, corrosion, fracture, failures, chlorides, grout, grout deficiency	18. Distribution Statement No restrictions. This document is available to the public through the National Technical Information Service, Springfield, VA 22161. http://www.ntis.gov		
19. Security Classif. (of this report) Unclassified	20. Security Classif. (of this page) Unclassified	21. No. of Pages 235	22. Price

Form DOT F 1700.7 (8-72) Reproduction of completed pages authorized.

SI* (MODERN METRIC) CONVERSION FACTORS

APPROXIMATE CONVERSIONS TO SI UNITS

Symbol	When You Know	Multiply By	To Find	Symbol
		LENGTH		
in	inches	25.4	millimeters	mm
ft	feet	0.305	meters	m
yd	yards	0.914	meters	m
mi	miles	1.61	kilometers	km
		AREA		
in^2	square inches	645.2	square millimeters	mm^2
ft^2	square feet	0.093	square meters	m^2
yd^2	square yard	0.836	square meters	m^2
ac	acres	0.405	hectares	ha
mi^2	square miles	2.59	square kilometers	km^2
		VOLUME		
fl oz	fluid ounces	29.57	milliliters	mL
gal	gallons	3.785	liters	L
ft^3	cubic feet	0.028	cubic meters	m^3
yd^3	cubic yards	0.765	cubic meters	m^3
		NOTE: volumes greater than 1000 L shall be shown in m^3		
		MASS		
oz	ounces	28.35	grams	g
lb	pounds	0.454	kilograms	kg
T	short tons (2000 lb)	0.907	megagrams (or "metric ton")	Mg (or "t")
		TEMPERATURE (exact degrees)		
^oF	Fahrenheit	5 (F-32)/9 or (F-32)/1.8	Celsius	^oC
		ILLUMINATION		
fc	foot-candles	10.76	lux	lx
fl	foot-Lamberts	3.426	candela/m^2	cd/m^2
		FORCE and PRESSURE or STRESS		
lbf	poundforce	4.45	newtons	N
lbf/in^2	poundforce per square inch	6.89	kilopascals	kPa

APPROXIMATE CONVERSIONS FROM SI UNITS

Symbol	When You Know	Multiply By	To Find	Symbol
		LENGTH		
mm	millimeters	0.039	inches	in
m	meters	3.28	feet	ft
m	meters	1.09	yards	yd
km	kilometers	0.621	miles	mi
		AREA		
mm^2	square millimeters	0.0016	square inches	in^2
m^2	square meters	10.764	square feet	ft^2
m^2	square meters	1.195	square yards	yd^2
ha	hectares	2.47	acres	ac
km^2	square kilometers	0.386	square miles	mi^2
		VOLUME		
mL	milliliters	0.034	fluid ounces	fl oz
L	liters	0.264	gallons	gal
m^3	cubic meters	35.314	cubic feet	ft^3
m^3	cubic meters	1.307	cubic yards	yd^3
		MASS		
g	grams	0.035	ounces	oz
kg	kilograms	2.202	pounds	lb
Mg (or "t")	megagrams (or "metric ton")	1.103	short tons (2000 lb)	T
		TEMPERATURE (exact degrees)		
^oC	Celsius	1.8C+32	Fahrenheit	^oF
		ILLUMINATION		
lx	lux	0.0929	foot-candles	fc
cd/m^2	candela/m^2	0.2919	foot-Lamberts	fl
		FORCE and PRESSURE or STRESS		
N	newtons	0.225	poundforce	lbf
kPa	kilopascals	0.145	poundforce per square inch	lbf/in^2

*SI is the symbol for the International System of Units. Appropriate rounding should be made to comply with Section 4 of ASTM E380.
(Revised March 2003)

TABLE OF CONTENTS

LIST OF FIGURES

LIST OF TABLES

LIST OF ABBREVIATIONS AND SYMBOLS

Abbreviations

CDF	cumulative distribution function
DOT	department of transportation
F	fully grouted
FDOT	Florida Department of Transportation
FHWA	Federal Highway Administration
FS	fracture stress
GUTS	guaranteed ultimate tensile strength
I_{macro}	macrocell corrosion current
MMFM	magnetic main flux method
mpy	mils per year
MS	multistrand
NDE	nondestructive evaluation
NDT	nondestructive testing
PDF	probability density function
POO	probability of occurrence
PT	post-tensioned
PTI	Post-Tensioning Institute
PVC	polyvinyl chloride
R	grout resistance
RCSA	remaining cross-section area
RH	relative humidity
R_p	polarization resistance
S	stressed
T_f	time to initial fracture/failure
US	unstressed
V	grout void

Symbols

μ	mean
$\mu(CRE)$	mean of corrosion rate equivalent
σ	standard deviation
$\sigma(CRE)$	standard deviation of corrosion rate equivalent
A	original wire cross-section area
$[Cl^-]$	chloride concentration
CRE	corrosion rate equivalent
FS	fracture stress
R	grout resistance
$RCSA$	remaining cross-section area
SA	sector area
T	time
T'	a time later than the initial time (T)

TA	triangle area
T_f	time to initial fracture/failure
TRA(-)	area of successive approximated trapezoids

CHAPTER 1. INTRODUCTION

Post-tensioned (PT) concrete construction was first introduced over 60 yr ago and has evolved to become a prime methodology for affecting the integrity of large reinforced concrete structures, including bridges. Potential advantages of PT construction include longer spans, reduced construction time, thinner sections with a more streamlined appearance, improved concrete crack control, and overall cost savings compared to structures that are conventionally reinforced. The majority of prestressing employed in PT construction is seven-wire strand, where six high-strength, high-carbon, cold-drawn, 270-ksi-minimum guaranteed ultimate tensile strength (GUTS), pearlitic steel wires that conform to ASTM A416 are spirally wound around a central straight wire.[(2)] PT bridges invariably employ grouted tendons, which consist of dead- and live-end anchorages, a prestressing strand, and a plastic or metal duct, which after strand stressing, is filled with grout. Likewise, anchorages comprise an anchor, a wedge plate, and a cap over the strand tails. Figure 1 schematically illustrates a PT anchorage with various components identified. Installation subsequent to concrete setting involves fixing one end of the strands at an embedded dead-end anchor and then stressing the other (live) end to a jacking force of 80 percent of the GUTS. On release, this force drops to approximately 70 percent of GUTS and is termed the "initial force." Further prestress relaxation occurs with time from 60 to 63 percent of GUTS; this being referred to as the "effective force." The rate of this long-term loss progressively moderates with time, and structural engineers generally assume (conservatively) that 27 yr (approximately 10,000 d) are required for completion. Grouted tendons can be either bonded or unbonded; the former are cast into concrete, and the latter are external, except at tiebacks and deviation blocks.

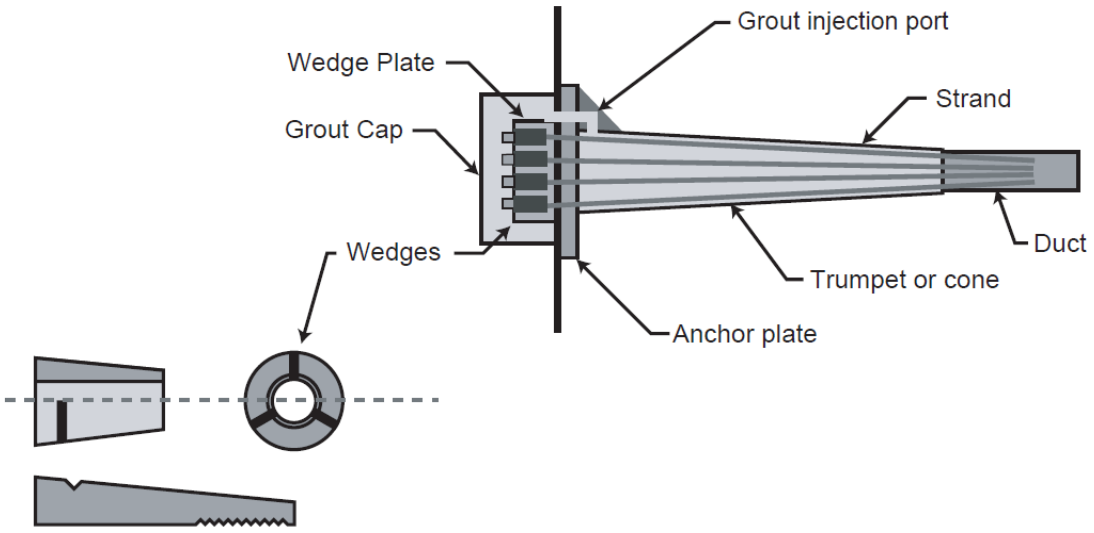

Source: FHWA.

Figure 1. Illustration. Schematic drawing of a PT tendon with various components identified.

As an offset to the advantages of PT construction, premature bridge tendon repair and replacement have been required in some instances because of strand corrosion, resultant fracture,

and even tendon failure. In the extreme, this can lead to structure collapse. Corrosion issues for bridge PT tendons became apparent in the United States in 1999 with disclosure of tendon failures that resulted from grout voids and associated bleed water at higher elevations along tendon profiles such as at anchorages and crest areas.[3–6] Some 10 States, to date, have reported tendon problems that stem from this cause. Grouts employed for PT bridge construction at the time of these initial problem disclosures and prior to 2002 consisted of a mixture of cement, water, and admixtures and were typically mixed at the project site. In an effort to improve grout performance as the primary corrosion protection method for PT tendons, the Post-Tensioning Institute (PTI) and some State departments of transportation (DOTs) revised their grout specifications in the 2001–2002 timeframe. This resulted in prepackaged, preapproved thixotropic grouts formulated with the goal of eliminating bleed water and thus improving the level of protection provided to strands. However, while these grouts were thought to provide a solution to the bleed-water problem, corrosion and even resultant tendon failures on relatively new PT bridges have been reported, and the limited forensic studies involving these newer grouts that have been performed to date have revealed the presence of separated, segregated, soft, chalky, unhardened material; free water; and high chloride and sulfate contents.[7–10] A European bridge was reported to have experienced tendon failures after less than 2 yr of service, and this was attributed to a combination of physical grout deficiencies and elevated sulfates.[11] Further, Sika Corporation U.S. informed the Federal Highway Administration (FHWA) in 2011 that their prepackaged SikaGrout® 300 PT for bridge PT tendons produced at the company's Marion, Ohio, facility from 2002 to 2010 may contain elevated concentrations of chloride. In response to concerns that these issues raise regarding tendon and bridge integrity, FHWA issued the following: a memorandum alerting State DOTs to the Sika PT grout issue; a literature survey to identify chloride concentration corrosion initiation threshold(s) for PT strand; a technical memorandum advising bridge owners regarding assessing and managing long-term performance of PT bridges having tendons with grout containing elevated chloride levels; a study that provides guidelines for sampling, assessing, and restoring defective grout in bridge PT tendons; and a series of two laboratory research studies, designated "phase 1" and "phase 2," that simulated and characterized PT strand corrosion as a consequence of variables associated with deficient grout, phase 1 having been previously completed and a final report issued.[12–15,1] References to data, figures, and findings from *An FHWA Special Study: Post-Tensioning Tendon Grout Chloride Thresholds* will herein be referred to as "phase 1."[1]

The purpose of this report is to document results from the phase 2 study and introduce an analytical modeling methodology that, given information regarding the extent of PT wire corrosion, projects the time to initial wire and strand fractures and tendon failures and the rate of subsequent fractures and failures. The approach is substantiated by the comparison of model projections with results from one of the previously referenced FHWA studies and with timing of strand fractures associated with bridge tendon failures.[1]

CHAPTER 2. EXPERIMENTAL AND MODELING ANALYSIS APPROACHES

PHASE 1 EXPERIMENTAL GROUT STUDY

Results from what is termed the "phase 1 laboratory study" served as a basis for the present tendon failure projecting modeling. In addition to a literature review (task 1), the phase 1 effort consisted of three experimental tasks, each of which involved exposures of approximately 6 mo, as listed below:

- Task 2.1: Single-wire specimens in an aqueous solution.
- Task 2.2: Single-strand specimens in grout with and without an air void.
- Task 2.3: Multistrand specimens in grouted duct with an air void.

Strands were 0.6 inch in diameter and conformed to ASTM A416 with 270-ksi GUTS.[(2)] A prepackaged grout mix was employed with admixed chloride concentrations of 0, 0.08, 0.20, 0.40, 0.60, 0.80, 1.00, and 2.00 percent by weight of cement. To accelerate any corrosion activity and also to represent environmental conditions that are likely to be experienced in service, the exposures were performed within an environmental chamber where successive 2-week subcycles of the following conditions were affected:

- Ambient (25 °C/60-percent relative humidity (RH)).
- Hot and humid (40 °C/90-percent RH).
- Ambient (25 °C/60-percent RH).
- Freezing and drying (–10 °C/40-percent RH).

Three full cycles were conducted during the approximate 6-mo period, although the final freezing and drying cycle was replaced by a hot and humid one as little corrosion activity was detected earlier for the former. Also, for grouted specimens with a void, provisions were made whereby water and fresh air could be introduced into the duct during the exposure. Parameters that were periodically monitored and recorded were corrosion potential, instantaneous corrosion rate (single-strand specimens only), macrocell corrosion current (I_{macro}) density (multistrand specimens only), and apparent grout resistance (R) and resistivity. The former three provide information regarding the propensity for corrosion or corrosion rate, and the last affects the magnitude of any micro- and macrocell corrosion.

Figure 2 reproduces figure 21 from the phase 1 report and shows a schematic representation of the task 2.1 specimens and experimental arrangement, whereas figure 3 and figure 4 reproduce figure 22 and figure 23 from that report and show photographs of stressed and unstressed wire specimens, respectively, under test. Likewise, figure 5 and figure 6 reproduce figure 25 and figure 24, respectively, and show schematic illustrations of single-strand specimens and the testing arrangement, whereas figure 7 shows a photograph of these specimens under test, as reproduced from figure 31 of the report. Finally, figure 8 reproduces figure 35 and provides a schematic representation of a multistrand specimen contained in a clear high-density polyethylene tube, and figure 9 reproduces figure 38, showing a photograph of fully assembled multistrand specimens under test. For stressed specimens, loading was, in all cases, to 60 percent of the GUTS.

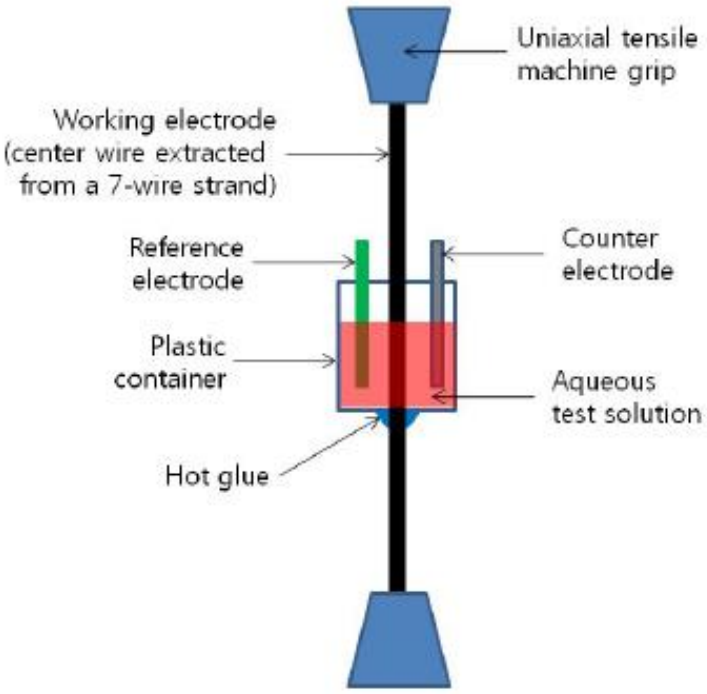

Source: FHWA.

Figure 2. Illustration. Schematic representation of the testing arrangement for single-wire specimens.[(1)]

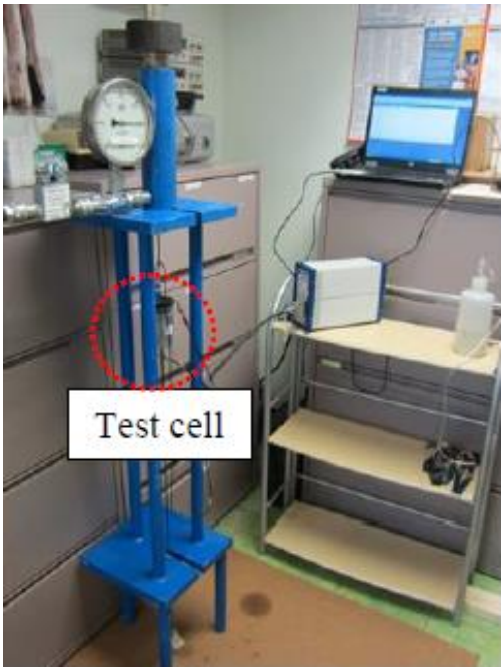

Source: FHWA.

Figure 3. Photo. Load frame and cell for loading single-wire specimens.[(1)]

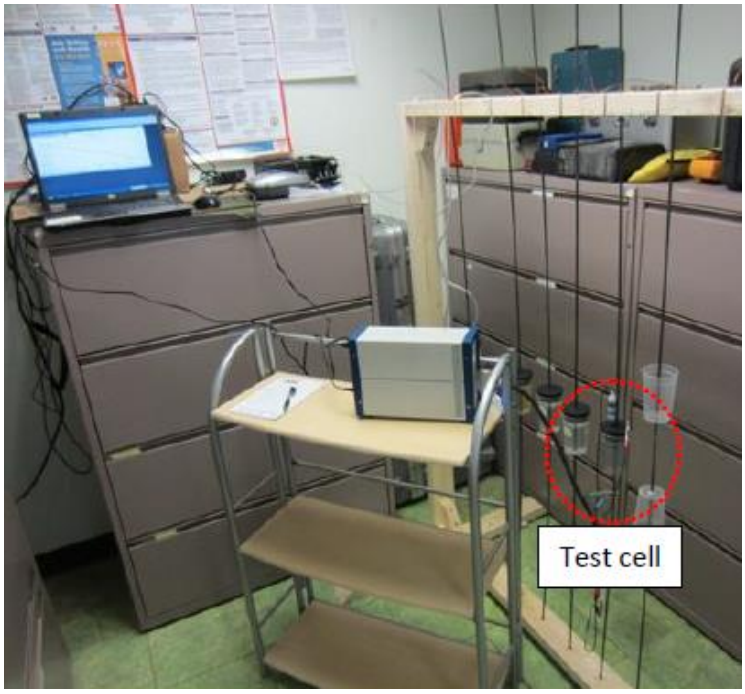

Source: FHWA.

Figure 4. Photo. Multiple unstressed single-wire specimens and test cells.[1]

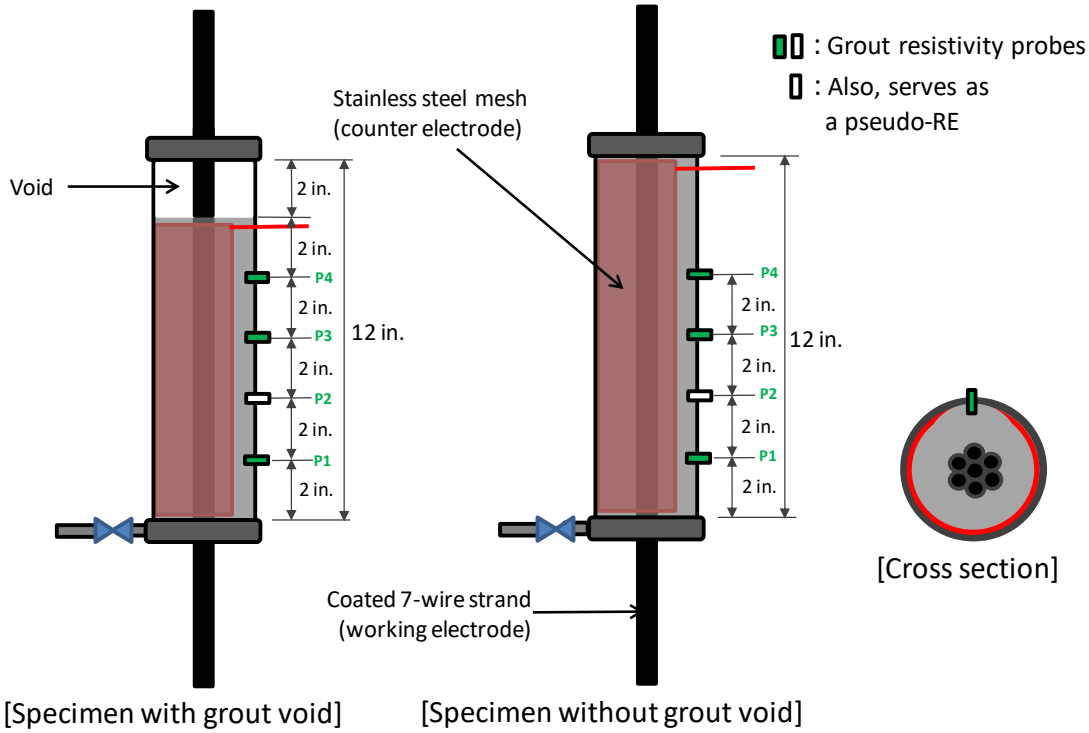

Source: FHWA.

Figure 5. Illustration. Schematic representation of grouted single-strand specimens with and without a grout void.[1]

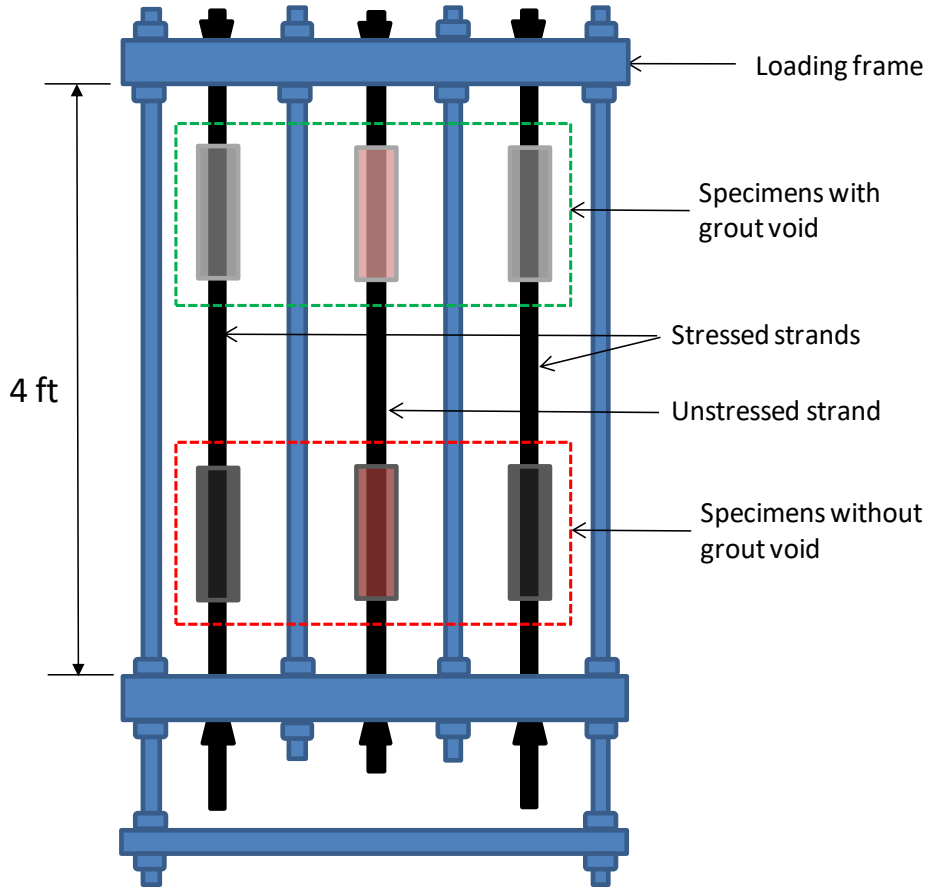

Source: FHWA.

Figure 6. Illustration. Schematic representation of grouted single-strand specimens in a loading frame.[(1)]

Source: FHWA.

Figure 7. Photo. Grouted single-strand specimens in loading frames.[(1)]

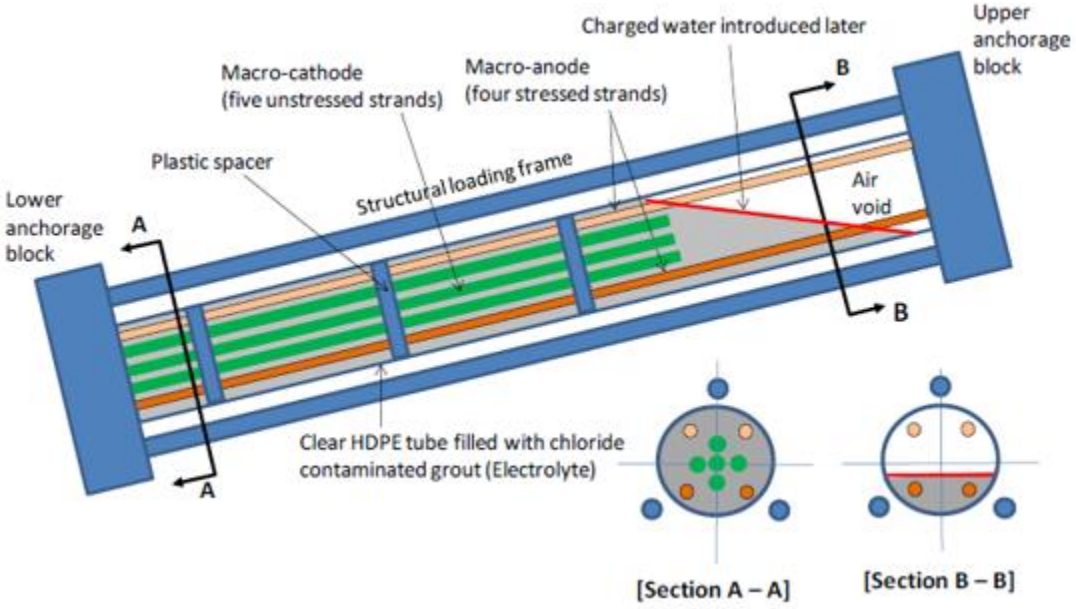

Source: FHWA.

Figure 8. Illustration. Schematic representation of a grouted multistrand specimen in a loading frame.[(1)]

Source: FHWA.

Figure 9. Photo. Multistrand specimens in loading frames under test.[(1)]

The tendon failure projection methodology developed in the present study utilized data from tasks 2.2 and 2.3 of the phase 1 FHWA study as these were considered to be particularly applicable to actual tendons. Results from the subsequent two studies are related to and discussed in respect to quantitative projections of the present study.

PHASE 2 EXPERIMENTAL GROUT STUDY

General

The phase 2 grout study was performed to assess corrosion damage in the presence of sulfate ions under several conditions that simulate what might occur in service, including grout segregation and carbonation. The corrosion damage data, in terms of pit depth, were used to refine and validate the failure forecasting model developed in this study. Experiments were performed at the FHWA Nondestructive Evaluation (NDE) Laboratory and also at two field PT bridges. The following describes experimental details and major test results of the phase 2 study.

Initial accelerated corrosion tests were performed for 80 d. This pilot testing was intended to develop a new experimental methodology for full-scale testing by addressing the following questions:

- Can multiple specimens be stressed and tested in the existing loading frames used in the phase 1 study?
- What variables are effective to introduce significant corrosion damage in a relatively short period of time?
- Is it necessary to include a grout coating to duplicate a certain field condition?
- What is the optimum volume of recharging water and most appropriate method of water injection?

- What is the amount of mixing water that consistently produces segregated grout?
- What is the best way of accelerating grout carbonation?
- What is the potential risk during testing of an unexpected fracture of stressed wires as a consequence of excessive corrosion damage?
- What is the highest rate of corrosion for stressed wires in the most corrosive test condition?

The pilot test specimens employed the straight, cleaned, 12-ft-long center (king) wire removed from a 0.6-inch diameter, low-relaxation, 270-ksi GUTS strand. These single-wire specimens were used to simulate grouted PT tendons. Once a sufficient number of wires were prepared, four wires were installed and stressed in each of three different loading frames. Six test cells were distributed evenly along each of the wires. This arrangement allowed placement of 24 test cells in each loading frame and a total of 72 test cells for the pilot program. Each cell was filled with one of three PTI class C prepackaged grout products acquired from local distributors. These are designated as "product A," "product B," and "product C" and served as the electrolyte. For each grout product, some test cells were filled with normal hardened grout, and others contained segregated grout that was mixed with extra water to trigger segregation. Additional details are described in the full-scale testing section below.

Custom-made wedges and anchor grips were fabricated for stressing individual wires. The wires were individually stressed at 60 percent of GUTS by applying approximately 5.3 kips of load. Subsequent to stressing, grout was pumped into the individual cells until the predetermined height was reached such that an artificial grout void resulted at the top of each test cell. Recharging water was periodically introduced into the voids during the testing. The test variables for the pilot testing included the following:

- Grout material (3): product A, product B, and product C, as noted previously.
- Working electrode (1): center wire extracted from a 0.6-inch seven-wire strand supplied by one supplier.
- Grout condition (3): normally hardened, segregated, and grout coated.
- Stress condition (1): stressed at 60 percent of GUTS.
- Grout void type (1): inclined.
- pH of recharging water (2): uncarbonated (pH 13.6) and carbonated (pH 9.0).
- Free sulfate concentration (4): 0, 0.4, 0.8, and 1.5 percent by weight of cement dissolved in the recharging water.
- Temperature (1): 40 °C (maintained in an environmental chamber).

For each grout product, eight normal grout specimens were fabricated with the mixing water dosage recommended by the manufacturer, and eight segregated grout specimens were prepared by adding 20 percent more water than the recommended amount. Specimens having a grout coating on the wire were fabricated by first pumping grout to the top of the test cell and then slowly discharging it until a uniform grout coating was adhered to the top 1 inch of the wire. As a result, 24 specimens were fabricated per grout product, and a total of 72 specimens were tested for 80 d.

At the end of the pilot testing and subsequent autopsy, the following observations were made:

- Segregated grout could not be consistently produced with 20 percent extra water regardless of the grout product.
- A thin grout coating prevented corrosion from taking place in most cases.
- Visible corrosion damage occurred on 20 wire specimens (about 27 percent), but depth of the attack was not measurable with a pit gauge.
- All of the observed damage was concentrated near the void/grout interface.
- Attempts to produce grout carbonation by placing dry ice pellets in the voids were not practical because CO_2 gas was not retained for an extended time.
- Macrocell current and linear polarization resistance (R_p) data indicated that adding low pH (9.0) recharging water could enhance corrosion in proportion to free sulfate concentration. On the other hand, the high pH (13.6) recharging water did not induce corrosion irrespective of sulfate concentration.
- I_{macro} measurement via a test panel mounted on the exterior wall of the environmental chamber was convenient and time saving.

Based on findings from the pilot program, full-scale accelerated corrosion testing was performed for 200 d with the following variables:

- Grout material (3): product A, product B, and product C.
- Working electrode (1): clean center wire extracted from a 0.6-inch seven-wire strand supplied by one supplier.
- Condition of grout (4): normally hardened, segregated grout; normally hardened admixed with sulfate; and segregated grout admixed with sulfate.
- Stress condition (2): stressed at 60 percent of GUTS and unstressed (control).
- Grout void (1): inclined.
- Sulfate concentration (4): 0, 0.4, 0.8, and 1.5 percent by weight of cement.

- Introduction of sulfate (2): dissolved in recharging water and sodium sulfate admixed with fresh grout.
- Recharging water pH (2): uncarbonated (pH 13.6) and carbonated (pH 8.0).
- Temperature (2): 25 °C (ambient) and 40 °C (maintained in two environmental chambers).

Combinations of these variables were expected to produce realistic corrosion damage. In most cases, there were three specimens for each set of test variables in cases of elevated temperature. Only single specimens were prepared in the case of control (ambient temperature) specimens.

Table 1. Test matrix for full-scale corrosion testing per grout product.

Grout Condition	Recharging Water	Sulfate Concentration	Number of Specimens (Testing Condition)	Number of Specimens (Testing Condition)	Number of Specimens (Testing Condition)	Number of Specimens (Testing Condition)
Segregated grout	No recharging water	Admixed sulfate 0%	—	1 (no stress; no carbonation; 25 °C)	—	3 (60% GUTS; pH 8.0 water added; 40 °C)
Segregated grout	No recharging water	Admixed sulfate 0.4%	1 (60% GUTS; no carbonation; 25 °C)	1 (no stress; no carbonation; 25 °C)	—	3 (60% GUTS; pH 8.0 water added; 40 °C)
Segregated grout	No recharging water	Admixed sulfate 0.8%	1 (60% GUTS; no carbonation; 25 °C)	1 (no stress; no carbonation; 25 °C)	—	3 (60% GUTS; pH 8.0 water added; 40 °C)
Segregated grout	No recharging water	Admixed sulfate 1.5%	—	1 (no stress; no carbonation; 25 °C)	—	3 (60% GUTS; pH 8.0 water added; 40 °C)
Segregated grout	Recharging water (pH 8.0)	Free sulfate 0%	—	—	3 (60% GUTS; no carbonation; 40 °C)	—
Segregated grout	Recharging water (pH 8.0)	Free sulfate 0.4%	—	—	3 (60% GUTS; no carbonation; 40 °C)	—
Segregated grout	Recharging water (pH 8.0)	Free sulfate 0.8%	—	—	3 (60% GUTS; no carbonation; 40 °C)	—
Segregated grout	Recharging water (pH 8.0)	Free sulfate 1.5%	—	—	2 (60% GUTS; no carbonation; 40 °C)	—
Segregated grout	Recharging water (pH 13.6)	Free sulfate 0%	—	—	—	3 (60% GUTS; pH 8.0 water added; 40 °C)

Grout Condition	Recharging Water	Sulfate Concentration	Number of Specimens (Testing Condition)	Number of Specimens (Testing Condition)	Number of Specimens (Testing Condition)	Number of Specimens (Testing Condition)
Segregated grout	Recharging water (pH 13.6)	Free sulfate 0.4%	—	—	—	3 (60% GUTS; pH 8.0 water added; 40 °C)
Segregated grout	Recharging water (pH 13.6)	Free sulfate 0.8%	—	—	—	3 (60% GUTS; pH 8.0 water added; 40 °C)
Segregated grout	Recharging water (pH 13.6)	Free sulfate 1.5%	—	—	—	3 (60% GUTS; pH 8.0 water added; 40 °C)
Normal grout	No recharging water	Admixed sulfate 0%	—	1 (no stress; no carbonation; 25 °C)	—	3 (60% GUTS; pH 8.0 water added; 40 °C)
Normal grout	No recharging water	Admixed sulfate 0.4%	1 (60% GUTS; no carbonation; 25 °C)	1 (no stress; no carbonation; 25 °C)	—	3 (60% GUTS; pH 8.0 water added; 40 °C)
Normal grout	No recharging water	Admixed sulfate 0.8%	1 (60% GUTS; no carbonation; 25 °C)	1 (no stress; no carbonation; 25 °C)	—	—
Normal grout	No recharging water	Admixed sulfate 1.5%	—	1 (no stress; no carbonation; 25 °C)	—	—
Normal grout	Recharging water (pH 8.0)	Free sulfate 0%	—	—	3 (60% GUTS; no carbonation; 40 °C)	—
Normal grout	Recharging water (pH 8.0)	Free sulfate 0.4%	—	—	3 (60% GUTS; no carbonation; 40 °C)	—
Normal grout	Recharging water (pH 8.0)	Free sulfate 0.8%	—	—	3 (60% GUTS; no carbonation; 40 °C)	—
Normal grout	Recharging water (pH 8.0)	Free sulfate 1.5%	—	—	1 (60% GUTS; no carbonation; 40 °C)	—
Normal grout	Recharging water (pH 13.6)	Free sulfate 0%	—	—	—	3 (60% GUTS; pH 8.0 water added; 40 °C)
Normal grout	Recharging water (pH 13.6)	Free sulfate 0.4%	—	—	—	3 (60% GUTS; pH 8.0 water added; 40 °C)

Grout Condition	Recharging Water	Sulfate Concentration	Number of Specimens (Testing Condition)	Number of Specimens (Testing Condition)	Number of Specimens (Testing Condition)	Number of Specimens (Testing Condition)
Normal grout	Recharging water (pH 13.6)	Free sulfate 0.8%	—	—	—	3 (60% GUTS; pH 8.0 water added; 40 °C)
Normal grout	Recharging water (pH 13.6)	Free sulfate 1.5%	—	—	—	3 (60% GUTS; pH 8.0 water added; 40 °C)

Note: Testing conditions—stressed at 60 percent of GUTS versus no stress; no carbonation versus carbonation by adding pH 8.0 water; temperature 25 °C versus 40 °C.
—No information available.

Specimen Configuration

Figure 10 schematically illustrates the specimen, which consisted of a clear polyvinyl chloride (PVC) pipe 10 inches in length and 2 inches in diameter and a cylindrical type 316 stainless steel mesh fitted inside the pipe.

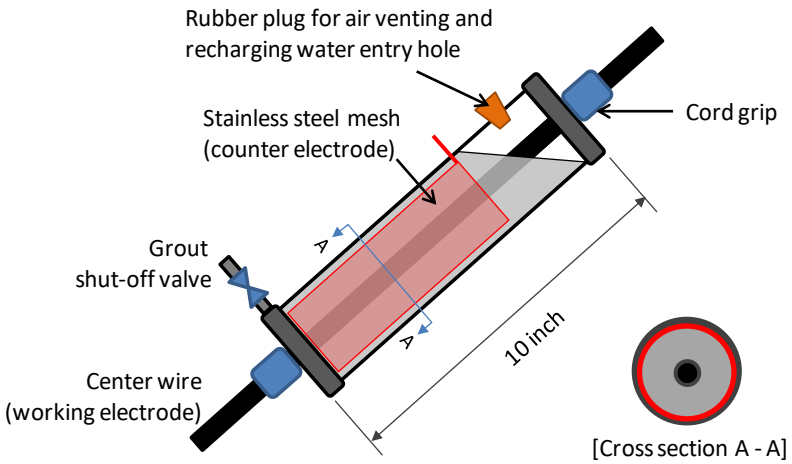

Source: FHWA.

Figure 10. Illustration. Schematic of test specimen containing an artificial void.

The stainless steel mesh served as the counter electrode in relation to a section of the encased wire (working electrode), which was stressed to 60 percent of GUTS. Both ends of the pipe were fitted with PVC caps. A pair of cord grips inserted into the center of the top and bottom caps was used to hold the wire and pipe together at a predetermined location without leaking. The specimens were partially filled with fresh grout to create an inclined artificial air void as shown in figure 10. A 0.5-inch ball valve installed at the bottom of the pipe allowed the injection of fresh grout mix, and this was permanently closed when the grout reached the target level. A 0.75-inch hole and a matching rubber plug were introduced at the top of the pipe for purging air during grout pumping and injecting recharging water to the void space during the exposure testing. Figure 11 shows a photograph of several specimens.

Source: FHWA.

Figure 11. Photo. Test specimens.

Specimen Fabrication

The full-scale corrosion testing required 16 mixes per grout product, and a total of 48 separate batches were prepared. Since each batch required only a small volume, every mix was prepared using a motorized small mixer equipped with a high-shear paddle. The segregated grout mixes were produced with 35 percent more water than the grout manufacturers' recommended water dosage. This increase from 20 percent in the pilot testing was necessary because the 20-percent mix did not produce the segregated grout consistently. When fresh grout was thoroughly mixed, it was injected into the designated test cells using a special small-volume hand pump designed for grout.

Elevated Temperature Exposure Testing

The majority of specimens were tested in two walk-in environmental chambers at 40 °C with relative humidity maintained at 80 to 95 percent. In most cases, three specimens were fabricated per test condition. This resulted in a total of 63 specimens for each grout product as indicated in table 1. Each loading frame accommodated four 12-ft-long center wires that were stressed individually at 60 percent of GUTS with each wire having eight specimens in series. With this arrangement, there were 32 specimens per loading frame, and 192 specimens could be tested concurrently. Figure 12 illustrates specimens arranged in a loading frame, and figure 13 shows actual specimens in an environmental chamber.

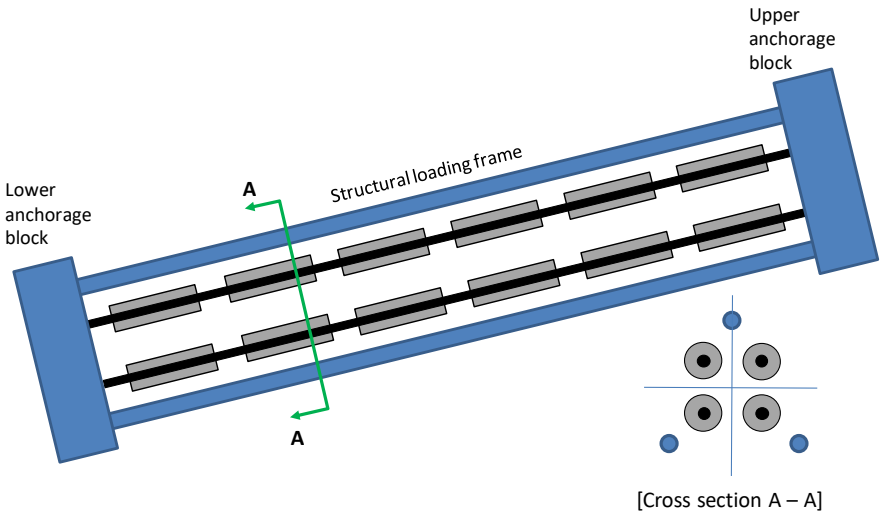

Source: FHWA.

Figure 12. Illustration. Specimen arrangement in the large loading frame.

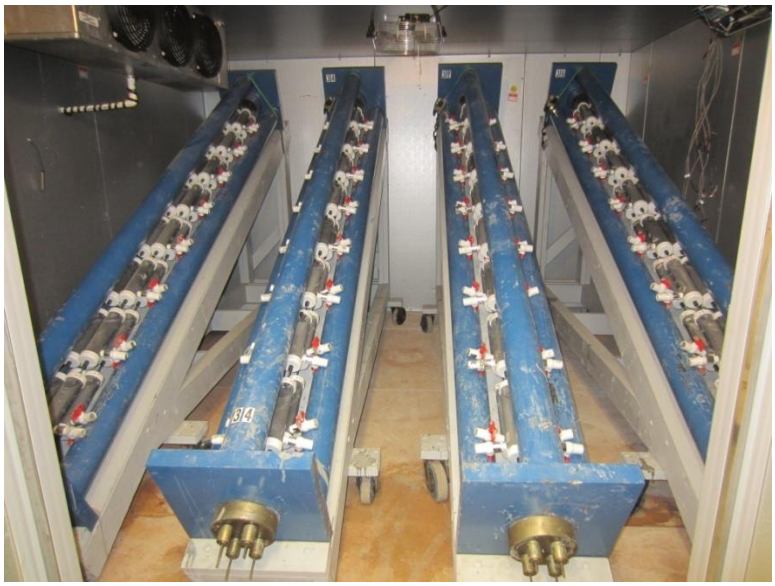

Source: FHWA.

Figure 13. Photo. Test setup in an environmental chamber.

During testing, each wire was electrically connected to the respective stainless steel mesh through a toggle switch mounted on the exterior test panel. This facilitated measurement of the macrocell current, to which corrosion rate is directly proportional. To simulate recharging water events, as these might occur on PT bridges, 0.34-oz solutions were injected according to the following protocols. For carbonated specimens (group 1), there were four recharging events with pH 8.0 water, each consisting of four sulfate concentrations after 35, 70, 122, and 175 d. For initially uncarbonated specimens (group 2), there were three recharging events with pH 13.6 water and four sulfate concentrations after 35, 70, and 122 d, followed by one recharging event after 175 d with pH 8.0 water containing the same sulfate concentrations. The latter was intended

to initiate carbonation. For sulfate admixed specimens (group 3), there was a recharging event after 122 and 175 d with pH 8.0 sulfate-free water for the purpose of initiating carbonation. Additionally, at each recharging event, the wire/grout interface was visually inspected.

Ambient Exposure Testing

Ambient exposures at 25 °C were for the purpose of better understanding corrosion behavior in the absence of recharging water with sulfates as might occur in a mild environment. The resultant control data were intended to provide a baseline to which effects of recharging water, sulfates, and exposure temperature/relative humidity on wire corrosion could be compared. As indicated in table 1, 12 specimens (4 stressed and 8 unstressed) were fabricated for each grout product, and they were accommodated in the smaller loading frame as shown in figure 14.

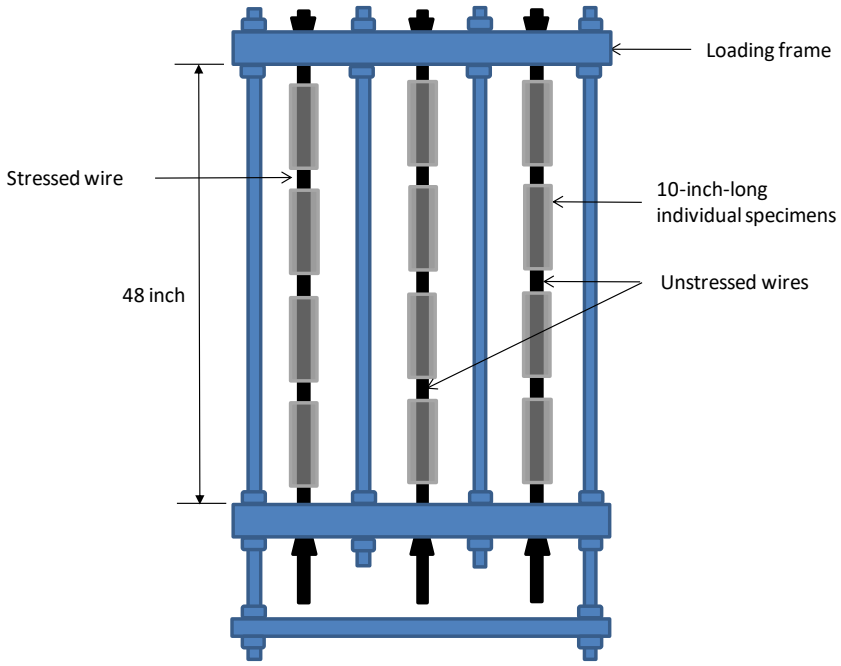

Source: FHWA.

Figure 14. Illustration. Specimen arrangement for the ambient exposure testing.

Data Collection

The state of corrosion was monitored using two established electrochemical techniques. The first test involved measurement of I_{macro}, which flows between the PT wire specimen and stainless steel mesh. A positive reading indicates current flow from the wire to the stainless steel mesh with the former serving as a macro-anode and undergoing corrosion. An increase in positive current with time indicates a proportional increase in metal loss. Conversely, a negative macrocell current indicates no corrosion at the PT wire.

The second electrochemical technique involved measurement of linear R_p, which is inversely proportional to the rate of corrosion. These measurements were made about 1 h subsequent to the

I_{macro} determinations with the circuit being open. These measurements (R_p) reflect the level of microcorrosion intensity in the absence of I_{macro}.

In addition to the electrochemical tests, R between the wire and the stainless steel mesh was also measured using a digital soil resistance meter with a two-pin configuration. These determinations were made subsequent to the I_{macro} and R_p measurements with the electrical circuit still open. This parameter (R) serves as an indirect moisture-content indicator and was an indicator of grout-moisture content changes that occurred in conjunction with recharging water events.

A total of 13 rounds of periodic data collection were made for I_{macro}, R_p, and R during the accelerated corrosion testing at the elevated temperature. For the control specimens, only two sets of the data were collected regardless of test conditions. This was because these specimens remained mostly passive.

WIRE AND STRAND FRACTURE TENDON FAILURE PREDICTIVE MODELING

Wire Fracture Criterion

The analysis methodology is based on previously reported data for residual strength of a precorroded ASTM A416 270-ksi GUTS center (straight), low-relaxation strand wire.[16,17] Figure 15 shows results from this study as a plot of stress at the time of fracture versus the percentage of the original wire cross-section area that remained at the most corroded location, which is where fracture occurred, and reveals a linear decrease in wire strength with increasing cross-section loss. The corrosion morphology for these wires consisted of localized, crater-like depressions similar to what was reported for specimens in the phase 1 study, examples of which are shown in figure 16. The baseline analyses assumed a wire/strand tension stress of 63 percent of GUTS (270 ksi), or 170 ksi, and any time dependence for this was not taken into account. Supplementary analyses consider higher wire/strand tensions since fractures/failures are often projected to occur at times less than the 27 yr assumed for completion of long-term relaxation as noted on page 1. Also considered is that actual wire and strand strength may be greater than the 270-ksi specified minimum. These latter considerations aside, the equation of the best fit line for the figure 15 data is as shown in figure 17.

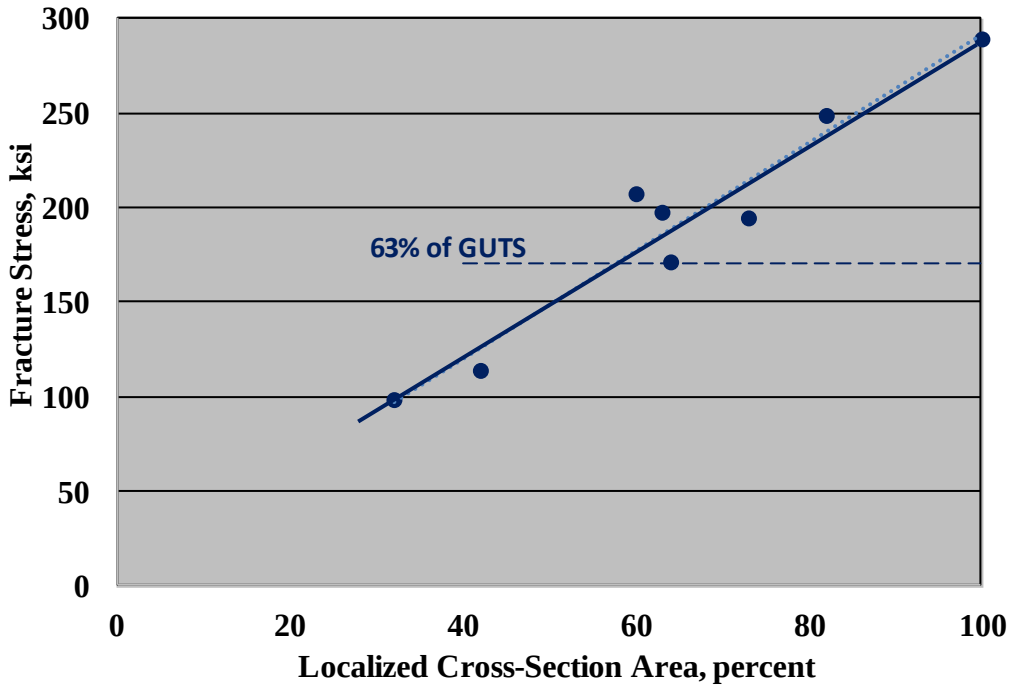

Source: FHWA.

Figure 15. Graph. Plot of prestressing steel wire fracture stress (FS) as a function of the remaining cross-section area (RCSA) of the wire at the most corroded location.

Source: FHWA.

Figure 16. Photo. Corroded wires of a strand as reproduced from figure 217 from the phase 1 study.[(1)]

$$FS = 2.86 \cdot RCSA + 5.47 (R^2 = 0.93)$$

Figure 17. Equation. Relationship between *FS* and *RCSA* based on the figure 15 data.

No correction was made to have the best fit line intersect the origin. This equation was modified for the present analyses such that *FS* at *RCSA* equals 100 percent equals the GUTS (270 ksi) as follows in figure 18:

$$FS = 2.86 \cdot RCSA - 16.0$$

Figure 18. Equation. Relationship between *FS* and *RCSA* modified such that *FS* = 270 ksi at *RCSA* = 100 percent.

Also, to be conservative, structural engineers typically assume that load from broken wires or strands is transmitted to unbroken ones; however, this possibility was not incorporated into the present test methodology. Instead, wire fractures were assumed to occur once corrosion sufficiently consumed the cross section locally such that the post-tension stress became elevated to the GUTS, irrespective of the condition of adjacent wires. Strand fracture was assumed to occur, however, on fracture of a third wire, which is consistent with load transfer from broken to unbroken wires.

It is recognized that a number of factors can influence PT strand corrosion rate, as listed below:

- Concentration of free chlorides.
- Concentration of free sulfates.
- Grout quality, including pH and physical defects such as segregation, separation, soft, unhardened material, chalkiness, and presence of free water.
- Water charging from an external source.
- Elevated temperature or relative humidity (or both) in combination with any of the above.

Individually or collectively, these determine the wire corrosion rate, which in turn, governs timing of any wire and strand fractures and tendon failures. The presently developed and employed analysis methodology is based on the dependence of the number of wire and strand fractures and tendon failures at specific times on the distribution of remaining cross-section area of wires, as represented by the mean (μ) and standard deviation (σ) of corrosion rate, considering that fracture occurs at the most corroded location on each wire. It is ultimately advantageous that the relationship between deficient grout condition and corrosion rate, as determined by the factors listed previously, be understood. Acquiring this information on actual structures may necessitate nondestructive testing or invasive inspection of tendons and sample taking, or both. Alternatively, it may be feasible to characterize the extent of grout deficiency or deficiencies on a bridge of interest, place this condition within the spectrum of conditions reported in the above-referenced FHWA study, and from this, estimate the mean and standard deviation of corrosion rate. The base model that was employed consists of 162 tendons, each with 22 Designation No.

15 (0.600-inch diameter) seven-wire strands (3,564 strands and 21,384 outer wires total).[1(1,2)] Tendons of this makeup were selected because this design is the same as for tendons that failed on the Ringling Causeway Bridge in Florida; however, analysis results are independent of the number of strands per tendon subject possibility to a rounding error.[(10)]

Corrosion Modeling

Based on the above, the fundamental input to the present failure projection modeling is the remaining cross-sectional area of the wires at the most corroded location, which is where fracture is assumed to occur, and how this remaining area decreases with exposure time. FHWA studies reported depths of localized attack along wires, and from these data, the corresponding corrosion rate was calculated. However, while the initial corrosion morphology consisted of spherical or conical depressions, these were considered to have morphed with time into a planar front. As examples, figure 19 shows a photograph of initial localized corrosion on a wire from the phase 1 study, and figure 20 provides an example of more advanced attack. As indicated in the figure 20 caption, depth of corrosion was 18 mils. Based on the width of attack around the wire circumference, wire dimensions, and geometry, and assuming a planar corrosion front, a corrosion depth of 16 mils was calculated, which is in good agreement with the measured value (18 mils). Figure 21 shows a micrograph of a heavily corroded wire from another study, which further supports the planar front assumption; however, as is apparent in the latter, there can be multiple initiation sites around the circumference.

Source: FHWA.

Figure 19. Photo. Example of initial localized corrosion on a wire from a fully grouted single-strand specimen of the phase 1 study (figure 239) for which grout chloride concentration was 0.80 wt% (pit depth is 4.7 mils).[(1)]

[1]It was considered that the initial three wires to fracture, thus causing strand fracture as noted above, are outer ones, given that the center wire is of slightly greater diameter and is more protected.

Source: FHWA.

Figure 20. Photo. Example of a more advanced attack on a wire from a single-strand specimen with a grout void from the phase 1 study (figure 243) for which grout chloride concentration was 2.00 wt% (pit depth is 18 mils).[(1)]

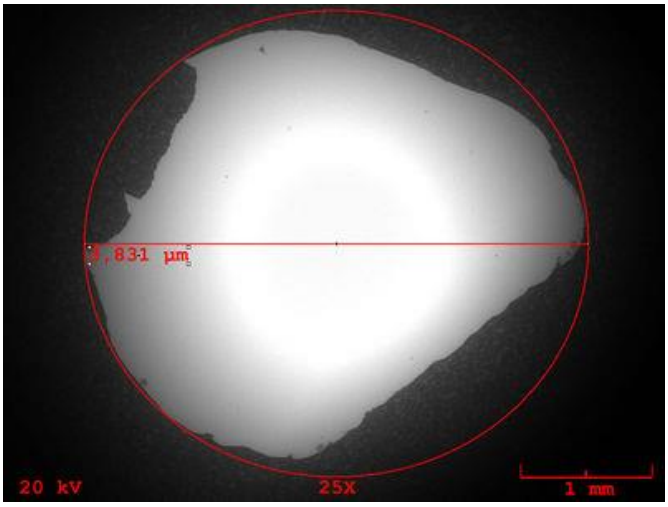

Source: FHWA.

Figure 21. Photo. Micrograph of a corroded wire cross section with approximately planar penetration fronts at multiple corrosion initiation sites.

Corrosion invariably involves an initiation time and a time of propagation. However, in the present analysis approach, the former (initiation time) was assumed to be negligible compared to time of overall exposure. Also, it is likely that corrosion rate within occluded sites of attack increases with time to a steady-state value as acidification develops. Modeling this would be complex and involve its own set of assumptions, and so, corrosion rate was assumed to be constant with time. For the example in figure 20, a corrosion penetration of 18 mils over the 178 d of exposure corresponds to an average attack rate of 37 mils per year (mpy). Corrosion rate for a penetration of 16 mils, as was determined based on assuming a planar corrosion front, is 33 mpy.

For some of the phase 1 specimens with a grout void, a hole was drilled in the duct at the void elevation after 120 to130 d, and water and fresh air were introduced. For specimens with 0.40 wt% chloride concentration and greater, this typically resulted in a negative potential shift

and elevated corrosion rate for some time thereafter, the effect being greater the higher the chloride concentration. Both single-strand specimens cited above (figure 19 and figure 20) are examples of this treatment.

Modeling of the *RCSA* was performed at time increments ranging from 0.10 to 2.00 yr based on a mean effective corrosion rate ($\mu(CRE)$) and a standard deviation ($\sigma(CRE)$) that were determined as explained below. Here, *CRE* is an abbreviation for corrosion rate equivalent. As such, any corrosion rate enhancement from periodic or occasional water charging events was averaged over time. Attack was assumed to initiate at a point on the wire circumference and proceed as a planar front, as discussed previously. The algorithm represented schematically in figure 22 was employed for times when cross-sectional loss was less than 50 percent. The RCSA of the wire, at a particular time (T) subsequent to exposure recommencing, was calculated using the equation in figure 23, where A is the original wire cross-section area, TA is the triangle area for which one side defines the corrosion front (shown in figure 22 for $T = 1$), and SA is the corresponding sector area.

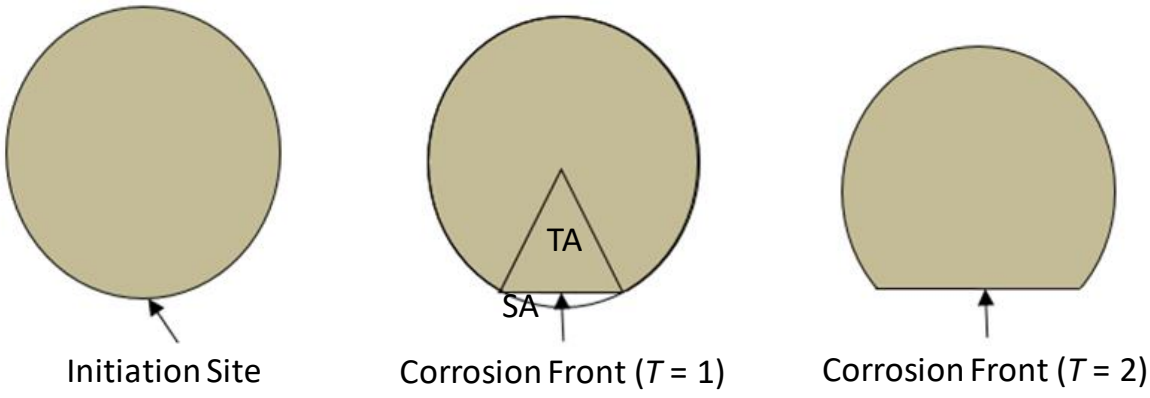

Source: FHWA.
A. Initiation Site.

Source: FHWA.
B. Corrosion Front (T = 1) (yr).

Source: FHWA.
C. Corrosion Front (T = 2) (yr).

Figure 22. Illustration. Schematic representation of the algorithm employed to project remaining wire cross-section area up to 50-percent loss.

$$RCSA = A - SA + TA$$

Figure 23. Equation. Projection of remaining wire cross-section area for cases where more than 50 percent of the original area remains.

RCSA beyond 50-percent loss was determined for different time increments using the equation in figure 24, where *TRA*(-) is the area of successive approximated trapezoids, the height of each ranging from 0.10 to 2.00 yr of penetration depending on the particular analysis and width as the average of the two contiguous cords.

$$RCSA = 0.5 \cdot A - TRA(1) - TRA(2) - \cdots$$

Figure 24. Equation. Projection of remaining wire cross-section area for cases where less than 50 percent of the original area remains.

Figure 25(a) then schematically illustrates this corrosion penetration model for losses less than 50 percent of the original cross section as the product of *CRE* and *T*, and figure 25(b) for losses beyond this, where *T´* is time subsequent to the 50-percent loss. *RCSA* calculations were performed using an Excel spreadsheet format that included a singular address of the final loss increment as the 50-percent *RCSA* was approached.

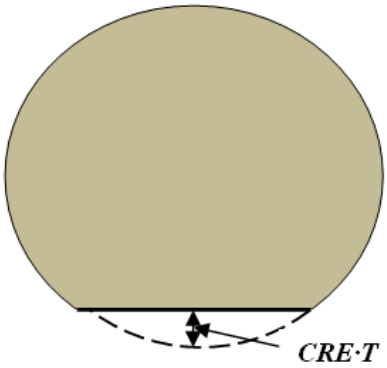

Source: FHWA.

A. Corrosion penetration model for losses less than 50 percent of the original section loss.

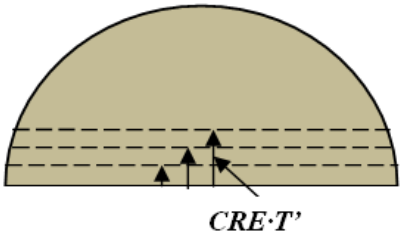

Source: FHWA.

B. Corrosion penetration model for losses more than 50 percent of the original section loss.

Figure 25. Illustration. Algorithm employed to calculate remaining wire cross-section area for each successive time increment of corrosion.

The distribution of *CRE*s was assumed to be normal, as justified subsequently, with $\mu(CRE)$ and $\sigma(CRE)$ being either assumed or determined from the phase 1 data. The *CRE* distribution for specific analyses ranged from $\mu(CRE)+2.25\cdot\sigma(CRE)$ to $\mu(CRE)-2.0\cdot\sigma(CRE)$ in mostly $0.2\cdot\sigma(CRE)$ increments with the corresponding *RCSA* being determined for each.

Figure 26 provides a plot of projected remaining wire cross-section area $\mu(CRE)$ = 3.6 mpy, $\sigma(CRE)$ = 0.42,[2] and various $\mu \pm x\cdot\sigma$ increments, where *x* ranges from +2.25 to –2.00, to 75 yr based on the algorithm illustrated in figure 25. This shows that the remaining area decreases with time at a progressively increasing rate initially but, eventually, reaches an inflection point, beyond which the rate of decrease moderates with further time. Such a trend is a consequence of, first, $\mu(CRE)$ (being considered as normally distributed and, second, the planar corrosion front assumption. Also, the results are shifted to shorter time with increasing $\mu(CRE)$ and become more spread with increasing $\sigma(CRE)$.

[2]These values were calculated from the phase 1 study results for a fully grouted specimen with 0.80 wt% chloride.

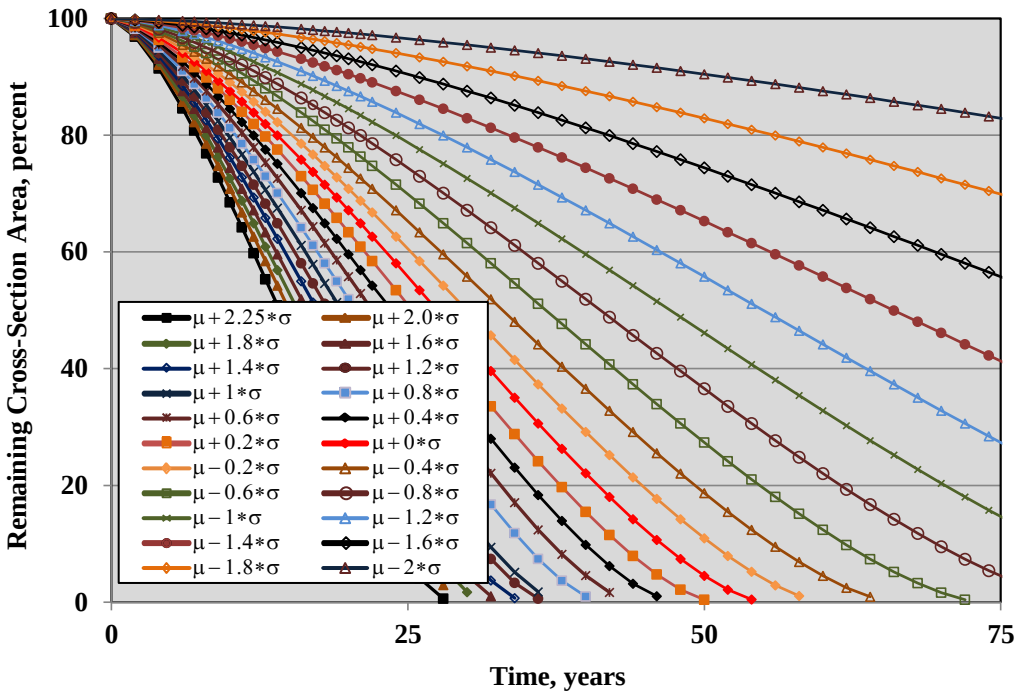

Source: FHWA.

Figure 26. Graph. Projected remaining wire cross-section area as a function of time for a range of $\mu \pm x \cdot \sigma$ increments.

For individual analyses, the wire *RCSA* was determined at successive times for each $\mu(CRE) \pm x \cdot \sigma(CRE)$ increment. Next, the number of wires in each increment and the probability of occurrence (POO) for each were calculated. The product of each POO and the total number of outer wires (21,384 for the baseline case) yielded the number of wires currently experiencing corrosion in each cross-sectional area increment at each time step. The product of the number of wires in each increment and the probability of fracture according to the mean and standard deviation of the figure 15 data yielded the corresponding number of fractured wires. As noted above, baseline analyses considered that strands are stressed to 63 percent of the GUTS. The mean remaining area to cause fracture at this stress was determined from the equation in figure 18 as 64.97 percent, and standard deviation was taken as determined from the data illustrated in figure 15 (σ = 6.33 percent). The total number of fractured outer wires was then determined for each time as the sum of such wires in each area increment.

For the baseline case, the 21,384 wires were partitioned into groups of 6, where each group represented the outer wires of a strand. Likewise, the groups of 6 were partitioned into groups of 22, with each of the latter representing a tendon. This results in there being 3,564 strands and 162 tendons. A random number was then assigned to each wire according to the total number of wires (21,384). For each time increment, the number of wires with a random number equal to or less than the model-determined number of fractured wires for that time increment was summed. Except where noted otherwise, the same order of random numbers was employed for all analyses.

Because wires were assigned to strands and strands to tendons, the time at which a strand fractured was determined according to when three of its wires had fractured. Likewise, tendon failure was considered to occur when 7 of its 22 strands had fractured. In both cases, these numbers of fractures elevate stress in the remaining wires/strands to above the GUTS (270 ksi), assuming load transfer from fractured to unfractured wires.[18,19] In the analyses that follow, the number and percentage of wire and strand fractures and tendon failures at successive time increments were determined.

CHAPTER 3. RESULTS AND DATA ANALYSIS

PHASE 2 TESTING

Autopsy and Pit Depth Measurements

Subsequent to the elevated temperature testing, specimens were dissected. The extracted wires were cleaned, and pit depths were measured with a digital pit gauge. All corrosion damage was found to have occurred at or near the void/grout interface. Figure 27 and figure 28 show a severely corroded wire near a segregated void/grout interface and the section loss that occurred, respectively. This particular specimen had been exposed to 0.8-percent sulfate by weight of cement dissolved in pH 8.0 recharging water.

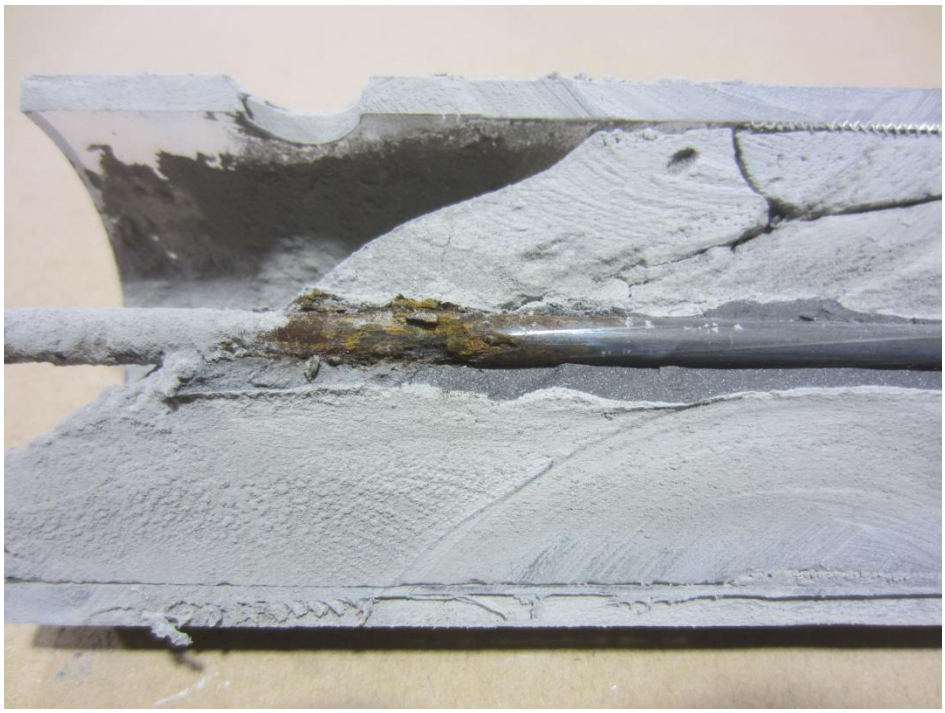

Source: FHWA.

Figure 27. Photo. A corroded wire that had been exposed in segregated grout.

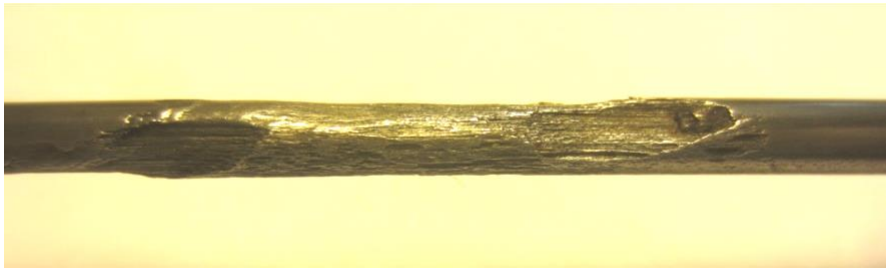

Source: FHWA.

Figure 28. Photo. Corrosion morphology of the cleaned wire shown in figure 27.

Major Findings

The accelerated corrosion testing at the elevated temperature resulted in sufficient corrosion damage for the modeling work. It also provided useful results for better understanding tendon corrosion associated with presence of grout segregation, recharging water, and sulfates, as well as the role of pH and temperature. In this regard, figure 29 through figure 31 present mean grout resistance, R, versus time plots for group 1 specimens (pH 8.0 recharging water), group 2 specimens (pH 13.6 recharging water plus pH 8.0 recharging water), and group 3 specimens (admixed sulfate plus deionized water), respectively. In every group, the segregated grout specimens exhibited lower mean R than the normal grout ones. On adding recharging water into the voids, the latter showed inconsistent resistance reductions, whereas the former showed little resistance change. This finding may suggest that the segregated grout was already near saturation. Moreover, the segregated grout specimens showed less mean R variation with time under the same condition compared to the normal grout specimens. The admixed grout specimens exhibited higher mean R than the nonadmixed grout counterparts. Finally, sulfate concentration did not influence mean R.

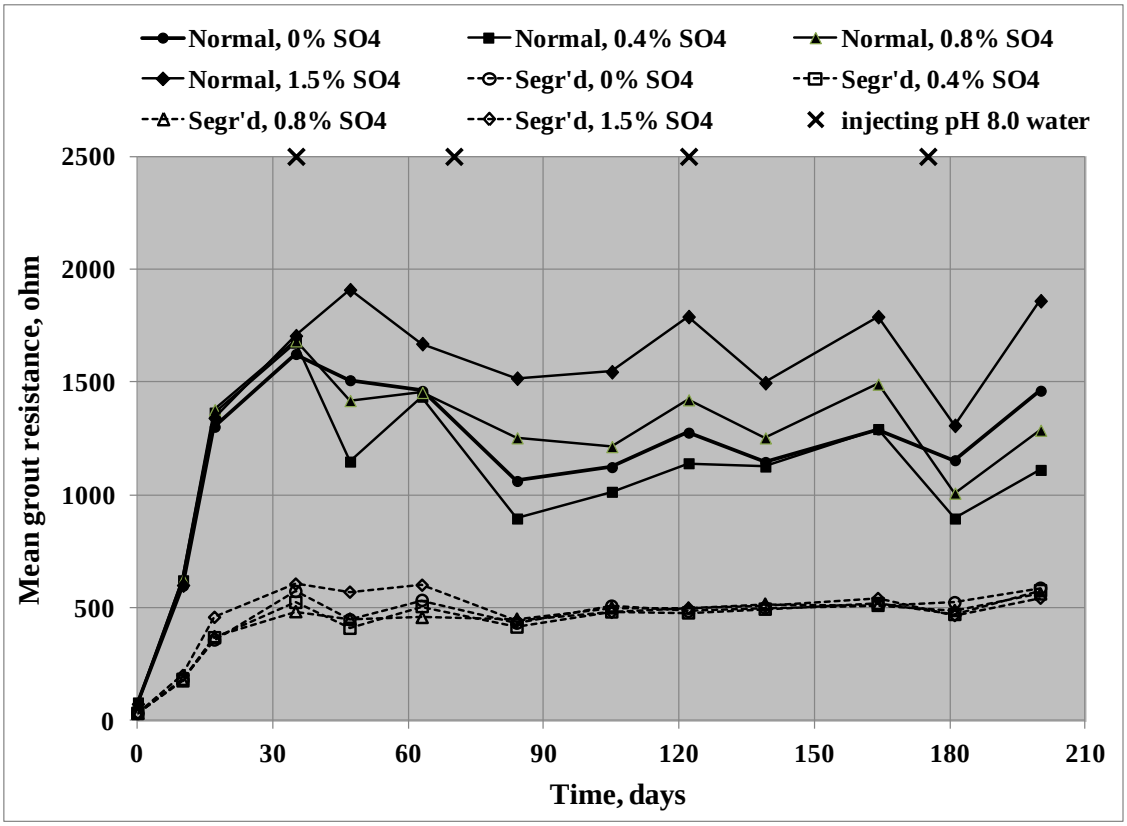

Source: FHWA.

Figure 29. Graph. Mean R versus time plot for group 1 specimens.

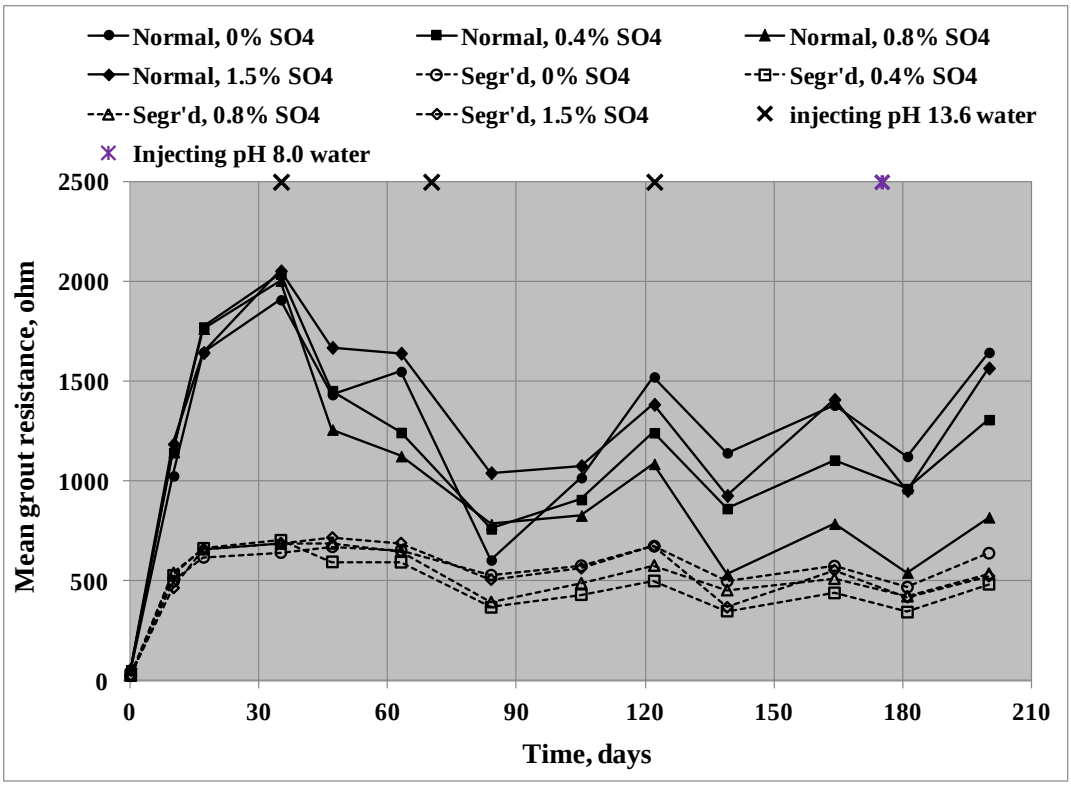

Source: FHWA.

Figure 30. Graph. Mean R versus time plot for group 2 specimens.

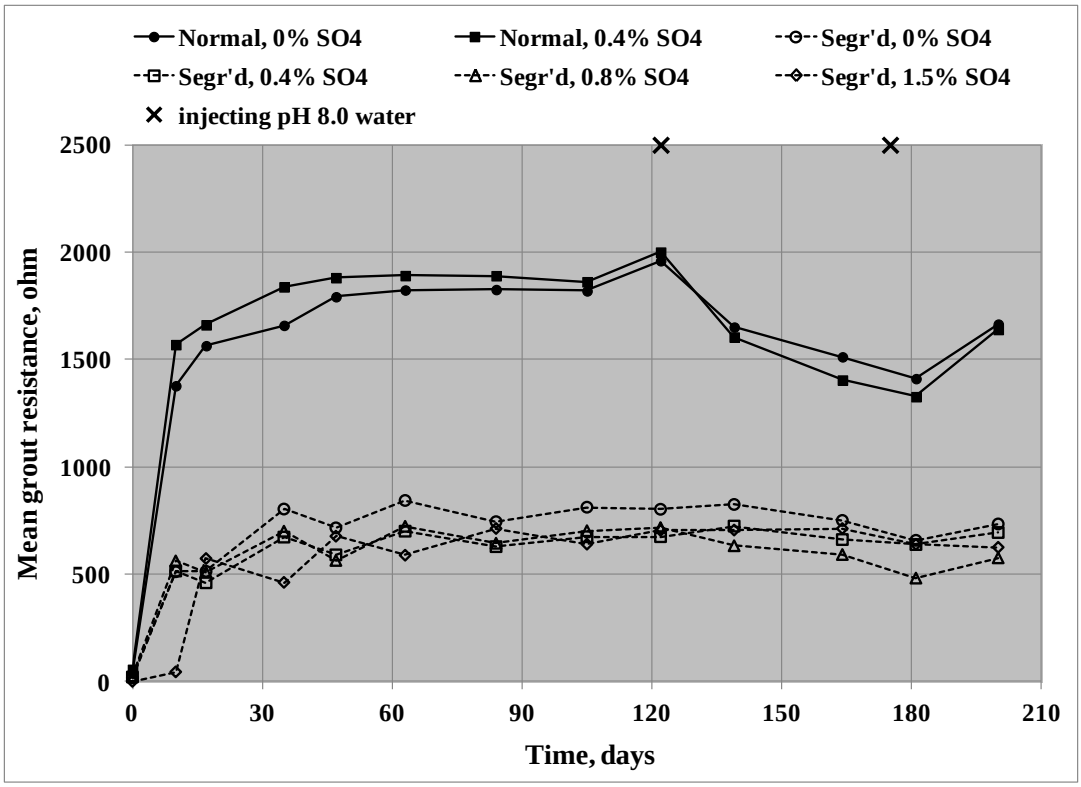

Source: FHWA.

Figure 31. Graph. Mean R versus time plot for group 3 specimens.

Figure 32 through figure 34 present mean I_{macro} versus time plots for the specimens in groups 1, 2, and 3, respectively. Only four datasets were included in the plots.

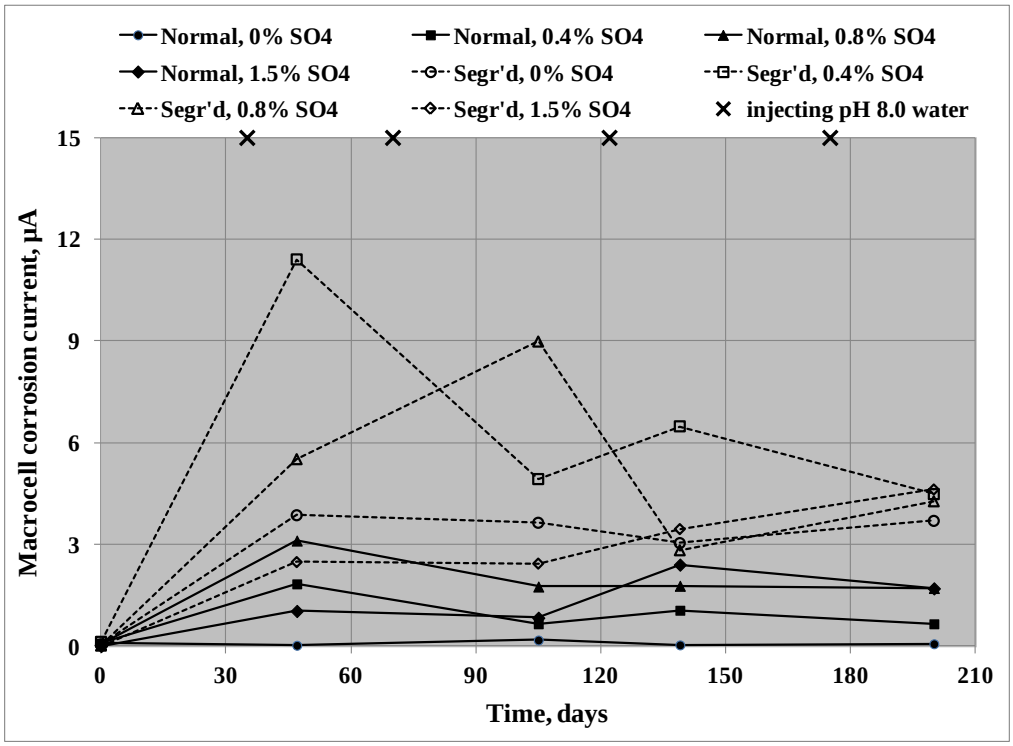

Source: FHWA.

Figure 32. Graph. Mean I_{macro} versus time plot for group 1 specimens.

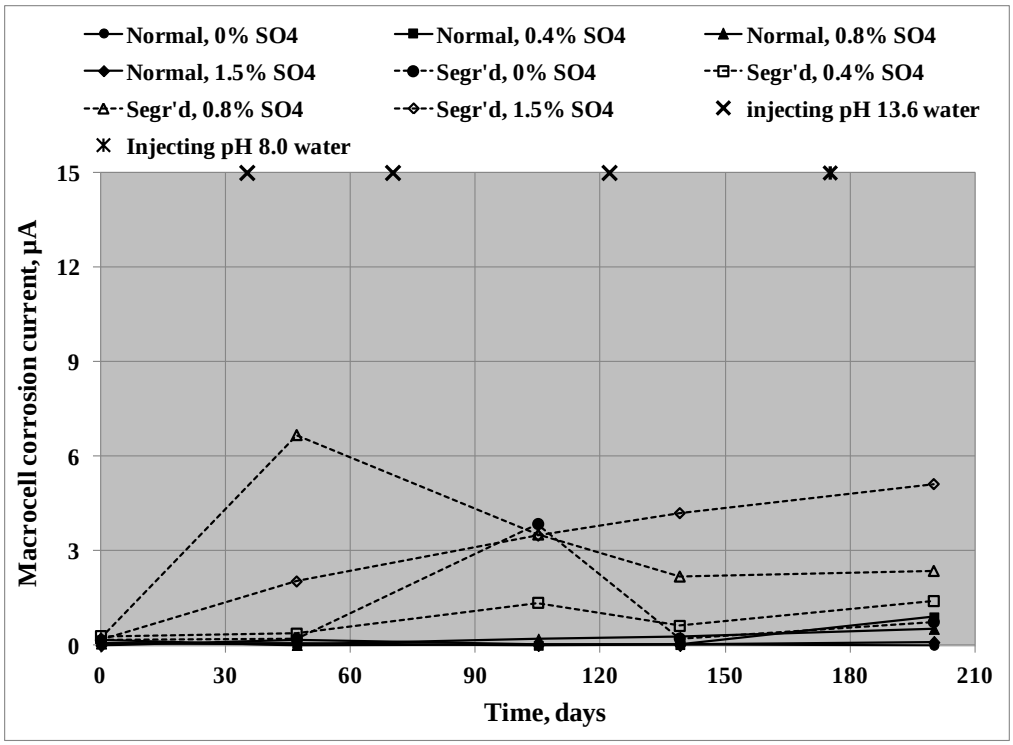

Source: FHWA.

Figure 33. Graph. Mean I_{macro} versus time plot for group 2 specimens.

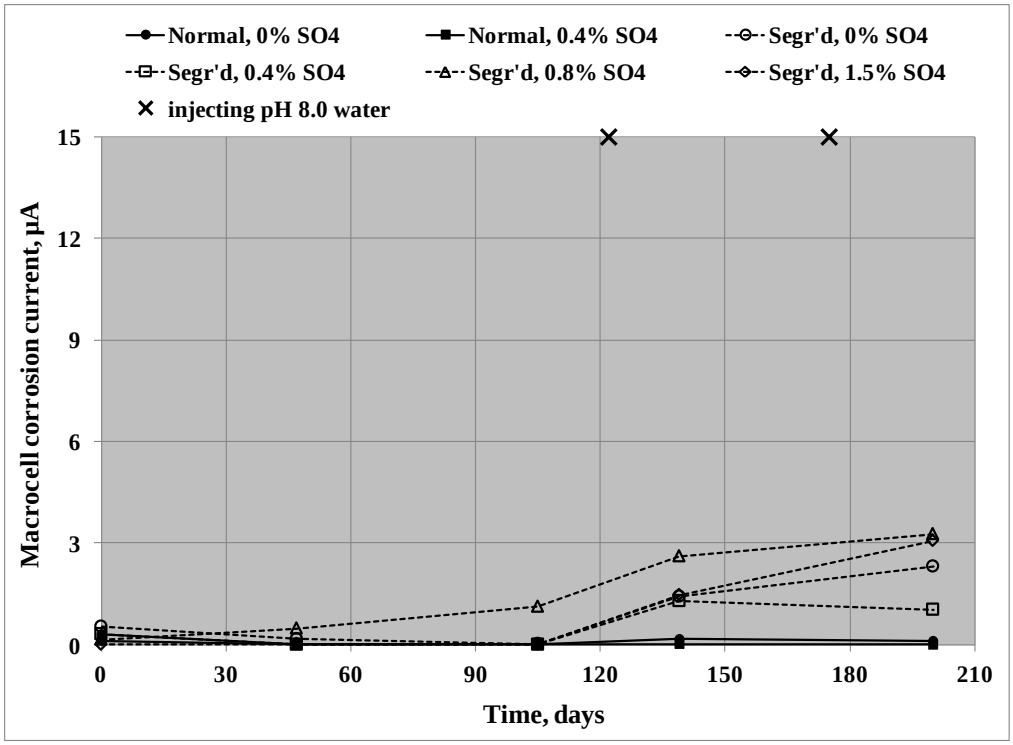

Source: FHWA.

Figure 34. Graph. Mean I_{macro} versus time plot for group 3 specimens.

It can be seen in figure 32 that segregation of grout created a more corrosive condition in the low pH (carbonated) environment, indicated by higher I_{macro}, than the normal grout in the same environment. In addition, mean I_{macro} values at 200 d for the segregated grout specimens were fairly similar, irrespective of sulfate concentration. The segregated grout specimens in groups 2 and 3 also exhibited higher mean I_{macro} values than the normal grout specimens, which exhibited negligible I_{macro}. This trend was observed under certain test conditions. The normal grout specimens in these groups were minimally influenced by the change of pH from 13.6 to 8.0 and presence of sulfate at any concentration. On the other hand, all of the segregated grout specimens containing admixed sulfate became noticeably active at 200 d, when deionized water was injected. However, they did not show a clear relationship between I_{macro} increase and sulfate concentration.

A total of 1,901 pit depth data were collected from the autopsied 189 specimens. Table 2 summarizes statistical analysis results of pit depth data for specimens in groups 1 and 2. Table 3 lists the same information for group 3 specimens.

Table 2. Pit depth statistics of group 1 and group 2 specimens.

Pit Depth (mil)	Normal Grout With pH 8.0 Recharging Water (Group 1). Sulfate Concentration Dissolved in Recharging Water by Weight of Cement (0%)	Normal Grout With pH 8.0 Recharging Water (Group 1). Sulfate Concentration Dissolved in Recharging Water by Weight of Cement (0.4%)	Normal Grout With pH 8.0 Recharging Water (Group 1). Sulfate Concentration Dissolved in Recharging Water by Weight of Cement (0.8%)	Normal Grout With pH 8.0 Recharging Water (Group 1). Sulfate Concentration Dissolved in Recharging Water by Weight of Cement (1.5%)	Segregated Grout With pH 8.0 Recharging Water (Group 1). Sulfate Concentration dissolved in Recharging Water by Weight of Cement (0%)	Segregated Grout With pH 8.0 Recharging Water (Group 1). Sulfate Concentration Dissolved in Recharging Water by Weight of Cement (0.4%)	Segregated Grout With pH 8.0 Recharging Water (Group 1). Sulfate Concentration Dissolved in Recharging Water by Weight of Cement (0.8%)	Segregated Grout With pH 8.0 Recharging Water (Group 1). Sulfate Concentration Dissolved in Recharging Water by Weight of Cement (1.5%)	Normal Grout With pH 13.6 Recharging Water (Group 2). Sulfate Concentration Dissolved in Recharging Water by Weight of Cement (0%)	Normal Grout With pH 13.6 Recharging Water (Group 2). Sulfate Concentration Dissolved in recharging Water by Weight of Cement (0.4%)	Normal Grout With pH 13.6 Recharging Water (Group 2). Sulfate Concentration Dissolved in Recharging Water by Weight of Cement (0.8%)	Normal Grout With pH 13.6 Recharging Water (Group 2). Sulfate Concentration Dissolved in Recharging Water by Weight of Cement (1.5%)	Segregated Grout With pH 13.6 Recharging water (Group 2). Sulfate Concentration Dissolved in Recharging Water by Weight of Cement (0%)	Segregated Grout With pH 13.6 Recharging Water (Group 2). Sulfate Concentration Dissolved in Recharging Water by Weight of Cement (0.4%)	Segregated Grout With pH 13.6 Recharging Water (Group 2). Sulfate concentration dissolved in Recharging Water by Weight of Cement (0.8%)	Segregated Grout With pH 13.6 Recharging Water (Group 2). Sulfate Concentration Dissolved in Recharging Water by Weight of Cement (1.5%)
Maximum	17.5	37.0	51.0	26.0	49.5	46.5	48.5	36.5	8.5	10.5	18.5	22.0	33.0	20.5	49.0	37.5
Mean of 5 highest	15.3	35.9	44.0	19.2	41.0	41.2	40.0	31.3	7.4	9.6	15.7	17.4	30.8	19.4	41.2	29.2
Mean of 10 highest	13.4	33.8	39.0	15.0	33.7	30.5	33.7	27.8	5.5	7.8	13.4	14.3	29.0	17.8	29.0	24.4
Mean	6.4	12.2	12.7	7.8	10.6	10.2	9.9	10.4	2.9	2.8	5.6	6.4	9.4	8.3	8.2	9.0
Median	5.5	10.5	9.5	6.8	8.5	8.5	7.0	7.5	2.3	1.5	5.0	6.0	5.5	7.0	6.0	7.5
Standard deviation	4.8	8.2	10.8	5.5	9.3	7.7	9.1	8.3	2.7	3.1	4.3	4.8	9.3	4.9	9.3	6.8

Table 3. Pit depth statistics of group 3 specimens.

Pit Depth (mil)	Sulfate Concentration Admixed in Normal Grout by Weight of Cement (0%)	Sulfate Concentration Admixed in Normal Grout by Weight of Cement (0.4%)	Sulfate Concentration Admixed in Normal Grout by Weight of Cement (0.8%)	Sulfate Concentration Admixed in Normal Grout by Weight of Cement (1.5%)	Sulfate Concentration Admixed in Segregated Grout by Weight of Cement (0%)	Sulfate Concentration Admixed in Segregated Grout by Weight of Cement (0.4%)	Sulfate Concentration Admixed in Segregated Grout by Weight of Cement (0.8%)	Sulfate Concentration Admixed in Segregated Grout by Weight of Cement (1.5%)
Maximum	10.5	5.0	—	—	23.5	14.5	12.0	29.0
Mean of 5 highest	7.9	2.9	—	—	20.0	13.1	11.2	24.7
Mean of 10 highest	6.1	1.5	—	—	15.6	10.5	10.6	21.9
Mean	3.6	1.2	—	—	5.4	4.1	5.2	8.3
Median	4.0	0.8	—	—	4.0	3.0	4.5	6.5
Standard Deviation	3.5	1.6	—	—	5.4	3.4	2.9	6.4

—No information available.

It can be seen in table 2 that the accelerated corrosion testing was able to produce significant corrosion damage in that the deepest measured pit was 51 mils, which is equivalent to 93 mpy. This particular pit represents about 26 percent of the section loss of the outer wire. Actual pit depth data are employed in the modeling work in chapter 4.

Figure 35 shows a plot of mean pit depth versus mean I_{macro} at 200 d for each of the three groups. No clear correlation is apparent between the two variables. A lack of any correlation is thought to be due to the fundamentally different characteristics of these parameters; that is, pits are formed by localized corrosion, whereas I_{macro} is related to the macroscopic corroding area, which could not be determined accurately.

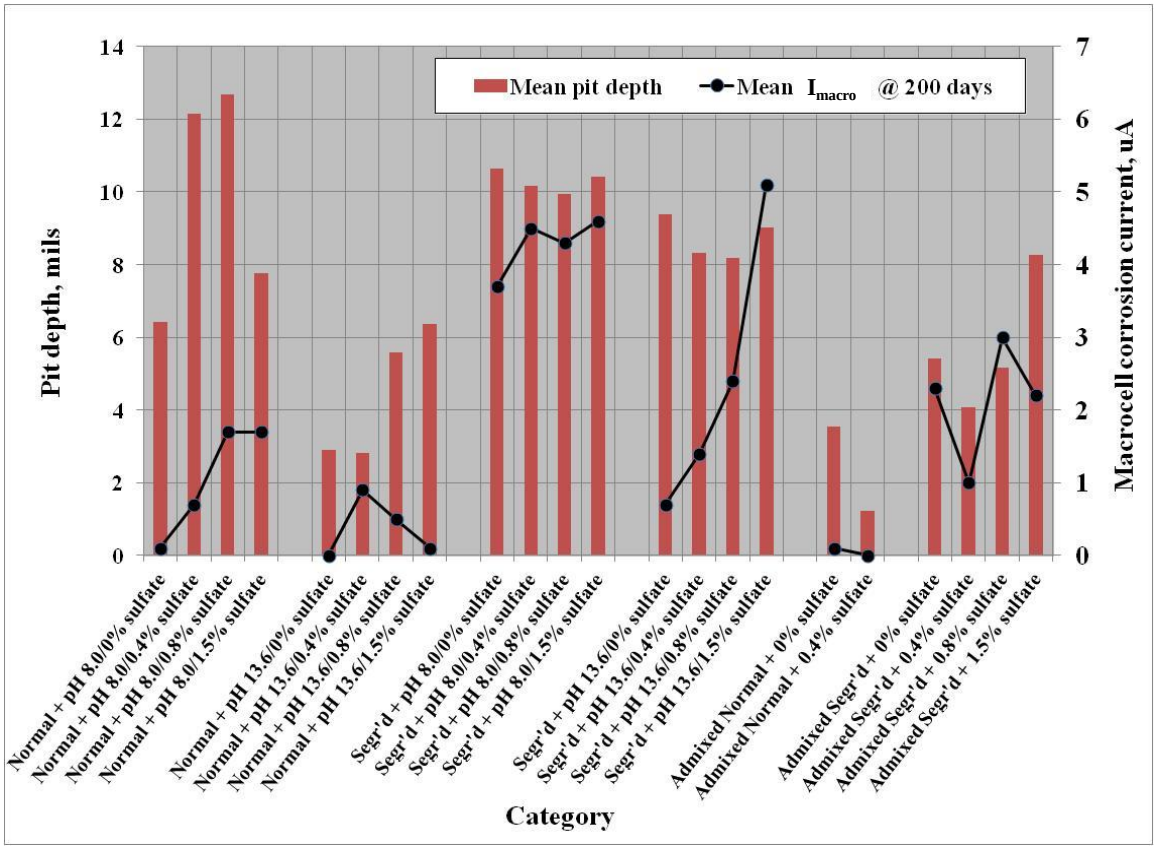

Source: FHWA.

Figure 35. Graph. Mean pit depth versus mean I_{macro} plot.

Figure 36 shows maximum pit depth and mean I_{macro} at 200 d for the same groups of specimens. Like figure 35, no correlations were found between the two variables for the same reason; that is, the maximum pit depth is related to the localized corrosion process, and I_{macro} is related to the macroscopic corrosion process.

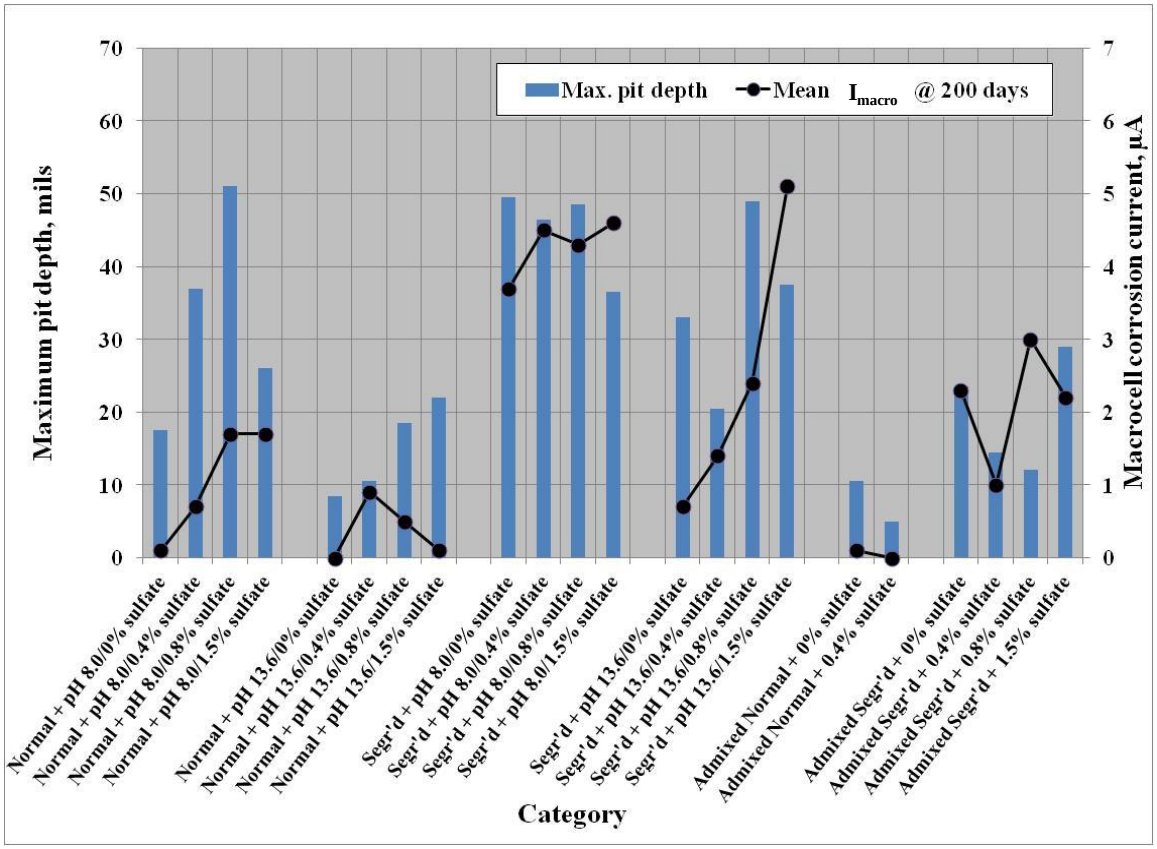

Source: FHWA.

Figure 36. Graph. Maximum pit depth versus mean I_{macro} plot.

Figure 37 is a scatterplot of R_p versus I_{macro} at 200 d. Even though there is no well-defined one-to-one relationship, the specimens exhibiting lower R_p (i.e., a higher corrosion rate) tended to yield larger I_{macro}. The segregated grout specimens showed this trend more definitively than the normal grout specimens.

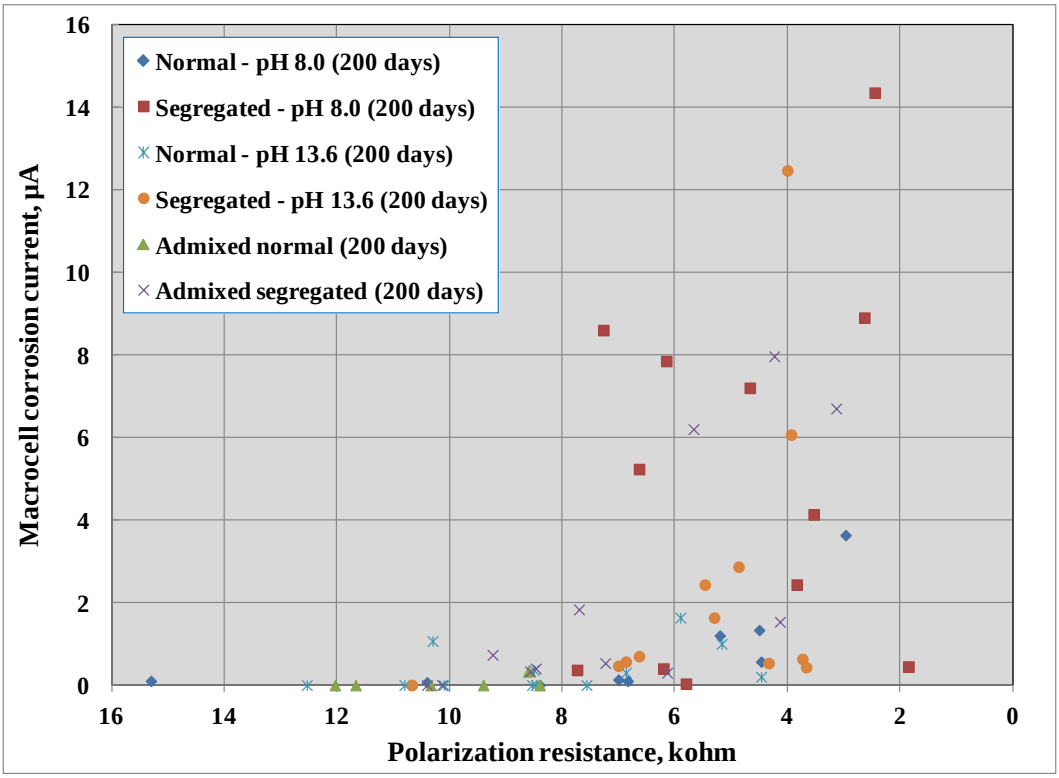

Source: FHWA.

Figure 37. Graph. R_p versus I_{macro} at 200 d plot.

PHASE 1 TESTING: SINGLE-STRAND SPECIMENS

General

In task 2 of the phase 1 study, both stressed and unstressed single-strand specimens with and without a grout void and with chloride concentrations ranging from 0 to 2.00 wt% cement were exposed for 178 d. These tests included successive 2-week periods of the three environmental conditions defined earlier (ambient (25 °C, 60% RH), hot and humid (40 °C, 90% RH), and freezing and drying (–10 °C, 40% RH)).

Fully Grouted Specimens

The phase 1 study reported the number and depth of pits for Specimen Numbers 0.8%–F–S and 2.0%–F–S (0.80 and 2.00 wt% chloride concentration, respectively, fully grouted (F), and stressed (S)) measured after specimen dissection and wire separation and cleaning with results being as listed in table 4, where statistical parameters assume normality.[1] Figure 38 through figure 40 plot the projected number of wire and strand fractures and tendon failures, respectively, versus time to 75 yr for Specimen Number 0.8%–F–S; figure 41 summarizes these results in a single plot. Likewise, figure 42 provides a summary plot of wire and strand fractures and tendon failures for Specimen Number 2.0%–F–S. The trends exhibited here show that initial fractures and failures are

[1]There are insufficient data here to test for normality; however, this was done for specimens with a grout void, as explained subsequently in conjunction with figures 48–51.

projected to commence after some period during which wire cross section progressively reduces, with subsequent fracture and failure rates progressively increasing with time to an inflection point beyond which these rates moderate. These trends track the progression of cross-section area reduction with time, as was illustrated in figure 26. Correspondingly, table 5 lists the times of initial fractures and failures (T_f) and the subsequent fracture and failure rates near the inflection point for both specimens. Thus, T_f and fracture rate were least for wires, and failure rate was greatest for tendons. This resulted because for a strand to fracture only 3 of its wires need to break, and failure of a 22-strand tendon requires only 7 of its strands to fracture in order for stress to become elevated to above the GUTS. Also, while T_f is less for the higher chloride specimen, there is little difference in subsequent wire and strand fracture and tendon failure rates. Possible reasons for this are provided subsequently.

Table 4. Listing of specimen dissection results for single-strand, fully grouted specimens for which measurements were made.

Specimen No.[1]	Count	Min Pit Depth (mil)	Max Pit Depth (mil)	Mean (μ) Pit Depth (mil)	Standard Deviation (σ)	Ratio (σ/μ)
0.8%–F–S	5	2	5	3.60	1.52	0.42
2.0%–F–S	35	2	12	4.11	2.01	0.49

[1]Percentage = wt% chloride; F = fully grouted; S = stressed.

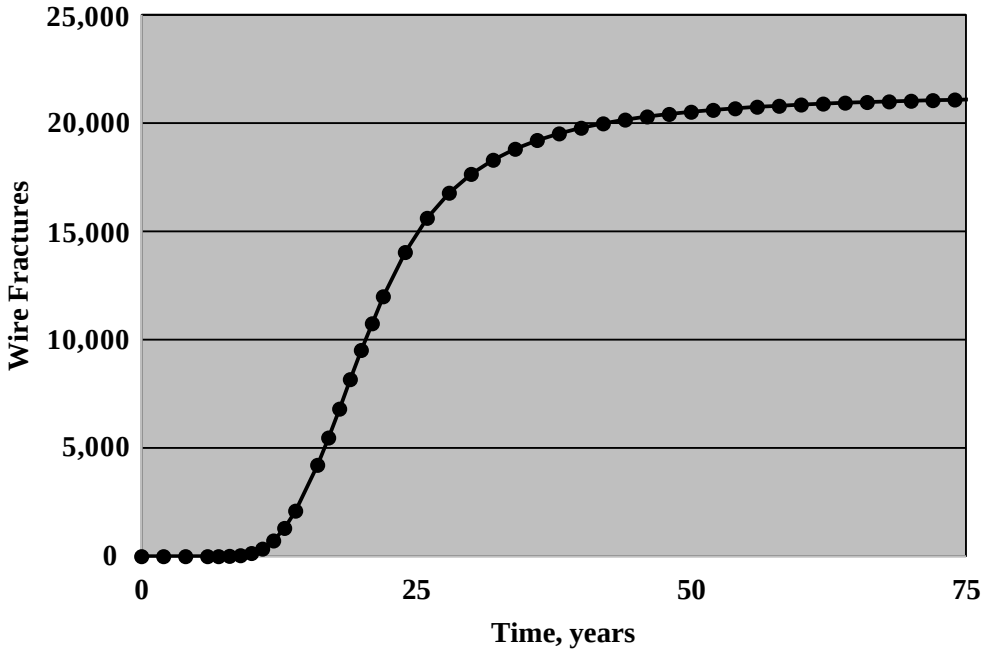

Source: FHWA.

Figure 38. Graph. Number of wire fractures as a function of time for the case of sound grout with 0.80 wt% chloride based on pit depth determinations for phase 1 Specimen Number 0.8%–F–S.(1)

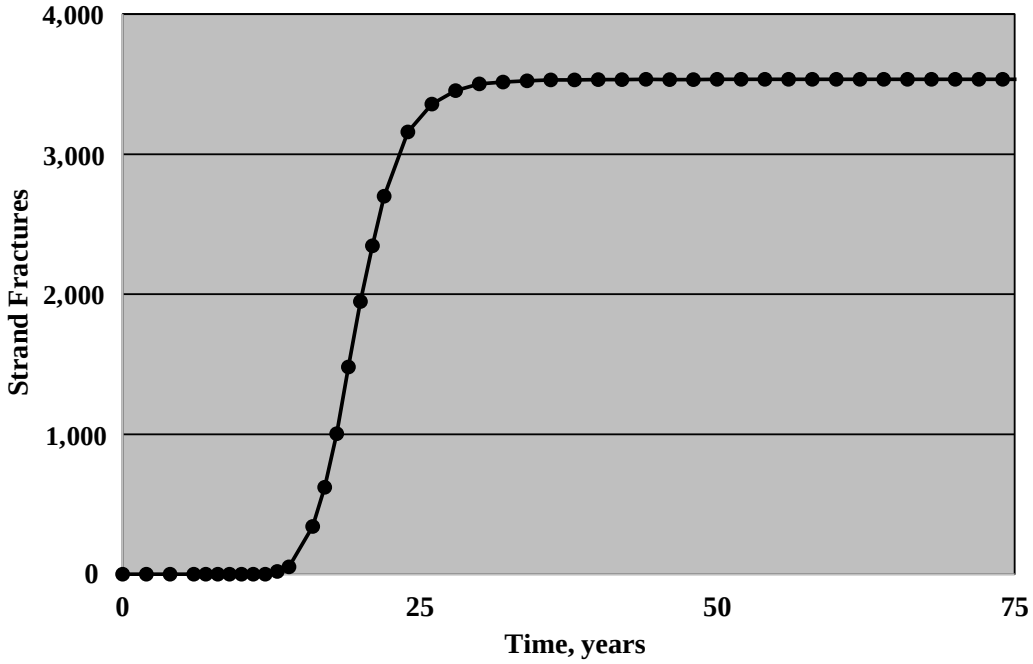

Source: FHWA.

Figure 39. Graph. Number of strand fractures as a function of time for the case of sound grout with 0.80 wt% chloride based on pit depth determinations for phase 1 Specimen Number 0.8%–F–S.[(1)]

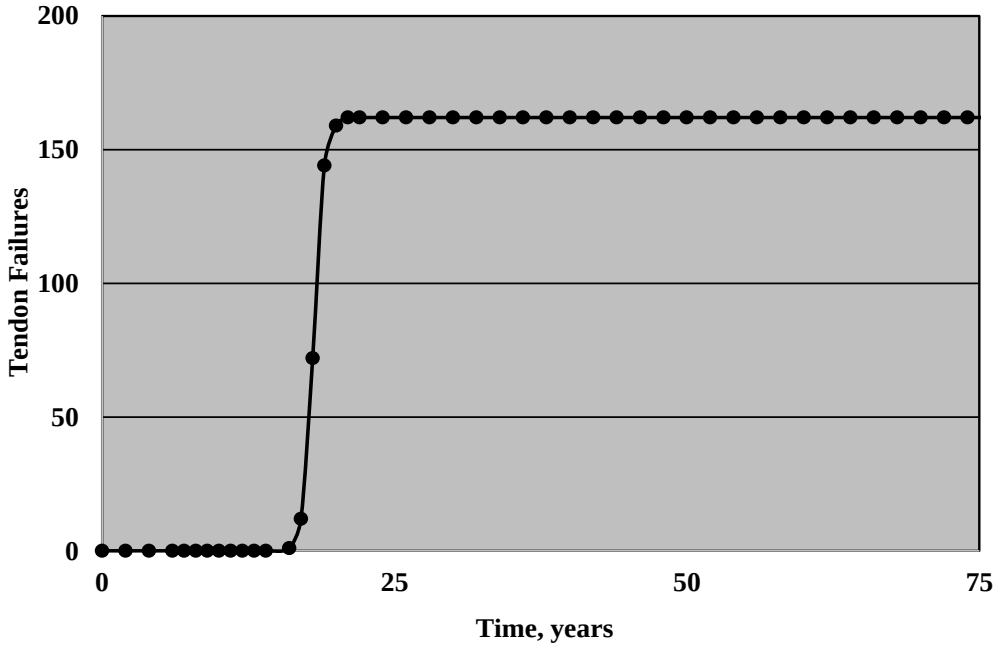

Source: FHWA.

Figure 40. Graph. Number of tendon failures as a function of time for the case of sound grout with 0.80 wt% chloride based on pit depth determinations for phase 1 Specimen Number 0.8%–F–S.[(1)]

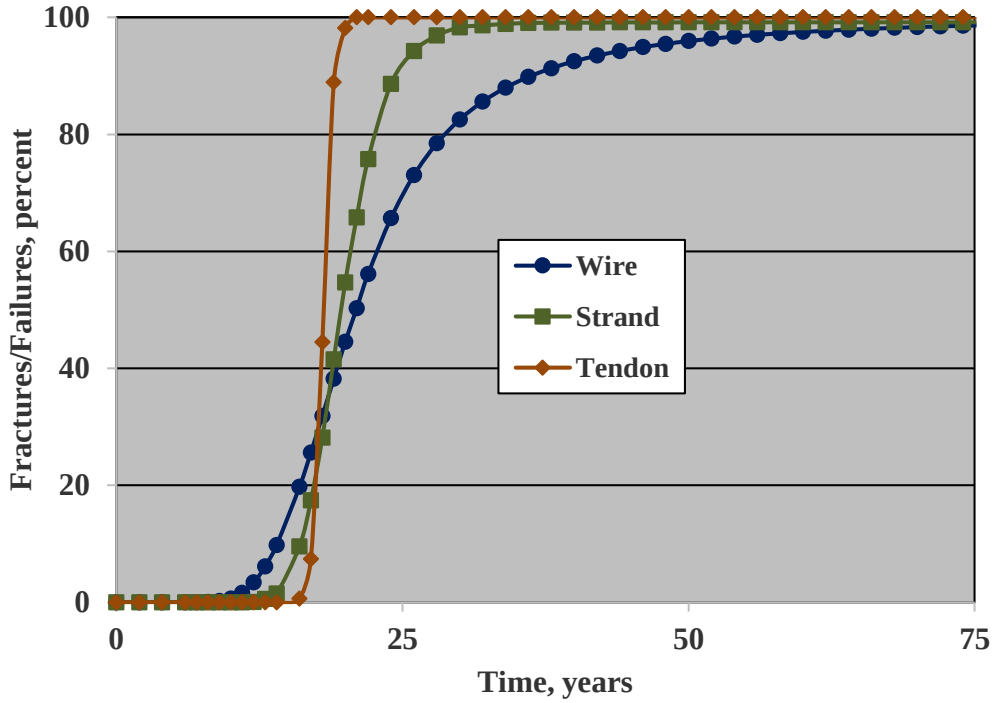

Source: FHWA.

Figure 41. Graph. Combined plot of the percentage of wire and strand fractures and tendon failures as a function of time based on pit depth determinations for phase 1 Specimen Number 0.8%–F–S.[(1)]

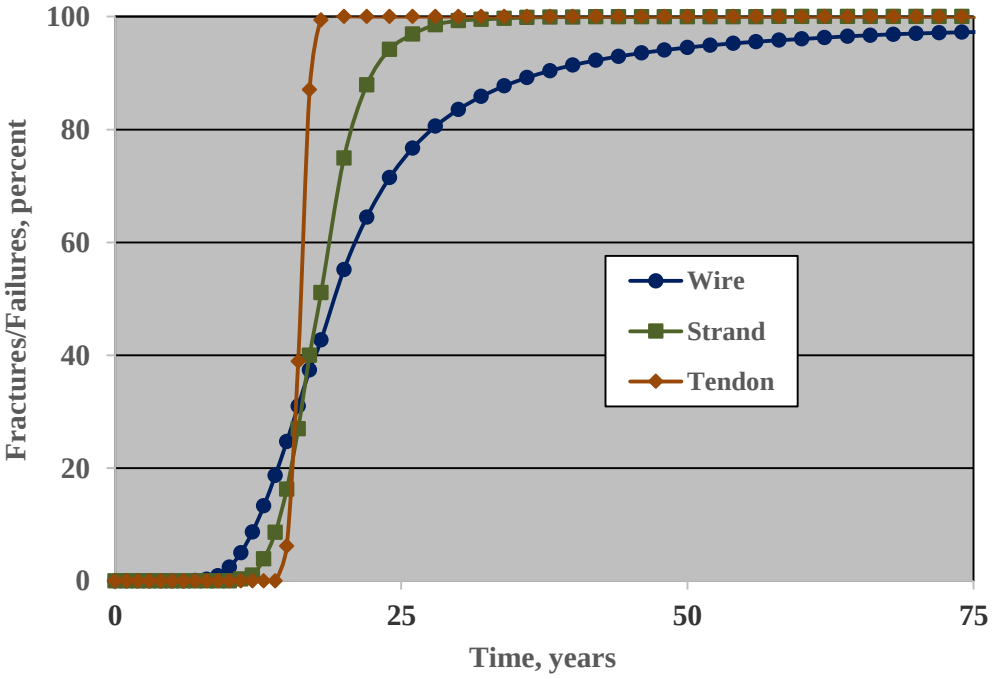

Source: FHWA.

Figure 42. Graph. Percentage of wire and strand fractures and tendon failures as a function of time based on pit depth determinations for phase 1 Specimen Number 2.0%–F–S.[(1)]

Table 5. T_f and rate of subsequent fractures for wires and strands and of failures for tendons for fully grouted single-strand specimens with two grout chloride concentrations.

Specimen Number	Member	T_f (Year)	Number of Fractures or Failures/Year*	Percent of Fractures or Failures/Year*
0.8%–F–S	Wire	6.3	1,363	6.4
0.8%–F–S	Strand	12.7	476	13.4
0.8%–F–S	Tendon	16.8	70	43.2
2.0%–F–S	Wire	5.2	1,398	6.5
2.0%–F–S	Strand	10.1	492	13.8
2.0%–F–S	Tendon	13.8	77	47.5

*Determined as slope of the curve near the inflection point.

The listed fracture/failure rates at the inflection point are of no practical significance and simply provide a comparison. Such rates in the timeframe just subsequent to T_f are of significance, however, and data for these are presented and discussed subsequently.

Table 4 indicates a relatively high standard deviation-to-mean ratio (σ/μ) for pit depth (0.42 for Specimen Number 0.8%–F–S and 0.49 for Specimen Number 2.0%–F–S), which may reflect the relatively small sample size. It can be reasoned that, for physically sound grout and a larger sample size, this ratio would be smaller. Considering this, calculations for Specimen Number 0.8%–F–S were repeated but with $\sigma(CRE) = 0.30\ \mu(CRE)$ and $0.15\ \mu(CRE)$, with results being shown in figure 43 and figure 44, respectively, for each of the two cases ($\mu(CRE) = 3.60$ mpy (table 1)). These are summarized in table 6 in comparison to actual results for Specimen Number 0.8%–F–S ($\sigma(CRE) = 0.42\ \mu(CRE)$). This shows that T_f and the rate of fracture/failure increase, the latter once initiated, with decreasing σ/μ.

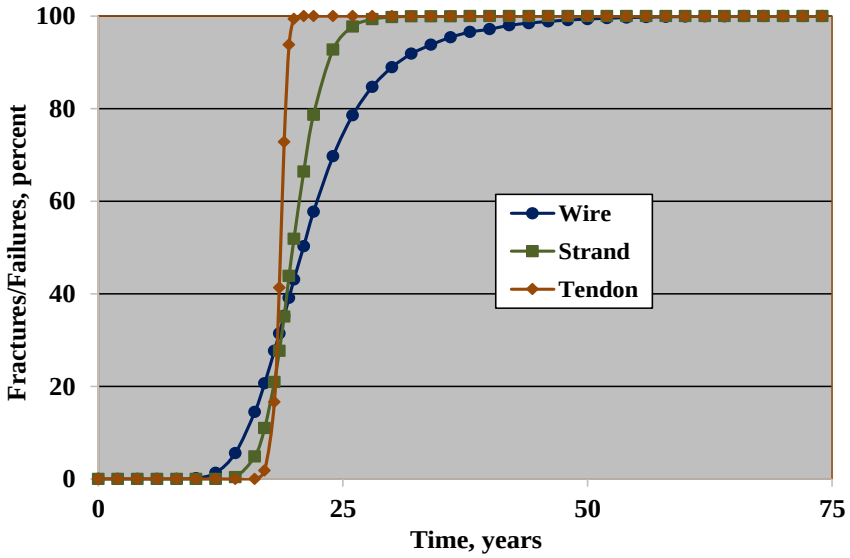

Source: FHWA.

Figure 43. Graph. Plot of the percentage of wire and strand fractures and tendon failures as a function of time for the case of sound grout with 0.80 wt% chloride and $\sigma(CRE)$ on corrosion rate equal to 0.30 $\mu(CRE)$.

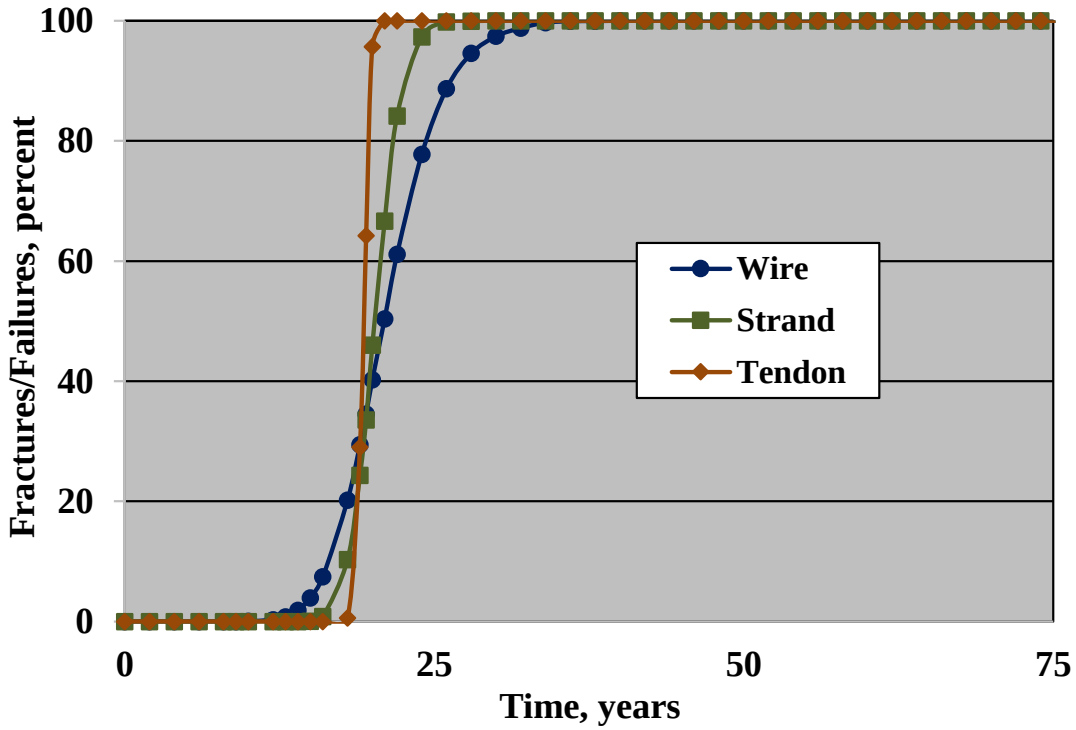

Source: FHWA.

Figure 44. Graph. Percentage of wire and strand fractures and tendon failures as a function of time for the case of sound grout with 0.80 wt% chloride and $\sigma(CRE)$ on corrosion rate equal to 0.15 $\mu(CRE)$.

Table 6. T_f and fracture/failure rates for Specimen Number 0.8%–F–S based on the measured mean corrosion rate (3.60 mpy (table 1)) and standard deviations on corrosion rate of 0.42, 0.30, and 0.15.

Standard Deviation on Corrosion Rate	Member	T_f (Year)	Number of Fractures or Failures/Year*	Percent of Fractures or Failures/Year*
$0.42 \cdot \mu$	Wire	6.3	1,363	6.4
$0.42 \cdot \mu$	Strand	12.7	476	13.4
$0.42 \cdot \mu$	Tendon	16.8	70	43.2
$0.30 \cdot \mu$	Wire	7.8	1,678	7.8
$0.30 \cdot \mu$	Strand	13.8	598	16.8
$0.30 \cdot \mu$	Tendon	16.9	102	63.0
$0.15 \cdot \mu$	Wire	9.2	2,167	10.1
$0.15 \cdot \mu$	Strand	15.0	884	24.8
$0.15 \cdot \mu$	Tendon	18.0	114	70.4

*Determined as slope of the curve near the inflection point.

Grout Void Specimens

Some single-strand specimens had a 2-inch-long air void at the top of the 12-inch test section. After approximately 129 d of exposure, a hole was drilled into the duct at the void elevation, and water was injected and outside air provided access. The general trend was that this resulted in a corrosion rate increase for some subsequent time, the magnitude of which increased with increasing chloride concentration for specimens with greater than 0.40 wt% chloride. Subsequent to the 178-d exposure, specimens were dissected and pit depth measurements made on three of these (Specimen Numbers 1.0%–V–S, 1.0%–V–US, and 2.0%–V–S), where V indicates presence of a grout void and US that the specimen was unstressed with results displayed in table 7. Figure 45 through figure 47 show corrosion rate versus time data for these three specimens, respectively, as reported in figures 126 and 127 of the phase 1 report, where corrosion rates are based on the entire 12-inch test specimen surface area and considering all seven wires. Red arrows designate periods of hot and humid exposure and blue ones freezing and drying. Conditions were ambient at other times. The results indicate that corrosion rate was highest during the hot and humid periods and lowest during the freezing and drying ones. Also, the corrosion rate increase that accompanied introduction of water and fresh air is also apparent, the magnitude of this being relatively small for 1.00 wt% chloride specimens but greater for 2.00 wt% chloride.

Table 7. Summary of pit depth measurement results for single-strand, grout-void specimens for which such determinations were made.

Specimen No.*	Count	Min Pit Depth (mil)	Max Pit Depth (mil)	Mean (μ) Pit Depth (mil)	Standard Deviation (σ)	Ratio (σ/μ)
1.0%–V–S	34	2	7	4.40	1.60	0.36
1.0%–V–US	26	2	12	5.94	3.11	0.52
2.0%–V–S	102	2	18	5.60	3.60	0.64

*Percentage = wt% chloride; V = grout void; S = stressed; US = unstressed.

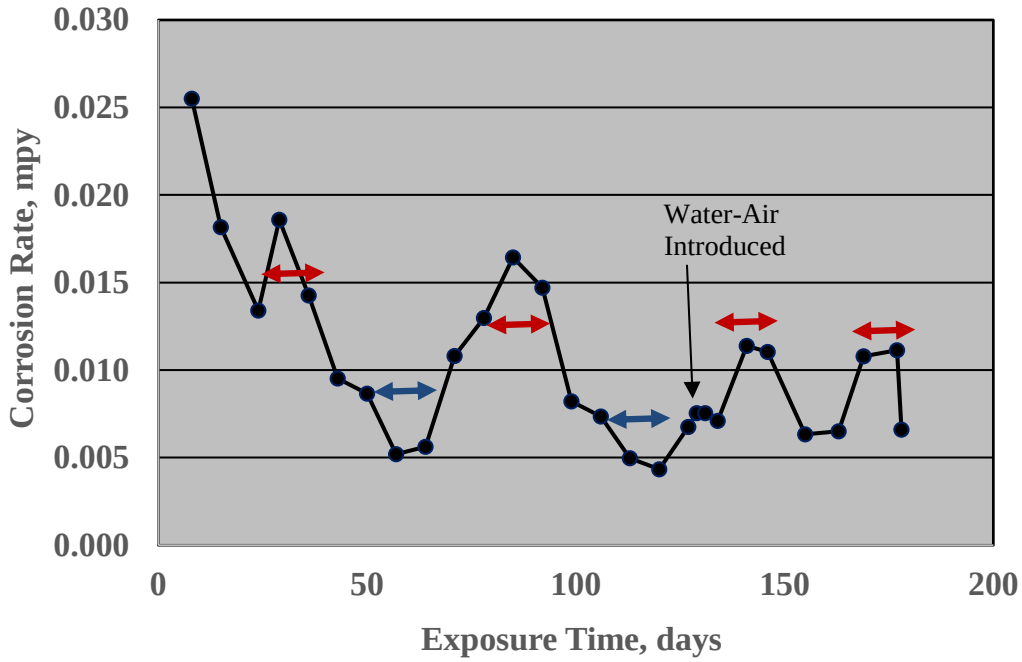

Source: FHWA.

Figure 45. Graph. Plot of corrosion rate versus time for Specimen Number 1.0%–V–S.

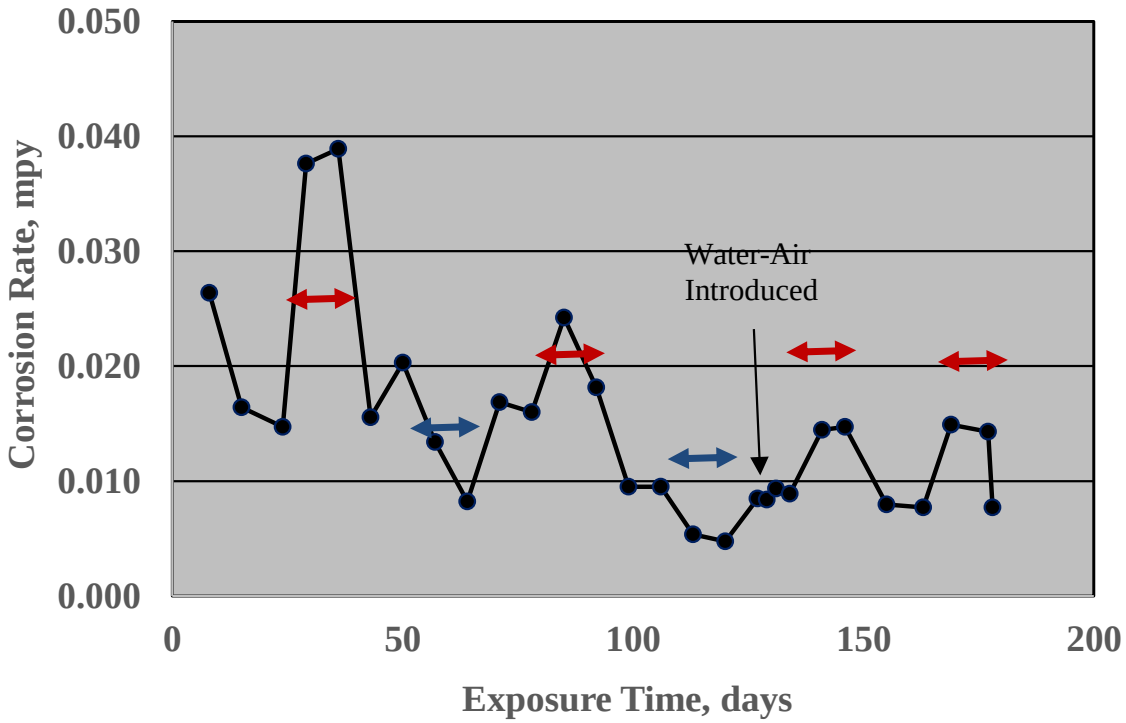

Source: FHWA.

Figure 46. Graph. Plot of corrosion rate versus time for Specimen Number 1.0%–V–US.

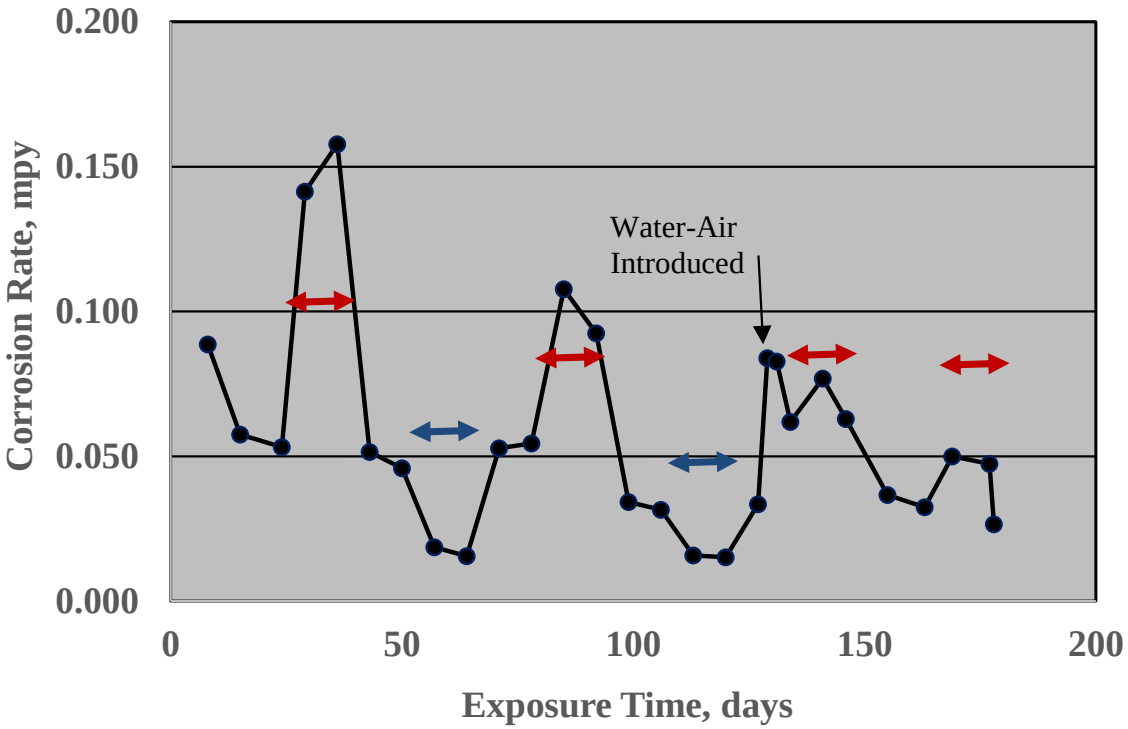

Source: FHWA.

Figure 47. Graph. Plot of corrosion rate versus time for Specimen Number 2.0%–V–S.

It is generally recognized that moisture or water at locations where steel penetrates a cementitious material, such as grout, establishes a corrosion cell with the bare steel at the interface serving as anode and the embedded steel as cathode. A small anode–large cathode area ratio can result and cause a high corrosion rate for the bare steel at such locations.[(20)] Based on the corrosion rate data subsequent to water and air introduction, little additional corrosion occurred for the two specimens with 1.00 wt% admixed chloride; however, the mean corrosion rate still exceeded that for the fully grouted specimens (table 4). Consistent with this, the deepest penetration (18 mils) for Specimen Number 1.0%–V–S occurred near the void/grout interface. (See figure 243 from the phase 1 report.)

The data in

indicate that mean pit depth was greater for Specimen Number 1.0%–V–US than for 2.0%–V–S. While this may have resulted because of the relatively small specimen size and scatter of the limited data, it is also possible that corrosion and associated anodic polarization of the Specimen Number 2.0%–V–S strand in the vicinity of the void/grout interface, as explained above, resulted in some cathodic polarization of the embedded metal. The finding that the greatest pit depths were recorded for this specimen and that at least some of these occurred at or near the void/grout interface is consistent with this. Such a projection is also supported by data from the phase 1 multistrand specimens, which indicate higher corrosion rate with 1.00 wt% chloride than for 2.00 wt% chloride, as discussed subsequently, apparently for the same reason given above.

Table 8 reports the results of pit depth measurements for the above three single-strand, void/grout specimens, as reported from the phase 1 study; and figure 48 and figure 49 show cumulative distribution function (CDF) plots of these data for Specimen Numbers 1.0%–V–US and 2.0%–V–S and reveal a sigmoidal trend between the two parameters, more so for the latter specimen. Specimen Number 1.0%–V–S is excluded because data are limited. However, while the sigmoidal trends are consistent with normality, the lack of symmetry, particularly in the case of Specimen Number 2.0%–V–S, suggests otherwise. However, it is likely that at least some of the deep pits occurred in the vicinity of the grout air void interface, as explained above, and if this was the case, then the distributions may be bimodal, at least for Specimen Numbers 1.0%–V–US and 2.0%–V–S. Figure 50 provides a probability density function (PDF) plot of these data for pit depths of 10 mils and less and shows that these conform to a relatively well-defined, bell-shaped curve. For a perfectly normal distribution, the mean and medium are identical, but in this case, these parameters are 4.75 and 4.00 mils, respectively. However, no data for pits of depth less than 2.0 mils were recorded because of the difficulty in making such measurements. It is projected that, if such data were available, then the mean and median would be closer. In addition, figure 51 shows a PDF plot for this same specimen for pit depths greater than or equal to 13 mils. These also exhibit a relatively well-defined, bell-shaped curve. There was some data manipulation in this case, however, as there were only four specific values but eight measurements. To increase the dataset without affecting the statistics, two pit depths of 13 mils were reassigned values of 12.5 and 13.5 mils. Likewise, three pit depths of 15 mils were reassigned as 14.5, 15.0, and 15.5 mils. In this case the mean and medium are 15.50 and 15.25 mils, respectively. Data for the two 1.0 wt% chloride specimens also exhibited well-defined bell-shaped curves. The mean and medium pit depths for Specimen Number 1.0%–V–US are 4.55 and 4.00 mils, respectively. That the value pairs are not closer probably resulted for the same reason given above for Specimen Number 2.0%–V–S. Based on these determinations, it was considered reasonable to treat the corrosion rate equivalent data as normally distributed.

Table 8. Pit depth data for single-strand specimens with a grout void.

Specimen No.	Wire No.	Pit Depth (mil)	Pit Depth (mil)	Pit Depth (mil)	Pit Depth (mil)	Pit Depth (mil)	Pit Depth (mil)	Pit Depth (mil)	Pit Depth (mil)	Pit Depth (mil)	Pit Depth (mil)	Pit Depth (mil)
1.0%–V–S	1	2	4	4	4	3	6	5	7	—	—	—
1.0%–V–US	1	3	5	10	5	4	11	12	6	3	—	—
1.0%–V–US	2	8	5	2	4	—	—	—	—	—	—	—
1.0%–V–US	3	7	2	8	7	11	5	5	4	3	2	12
1.0%–V–US	3	10	6	—	—	—	—	—	—	—	—	—
2.0%–V–S	1	3	3	8	3	7	2	5	2	4	4	7
2.0%–V–S	1	7	9	8	8	7	4	6	5	13	13	10
2.0%–V–S	1	2	5	3	17	18	7	2	4	4	4	5
2.0%–V–S	1	4	4	5	4	4	2	4	2	5	2	15

Specimen No.	Wire No.	Pit Depth (mil)	Pit Depth (mil)	Pit Depth (mil)	Pit Depth (mil)	Pit Depth (mil)	Pit Depth (mil)	Pit Depth (mil)	Pit Depth (mil)	Pit Depth (mil)	Pit Depth (mil)	Pit Depth (mil)
2.0%–V–S	2	3	4	4	5	10	7	6	3	6	5	2
2.0%–V–S	3	5	3	8	4	5	3	2	3	4	7	15
2.0%–V–S	3	15	18	8	8	5	4	4	2	—	—	—
2.0%–V–S	4	3	4	4	3	3	4	4	7	5	7	4
2.0%–V–S	5	3	3	5	5	2	2	9	4	5	5	6
2.0%–V–S	5	9	8	6	9	6	3	—	—	—	—	—

—No information available.

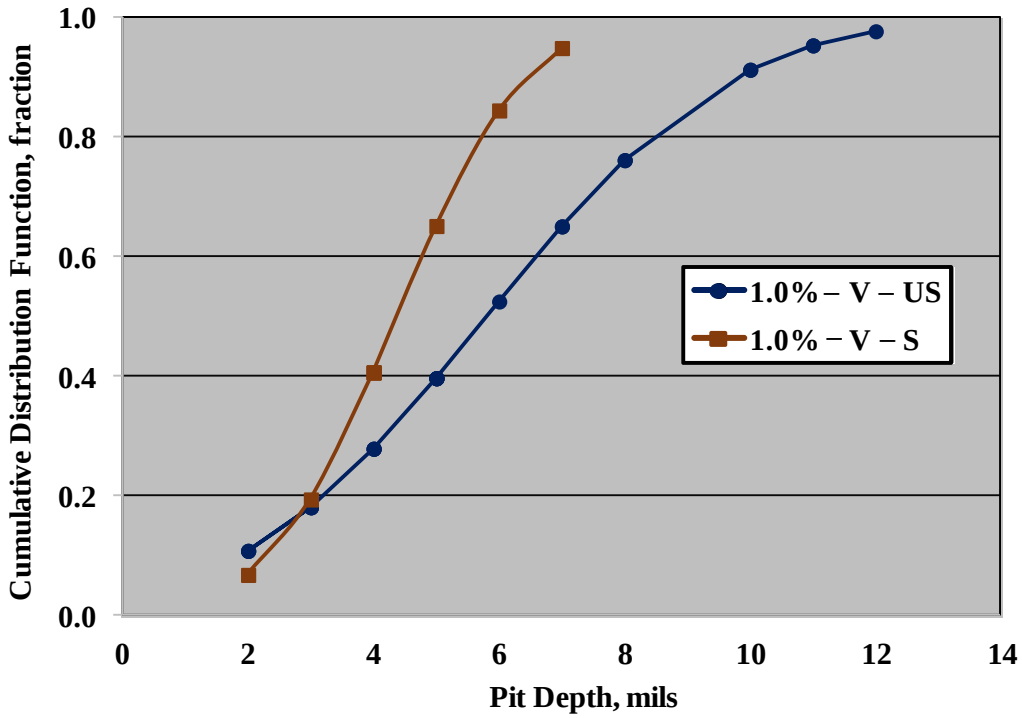

Source: FHWA.

Figure 48. Graph. Normal CDF plot of pit depth for Specimen Numbers 1.0%–V–US and 1.0%–V–S.

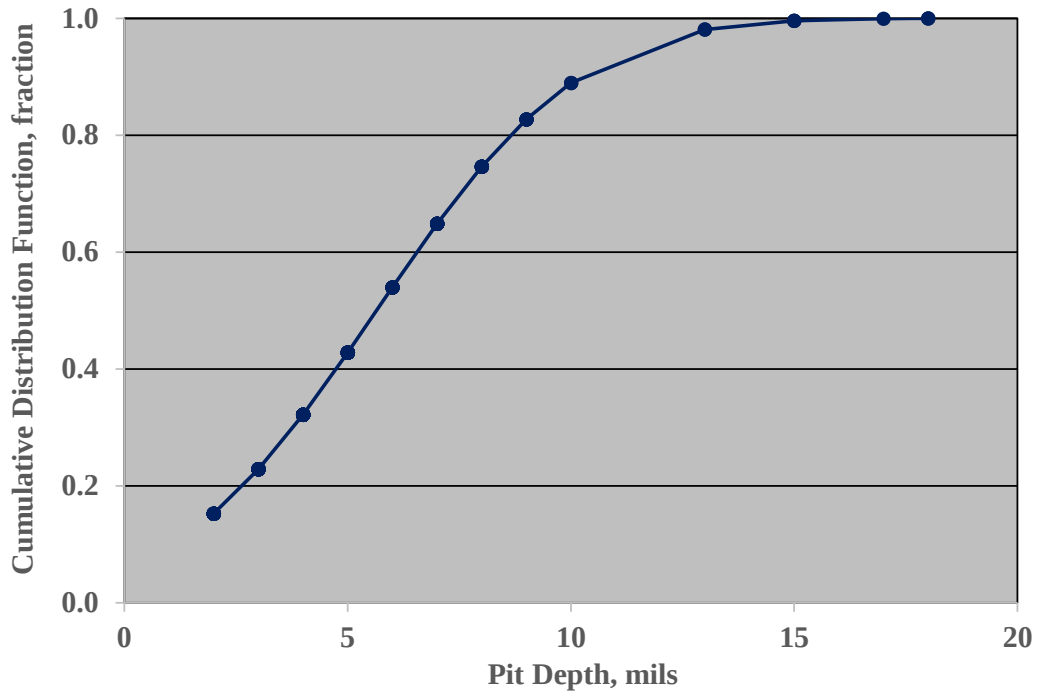

Source: FHWA.

Figure 49. Graph. Normal CDF plot of pit depths for Specimen 2.0%–V–S.

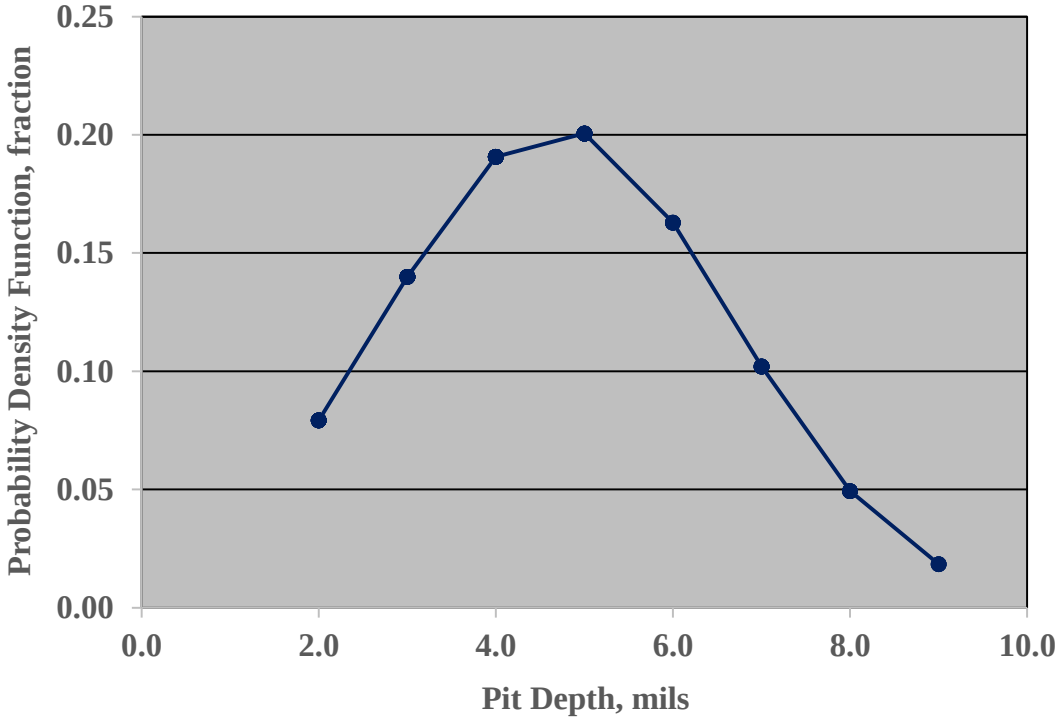

Source: FHWA.

Figure 50. Graph. Normal PDF plot of pit data for depths less than or equal to 9.0 mils for Specimen Number 2.0%–V–S.

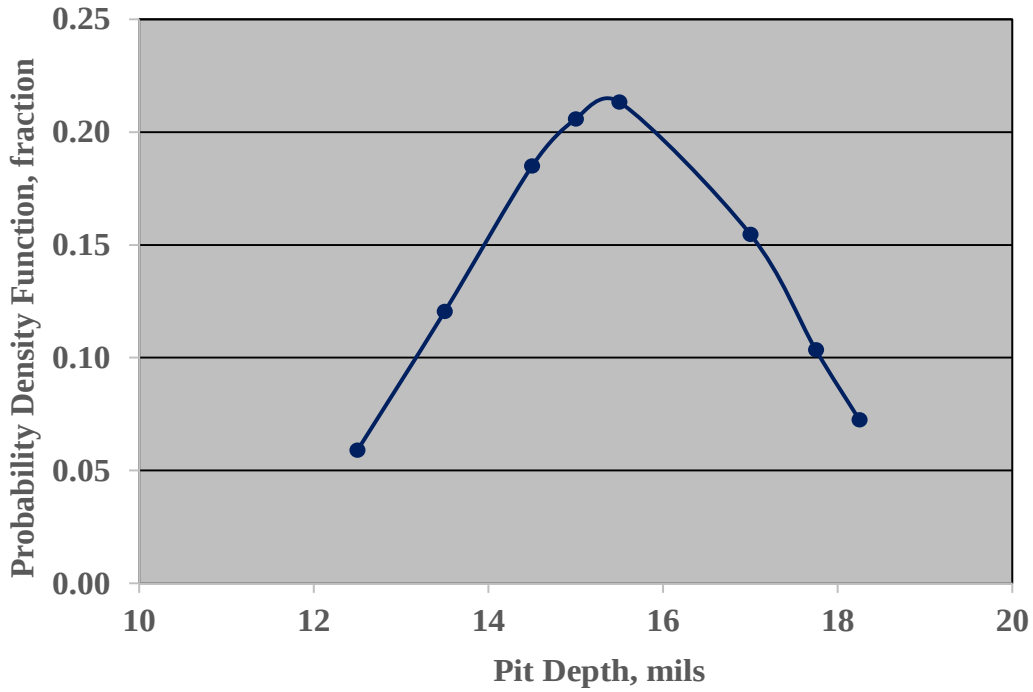

Source: FHWA.

Figure 51. Graph. Normal PDF plot of pit depth data for depths greater than 10 mils for Specimen Number 2.0%–V–S.

Figure 52 and figure 53 show analysis results for wire and strand fractures with time, respectively, and figure 54 does the same for tendon failures based on the σ and μ of pit depth for Specimen Number 1.0%–V–S. Likewise, figure 55 shows these trends superimposed on a common plot. Figure 56 presents superimposed results for Specimen Number 1.0%–V–US and figure 57 for Specimen Number 2.0%–V–S. The same general trends are apparent in all three cases, and these are similar to what was determined for the fully grouted specimens (figure 38 through figure 44). Table 9 summarizes these results in terms of T_f and fracture/failure rate near the inflection point for each of the three specimens. It is unclear whether or not differences in T_f and fracture/failure rate, where these occur, are other than data scatter.

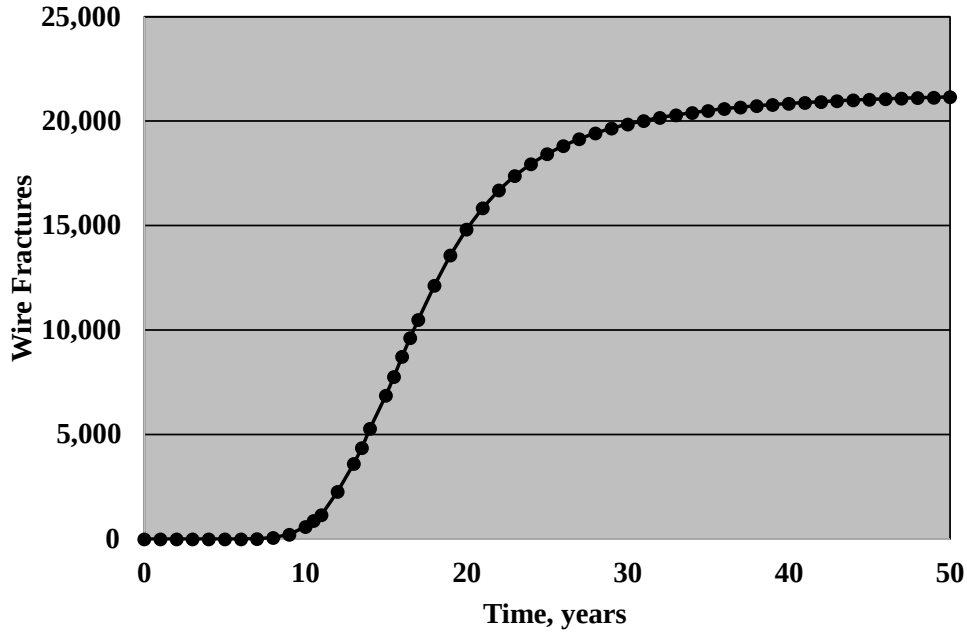

Source: FHWA.

Figure 52. Graph. Plot of the number of wire fractures as a function of time for Specimen Number 1.0%–V–S (grout with 1.0 wt% chloride and an air void).

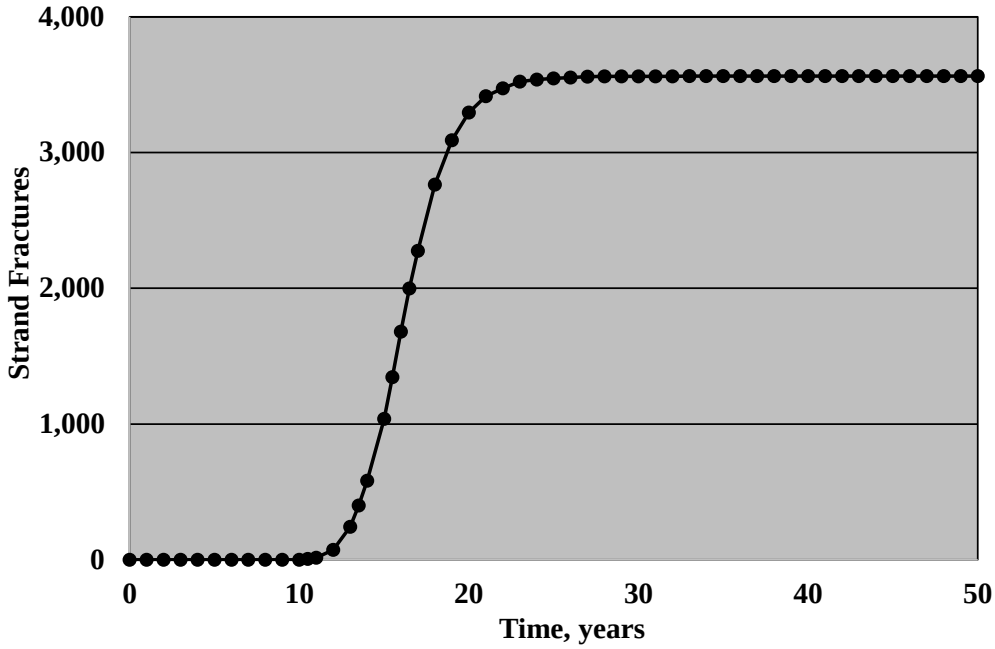

Source: FHWA.

Figure 53. Graph. Plot of the number of strand fractures as a function of time for Specimen Number 1.0%–V–S (grout with 1.0 wt% chloride and an air void).

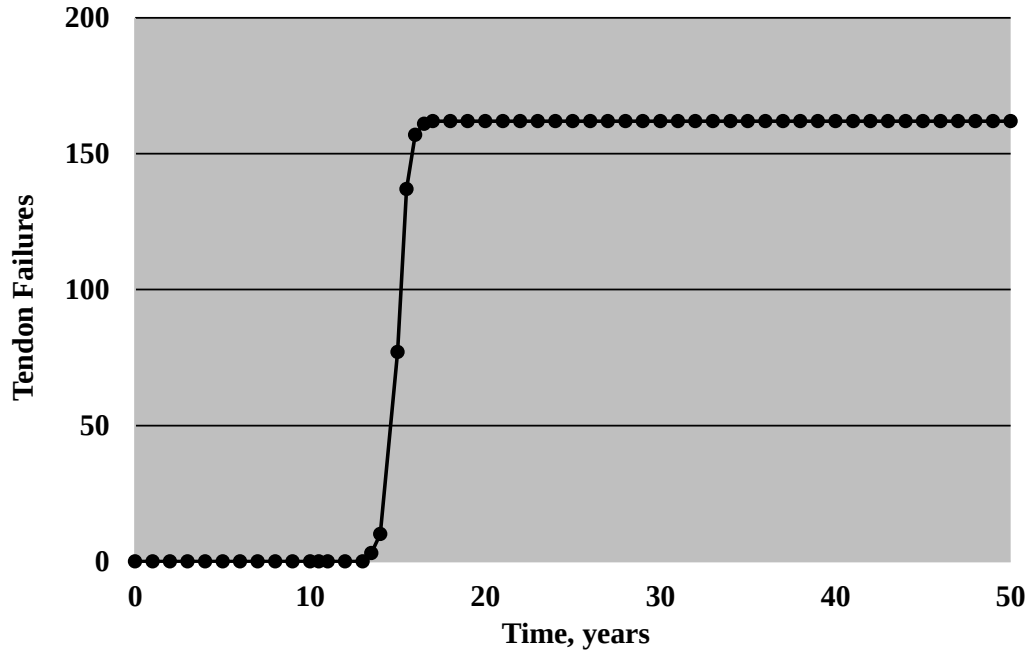

Source: FHWA.

Figure 54. Graph. Plot of the number of tendon failures as a function of time for Specimen Number 1.0%–V–S (grout with 1.0 wt% chloride and an air void).

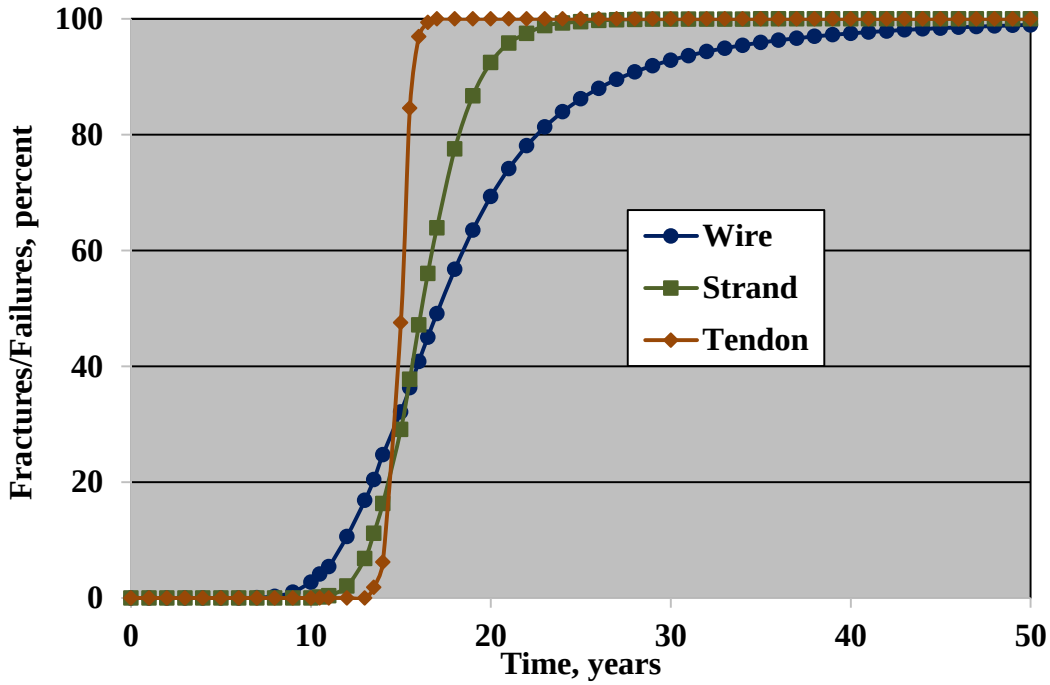

Source: FHWA.

Figure 55. Graph. Plot of the percentage of wire and strand fractures and tendon failures as a function of time based on phase 1 corrosion data for Specimen Number 1.0%–V–S (grout with 1.0 wt% chloride and an air void).[(1)]

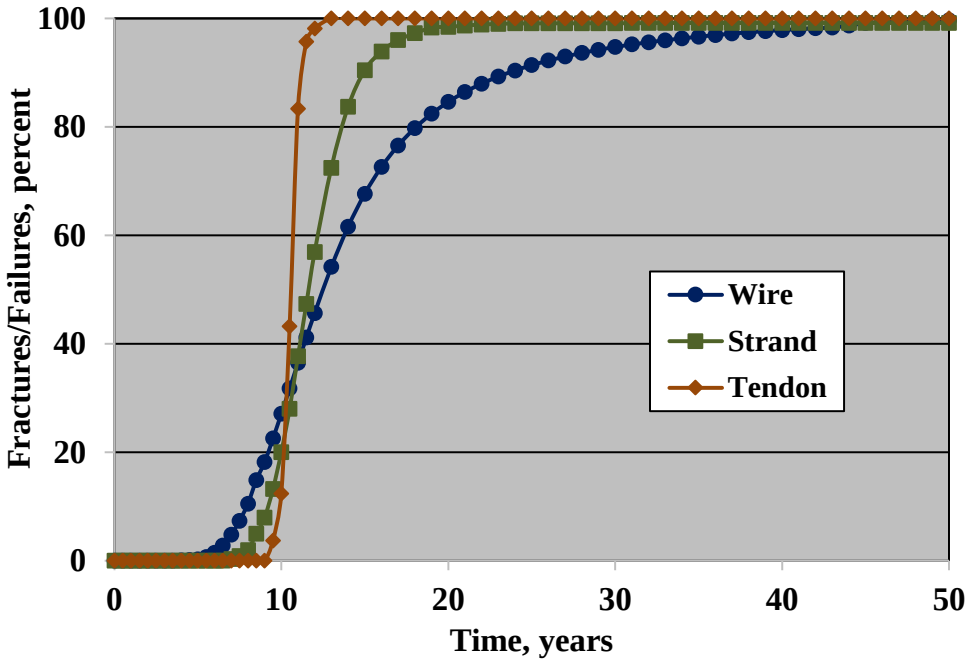

Source: FHWA.

Figure 56. Graph. Plot of the percentage of wire and strand fractures and tendon failures as a function of time based on phase 1 corrosion data for Specimen Number 1.0%–V–US (grout with 1.0 wt% chloride and an air void).[(1)]

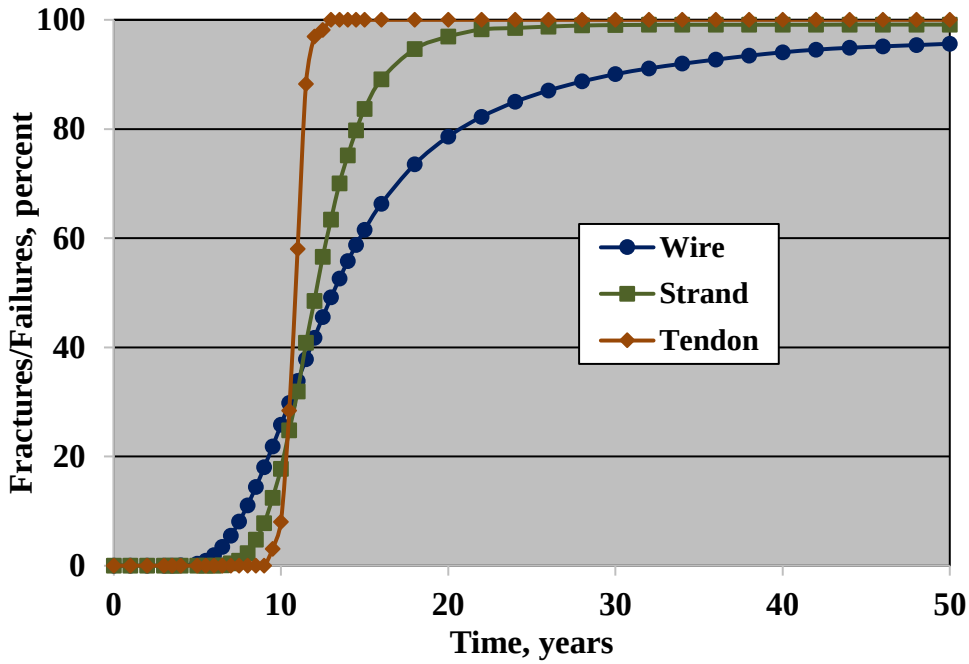

Source: FHWA.

Figure 57. Graph. Plot of the percentage of wire and strand fractures and tendon failures as a function of time based on phase 1 corrosion data for Specimen Number 2.0%–V–S (grout with 2.0 wt% chloride and an air void).[(1)]

Table 9. T_f and fracture/failure rate results for single-strand specimens with a grout void.

Specimen No.	Member	T_f (Year)	Number of Fractures or Failures/Year*	Percent of Fractures or Failures/Year*
1.0%–V–S	Wire	5.4	1,764	8.2
1.0%–V–S	Strand	10.1	670	18.8
1.0%–V–S	Tendon	13.4	120	74.1
1.0%–V–US	Wire	3.5	1,964	9.2
1.0%–V–US	Strand	6.7	685	19.2
1.0%–V–US	Tendon	9.3	130	80.2
2.0%–V–S	Wire	3.4	1,724	8.1
2.0%–V–S	Strand	6.5	590	16.6
2.0%–V–S	Tendon	9.2	96	59.3

*Determined as slope of the curve near the inflection point.

While results from the phase 1 study where water was introduced into the grout–air void of the single-strand specimens with 1.0 wt% chloride (Specimen Numbers 1%–V–S and 1%–V–US) indicate a relatively small corrosion rate increase, those for Specimen Number. 2.0%–V–S show an increase by a factor of about 2.5 (figure 45 through figure 47). Also, for the analysis reported in figure 51, mean pit depth was 15.50 mils with a standard deviation of 1.87, which translates to a corrosion rate of 31.8 mpy with standard deviation 3.8, considering the 178-d exposure period. Consequently, wire and strand fracture and tendon failure analyses were performed considering that these higher rates occurred near the grout-void interface for reasons discussed above. Figure 58 shows wire and strand fracture and tendon-failure progression with time based on the above higher mean corrosion rate and the corresponding standard deviation. Further, table 10 lists T_f and fracture/failure rate near the inflection point for these analyses (note the units change for the latter compared to the previous analyses). Clearly, the corrosion rate distribution analyzed here, which is considerably greater than for previous ones, results in much reduced T_f and higher fracture/failure rates. No situation was considered in which water was continually present at the void/grout interface, in which case T_f should be even less.

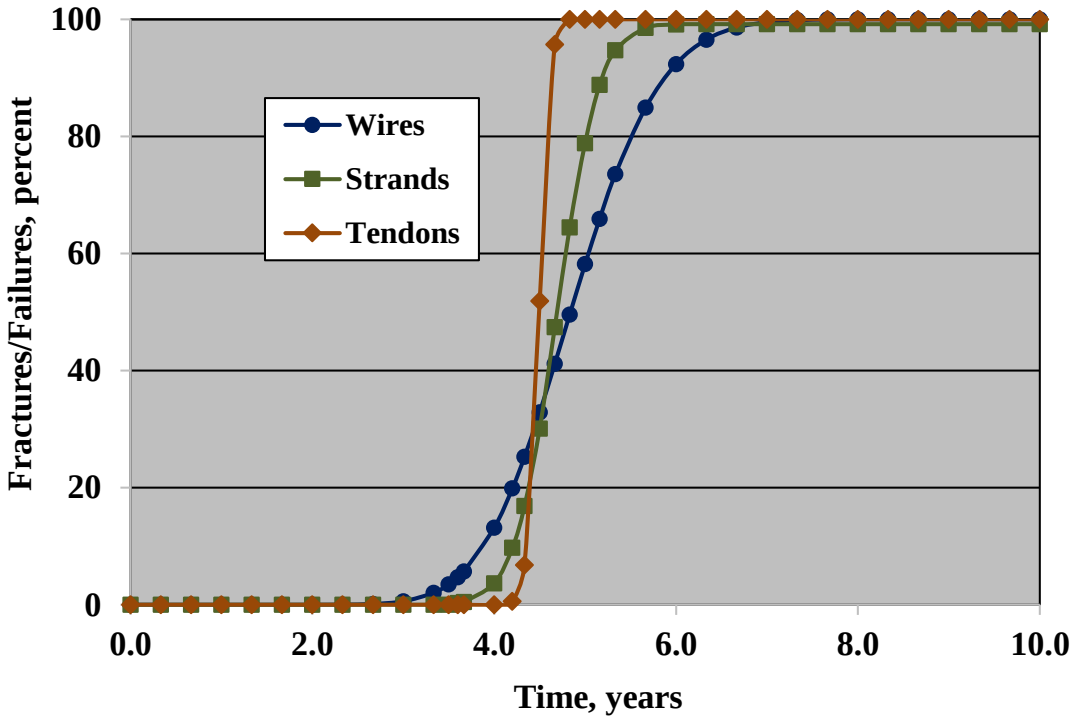

Source: FHWA.

Figure 58. Graph. Plot of the percentage of wire and strand fractures and tendon failures as a function of time for Specimen Number 2.0%–V–S (grout with 2.0 wt% chloride and an air void) assuming a mean corrosion rate of 15.50 mpy and standard deviation on corrosion rate of 1.87 mpy.

Table 10. T_f and fracture/failure rate results for Specimen Number 2.0%–V–S based on a mean corrosion rate of 15.50 mpy and standard deviation on corrosion rate of 1.87 mpy.

Specimen Number	Member	T_f (Year)	Number of Fractures or Failures/Year*	Percent of Fractures or Failures/Year*
2.0%–V–S	Wire	1.9	912	4.3
2.0%–V–S	Strand	3.5	309	8.7
2.0%–V–S	Tendon	4.2	37	22.5

*Determined as slope of the curve near the inflection point.

PHASE 1 TESTING: MULTISTRAND SPECIMENS

General

A total of eight tendons in this category were fabricated and tested (figure 8 and figure 9), and table 11 lists these according to designation and grout chloride concentration. Observations made on exposure termination, dissection, and analysis revealed the following:

- Corrosion of the stressed strands was greatest at or near the void/grout interface.

- Specimens with grout chloride concentrations 0, 0.40, and 2.00 wt% chloride exhibited a black deposit on the grout near the void/grout interface, an example of which is shown in figure 59, and exceptionally high corrosion losses occurred locally here. The deposits were determined to have a relatively high concentration of soluble sulfates, and the high corrosion rates at this location were attributed to this.

- For specimens that did not develop high-sulfate deposits, ones with less than 0.80 wt% chloride exhibited mostly localized rusting, and relatively little pit depth data were recorded for these.

Table 11. Listing of multistrand tendons and the admixed chloride concentration for each.

Tendon Designation	Chloride Concentration (wt%)
MS–0	0
MS–0.08	0.08
MS–0.2	0.2
MS–0.4	0.4
MS–0.6	0.6
MS–0.8	0.8
MS–1.0	1.0
MS–2.0	2.0

Source: FHWA.

Figure 59. Photo. Appearance of black deposits at the void/grout interface as shown by figure 213 from the phase 1 report.[(1)]

The tendons from the phase 1 study were dissected subsequent to the 178-d exposure, and strands were removed and sectioned into 12-inch lengths. Wires were then separated from strands, and corrosion products were removed. Pits depths were measured for a number of these wires and reported in cases where depth was 2 mils or greater. The focus of the present analyses was limited to the stressed strands since these passed through the void/grout interface, whereas the unstressed ones were fully embedded and experienced more modest attack. Corrosion was generally greatest at or near the grout-void interface, presumably for the reasons discussed above. Consequently, the present analyses used pit depth data from the uppermost 12-inch length of the two bottom strands of each tendon and from the second such length for the two top strands of each tendon since the void/grout interface occurred along these. It was assumed that the deepest pit on each of these wire lengths would lead to fracture of that wire on continued exposure and eventually of the strand when a third wire fractured. Thus, while analyses of single-strand specimens were necessarily based on the mean and standard deviation of all measured pit depths, those for multistrand specimens used the distribution of maximum pit depth per wire in the air-void region, since depths were greatest here and, hence, this is where fracture would be expected to occur. Analyses projecting wire and strand fracture and tendon failure progression were grouped according to whether or not the above-referenced black deposit was present.

Specimens Without Black, High-Sulfate Deposits

Analyses, as reported above for single-strand specimens, were also performed for multistrand (MS) ones with 0.80 and 1.00 wt% chloride (Specimen Numbers MS–0.8 and MS–1.0). Table 12 lists the maximum pit depth on each of the six outer wires of the top left strand for the former specimen. Here, the mean is 10.7 mils with standard deviation 4.41. Since the exposure was for 178 d, these translate to a mean corrosion rate of 21.4 mpy with standard deviation 8.8. Figure 60 shows fracture/failure analysis results for Specimen Number MS–0.8 as a plot of the percent of wire and strand fractures and tendon failures versus time, and table 13 lists T_f and failure rate near the inflection point for each.

Table 12. Maximum pit depths for each outer wire of top left strand from Specimen Number MS–0.8.

Maximum Pit Depth (mil)
19
9
7
8
9
12

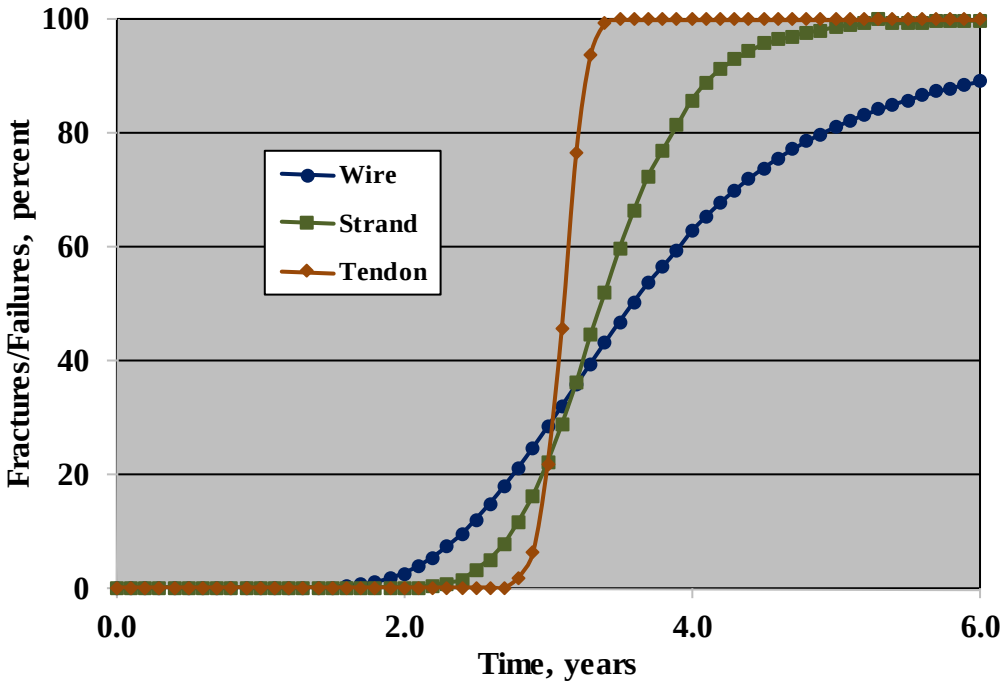

Source: FHWA.

Figure 60. Graph. Plot of the percentage of wire and strand fractures and tendon failures as a function of time based on phase 1 multistrand pit depth distribution data for Specimen Number MS–0.8 (0.80 wt% admixed chloride).[(1)]

Table 13. T_f and fracture/failures rates for Specimen Number MS–0.8 (0.80 wt% chloride).

Mean Corrosion Rate, mpy	Standard Deviation on Corrosion Rate	Component	T_f (Year)	Number of Fractures or Failures/Month*	Percent of Fractures or Failures/Month*
21.3	8.8	Wire	1.1	673	3.1
21.3	8.8	Strand	2.0	278	7.2
21.3	8.8	Tendon	2.7	31	19.0

*Determined as slope of the curve near the inflection point.

Analyses for Specimen MS–1.0 (1.00 wt% admixed chloride), on the other hand, used maximum pit depth for each outer wire of the top left and top right strands as listed in table 14. Data for these strands were the most extensive and included measurements on all six outer wires. No distinction is made between the two strands because the mean for both was essentially the same. Figure 61 plots the percentage of wire and strand fractures and tendon failures as a function of time for this tendon, and table 15 lists T_f and fracture/failure rates near the inflection point. Comparison of these results with those in table 13 (Specimen MS–0.80) indicates T_f to be slightly less and fracture/failure rates greater for the tendon with higher grout chloride concentration. An initial tendon failure is projected to occur for Specimen MS–0.80 in less than 3 yr and for Specimen MS–1.00 after a little more than 1 yr.

Table 14. Maximum pit depths for each outer wire of top left and top right strands for Specimen Number MS–1.0.

Strand Top Right Maximum Pit Depth (mil)	Strand Top Left Maximum Pit Depth (mil)
11	25
16	12
13	12
11	9
12	8
10	10

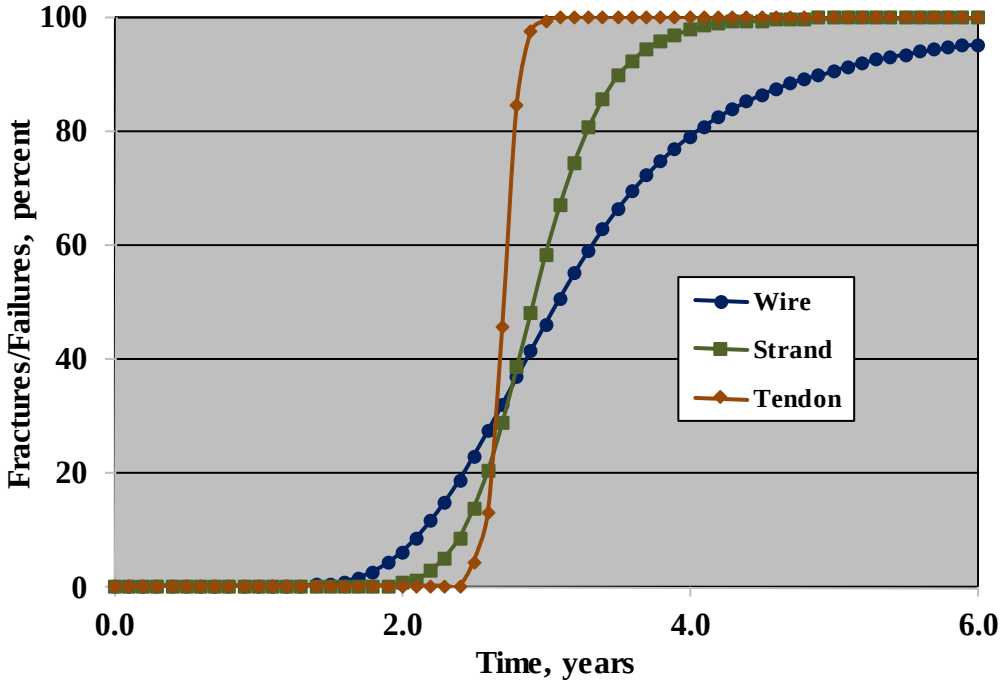

Source: FHWA.

Figure 61. Graph. Plot of the percentage of wire and strand fractures and tendon failures as a function of time based on phase 1 multistrand Specimen Number MS–1.0 (mean corrosion rate 24.8 mpy and standard deviation 8.9).[(1)]

Table 15. T_f and fracture/failures rates for Specimen Number MS–1.0 (1.0 wt% chloride).

Mean Corrosion Rate, mpy	Standard Deviation on Corrosion Rate	Component	T_f (Year)	Number of Fractures or Failures/Month*	Percent of Fractures or Failures/Month*
24.8	8.9	Wire	1.0	858	4.0
24.8	8.9	Strand	1.8	292	8.2
24.8	8.9	Tendon	2.4	45	27.8

*Determined as slope of the curve near the inflection point.

Specimens with Black, High-Sulfate Deposits

As noted above, specimens in this category were ones with 0, 0.40, and 2.00 wt% chloride. Because of the severity of the attack on strands of these tendons, analyses were performed in each of the three cases. Table 16 lists the maximum pit depth that was measured for each outer wire from the uppermost 12-inch length of the bottom right and bottom left strands from Specimen Number MS–0.0 (0.0 wt% chloride), and figure 62 shows the analysis results. Likewise, table 17 lists T_f and fracture/failure rate near the inflection point.

Table 16. Maximum pit depths for each outer wire of two strands from Specimen Number MS–0.0 (data were reported for only five wires in the case of the bottom left strand).

Bottom Right Strand Maximum Pit Depth (mil)	Bottom Left Strand Maximum Pit Depth (mil)
19	32
32	23
14	27
16	27
36	22
30	—

—No information available.

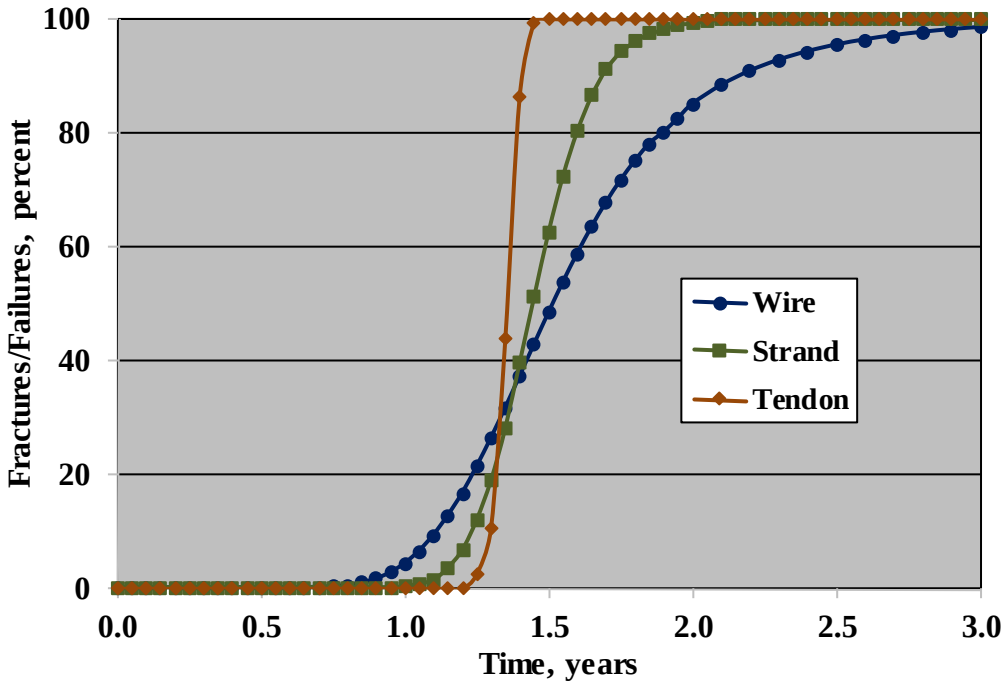

Source: FHWA.

Figure 62. Graph. Plot of the percentage of wire and strand fractures and tendon failures as a function of time for phase 1 multistrand Specimen Number MS–0.0 (mean corrosion rate 50.6 mpy and standard deviation 14.2).(1)

Table 17. T_f and fracture/failures rates for Specimen Number MS–0.0 (0.0 wt% chloride).

Mean Corrosion Rate, mpy	Standard Deviation on Corrosion Rate	Component	T_f (Year)	Number of Fractures or Failures/Month*	Percent of Fractures or Failures/Month*
50.6	14.2	Wire	0.52	2,013	9.4
50.6	14.2	Strand	0.95	715	20.1
50.6	14.2	Tendon	1.24	102	62.8

*Determined as slope of the curve near the inflection point.

Table 18 lists maximum pit depth for each wire along the uppermost 12-inch length of the bottom left strand from Specimen Number MS–0.4, whereas table 19 does this for the same strand of Specimen Number MS–2.0. Mean corrosion rate and standard deviation for the former are 74.3 mpy and 28.3, respectively and, for the latter, are 42.7 mpy and 15.1, respectively. There were extensive pit depth measurements in each of these two cases. Projected fracture/failure results for the former specimen are presented in figure 63 and summarized in table 20, and those for Specimen Number MS–2.0 are shown in figure 64 and table 21. Note that the corrosion rate was more severe for the specimen with lesser chloride, suggesting that the nature and aggressiveness of the sulfate-rich deposit was controlling.

Table 18. Maximum pit depths for the bottom left strand of Specimen Number MS–0.4 with black deposit.

Maximum Pit Depth (mil)
52
19
39
50
42
21

Table 19. Maximum pit depths for the bottom left strand of Specimen Number MS–2.0 with black deposit.

Maximum Pit Depth (mil)
25
33
11
23
17
19

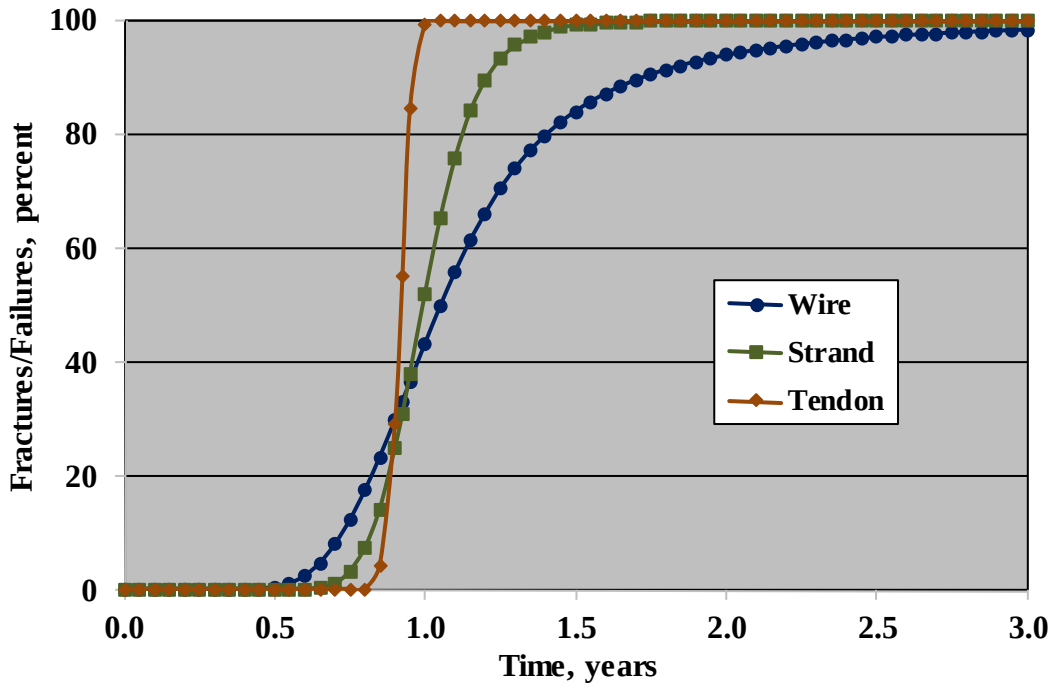

Source: FHWA.

Figure 63. Graph. Plot of the percentage of wire and strand fractures and tendon failures as a function of time based on measurements made on phase 1 multistrand Specimen Number MS–0.4 (0.4 wt% admixed chloride).[(1)]

Table 20. T_f and fracture/failures rates for Specimen Number MS–0.4 (0.40 wt% chloride).

Mean Corrosion Rate, mpy	Standard Deviation on Corrosion Rate	Component	T_f (Year)	Number of Fractures or Failures/Month*	Percent of Fractures or Failures/Month*
74.3	28.3	Wire	0.33	2,473	11.6
74.3	28.3	Strand	0.60	877	24.6
74.3	28.3	Tendon	0.80	130	80.2

*Determined as slope of the curve near the inflection point.

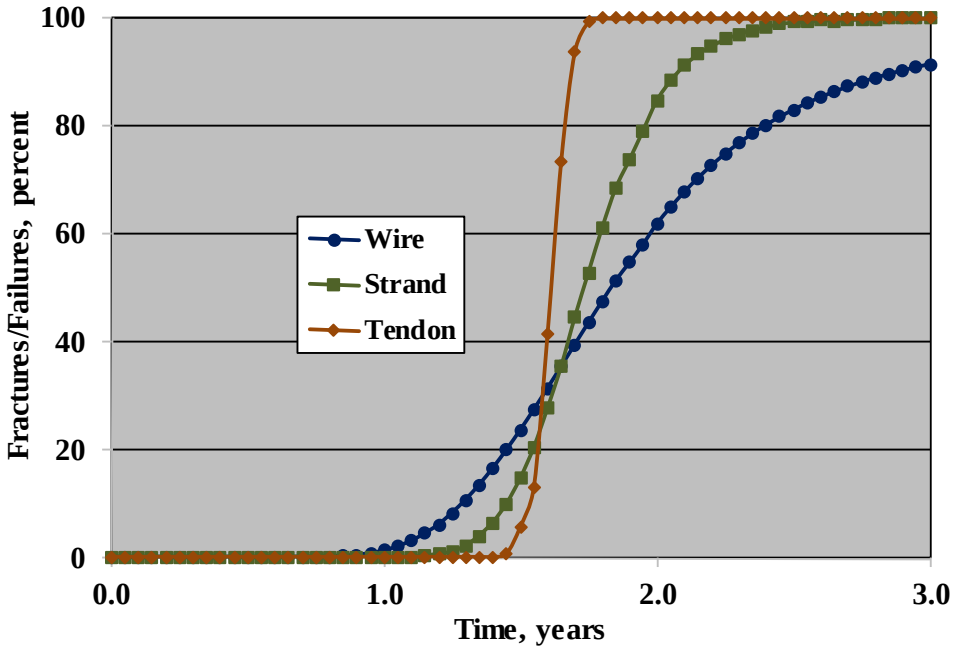

Source: FHWA.

Figure 64. Graph. Plot of the percentage of wire and strand fractures and tendon failures as a function of time based on phase 1 multistrand Specimen Number MS–2.0 (2.00 wt% admixed chloride). (1)

Table 21. T_f and fracture/failures rates for Specimen Number MS–2.0 (2.00 wt% chloride).

Mean Corrosion Rate, mpy	Standard Deviation on Corrosion Rate	Component	T_f (Year)	Number of Fractures or Failures/Month*	Percent of Fractures or Failures/Month*
42.7	15.1	Wire	0.58	1,457	6.8
42.7	15.1	Strand	1.05	517	14.5
42.7	15.1	Tendon	1.39	72	44.2

*Determined as slope of the curve near the inflection point.

Comparison of Single- and Multistrand Analysis Projections

Figure 65 through figure 67 graphically summarize the T_f results presented above for wires, strands, and tendons, respectively. These indicate, in all cases, as above, that T_f is greatest for tendons and least for wires with T_f for strands being between the two. Also, T_f is less for multistrand specimens compared to single-strand specimens (figure 55 through figure 58 compared to figure 60 through figure 64, and table 9 and table 10 compared to table 13, table 15, table 17, table 20, and table 21); fully grouted specimens exhibited the highest T_f (figure 41 through figure 44 and table 5 and table 6). However, with the higher mean corrosion rates that are projected to occur near the void/grout interface of single-strand specimens (figure 55 through figure 58 and table 9 and table 10), T_f was reduced to near that for the multistrand tendon specimens as also shown in figure 65 through figure 67. These results indicate that single-strand specimens, as configured in the phase 1 study, do not experience the same extent of corrosion-induced deterioration as multistrand ones; only the latter are likely to reflect service performance unless a correction factor is developed and employed.

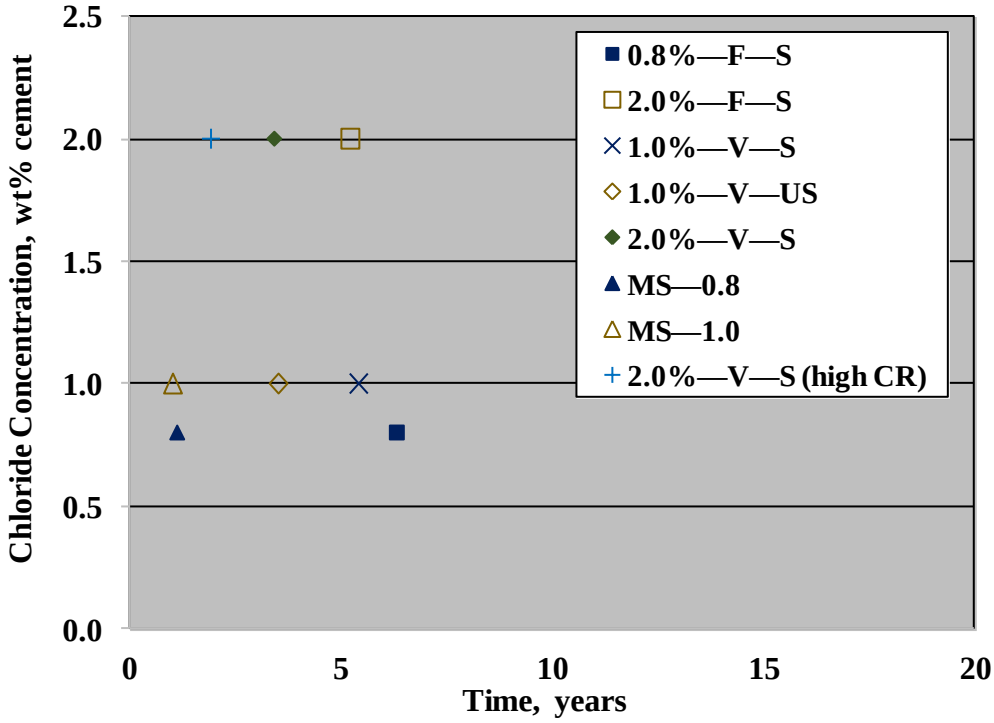

Source: FHWA.

Figure 65. Graph. Plot of the projected T_f for wires of single- and multistrand specimens with 0.8, 1.0, and 2.0 wt% chloride as a function of grout chloride concentration.

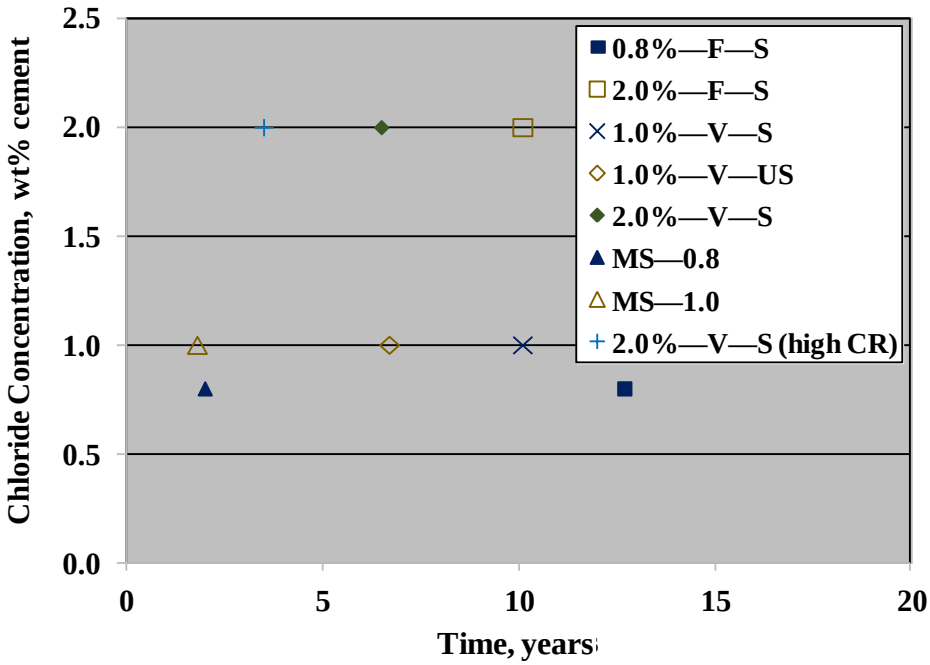

Source: FHWA.

Figure 66. Graph. Plot of the projected Tf for strands of single- and multistrand specimens with different grout chloride concentrations.

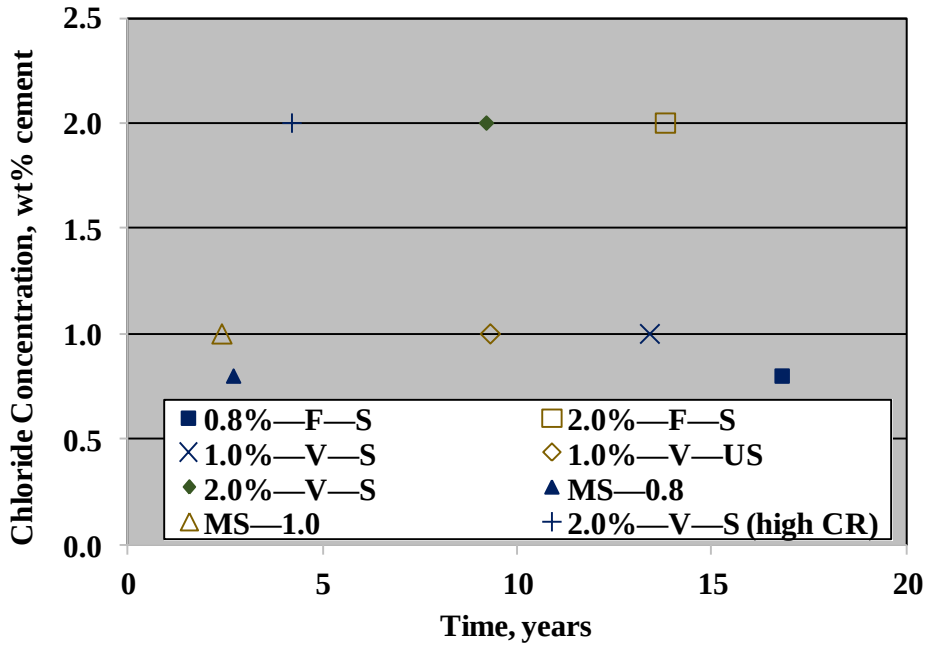

Source: FHWA.

Figure 67. Graph. Plot of the projected T_f for tendons of single- and multistrand specimens with different grout chloride concentrations.

SYSTEMATIC ANALYSIS

Approach and Results

In view of the above results, a more systematic set of analyses was performed that employed incremental mean corrosion rates as listed in table 22 and standard deviation 0.30 of the mean. The latter parameter approximates what occurred for the phase 1 tendon multistrand specimens (table 13, table 15, table 17, table 20, and table 21), where the ratio of standard deviation-to-mean corrosion rate is in the range of 0.28 to 0.41. This may better facilitate failure projection for actual in-place tendons given grout condition (extent of physical or chemical deficiency (or both)) and an understanding of how this affects corrosion rate, as illustrated in detail in chapter 5. Figure 68 through figure 81 then show plots of fracture/failure progression with time for wires, strands, and tendons that experience these mean corrosion rates and the above standard deviation, and table 23 through table 26 list the corresponding T_f and fracture/failure rate for each case. The general trend is that the onset of fractures/failures shifts to shorter time with increasing mean corrosion rate.

Table 22. Mean corrosion rates employed for systematic analyses.

Mean Corrosion Rate, (mpy)
1.0
2.0
3.0
4.0
5.0
7.5
10.0
15.0
20.0
30.0
40.0
50.0
60.0
80.0

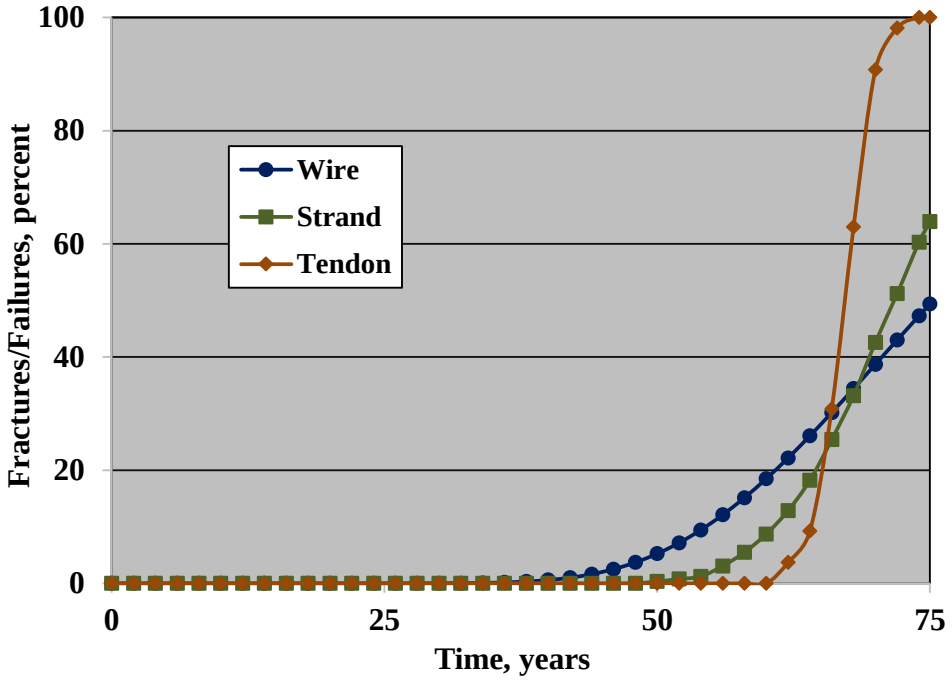

Source: FHWA.

Figure 68. Graph. Plot of the percentage of wire and strand fractures and tendon failures as a function of time based on a mean wire corrosion rate of 1.0 mpy and standard deviation 0.3 of the mean.

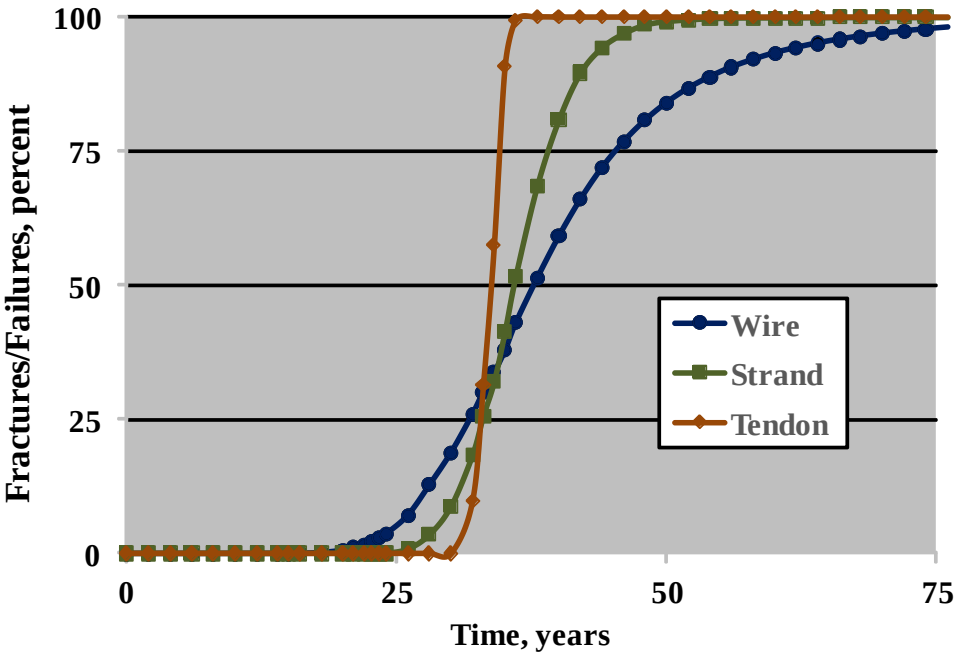

Source: FHWA.

Figure 69. Graph. Plot of the percentage of wire and strand fractures and tendon failures as a function of time based on a mean wire corrosion rate of 2.0 mpy and standard deviation 0.3 of the mean.

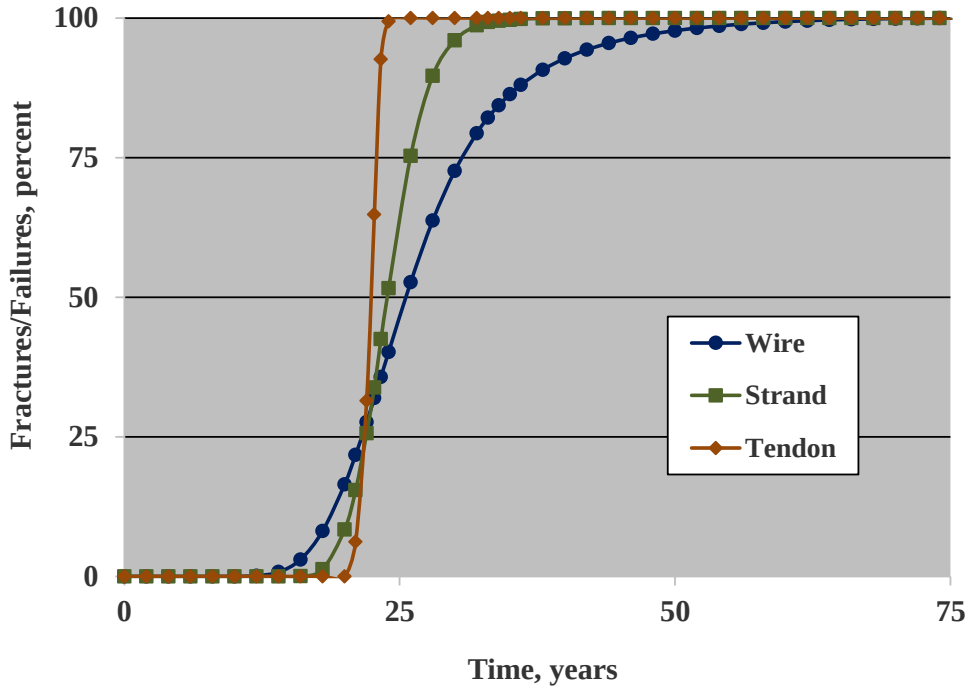

Source: FHWA.

Figure 70. Graph. Plot of the percentage of wire and strand fractures and tendon failures as a function of time based on a mean wire corrosion rate of 3.0 mpy and standard deviation 0.3 of the mean.

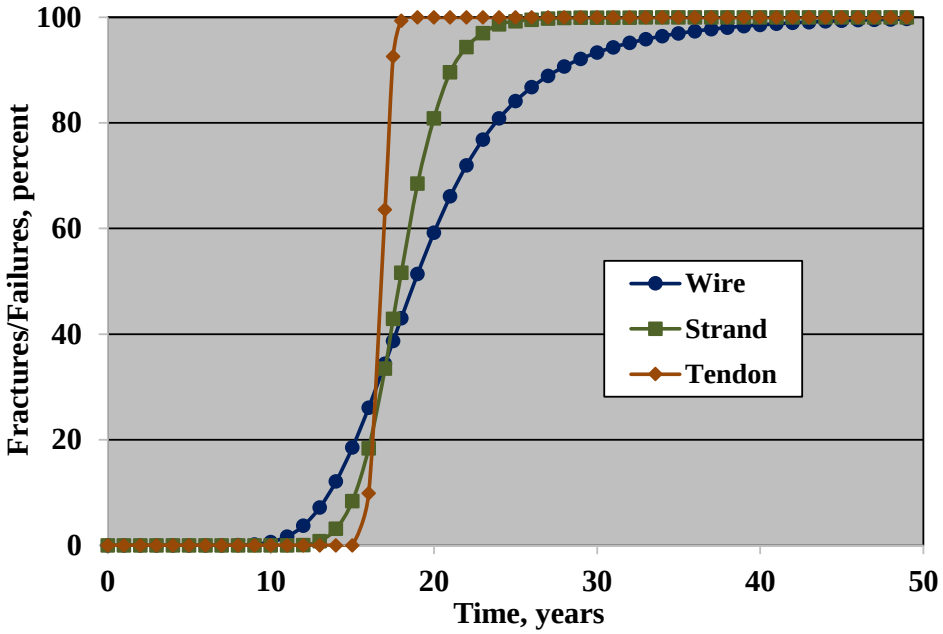

Source: FHWA.

Figure 71. Graph. Plot of the percentage of wire and strand fractures and tendon failures as a function of time based on a mean wire corrosion rate of 4.0 mpy and standard deviation 0.3 of the mean.

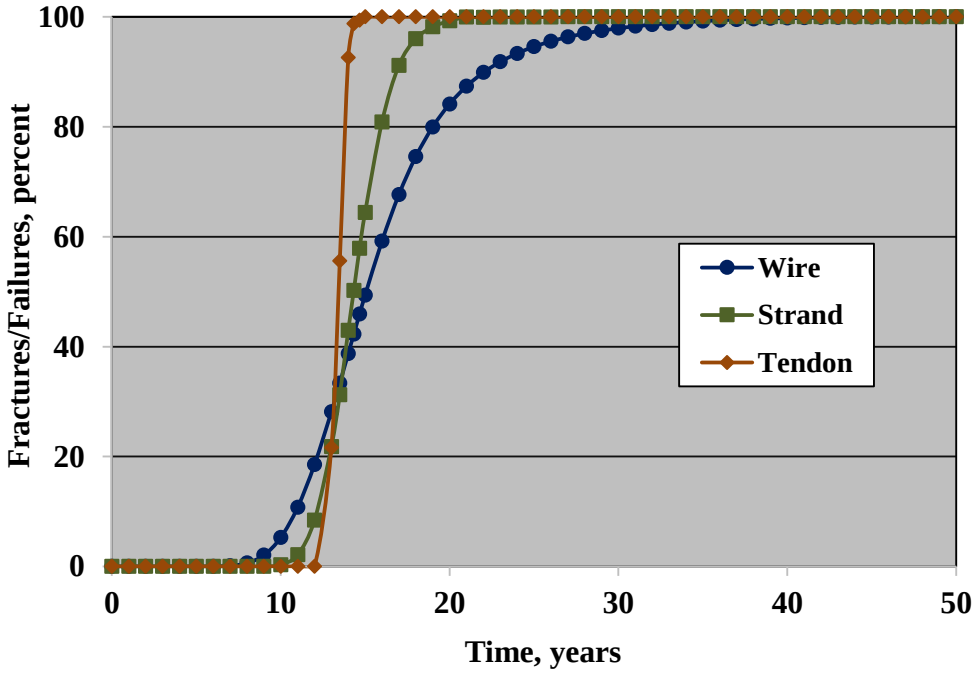

Source: FHWA.

Figure 72. Graph. Plot of the percentage of wire and strand fractures and tendon failures as a function of time based on a mean wire corrosion rate of 5.0 mpy and standard deviation 0.3 of the mean.

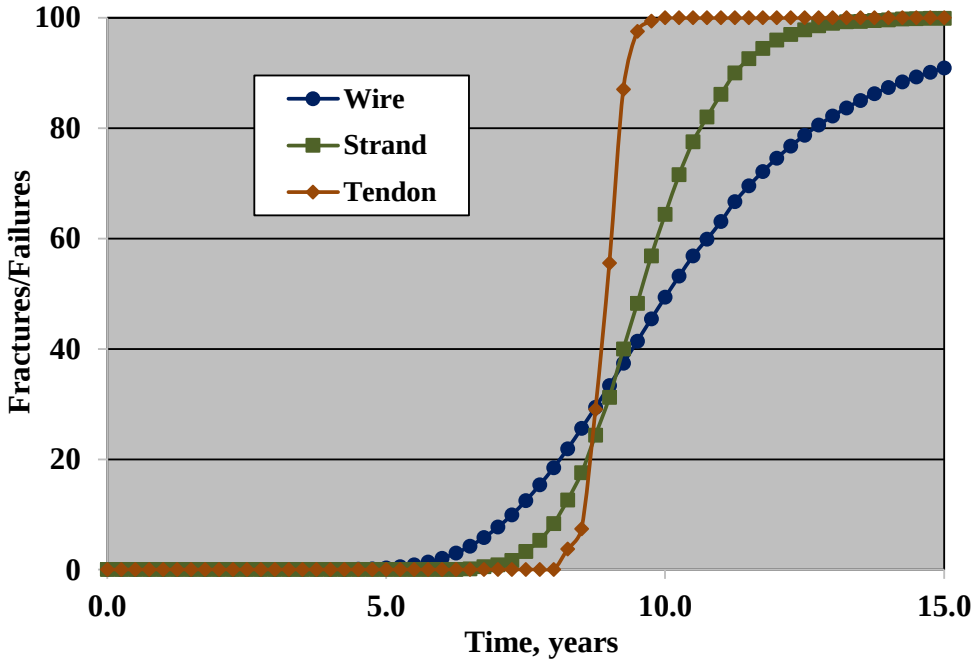

Source: FHWA.

Figure 73. Graph. Plot of the percentage of wire and strand fractures and tendon failures as a function of time based on a mean wire corrosion rate of 7.5 mpy and standard deviation 0.3 of the mean.

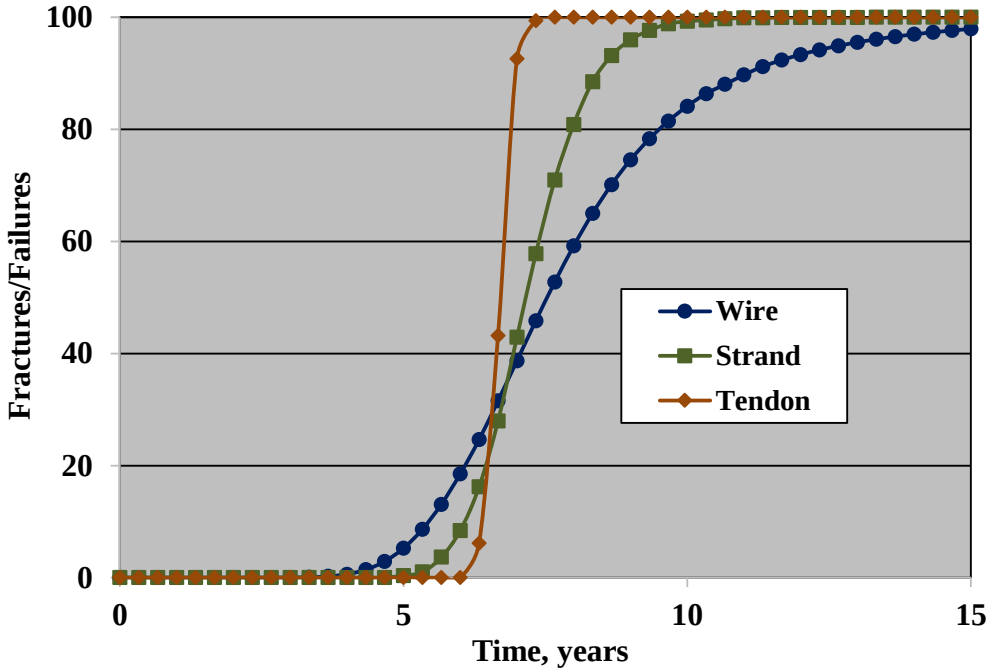

Source: FHWA.

Figure 74. Graph. Plot of the percentage of wire and strand fractures and tendon failures as a function of time based on a mean wire corrosion rate of 10.0 mpy and standard deviation 0.3 of the mean.

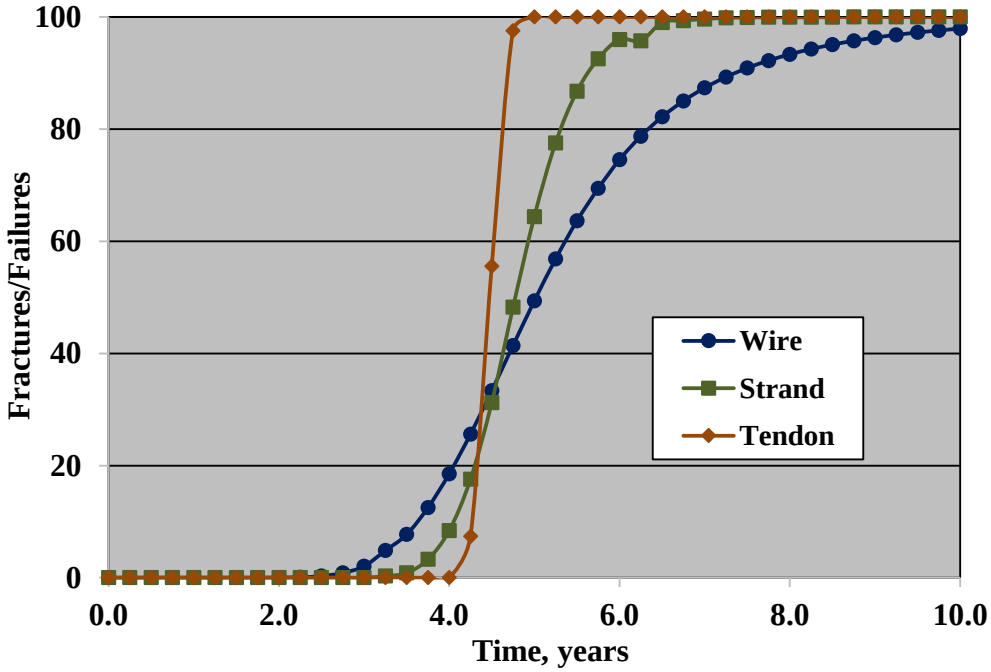

Source: FHWA.

Figure 75. Graph. Plot of the percentage of wire and strand fractures and tendon failures as a function of time based on a mean wire corrosion rate of 15.0 mpy and standard deviation 0.3 of the mean.

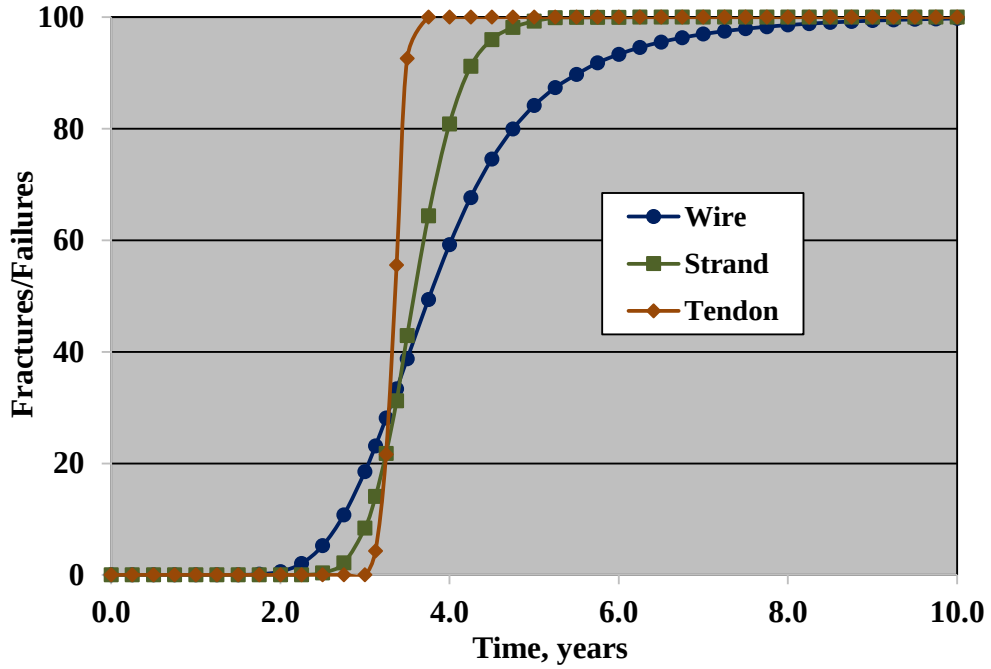

Source: FHWA.

Figure 76. Graph. Plot of the percentage of wire and strand fractures and tendon failures as a function of time based on a mean wire corrosion rate of 20.0 mpy and standard deviation 0.3 of the mean.

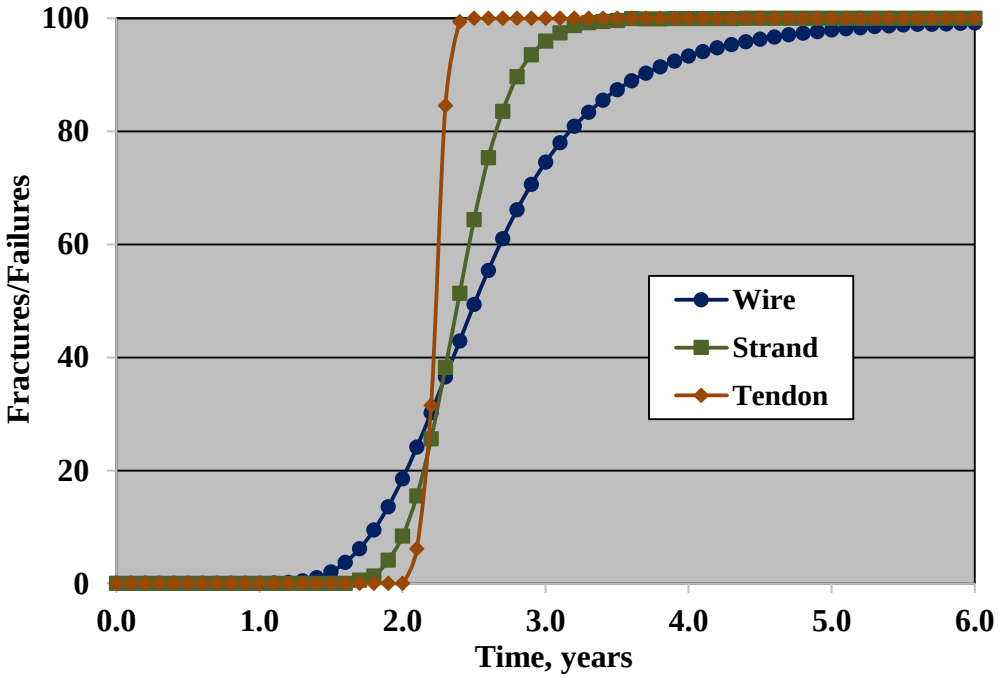

Source: FHWA.

Figure 77. Graph. Plot of the percentage of wire and strand fractures and tendon failures as a function of time based on a mean wire corrosion rate of 30.0 mpy and standard deviation 0.3 of the mean.

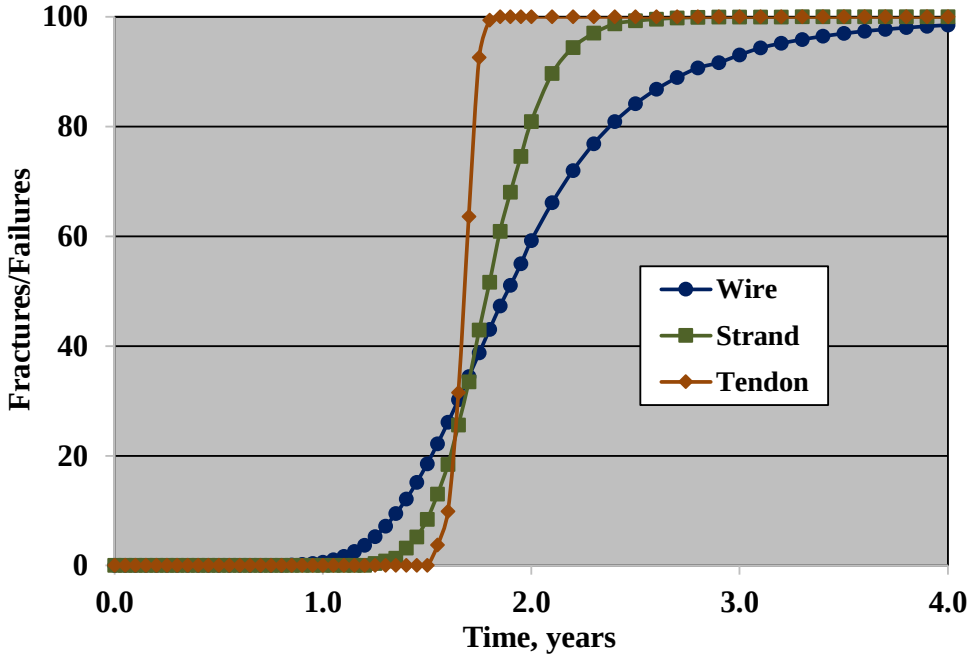

Source: FHWA.

Figure 78. Graph. Plot of the percentage of wire and strand fractures and tendon failures as a function of time based on a mean wire corrosion rate of 40.0 mpy and standard deviation 0.3 of the mean.

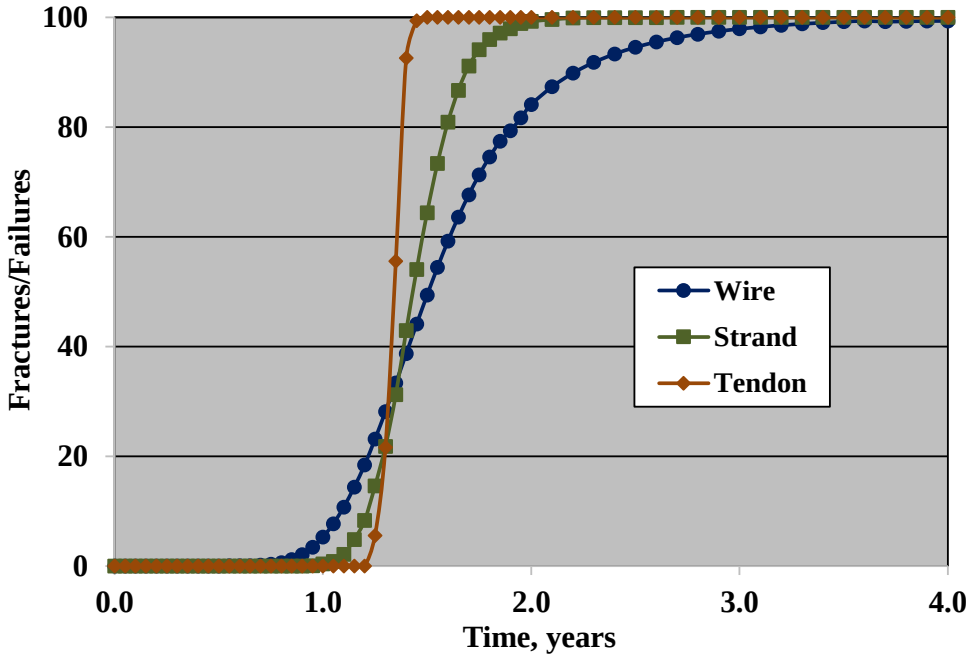

Source: FHWA.

Figure 79. Graph. Plot of the percentage of wire and strand fractures and tendon failures as a function of time based on a mean wire corrosion rate of 50.0 mpy and standard deviation 0.3 of the mean.

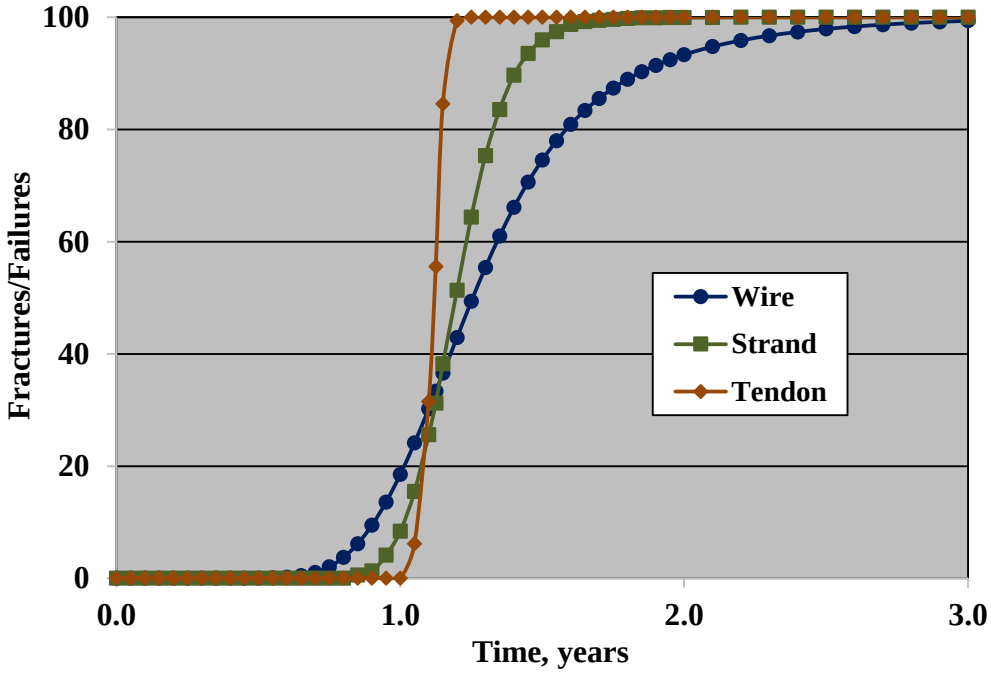

Source: FHWA.

Figure 80. Graph. Plot of the percentage of wire and strand fractures and tendon failures as a function of time based on a mean wire corrosion rate of 60.0 mpy and standard deviation 0.3 of the mean.

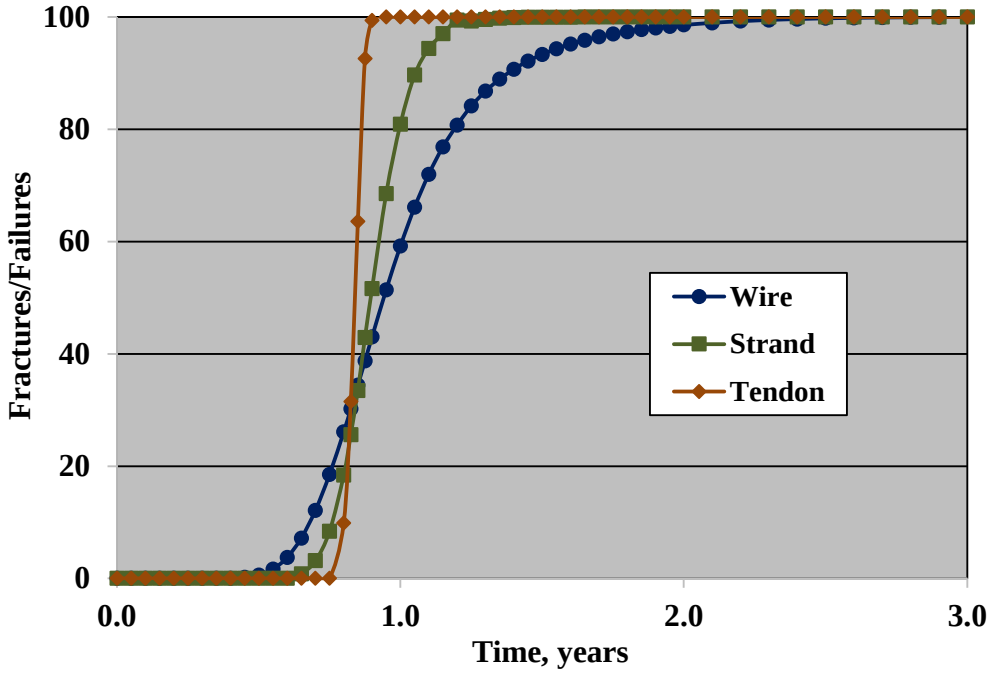

Source: FHWA.

Figure 81. Graph. Plot of the percentage of wire and strand fractures and tendon failures as a function of time based on a mean wire corrosion rate of 80.0 mpy and standard deviation 0.3 of the mean.

Table 23. Projected T_f and fracture/failure rate for mean corrosion rate of 1.0 mpy and standard deviation 0.3 of the mean.

Component	T_f (Year)	Number of Fractures or Failures/Year*	Percent of Fractures or Failures/Year*
Wire	25.9	460	2.2
Strand	48.0	139	3.9
Tendon	60.9	26	16.0

*Determined as slope of the curve near the inflection point.

Table 24. Projected T_f and fracture/failure rate for mean corrosion rate of 2.0 mpy and standard deviation 0.3 of the mean.

Component	T_f (Year)	Number of Fractures or Failures/Year*	Percent of Fractures or Failures/Year*
Wire	12.7	1,092	5.1
Strand	23.3	332	9.3
Tendon	31.6	42	25.9

*Determined as slope of the curve near the inflection point.

Table 25. Projected T_f and fracture/failure rate for mean corrosion rate of 3.0 mpy and standard deviation 0.3 of the mean.

Component	T_f (Year)	Number of Fractures or Failures/Year*	Percent of Fractures or Failures/Year*
Wire	8.6	1,382	6.5
Strand	15.8	478	13.4
Tendon	20.3	86	53.1

[1]Determined as slope of the curve near the inflection point.

Table 26. Projected T_f and fracture/failure rate for mean corrosion rate of 4.0 mpy and standard deviation 0.3 of the mean.

Component	T_f (Year)	Number of Fractures or Failures/Month*	Percent of Fractures or Failures/Month*
Wire	6.3	153	0.7
Strand	12.0	54	1.5
Tendon	15.8	7	4.5

*Determined as slope of the curve near the inflection point.

Table 27. Projected T_f and fracture/failure rate for mean corrosion rate of 5.0 mpy and standard deviation 0.3 of the mean.

Component	T_f (Year)	Number of Fractures or Failures/Month*	Percent of Fractures or Failures/Month*
Wire	5.1	190	0.9
Strand	9.8	64	1.8
Tendon	12.7	9	5.7

*Determined as slope of the curve near the inflection point.

Table 28. Projected T_f and fracture/failure rate for mean corrosion rate of 7.5 mpy and standard deviation 0.3 of the mean.

Component	T_f (Year)	Number of Fractures or Failures/Month*	Percent of Fractures or Failures/Month*
Wire	3.5	287	1.3
Strand	6.3	101	2.8
Tendon	8.1	14	8.8

*Determined as slope of the curve near the inflection point.

Table 29. Projected T_f and fracture/failure rate for mean corrosion rate of 10.0 mpy and standard deviation 0.3 of the mean.

Component	T_f (Year)	Number of Fractures or Failures/Month*	Percent of Fractures or Failures/Month*
Wire	2.6	381	1.8
Strand	4.7	133	3.7
Tendon	6.3	15	9.2

*Determined as slope of the curve near the inflection point.

Table 30. Projected T_f and fracture/failure rate for mean corrosion rate of 15.0 mpy and standard deviation 0.3 of the mean.

Component	T_f (Year)	Number of Fractures or Failures/Month*	Percent of Fractures or Failures/Month*
Wire	1.8	567	2.7
Strand	3.1	202	5.7
Tendon	4.2	26	16.0

*Determined as slope of the curve near the inflection point.

Table 31. Projected T_f and fracture/failure rate for mean corrosion rate of 20.0 mpy and standard deviation 0.3 of the mean.

Component	T_f (Year)	Number of Fractures or Failures/Month*	Percent of Fractures or Failures/Month*
Wire	1.3	756	3.5
Strand	2.5	278	7.8
Tendon	3.1	37	22.6

*Determined as slope of the curve near the inflection point.

Table 32. Projected T_f and fracture/failure rate for mean corrosion rate of 30.0 mpy and standard deviation 0.3 of the mean.

Component	T_f (Year)	Number of Fractures or Failures/Month*	Percent of Fractures or Failures/Month*
Wire	0.9	1,116	5.2
Strand	1.6	367	11.1
Tendon	2.1	58	35.5

*Determined as slope of the curve near the inflection point.

Table 33. Projected T_f and fracture/failure rate for mean corrosion rate of 40.0 mpy and standard deviation 0.3 of the mean.

Component	T_f (Year)	Number of Fractures or Failures/Month*	Percent of Fractures or Failures/Month*
Wire	0.65	1,535	7.2
Strand	1.20	517	14.5
Tendon	1.52	87	53.5

*Determined as slope of the curve near the inflection point.

Table 34. Projected T_f and fracture/failure rate for mean corrosion rate of 50.0 mpy and standard deviation 0.3 of the mean.

Component	T_f (Year)	Number of Fractures or Failures/Month*	Percent of Fractures or Failures/Month*
Wire	0.50	1,915	9.0
Strand	0.95	695	19.5
Tendon	1.23	100	61.7

*Determined as slope of the curve near the inflection point.

Table 35. Projected T_f and fracture/failure rate for mean corrosion rate of 60.0 mpy and standard deviation 0.3 of the mean.

Component	T_f (Year)	Number of Fractures or Failures/Month*	Percent of Fractures or Failures/Month*
Wire	0.43	2,303	10.8
Strand	0.80	748	21.0
Tendon	1.04	130	80.2

*Determined as slope of the curve near the inflection point.

Table 36. Projected T_f and fracture/failure rate for mean corrosion rate of 80.0 mpy and standard deviation 0.3 of the mean.

Component	T_f (Year)	Number of Fractures or Failures/Month*	Percent of Fractures or Failures/Month*
Wire	0.33	3,018	14.1
Strand	0.60	1,078	30.3
Tendon	0.79	>162	>100

*Determined as slope of the curve near the inflection point.

Summary of Wire and Strand Fracture and Tendon Failure Projections

Figure 82 provides a plot of T_f as a function of mean corrosion rate based on the results in figure 68 through figure 81 and table 23 through table 26. Also indicated are projected T_f results for Specimen Numbers MS–0.8 and MS–1.0, the grout of which exhibited minimal soluble sulfates. The slightly lower T_f for the latter two specimens probably resulted because of the higher standard deviation on mean corrosion rate (σ/μ = 0.41 for the former and 0.36 for the latter compared to 0.30 on which the systematic analyses were based (see above)). Likewise, figure 83

reproduces the three trend lines from figure 82 but with T_f data for Specimens MS–0.0, MS–0.4, and MS–2.0, which had relatively high soluble sulfates added.

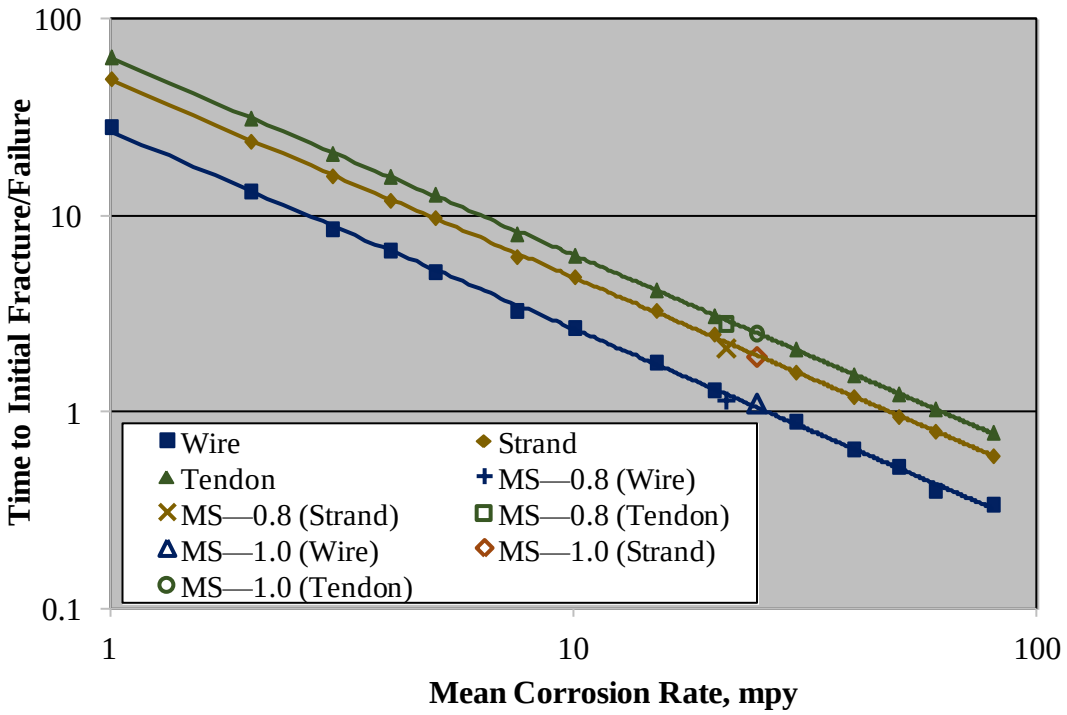

Source: FHWA.

Figure 82. Graph. Plot of T_f for wires, strands, and tendons as a function of corrosion rate as determined from the results in tables 10, 12, and 20–33.

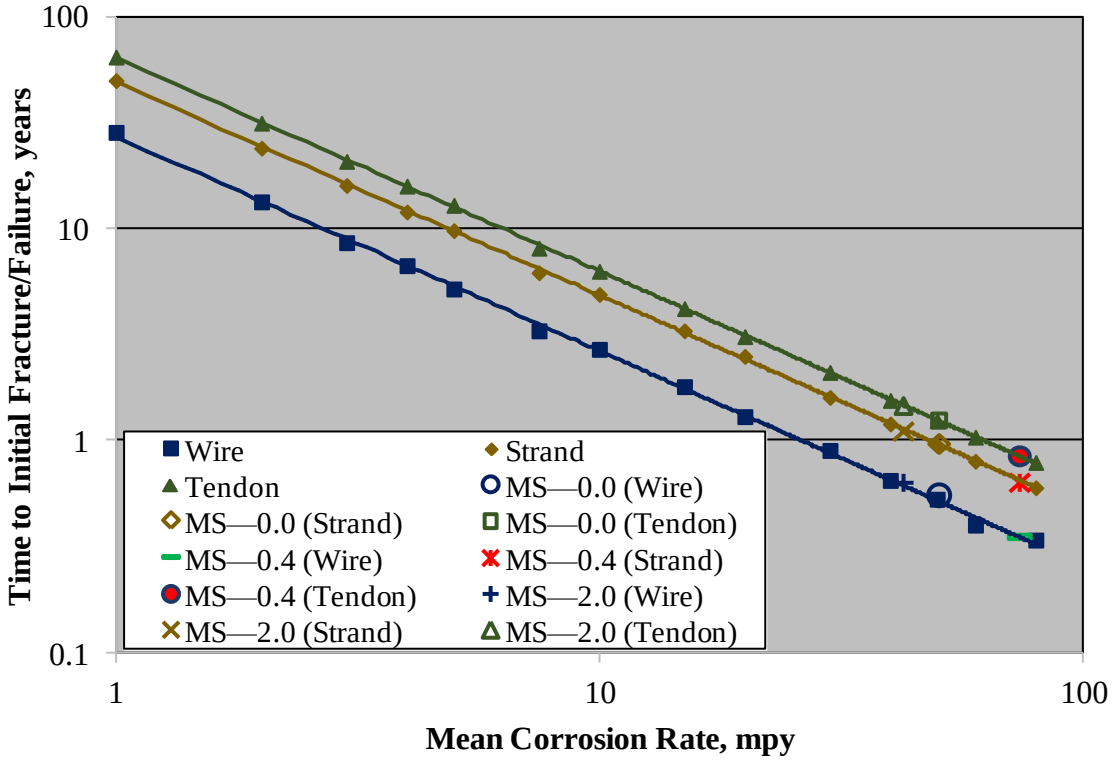

Source: FHWA.

Figure 83. Graph. Plot of T_f for wires, strands, and tendons as a function of corrosion rate as determined from the results in tables 14, 17, 18, and 20–33.

The following are equations (figure 84 through figure 86) for the best fit line through each of the three sets of data.

$$T_f = 27.05 \cdot \mu(CRE)^{-1.01} \ (R^2 > 0.99)$$

Figure 84. Equation. Analytical expression for the dependence of T_f for wires on corrosion rate.

$$T_f = 49.83 \cdot \mu(CRE)^{-1.01} \ (R^2 > 0.99)$$

Figure 85. Equation. Analytical expression for the dependence of T_f for strands on corrosion rate.

$$T_f = 63.60 \cdot \mu(CRE)^{-1.01} \ (R^2 > 0.99)$$

Figure 86. Equation. Analytical expression for the dependence of T_f for tendons on corrosion rate.

It should be recognized that these results are based on the phase 1 experimental conditions, specifically for water being injected into the void/grout space after some period of time during the exposure and for the temperature and relative humidity cycles that were employed. The former caused a corrosion rate increase for some time after injection for some specimens (figure 45

through figure 47), and so the T_f projections would probably change for a different injection history and if different temperature and relative humidity cycles had been employed.

MODELING APPROACH VALIDATION

Two opportunities arose whereby a degree of validation for the proposed fracture/failure methodology could be made. One occurred in conjunction with detensioning of Specimen Number MS–0.4, during which three wires on one strand fractured near the void/grout interface. Figure 88 reproduces figure 219 from the phase 1 report and shows this strand, where the red arrow identifies the three broken wires, and gray arrows point to black, sulfate-rich deposits. Further, figure 88 reproduces figure 220 from that report, showing a closeup view of the strand with fractured wires. Although the wire fractures were triggered by the detensioning activities, it is likely that they were on the verge of occurring irrespective of this. Consequently, T_f for these was taken as 0.60 yr (detensioning took place after 178 d, or 0.49 yr), considering that they would have remained unfractured for slightly longer than was actually the case.

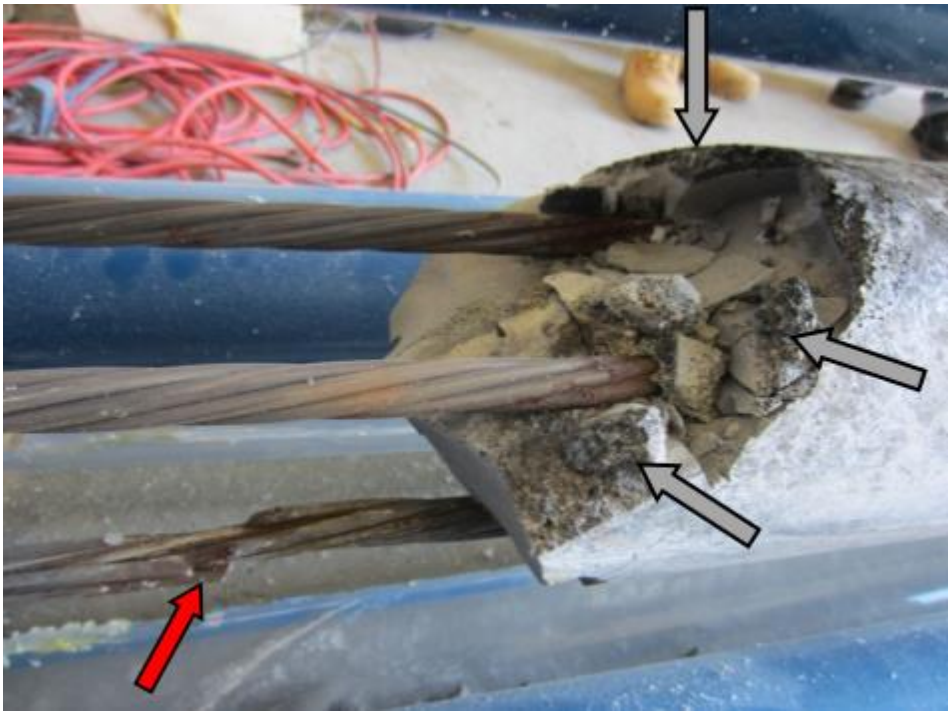

Source: FHWA.

Figure 87. Photo. Appearance of strands and fractured wires from Specimen Number MS–0.4 after duct removal.[(1)]

Source: FHWA.

Figure 88. Photo. Closeup view of the strand in figure 87 showing fractured wires.(1)

The fracturing of these three wires provides an opportunity to compare this timing with modeling predictions. In this regard, table 20 lists the projected T_f for wires based on corrosion rate data acquired from this strand as of 0.33 yr, which is about half of the 0.60 yr estimated above. In view of this difference, the analysis was refined to take into account that, first, the tendon was stressed to 60 percent of GUTS while the analysis employed a value of 63 percent,[2] and second, the tendon consisted of 24 outer stressed wires, whereas the analysis was based on 21,384 stressed wires. The latter factor resulted in a higher corrosion rate for wires at the extreme of the distribution and, hence, projection of an earlier initial fracture according to the greater the number of wires. Thus, repeating the analysis using, first, stress as 60 percent of GUTS and, second, a tendon composed of but four strands (24 outer wires) yielded a T_f of 0.66 yr, which all factors considered, is in good agreement with the assigned 0.60 yr. That the remaining wires on this strand did not fracture once three wires did so, as is projected to occur according to the analysis assumptions (see chapter 3), is attributed to the development length for transference of stress to remaining wires being relatively long compared to length of the tendon. Consequently, the unfractured wires were stressed in displacement control.

The second opportunity resulted in conjunction with pit depth measurements made on one of two failed tendons recovered from the Ringling Causeway in Florida, which are discussed in detail in chapter 6. Visual inspection subsequent to separating and cleaning wires revealed that corrosion was most advanced near the fractures and progressively moderated from there. In view of this, a 10-inch length was cut from the fractured end of three strands that were determined to have failed from excessive corrosion loss as opposed to tensile overload, and pit depths were measured on individual wires subsequent to separating these and cleaning. However, one of these had only three to eight pits per wire. Corrosion, in this case, occurred mostly at the fracture site, and so this strand

[2]Strand tension was measured shortly before detensioning and determined to be the same as it was initially.

was considered not representative and was not included in the analysis. Also, one wire of one of the strands had no measurable pits. Table 37 and table 38 list the depth of the five deepest pits per wire for the other two strands along with the average $\mu(CRE)$, $\sigma(CRE)$, and $\sigma(CRE)/\mu(CRE)$, assuming a 7.5-yr exposure.[3] Because the five deepest pits alone were included, this condition considers that these are likely to approach the extent of corrosion at the fracture location. Also listed is the average $\mu(CRE)$ for the three wires with the deepest pits, considering that fracture of these would result in strand breakage as discussed above. From the latter, strand T_f was calculated based on the equation in figure 85 above as 3.8 and 4.8 yr for the two strands.

Of course, it is not known when during the assumed 7.5 yr that these fractures occurred. In all likelihood, corrosion continued and pit depth increased further subsequent to the wire fractures. On this basis, the calculated times of fracture should be greater than calculated (3.8 and 4.8 yr). This may be offset to some extent, however, considering that pit depths at the fracture site were probably greater than elsewhere on the wires. Regardless, results from the Ringling Causeway failures are consistent with the proposed tendon failure methodology. Further qualification of the failure projection model might occur as additional information becomes available.

[3]The failures were disclosed approximately 8 yr subsequent to construction.

Table 37. Pit depth measurements and projected T_f for strand R2 from the Ringling Causeway.

Wire No.	Pit Depth—Five Deepest (mil)	Pit Depth—Five Deepest (mil)	Pit Depth—Five Deepest (mil)	Pit Depth—Five Deepest (mil)	Pit Depth—Five Deepest (mil)	Mean (mil)	Standard Deviation	$\mu(CRE)$ (mpy)	$\sigma(CRE)$	$\sigma(CRE)/\mu(CRE)$	$\mu(CRE)$ (mpy)—Three Deepest	T_f (Year) (Equation 71)
1	39.5	42.5	72.5	75.5	61.0	58.2	16.6	7.8	2.2	0.29	10.1	4.8
2	71.0	82.0	87.5	117.5	57.5	83.1	22.4	11.1	3.0	0.27	10.1	4.8
3	35.5	35.0	30.0	38.5	72.5	42.3	17.2	5.6	2.3	0.41	10.1	4.8
4	78.5	89.0	102.5	39.0	33.0	68.4	30.8	9.1	4.1	0.45	10.1	4.8
5	79.0	73.5	34.0	29.0	18.5	46.8	27.5	6.2	3.7	0.59	10.1	4.8
6	32.0	39.5	69.0	115.0	121.5	75.4	41.6	10.1	5.5	0.55	10.1	4.8
7	14.0	13.0	17.0	16.5	20.0	16.1	2.7	2.1	0.4	0.17	10.1	4.8

Table 38. Pit depth measurements and projected T_f for strand R6 from the Ringling Causeway.

Wire No.	Pit Depth—Five Deepest (mil)	Pit Depth—Five Deepest (mil)	Pit Depth—Five Deepest (mil)	Pit Depth—Five Deepest (mil)	Pit Depth—Five Deepest (mil)	Mean (mil)	Standard Deviation	$\mu(CRE)$ (mpy)	$\sigma(CRE)$	$\sigma(CRE)/\mu(CRE)$	$\mu(CRE)$ (mpy)—Three Deepest	T_f (Year) (Equation 71)
1	55.5	101.0	118.0	47.0	26.0	69.5	38.5	9.3	5.1	0.55	12.7	3.8
2	133.5	130.0	131.0	98.0	75.0	113.5	26.0	15.1	3.5	0.23	12.7	3.8
3	43.0	86.0	90.0	51.5	43.0	62.7	23.4	8.4	3.1	0.37	12.7	3.8
4	151.0	50.0	57.0	58.0	53.0	73.8	43.3	9.8	5.8	0.59	12.7	3.8
5	88.5	52.0	44.0	35.0	34.0	50.7	22.4	6.8	3.0	0.44	12.7	3.8
6	161.5	132.5	102.0	65.5	33.5	99.0	51.1	13.2	6.8	0.52	12.7	3.8

PROJECTED VERSUS ACTUAL WIRE AND STRAND FRACTURES

It should be recognized that the actual number of wire and strand fractures can differ from projection because the model does not count wires that fracture because of strand overload and, likewise, strands that fracture because of tendon overload. Thus, as noted above, strands fracture when three wires exhibit sufficient corrosion that they fracture, leading to seven fractures total but with only three projected by the model. Likewise, tendons fail on 7 strand fractures; however, this results in fracture of all 22 strands, even though only 7 fractures are projected by the model. Where this might become an issue is if all fractured wires or strands (or both) are being counted in one or more failed tendons with expectation that these should conform to model projections. Figure 89 plots the number of projected wire fractures versus time compared to the total number of such fractures that should be present. Likewise, figure 90 does the same for strands. In both cases, $\mu(CRE)$ = 5.0 mpy and $\sigma(CRE)$ = 0.5 of the mean. The plots demonstrate that any assessment of wire and strand fractures in tendons for the purpose of verifying model projections must take the above considerations into account.

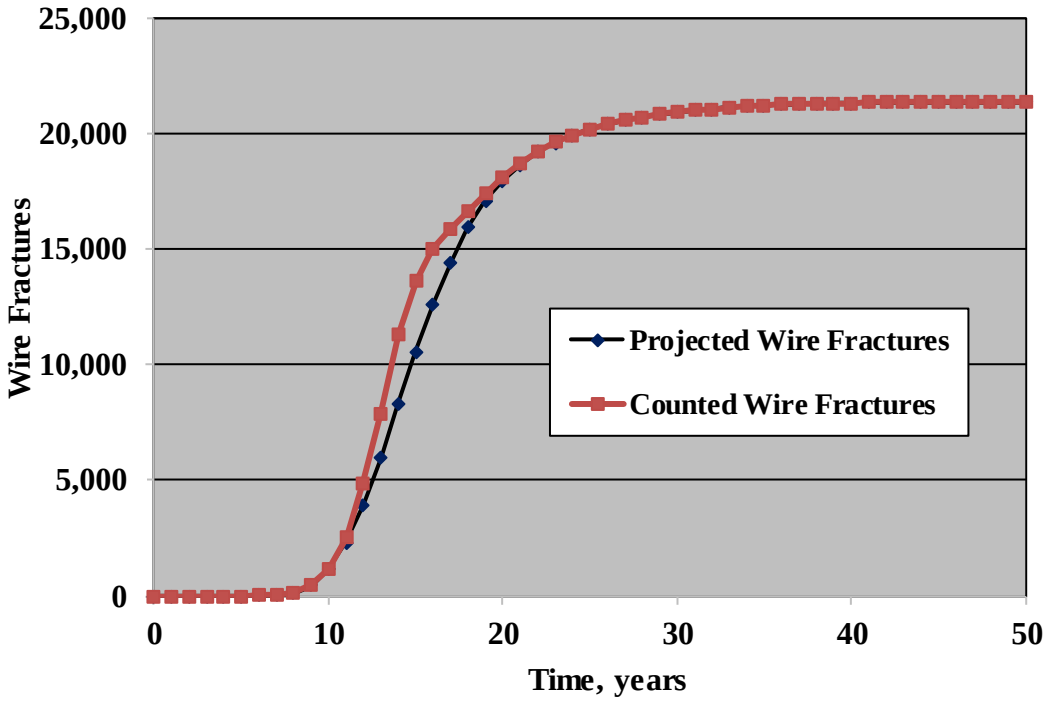

Source: FHWA.

Figure 89. Graph. Plot of the number of both model projected and actual count wire fractures versus time for $\mu(CRE)$ = 5.0 mpy and $\sigma(CRE)$ = 0.5 of the mean.

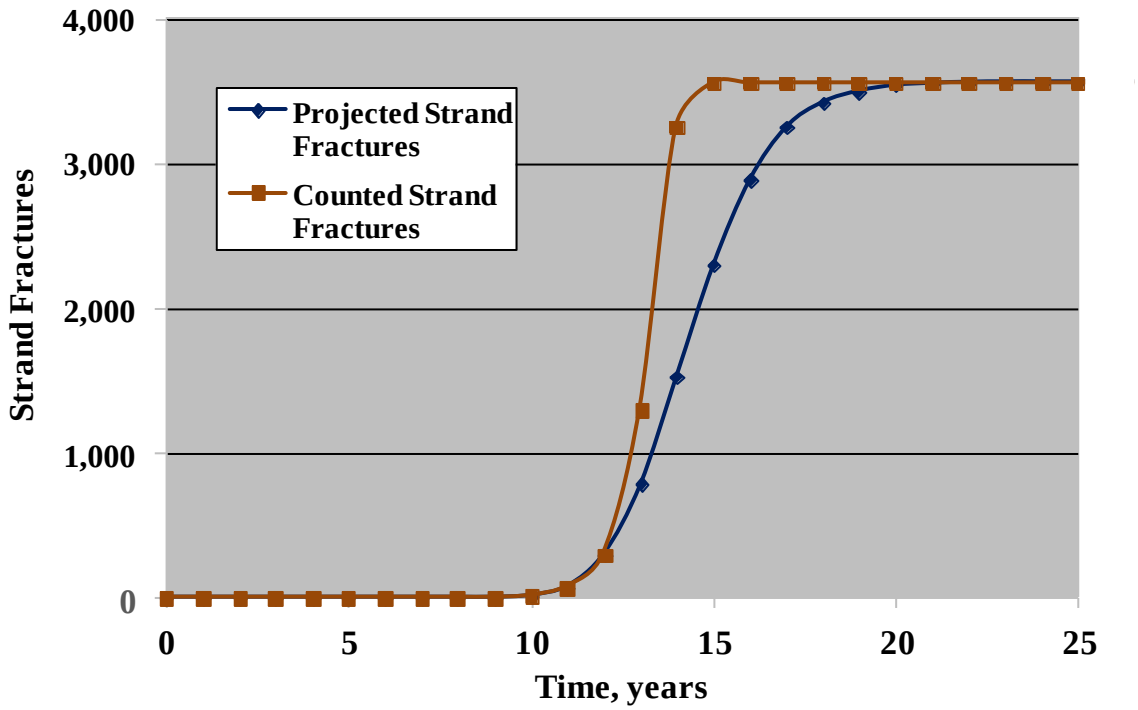

Source: FHWA.

Figure 90. Graph. Plot of the number of both model projected and actual count strand fractures versus time for $\mu(CRE)$ = 5.0 mpy and $\sigma(CRE)$ = 0.5 of the mean.

EFFECT OF ANALYSIS VARIABLES

General

Variables that potentially affect projected tendon performance and analysis results, in addition to the ones considered previously and which were investigated in the present study, include the following:

- Strand/tendon stress.
- Wire/strand strength.
- Random number sequence.
- Number of tendons.
- Tendon length.

Each of these is evaluated below.

Effect of Strand/Tendon Post-Tension Stress

As noted above, the initial jacking force for strands is typically 80 percent of GUTS (270 ksi). This reduces to about 70 percent on external load release, and over the long term, relaxation reduces this further to 60 to 64 percent of GUTS. The above analyses assumed a stress of 63 percent of GUTS, which is consistent with the long-term range of relaxed values. However, this choice could potentially result in nonconservative analysis findings, since the relaxation

period may exceed T_f, particularly in cases where mean corrosion rate is high. Consequently, additional analyses were performed for stresses of 66 and 68 percent of GUTS and mean corrosion rates of 2.0, 10.0, and 40.0 mpy with standard deviation being 30 percent of the mean in each case. Table 39 and table 40 list T_f and the number and percentage of fractures/failures per year for wires, strands, and tendons with a mean corrosion rate of 2.0 mpy and a post-tension stress of 66 and 68 percent of GUTS, respectively. Table 41 and table 42 do the same for mean corrosion rate of 10 mpy, and table 43 and table 44 for mean corrosion rate of 40 mpy (note that fracture/failure rates in these latter two cases are on a per-month basis). In each case, $\sigma(CRE)/\mu(CRE) = 0.30$. Figure 91 shows a plot of T_f versus post-tension stress for each of these three corrosion rates, and table 45 through table 47 list T_f and percent decrease for post-tension stresses of 66 and 68 percent compared to 63 percent of GUTS (270 ksi) for the same corrosion rates as above. Invariably, these percent changes are greater the higher the post-tension stress, and stressing to 68 percent of GUTS compared to 63 percent resulted in a T_f decrease in tendon failure rate of approximately 12 percent irrespective of corrosion rate.

Table 39. Projected T_f and fracture/failure rate for mean corrosion rate of 2.0 mpy and strand/tendon stress 66 percent of GUTS.

Component	T_f (Year)	Number of Fractures or Failures/Year*	Percent of Fractures or Failures/Year*
Wire	9.5	953	0.5
Strand	22.0	346	9.7
Tendon	29.7	56	34.6

*Determined as slope of the curve near the inflection point.

Table 40. Projected T_f and fracture/failure rate for mean corrosion rate of 2.0 mpy and strand/tendon stress 68 percent of GUTS.

Component	T_f (Year)	Number of Fractures or Failures/Year*	Percent of Fractures or Failures/Year*
Wire	8.8	971	4.5
Strand	21.5	336	9.4
Tendon	27.7	57	35.2

*Determined as slope of the curve near the inflection point.

Table 41. Projected T_f and fracture/failure rate for mean corrosion rate of 10.0 mpy and strand/tendon stress 66 percent of GUTS.

Component	T_f (Year)	Number of Fractures or Failures/Month*	Percent of Fractures or Failures/Month*
Wire	2.1	393	1.8
Strand	4.3	136	3.8
Tendon	5.7	20	12.3

*Determined as slope of the curve near the inflection point.

Table 42. Projected T_f and fracture/failure rate for mean corrosion rate of 10.0 mpy and strand/tendon stress 68 percent of GUTS.

Component	T_f (Year)	Number of Fractures or Failures/Month*	Percent of Fractures or Failures/Month*
Wire	1.8	410	1.9
Strand	4.2	140	3.9
Tendon	5.5	18	11.0

*Determined as slope of the curve near the inflection point.

Table 43. Projected T_f and fracture/failure rate for mean corrosion rate of 40.0 mpy and strand/tendon stress 66 percent of GUTS.

Component	T_f (Year)	Number of Fractures or Failures/Month*	Percent of Fractures or Failures/Month*
Wire	0.5	1,590	7.4
Strand	1.1	578	16.2
Tendon	1.4	93	57.6

*Determined as slope of the curve near the inflection point.

Table 44. Projected T_f and fracture/failure rate for mean corrosion rate of 40.0 mpy and strand/tendon stress 68 percent of GUTS.

Component	T_f (Year)	Number of Fractures or Failures/Month*	Percent of Fractures or Failures/Month*
Wire	0.5	1,620	7.6
Strand	1.1	560	15.7
Tendon	1.4	93	57.6

*Determined as slope of the curve near the inflection point.

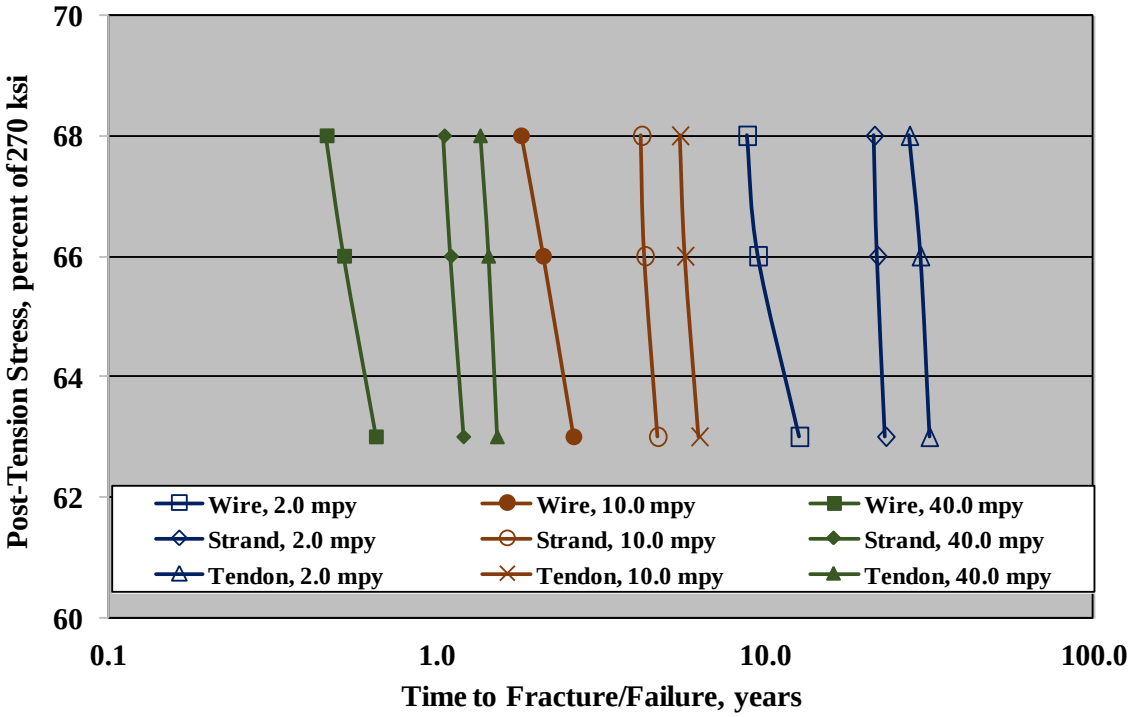

Source: FHWA.

Figure 91. Graph. Plot of T_f for wires, strands, and tendons as a function of post-tension stress for mean corrosion rates of 2.0, 10.0, and 40.0 mpy and standard deviation 0.3 of the mean.

Table 45. T_f and percent decrease in T_f for post-tension stresses of 66 and 68 percent of GUTS (270 ksi) compared to 63 percent for mean corrosion rate of 2.0 mpy.

Stress (% of 270 ksi)	Wire T_f (Year)	Strand T_f (Year)	Tendon T_f (Year)	Wire T_f Decrease (Year)	Strand T_f Decrease (%)	Tendon T_f Decrease (%)
63	12.7	23.3	31.6	—	—	—
66	9.5	22.0	29.7	—	—	—
68	8.8	21.5	27.5	—	—	—
63–66	—	—	—	25.2	5.6	6.0
63–68	—	—	—	30.7	7.7	13.0

—No information available.

Table 46. T_f and percent decrease in T_f for post-tension stresses of 66 and 68 percent of GUTS (270 ksi) compared to 63 percent for mean corrosion rate of 10.0 mpy.

Stress (% of 270 ksi)	Wire T_f (Year)	Strand T_f (Year)	Tendon T_f (Year)	Wire T_f Decrease (Year)	Strand T_f Decrease (%)	Tendon T_f Decrease (%)
63	2.6	4.7	6.3	—	—	—
66	2.1	4.3	5.7	—	—	—
68	1.8	4.2	5.5	—	—	—
63–66	—	—	—	19.2	7.5	9.2
63–68	—	—	—	30.8	9.7	12.4

—No information available.

Table 47. T_f and percent decrease in T_f for post-tension stresses of 66 and 68 percent of GUTS (270 ksi) compared to 63 percent for mean corrosion rate of 40.0 mpy.

Stress (% of 270 ksi)	Wire T_f (Year)	Strand T_f (Year)	Tendon T_f (Year)	Wire T_f Decrease (Year)	Strand T_f Decrease (%)	Tendon T_f Decrease (%)
63	0.65	1.20	1.52	—	—	—
66	0.52	1.10	1.43	—	—	—
68	0.46	1.05	1.35	—	—	—
63–66	—	—	—	20.0	8.3	5.9
63–68	—	—	—	29.2	12.5	11.2

—No information available.

Effect of Wire/Strand Strength

As noted above, 270 ksi is the specified minimum wire/strand strength (GUTS), and in order to ensure that this criterion is met, actual strength is likely to be greater. This was indicated, for example, by the single uncorroded wire datum in figure 15, for which GUTS is 289 ksi. Consequently, analyses were also performed for wire/strand tensile strengths of 280 and 290 ksi and post-tension stresses of 63, 66, and 68 percent of 270 ksi. As above, mean corrosion rates of 2, 10, and 40 mpy with $\sigma(CRE)/\mu(CRE) = 0.30$ were employed in all cases. Table 48 through table 65 list T_f and fracture/failure rate results for these analyses, and figure 92 through figure 94 show these graphically for each of the above three mean corrosion rates, respectively. Thus, T_f is seen to increase with increasing wire strength, but with the effect being progressively moderated with increasing post-tension stress.

Table 48. Projected T_f and fracture/failure rate for mean corrosion rate of 2.0 mpy, wire/strand strength 280 ksi, and strand/tendon stress 63 percent of GUTS.

Component	T_f (Year)	Number of Fractures or Failures/Year*	Percent of Fractures or Failures/Year*
Wire	14.9	860	4.0
Strand	26.0	306	8.6
Tendon	32.7	56	34.6

*Determined as slope of the curve near the inflection point.

Table 49. Projected T_f and fracture/failure rate for mean corrosion rate of 2.0 mpy, wire/strand strength 280 ksi, and strand/tendon stress 66 percent of GUTS.

Component	T_f (Year)	Number of Fractures or Failures/Year*	Percent of Fractures or Failures/Year*
Wire	10.8	939	4.4
Strand	23.3	331	9.3
Tendon	29.8	55	34.0

*Determined as slope of the curve near the inflection point.

Table 50. Projected T_f and fracture/failure rate for mean corrosion rate of 2.0 mpy, wire/strand strength 280 ksi, and strand/tendon stress 68 percent of GUTS.

Component	T_f (Year)	Number of Fractures or Failures/Year*	Percent of Fractures or Failures/Year*
Wire	10.1	950	4.4
Strand	21.7	326	9.1
Tendon	27.9	52	31.8

*Determined as slope of the curve near the inflection point.

Table 51. Projected T_f and fracture/failure rate for mean corrosion rate of 10.0 mpy, wire/strand strength 280 ksi, and strand/tendon stress 63 percent of GUTS.

Component	T_f (Year)	Number of Fractures or Failures/Month*	Percent of Fractures or Failures/Month*
Wire	3.1	367	1.7
Strand	5.2	121	3.7
Tendon	6.6	18	11.3

*Determined as slope of the curve near the inflection point.

Table 52. Projected T_f and fracture/failure rate for mean corrosion rate of 10.0 mpy, wire/strand strength 280 ksi, and strand/tendon stress 66 percent of GUTS.

Component	T_f (Year)	Number of Fractures or Failures/Month*	Percent of Fractures or Failures/Month*
Wire	2.4	392	1.8
Strand	4.6	136	3.8
Tendon	6.0	23	14.2

*Determined as slope of the curve near the inflection point.

Table 53. Projected T_f and fracture/failure rate for mean corrosion rate of 10.0 mpy, wire/strand strength 280 ksi, and strand/tendon stress 68 percent of GUTS.

Component	T_f (Year)	Number of Fractures or Failures/Month*	Percent of Fractures or Failures/Month*
Wire	2.0	392	1.8
Strand	4.3	143	4.0
Tendon	5.6	22	13.6

*Determined as slope of the curve near the inflection point.

Table 54. Projected T_f and fracture/failure rate for mean corrosion rate of 40.0 mpy, wire/strand strength 280 ksi, and strand/tendon stress 63 percent of GUTS.

Component	T_f (Year)	Number of Fractures or Failures/Month*	Percent of Fractures or Failures/Month*
Wire	0.77	1,532	7.2
Strand	1.30	490	13.7
Tendon	1.64	68	42.2

*Determined as slope of the curve near the inflection point.

Table 55. Projected T_f and fracture/failure rate for mean corrosion rate of 40.0 mpy, wire/strand strength 280 ksi, and strand/tendon stress 66 percent of GUTS.

Component	T_f (Year)	Number of Fractures or Failures/Month*	Percent of Fractures or Failures/Month*
Wire	0.6	1,548	7.2
Strand	1.2	552	15.5
Tendon	1.5	75	46.3

*Determined as slope of the curve near the inflection point.

Table 56. Projected T_f and fracture/failure rate for mean corrosion rate of 40.0 mpy, wire/strand strength 280 ksi, and strand/tendon stress 68 percent of GUTS.

Component	T_f (Year)	Number of Fractures or Failures/Month*	Percent of Fractures or Failures/Month*
Wire	0.5	1,608	7.5
Strand	1.1	543	15.2
Tendon	1.4	77	47.3

*Determined as slope of the curve near the inflection point.

Table 57. Projected T_f and fracture/failure rate for mean corrosion rate of 2.0 mpy, wire/strand strength 290 ksi, and strand/tendon stress 63 percent of GUTS.

Component	T_f (Year)	Number of Fractures or Failures/Month*	Percent of Fractures or Failures/Month*
Wire	17.3	859	4.0
Strand	28.0	271	7.6
Tendon	35.4	47	28.7

*Determined as slope of the curve near the inflection point.

Table 58. Projected T_f and fracture/failure rate for mean corrosion rate of 2.0 mpy, wire/strand strength 290 ksi, and strand/tendon stress 66 percent of GUTS.

Component	T_f (Year)	Number of Fractures or Failures/Year*	Percent of Fractures or Failures/Year*
Wire	15.7	845	4.0
Strand	26.0	319	9.0
Tendon	33.5	48	29.8

*Determined as slope of the curve near the inflection point.

Table 59. Projected T_f and fracture/failure rate for mean corrosion rate of 2.0 mpy, wire/strand strength 290 ksi, and strand/tendon stress 68 percent of GUTS.

Component	T_f (Year)	Number of Fractures or Failures/Month*	Percent of Fractures or Failures/Month*
Wire	14.3	878	1.7
Strand	25.5	323	9.1
Tendon	32.0	47	29.0

*Determined as slope of the curve near the inflection point.

Table 60. Projected T_f and fracture/failure rate for mean corrosion rate of 10.0 mpy, wire/strand strength 290 ksi, and strand/tendon stress 63 percent of GUTS.

Component	T_f (Year)	Number of Fractures or Failures/Month*	Percent of Fractures or Failures/Month*
Wire	3.5	351	1.6
Strand	5.7	121	3.4
Tendon	7.3	20	12.0

*Determined as slope of the curve near the inflection point.

Table 61. Projected T_f and fracture/failure rate for mean corrosion rate of 10.0 mpy, wire/strand strength 290 ksi, and strand/tendon stress 66 percent of GUTS.

Component	T_f (Year)	Number of Fractures or Failures/Month*	Percent of Fractures or Failures/Month*
Wire	3.1	349	1.6
Strand	5.3	129	3.6
Tendon	6.7	17	10.6

*Determined as slope of the curve near the inflection point.

Table 62. Projected T_f and fracture/failure rate for mean corrosion rate of 10.0 mpy, wire/strand strength 290 ksi, and strand/tendon stress 68 percent of GUTS.

Component	T_f (Year)	Number of Fractures or Failures/Month*	Percent of Fractures or Failures/Month*
Wire	2.9	372	1.7
Strand	5.0	130	3.6
Tendon	6.6	15	9.0

*Determined as slope of the curve near the inflection point.

Table 63. Projected T_f and fracture/failure rate for mean corrosion rate of 40.0 mpy, wire/strand strength 290 ksi, and strand/tendon stress 63 percent of GUTS.

Component	T_f (Year)	Number of Fractures or Failures/Month*	Percent of Fractures or Failures/Month*
Wire	0.9	1,404	6.6
Strand	1.4	527	14.8
Tendon	1.8	87	53.5

*Determined as slope of the curve near the inflection point.

Table 64. Projected T_f and fracture/failure rate for mean corrosion rate of 40.0 mpy, wire/strand strength 290 ksi, and strand/tendon stress 66 percent of GUTS.

Component	T_f (Year)	Number of Fractures or Failures/Month*	Percent of Fractures or Failures/Month*
Wire	0.8	1,475	6.9
Strand	1.3	509	13.7
Tendon	1.7	87	53.5

*Determined as slope of the curve near the inflection point.

Table 65. Projected T_f and fracture/failure rate for mean corrosion rate of 40.0 mpy, wire/strand strength 290 ksi, and strand/tendon stress 68 percent of GUTS.

Component	T_f (Year)	Number of Fractures or Failures/Month*	Percent of Fractures or Failures/Month*
Wire	0.7	1,397	6.5
Strand	1.3	542	15.2
Tendon	1.6	78	48.4

*Determined as slope of the curve near the inflection point.

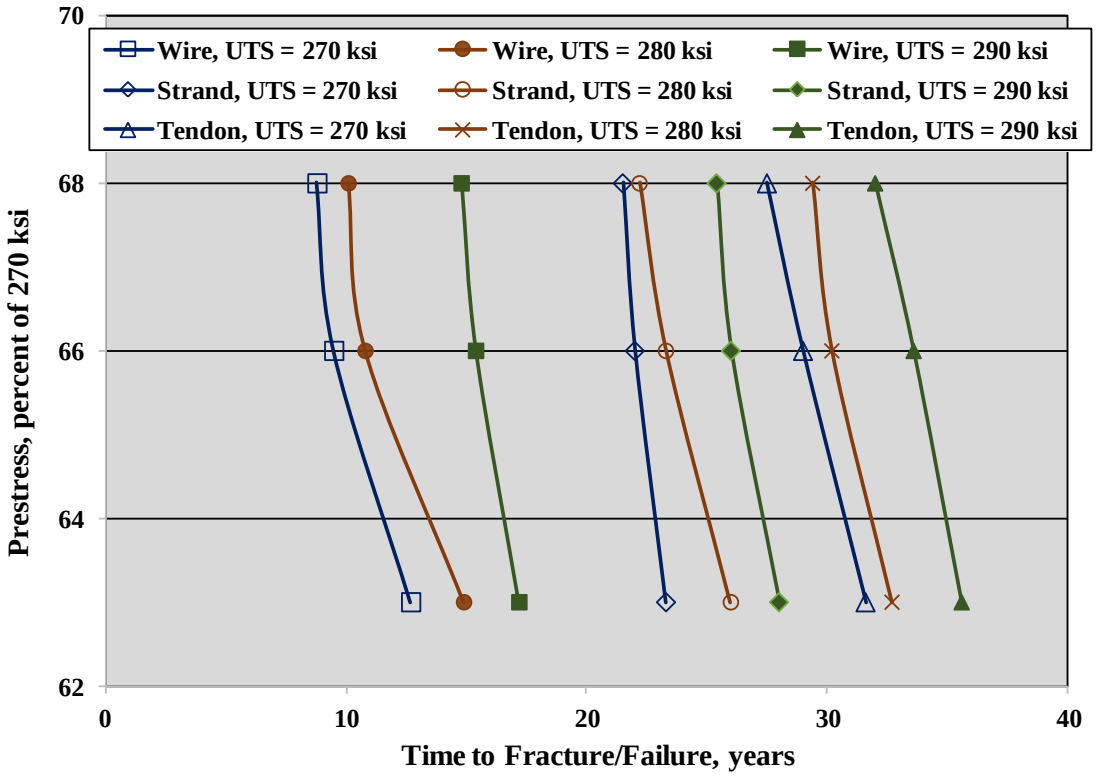

Source: FHWA.

Figure 92. Graph. Plot of T_f for wires, strands, and tendons as a function of post-tension stress and wire/strand strength for mean corrosion rates of 2.0 mpy and standard deviation 0.3 of the mean.

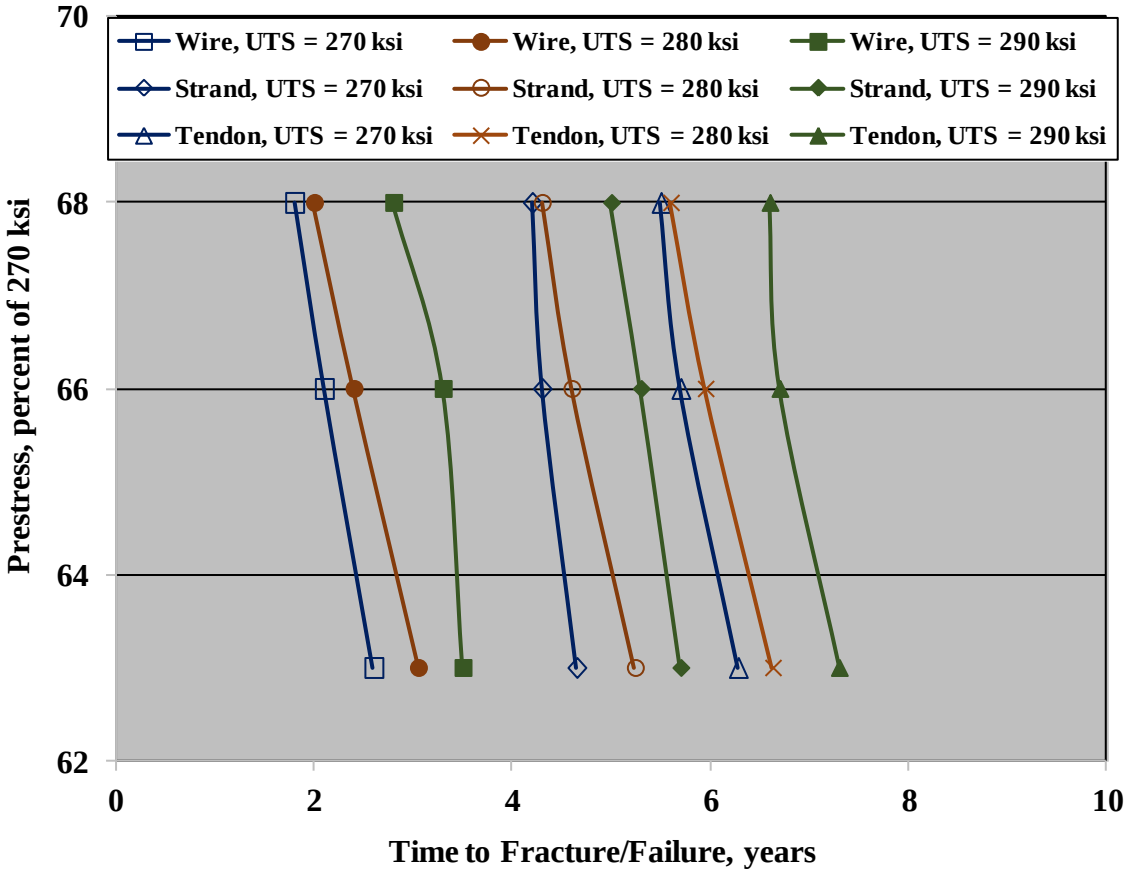

Source: FHWA.

Figure 93. Graph. Plot of T_f for wires, strands, and tendons as a function of post-tension stress and wire/strand strength for mean corrosion rates of 10.0 mpy and standard deviation 0.3 of the mean.

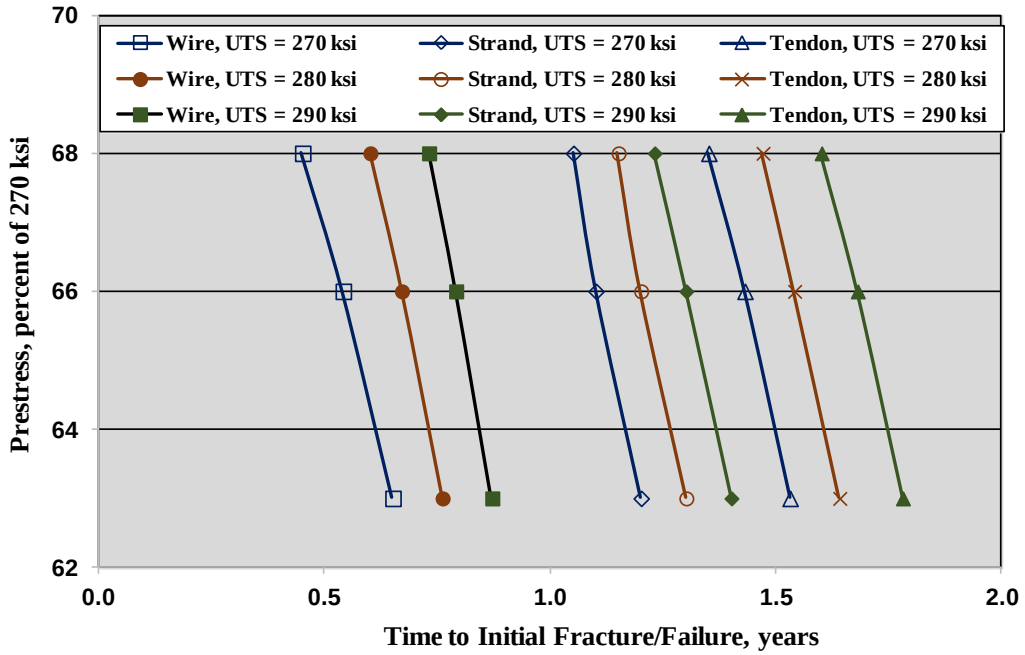

Source: FHWA.

Figure 94. Graph. Plot of T_f for wires, strands, and tendons as a function of post-tension stress and wire/strand strength for mean corrosion rates of 40.0 mpy and standard deviation 30 percent of the mean.

Effect of Different Analysis Random Number Sequences

The above analyses all employed the same random numbers and sequence thereof. However, it can be reasoned that different sequences may result in variations as to how these numbers are partitioned according to groups of six, which represent the outer wires of individual strands and, of 22 groups of six, which represent outer wires of strands comprising individual tendons. This, in turn, could lead to different projections for T_f and for the subsequent rate of fractures/failures. To investigate this, four additional analyses were performed for the case of mean corrosion rate 3.0 mpy and standard deviation 0.9 (see results in figure 70 and table 25), each with a unique random number sequence. Table 66 lists the results for these, where random number set 1 is the same as for all of the above analyses. Results for T_f of wires were determined to the nearest 0.01 yr, whereas for strands and tendons, resolution was to the nearest 0.05 yr. The results show that T_f for wires is identical in each case, as should be expected since each is based on the same set of random numbers, and how these are ordered is of no consequence. However, differences, although not major, occur in the case of strands and tendons because of the above-stated reason. Strand T_f for random number set 4 is somewhat of an outlier because, at 14.10 yr, 3 of the 21,384 random numbers for one group of 6 (representing a strand) had values below 245, the latter being the model projected number of wire fractures after this time. However, T_f for tendons in this set was the highest of the five analyses. This resulted because the model projected 382 strand fractures at 20.75 yr, where 7 of these occurred in one group of 22 strands.

Table 66. T_f results for different random number sequences.

Random Number Set	Wire T_f (Year)	Strand T_f (Year)	Tendon T_f (Year)
1	8.59	15.75	20.25
2	8.59	15.35	20.45
3	8.59	15.55	20.35
4	8.59	14.10	20.75
5	8.59	15.35	20.45

Number of Tendons

Consideration was also given to the possibility that the number of tendons in the model might affect fracture and failure projections. Results of an analysis related to this issue were described above for Specimen Number MS–0.4 (mean corrosion rate 74.3 mpy and standard deviation 28.3), where T_f for a system with 162 tendons was determined as 0.32 yr and, for 4 tendons, 0.66 yr. On a time-scale basis, this difference is not great (0.34 yr), but percentagewise, the T_f reduction for the 162-tendon system is by more than 50 percent. To further investigate any effect of this factor, analyses were also performed with models composed of 40, 81, and 121 tendons and compared to results with 162 tendons. The mean corrosion rate in all cases was 3.0 mpy with standard deviation 0.9 ($\sigma(CRE)/\mu(CRE) = 0.30$). Figure 95 and figure 96 provide wire and strand fracture projections for each of these four cases, and figure 97 does the same for tendon failures. While the four sets of data seem to superimpose, there are small differences; however, these may be due to different random number sets necessarily being employed in each case. It is concluded that, at least for these numbers of tendons, differences in the onset and subsequent rate of fractures/failures are not significant.

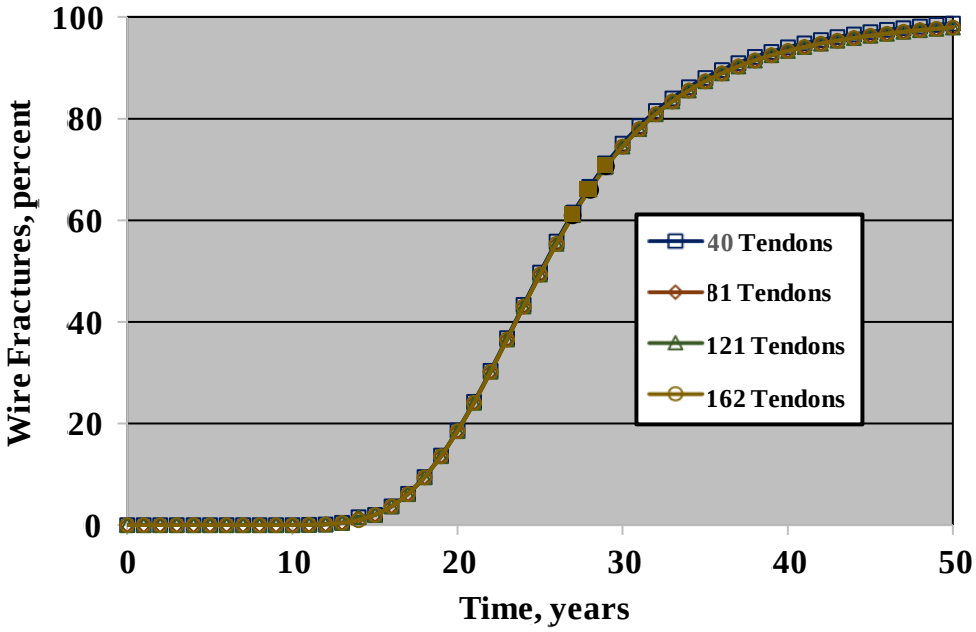

Source: FHWA.

Figure 95. Graph. Plot of the percentage of wire fractures as a function of time for systems with 40, 81, 121, and 162 tendons.

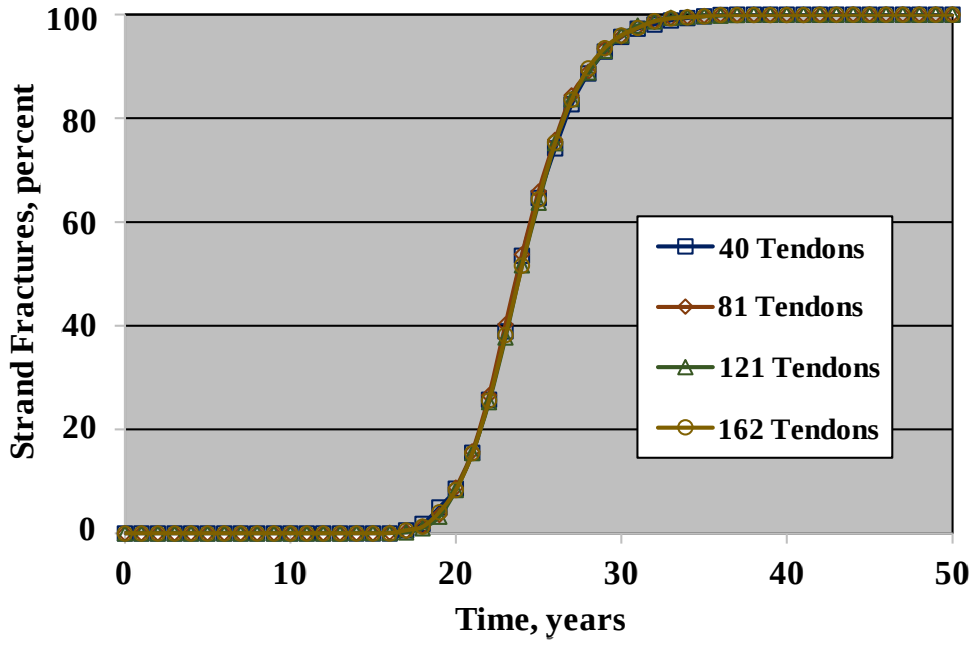

Source: FHWA.

Figure 96. Graph. Plot of the percentage of strand fractures as a function of time for systems with 40, 81, 121, and 162 tendons.

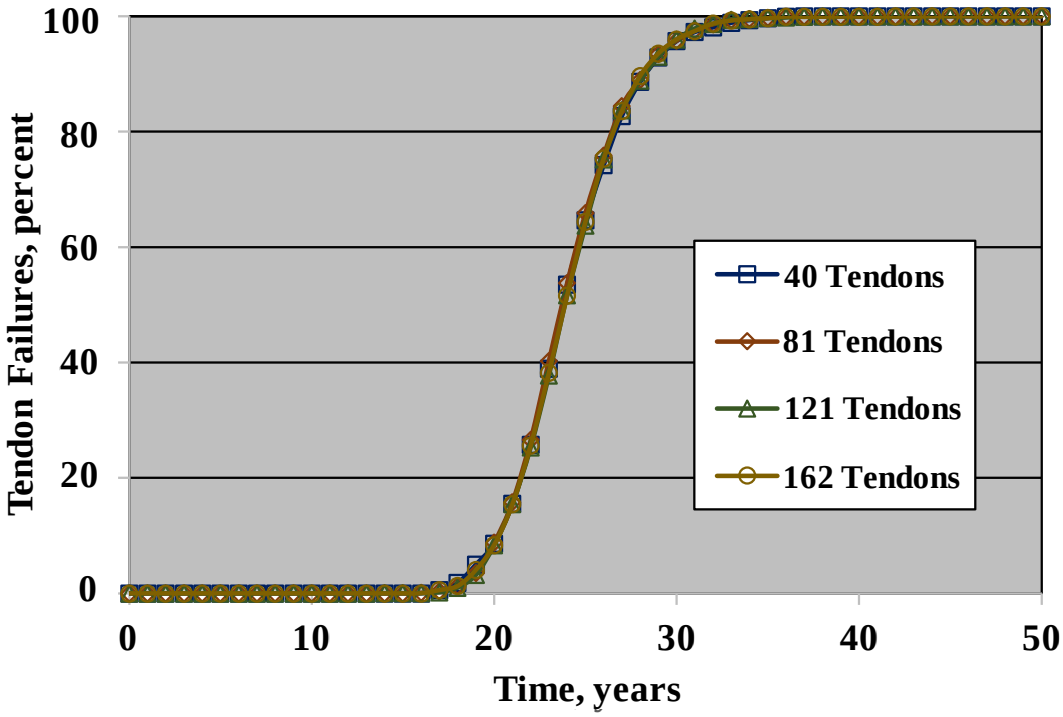

Source: FHWA.

Figure 97. Graph. Plot of the percentage of tendon failures as a function of time for systems with 40, 81, 121, and 162 tendons.

Effect of Tendon Length

Any effect of tendon length on onset of corrosion and resultant fractures/failures could arise from differences in exposed surface area and resultant corrosion rate distribution extremes. Consequently, the highest corrosion rate experienced at a local area on a relatively long tendon is likely to exceed that for a shorter one, all other factors being the same. The length of bridge PT tendons is typically in the range of 150 to 200 ft; however, these can be as short as 10 and as long as 500 ft. The present analysis methodology does not accommodate tendon length directly; however, insight into any effect of this variable can be gained by considering that a 500-ft-long tendon is equivalent, at least in a certain sense, to 50 10-ft ones, and so on. In this regard, the above analyses involving different numbers of tendons are relevant here. Thus, if a system with 162 tendons represents a length of 500 ft, then one with 121 tendons equates to a 375-ft length, 81 tendons to 250 ft, and 40 tendons to 123 ft. Table 67 lists T_f values for wires, strands, and tendons for each of these four numbers of tendons (40, 81, 121, and 162) and indicates a slight decrease in T_f for wires with an increasing number of tendons, but differences in the case of strands and tendons are probably random scatter (mean and standard deviation for corrosion rate were 3.0 mpy and 0.9, respectively). Reasons for this were discussed above, where apparently the different sets of random numbers that were necessarily employed for each analysis outweighed any effect of the number of tendons. However, this might not be the case for systems of shorter length, as represented by a smaller numbers of tendons. At the extreme, and employing the above rationale, a 10-ft-long tendon would be equivalent to a system composed of approximately 3 tendons, which is close to the case investigated above for Specimen Number

MS–0.4, where T_f for 162 tendons was determined as 0.32 yr, and for 4 tendons as 0.66 yr. However, the four tendons in this latter case had only four strands each.

Table 67. T_f for wires, strands, and tendons for four different numbers of tendons.

Component	40 Tendons T_f (Year)	81 Tendons T_f (Year)	121 Tendons T_f (Year)	162 Tendons T_f (Year)
Wire	9.8	9.2	8.9	9.1
Strand	16.5	15.8	14.0	16.0
Tendon	20.9	20.9	20.8	20.8

In view of the above, an analysis was performed for a system composed of three tendons, each with 22 strands, thus approximating the case of a 10-ft-long tendon. As above, mean corrosion rate was 3.0 mpy and standard deviation 0.9 in both cases. Figure 98 shows results of this analysis, and table 68 lists T_f for the 3 components in comparison to the case with 162 tendons. This shows that T_f is greater for the smaller tendon case, consistent with the difference in distribution extremes for the two instances. Particularly noteworthy is that strand fracture progression in the shorter tendon case, once initiated, does not follow a smooth trend but instead exhibits undulations. This is thought to be a consequence of the relatively small number of random numbers, in which case fractures/failures in very short tendons may be more unpredictable than for longer ones. Also, while the fracture progression rate for wires and strands, once initiated, is approximately the same in the two cases (3 versus 162 tendons), all three tendons are projected to fail within 2 yr. However, a moderating factor is that there is probably no load transference from fractured wires and strands to unfractured ones in the short tendon case, as assumed in the model. Consequently, unfractured wires and strands remain in displacement control and should be unaffected by fracture of others, except as possibly affected by an associated shock wave. Instead of attempting to take tendon length into account in analyzing specific situations, it is recommended that it simply be recognized that analysis results may be conservative in the case of very short tendons.

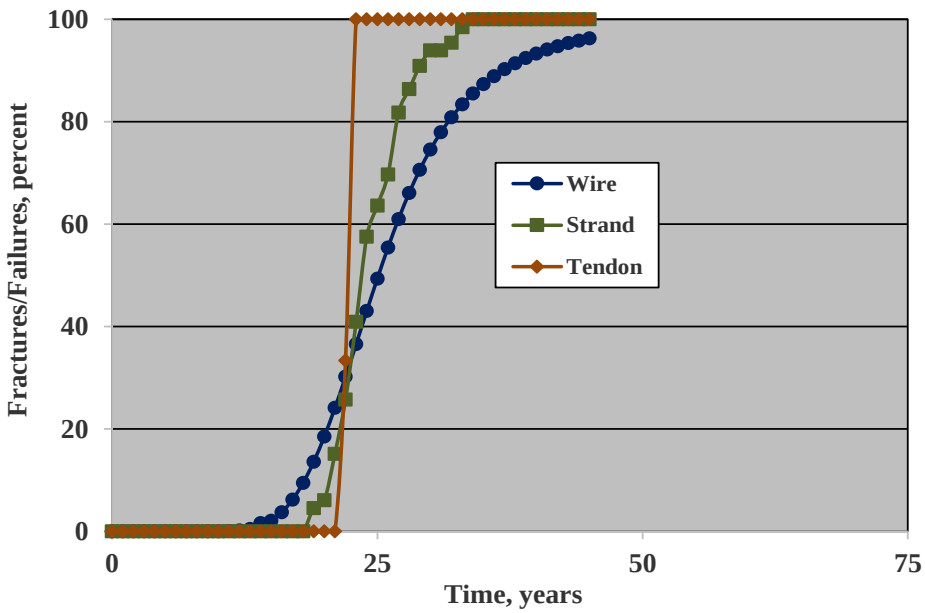

Source: FHWA.

Figure 98. Graph. Plot of fracture/failure progression for a 3-tendon system.

Table 68. T_f for wire, strand, and tendon T_f for systems with 3 compared to 162 tendons.

Component	3 Tendons T_f (Year)	162 Tendons T_f (Year)
Wire	12.7	9.1
Strand	18.3	16.0
Tendon	23.0	20.8

CHAPTER 4. FRACTURE AND FAILURE RATES SUBSEQUENT TO FIRST OCCURRENCE

GENERAL

As noted above, the fracture and failure rates listed in the preceding tables were determined at the inflection point of the T_f plots. These were provided for illustrative purposes only and are of little practical significance since. By the time they apply, fracture and failure rates would be unmanageable, and structure closure or collapse is likely to already have occurred. Of greater importance are such rates just subsequent to onset of fractures and failures since these provide bridge engineers with the degree of urgency at hand. To investigate these, such rates were determined for mean corrosion rates of 0.5, 0.6, 0.8, 1.0, 3.0, 4.0, 5.0, 10.0, and 20.0 mpy and $\sigma(CRE)/\mu(CRE)$ in each case of 0.3, 0.5, and 0.6.

Because the timeframe of wire and strand fractures and tendon failures differs widely for the above mean corrosion rates, results are presented in three ranges: $\mu(CRE)$ = 0.5–1.0, 3.0–5.0, and 10.0–20.0 mpy. Findings for each of these three groupings are presented in table 69 through table 104, and figure 99 through figure 116 for the specific case of $\sigma(CRE)/\mu(CRE) = 0.5$.[1] Results for $\sigma(CRE)/\mu(CRE)$ = 0.3 and 0.6 are shown in appendixes A and B, respectively. Both the number and percentage of fractures/failures versus time are shown, the former applying to the specific case of 162 tendons, and the latter being independent of the number of tendons. Also indicated are the number and percentage per time increment.

[1]Some T_f results for $\sigma(CRE)/\mu(CRE)$ = 0.3 are presented in tables 19–27 and figures 54–62.

Table 69. Number of wire fractures as a function of time for $\mu(CRE)$ in the range of 0.5–1.0 mpy and $\sigma(CRE)/\mu(CRE) = 0.5$.

Exposure Time (Year)	$\mu(CRE)$ = 0.5 mpy	$\mu(CRE)$ = 0.6 mpy	$\mu(CRE)$ = 0.8 mpy	$\mu(CRE)$ = 1.0 mpy
20	0	0	0	0
22	0	0	0	1
24	0	0	0	3
26	0	0	1	8
28	0	0	1	19
30	0	0	3	42
32	0	0	7	85
34	0	1	14	159
36	0	1	27	274
38	0	2	49	439
40	0	3	85	660
42	1	6	141	941
44	1	10	222	1,281
46	2	16	333	1,679
48	3	27	479	2,130
50	5	42	660	2,630
52	8	65	880	3,173
54	13	97	1,138	3,754
56	19	141	1,434	4,367
58	29	199	1,765	5,005
60	42	274	2,130	5,663
62	61	366	2,526	6,333
64	85	479	2,951	7,010
66	118	611	3,401	7,688
68	159	766	3,875	8,362
70	211	941	4,367	9,027
72	274	1,138	4,876	9,677
74	350	1,356	5,398	10,308
76	439	1,595	5,929	10,916

Table 70. Number of wire fractures in successive 2-yr time increments for $\mu(CRE)$ in the range of 0.5–1.0 mpy and $\sigma(CRE)/\mu(CRE) = 0.5$.

Exposure Time (Year)	$\mu(CRE)$ = 0.5 mpy	$\mu(CRE)$ = 0.6 mpy	$\mu(CRE)$ = 0.8 mpy	$\mu(CRE)$ = 1.0 mpy
20	0	0	0	0
22	0	0	0	1
24	0	0	0	2
26	0	0	0	5
28	0	0	1	11
30	0	0	2	23
32	0	0	4	43
34	0	0	7	74
36	0	0	13	115
38	0	1	22	165
40	0	1	36	222
42	0	2	56	281
44	0	4	81	340
46	1	7	111	397
48	1	10	145	451
50	2	16	182	500
52	3	23	220	543
54	5	32	258	581
56	7	44	295	613
58	10	58	331	638
60	13	74	365	657
62	18	93	396	670
64	25	112	425	677
66	32	133	451	678
68	41	154	473	674
70	52	176	493	664
72	63	197	509	650
74	76	218	522	631
76	89	238	532	608

Table 71. Percent of wire fractures as a function of time for $\mu(CRE)$ in the range of 0.5–1.0 mpy and $\sigma(CRE)/\mu(CRE) = 0.5$.

Exposure Time (Year)	$\mu(CRE)$ = 0.5 mpy	$\mu(CRE)$ = 0.6 mpy	$\mu(CRE)$ = 0.8 mpy	$\mu(CRE)$ = 1.0 mpy
20	0.0	0.0	0.0	0.0
22	0.0	0.0	0.0	0.0
24	0.0	0.0	0.0	0.0
26	0.0	0.0	0.0	0.0
28	0.0	0.0	0.0	0.1
30	0.0	0.0	0.0	0.2
32	0.0	0.0	0.0	0.4
34	0.0	0.0	0.1	0.7
36	0.0	0.0	0.1	1.3
38	0.0	0.0	0.2	2.1
40	0.0	0.0	0.4	3.1
42	0.0	0.0	0.7	4.4
44	0.0	0.0	1.0	6.0
46	0.0	0.1	1.6	7.9
48	0.0	0.1	2.2	10.0
50	0.0	0.2	3.1	12.3
52	0.0	0.3	4.1	14.8
54	0.1	0.5	5.3	17.6
56	0.1	0.7	6.7	20.4
58	0.1	0.9	8.3	23.4
60	0.2	1.3	10.0	26.5
62	0.3	1.7	11.8	29.6
64	0.4	2.2	13.8	32.8
66	0.6	2.9	15.9	36.0
68	0.7	3.6	18.1	39.1
70	1.0	4.4	20.4	42.2
72	1.3	5.3	22.8	45.3
74	1.6	6.3	25.2	48.2
76	2.1	7.5	27.7	51.0

Table 72. Percent of wire fractures as a function of time for $\mu(CRE)$ in the range of 0.5–1.0 mpy and $\sigma(CRE)/\mu(CRE) = 0.5$.

Exposure Time (Year)	$\mu(CRE)$ = 0.5 mpy	$\mu(CRE)$ = 0.6 mpy	$\mu(CRE)$ = 0.8 mpy	$\mu(CRE)$ = 1.0 mpy
20	0.0	0.0	0.0	0.0
22	0.0	0.0	0.0	0.0
24	0.0	0.0	0.0	0.0
26	0.0	0.0	0.0	0.0
28	0.0	0.0	0.0	0.1
30	0.0	0.0	0.0	0.1
32	0.0	0.0	0.0	0.2
34	0.0	0.0	0.0	0.3
36	0.0	0.0	0.1	0.5
38	0.0	0.0	0.1	0.8
40	0.0	0.0	0.2	1.0
42	0.0	0.0	0.3	1.3
44	0.0	0.0	0.4	1.6
46	0.0	0.0	0.5	1.9
48	0.0	0.0	0.7	2.1
50	0.0	0.1	0.9	2.3
52	0.0	0.1	1.0	2.5
54	0.0	0.2	1.2	2.7
56	0.0	0.2	1.4	2.9
58	0.0	0.3	1.5	3.0
60	0.1	0.3	1.7	3.1
62	0.1	0.4	1.9	3.1
64	0.1	0.5	2.0	3.2
66	0.2	0.6	2.1	3.2
68	0.2	0.7	2.2	3.2
70	0.2	0.8	2.3	3.1
72	0.3	0.9	2.4	3.0
74	0.4	1.0	2.4	3.0
76	0.4	1.1	2.5	2.8

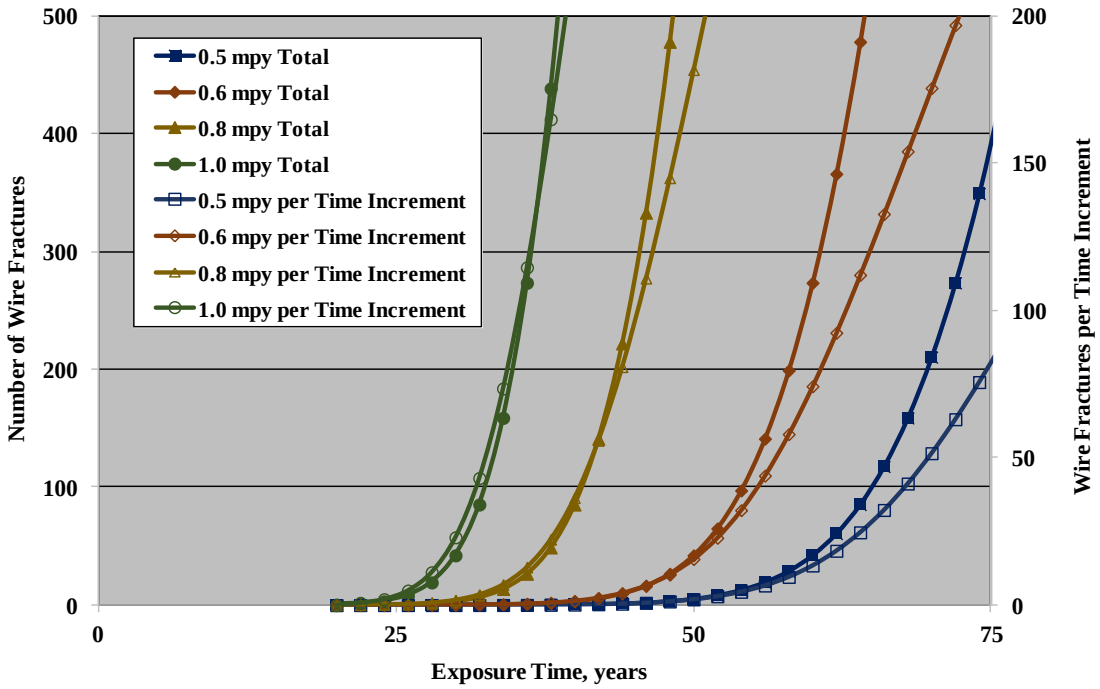

Source: FHWA.

Figure 99. Graph. Number of wire fractures and number per time increment versus time for $\mu(CRE)$ = 0.5, 0.6, 0.8, and 1.0 mpy and $\sigma(CRE)/\mu(CRE)$ = 0.5.

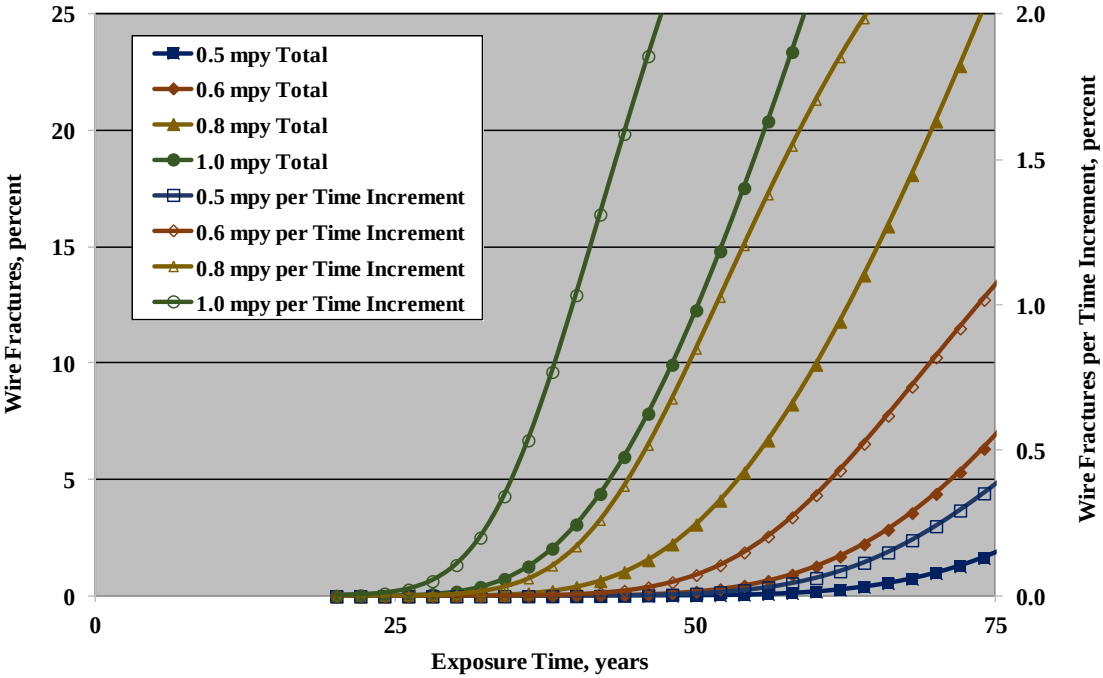

Source: FHWA.

Figure 100. Graph. Percent of wire fractures and percent per time increment versus time for $\mu(CRE)$ = 0.5, 0.6, 0.8, and 1.0 mpy and $\sigma(CRE)/\mu(CRE)$ = 0.5.

Table 73. Number of wire fractures as a function of time for $\mu(CRE)$ = 3.0, 4.0, and 5.0 mpy and $\sigma(CRE)/\mu(CRE)$ = 0.5.

Exposure Time (Year)	$\mu(CRE)$ = 3.0 mpy	$\mu(CRE)$ = 4.0 mpy	$\mu(CRE)$ = 5.0 mpy
0	0	0	0
1	0	0	0
2	0	0	0
3	0	0	0
4	0	0	0
5	0	0	5
6	0	3	42
7	1	19	211
8	3	85	660
9	13	274	1,473
10	43	660	2,630
11	120	1,281	4,057
12	278	2,130	5,663
13	551	3,173	7,349
14	956	4,367	9,027
15	1,495	5,663	—

—No information available.

Table 74. Number of wire fractures per time increment for $\mu(CRE)$ =3.0, 4.0, and 5.0 mpy and $\sigma(CRE)/\mu(CRE)$ = 0.5.

Exposure Time (Year)	$\mu(CRE)$ = 3.0 mpy	$\mu(CRE)$ = 4.0 mpy	$\mu(CRE)$ = 5.0 mpy
0	0	0	0
1	0	0	0
2	0	0	0
3	0	0	0
4	0	0	0
5	0	0	5
6	0	3	37
7	1	16	168
8	3	66	450
9	10	188	813
10	30	387	1,156
11	77	621	1,428
12	158	848	1,605
13	273	1,043	1,687
14	405	1,194	1,678
15	540	1,295	—

—No information available.

Table 75. Percent of wire fractures as a function of time for $\mu(CRE)$ = 3.0, 4.0, and 5.0 mpy and $\sigma(CRE)/\mu(CRE)$ = 0.5.

Exposure Time (Year)	$\mu(CRE)$ = 3.0 mpy	$\mu(CRE)$ = 4.0 mpy	$\mu(CRE)$ = 5.0 mpy
0	0.0	0.0	0.0
1	0.0	0.0	0.0
2	0.0	0.0	0.0
3	0.0	0.0	0.0
4	0.0	0.0	0.0
5	0.0	0.0	0.0
6	0.0	0.0	0.2
7	0.0	0.1	1.0
8	0.0	0.4	3.1
9	0.1	1.3	6.9
10	0.2	3.1	12.3
11	0.6	6.0	19.0
12	1.3	10.0	26.5
13	2.6	14.8	34.4
14	4.5	20.4	42.2
15	7.0	26.5	—

—No information available.

Table 76. Percent of wire fractures per time increment for $\mu(CRE)$ = 3.0, 4.0, and 5.0 mpy and $\sigma(CRE)/\mu(CRE)$ = 0.5.

Exposure Time (Year)	$\mu(CRE)$ = 3.0 mpy	$\mu(CRE)$ = 4.0 mpy	$\mu(CRE)$ = 5.0 mpy
0	0.0	0.0	0.0
1	0.0	0.0	0.0
2	0.0	0.0	0.0
3	0.0	0.0	0.0
4	0.0	0.0	0.0
5	0.0	0.0	0.0
6	0.0	0.0	0.2
7	0.0	0.1	0.6
8	0.0	0.2	1.3
9	0.0	0.6	1.7
10	0.1	0.9	1.6
11	0.2	1.1	1.3
12	0.4	1.1	0.8
13	0.5	0.9	—
14	0.6	—	—
15	0.6	—	—

—No information available.

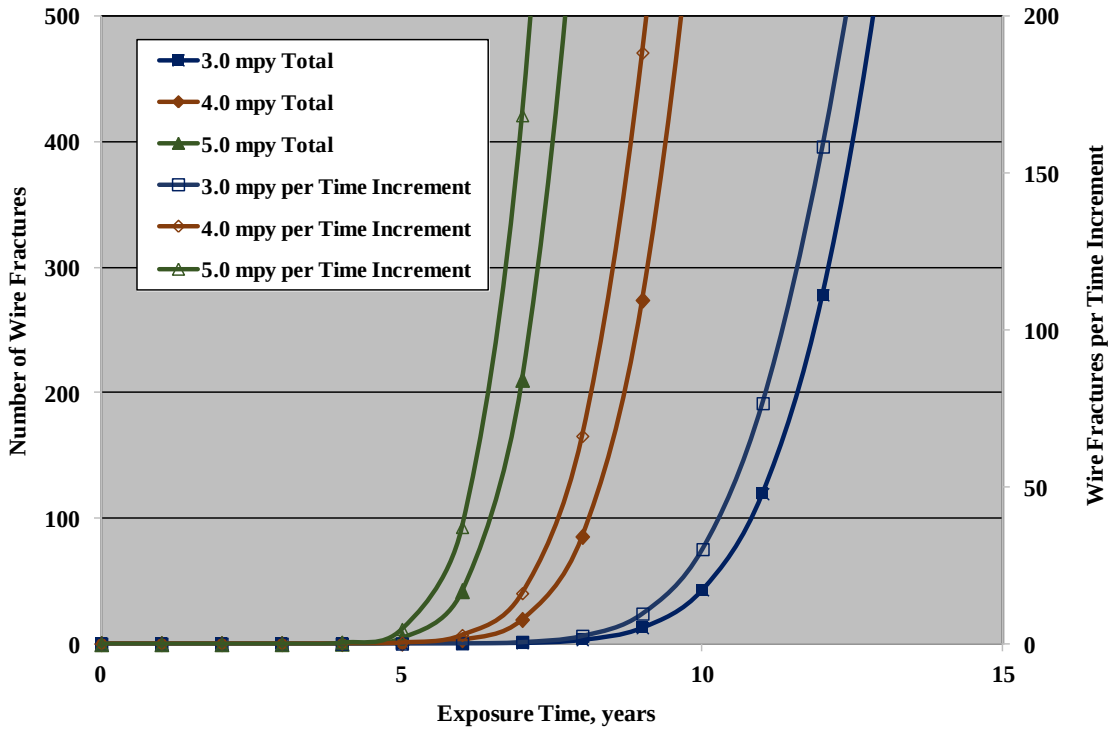

Source: FHWA.

Figure 101. Graph. Number of wire fractures and number per time increment versus time for $\mu(CRE)$ = 3.0, 4.0, and 5.0 mpy and $\sigma(CRE)/\mu(CRE)$ = 0.5.

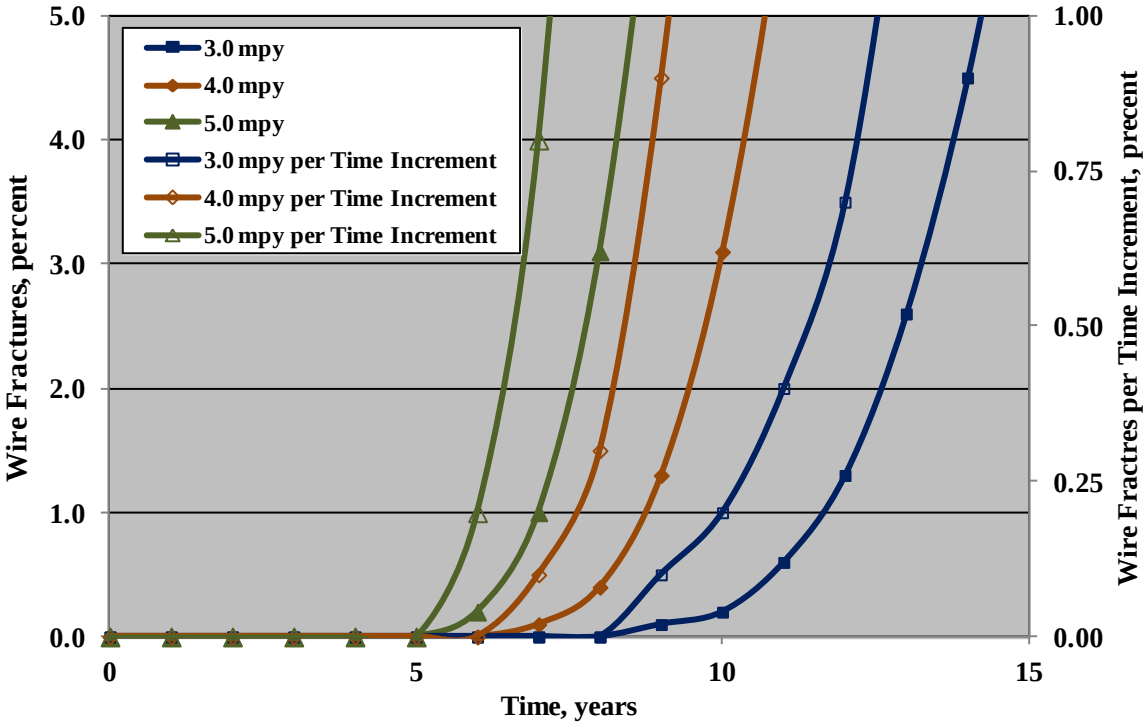

Source: FHWA.

Figure 102. Graph. Percent of wire fractures and percent per time increment versus time for $\mu(CRE)$ = 3.0, 4.0, and 5.0 mpy and $\sigma(CRE)/\mu(CRE)$ = 0.5.

Table 77. Number of wire fractures as a function of time for $\mu(CRE)$ = 10.0 and 20.0 mpy and $\sigma(CRE)/\mu(CRE)$ = 0.5.

Exposure Time (Year)	$\mu(CRE)$ = 10.0 mpy	$\mu(CRE)$ = 20.0 mpy
0.00	0	0
0.25	0	0
0.50	0	0
0.75	0	0
1.00	0	0
1.25	0	5
1.50	0	42
1.75	0	211
2.00	0	660
2.25	2	1,473
2.50	5	2,630
2.75	16	4,057
3.00	43	5,663
3.25	102	7,349
3.50	214	9,027
3.75	398	10,615
4.00	670	12,051
4.25	1,036	13,298
4.50	1,495	14,351
4.75	2,043	15,226
5.00	2,669	15,951

Table 78. Number of wire fractures per time increment for $\mu(CRE)$ = 10.0 and 20.0 mpy and $\sigma(CRE)/\mu(CRE)$ = 0.5.

Exposure Time (Year)	$\mu(CRE)$ = 10.0 mpy	$\mu(CRE)$ = 20.0 mpy
0.00	0	0
0.25	0	0
0.50	0	0
0.75	0	0
1.00	0	0
1.25	0	5
1.50	0	37
1.75	0	168
2.00	0	450
2.25	1	813
2.50	4	1,156
2.75	11	1,428
3.00	27	1,605
3.25	59	1,687
3.50	112	1,677
3.75	185	1,588
4.00	272	1,436
4.25	366	1,247
4.50	459	1,053
4.75	547	875
5.00	627	725

Table 79. Percent of wire fractures versus time for $\mu(CRE)$ = 10.0 and 20.0 mpy and $\sigma(CRE)/\mu(CRE)$ = 0.5.

Exposure Time (Year)	$\mu(CRE)$ = 10.0 mpy	$\mu(CRE)$ = 20.0 mpy
0.00	0.0	0.0
0.25	0.0	0.0
0.50	0.0	0.0
0.75	0.0	0.0
1.00	0.0	0.0
1.25	0.0	0.0
1.50	0.0	0.2
1.75	0.0	1.0
2.00	0.0	3.1
2.25	0.0	6.9
2.50	0.0	12.3
2.75	0.1	19.0
3.00	0.2	26.5
3.25	0.5	34.4
3.50	1.0	42.2
3.75	1.9	49.6
4.00	3.1	56.4
4.25	4.8	62.2
4.50	7.0	67.1
4.75	9.6	71.2
5.00	12.5	74.6

Table 80. Percent of wire fractures per time increment for $\mu(CRE)$ = 10.0 and 20.0 mpy and $\sigma(CRE)/\mu(CRE)$ = 0.5.

Exposure Time (Year)	$\mu(CRE)$ = 10.0 mpy	$\mu(CRE)$ = 20.0 mpy
0.00	0.0	0.0
0.25	0.0	0.0
0.50	0.0	0.0
0.75	0.0	0.0
1.00	0.0	0.0
1.25	0.0	0.0
1.50	0.0	0.2
1.75	0.0	0.8
2.00	0.0	2.1
2.25	0.0	3.8
2.50	0.0	5.4
2.75	0.0	6.7
3.00	0.1	7.5
3.25	0.3	7.9
3.50	0.5	7.8
3.75	0.9	7.4
4.00	1.3	6.7
4.25	1.7	5.8
4.50	2.1	4.9
4.75	2.6	4.1
5.00	2.9	3.4

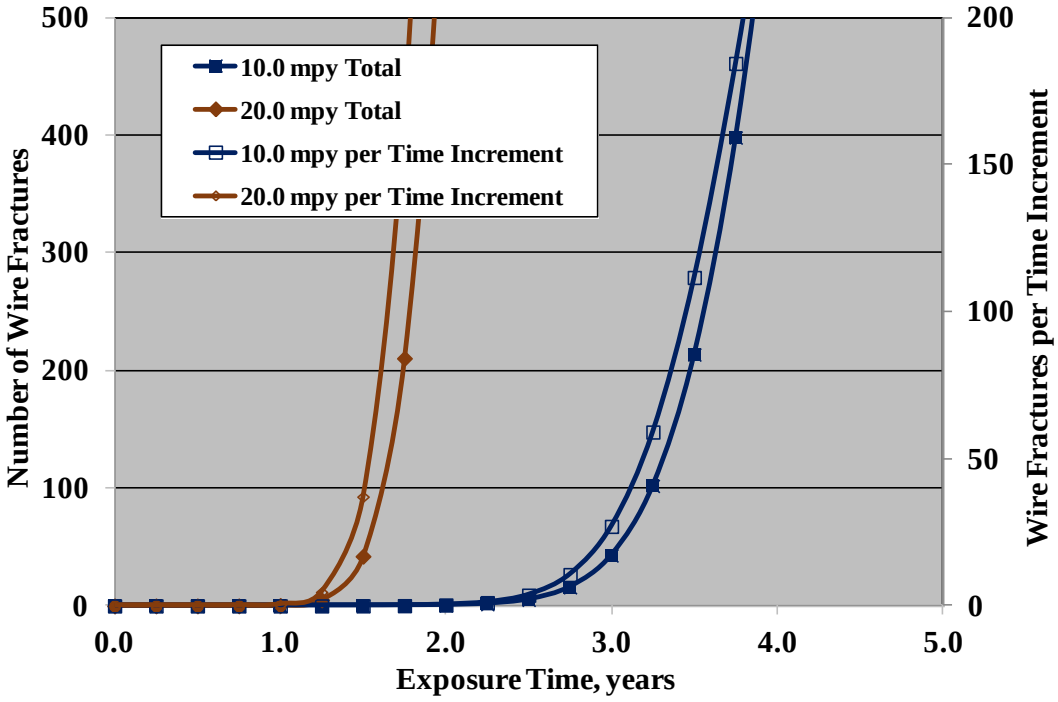

Source: FHWA.

Figure 103. Graph. Number of wire fractures and number per time increment versus time for $\mu(CRE)$ = 10.0 and 20.0 mpy and $\sigma(CRE)/\mu(CRE)$ = 0.5.

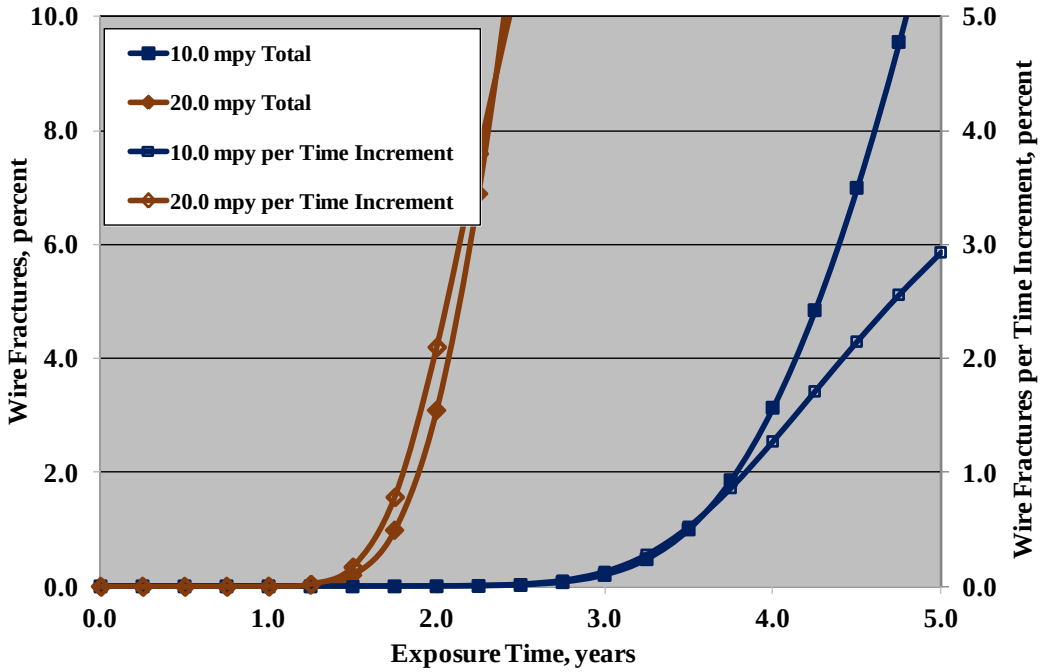

Source: FHWA.

Figure 104. Graph. Percent of wire fractures and percent per time increment versus time for $\mu(CRE)$ = 10.0 and 20.0 mpy and $\sigma(CRE)/\mu(CRE)$ = 0.5.

Table 81. Strand fractures versus time for $\mu(CRE)$ = 0.5, 0.6, 0.8, and 1.0 mpy and $\sigma(CRE)/\mu(CRE)$ = 0.5.

Exposure Time (Year)	$\mu(CRE)$ = 0.5 mpy	$\mu(CRE)$ = 0.6 mpy	$\mu(CRE)$ = 0.8 mpy	$\mu(CRE)$ = 1.0 mpy
36	0	0	0	0
38	0	0	0	0
40	0	0	0	1
42	0	0	0	6
44	0	0	0	13
46	0	0	0	10
48	0	0	0	27
50	0	0	1	56
52	0	0	4	64
54	0	0	8	84
56	0	0	11	114
58	0	0	11	136
60	0	0	22	165
62	0	0	44	197
64	0	0	48	191
66	0	0	56	237
68	0	0	76	210
70	0	1	94	258
72	0	0	110	—
74	0	7	115	—
76	0	6	142	—

—No information available.

Table 82. Strand fractures per time increment for $\mu(CRE)$ = 0.50, 0.60, 0.80, and 1.0 mpy and $\sigma(CRE)/\mu(CRE)$ = 0.5.

Exposure Time (Year)	$\mu(CRE)$ = 0.5 mpy	$\mu(CRE)$ = 0.6 mpy	$\mu(CRE)$ = 0.8 mpy	$\mu(CRE)$ = 1.0 mpy
36	0.0	0.0	0.0	0.0
38	0.0	0.0	0.0	0.0
40	0.0	0.0	0.0	0.0
42	0.0	0.0	0.0	0.2
44	0.0	0.0	0.0	0.4
46	0.0	0.0	0.0	0.3
48	0.0	0.0	0.0	0.8
50	0.0	0.0	0.0	1.6
52	0.0	0.0	0.1	1.8
54	0.0	0.0	0.2	2.4
56	0.0	0.0	0.3	3.2
58	0.0	0.0	0.3	3.8
60	0.0	0.0	0.6	4.6
62	0.0	0.0	1.2	5.5
64	0.0	0.0	1.3	5.4
66	0.0	0.0	1.6	6.6
68	0.0	0.0	2.1	5.9
70	0.0	0.0	2.6	7.2
72	0.0	0.0	3.1	—
74	0.0	0.2	3.2	—
76	0.0	0.2	4.0	—

—No information available.

Table 83. Percent of strand fractures versus time for $\mu(CRE)$ = 0.50, 0.60, 0.80, and 1.0 mpy and $\sigma(CRE)/\mu(CRE)$ = 0.5.

Exposure Time (Year)	$\mu(CRE)$ = 0.5 mpy	$\mu(CRE)$ = 0.6 mpy	$\mu(CRE)$ = 0.8 mpy	$\mu(CRE)$ = 1.0 mpy
36	0.0	0.0	0.0	0.0
38	0.0	0.0	0.0	0.0
40	0.0	0.0	0.0	0.0
42	0.0	0.0	0.0	0.2
44	0.0	0.0	0.0	0.6
46	0.0	0.0	0.0	0.8
48	0.0	0.0	0.0	1.6
50	0.0	0.0	0.0	3.2
52	0.0	0.0	0.1	5
54	0.0	0.0	0.4	7.3
56	0.0	0.0	0.7	10.5
58	0.0	0.0	1.0	14.3
60	0.0	0.0	1.6	19.0
62	0.0	0.0	2.8	24.5
64	0.0	0.0	4.2	29.9
66	0.0	0.0	5.8	36.5
68	0.0	0.0	7.9	42.4
70	0.0	0.0	10.5	49.6
72	0.0	0.0	13.6	—
74	0.0	0.2	16.8	—
76	0.0	0.4	20.8	—

—No information available.

Table 84. Percent of strand fractures per time increment for $\mu(CRE)$ = 0.50, 0.60, 0.80, and 1.0 mpy and $\sigma(CRE)/\mu(CRE)$ = 0.5.

Exposure Time (Year)	$\mu(CRE)$ = 0.5 mpy	$\mu(CRE)$ = 0.6 mpy	$\mu(CRE)$ = 0.8 mpy	$\mu(CRE)$ = 1.0 mpy
36	0.0	0.0	0.0	0.0
38	0.0	0.0	0.0	0.0
40	0.0	0.0	0.0	0.0
42	0.0	0.0	0.0	0.2
44	0.0	0.0	0.0	0.4
46	0.0	0.0	0.0	0.3
48	0.0	0.0	0.0	0.8
50	0.0	0.0	0.0	1.6
52	0.0	0.0	0.1	1.8
54	0.0	0.0	0.2	2.4
56	0.0	0.0	0.3	3.2
58	0.0	0.0	0.3	3.8
60	0.0	0.0	0.6	4.6
62	0.0	0.0	1.2	5.5
64	0.0	0.0	1.3	5.4
66	0.0	0.0	1.6	6.6
68	0.0	0.0	2.1	5.9
70	0.0	0.0	2.6	7.2
72	0.0	0.0	3.1	—
74	0.0	0.2	3.2	—
76	0.0	0.2	4.0	—

—No information available.

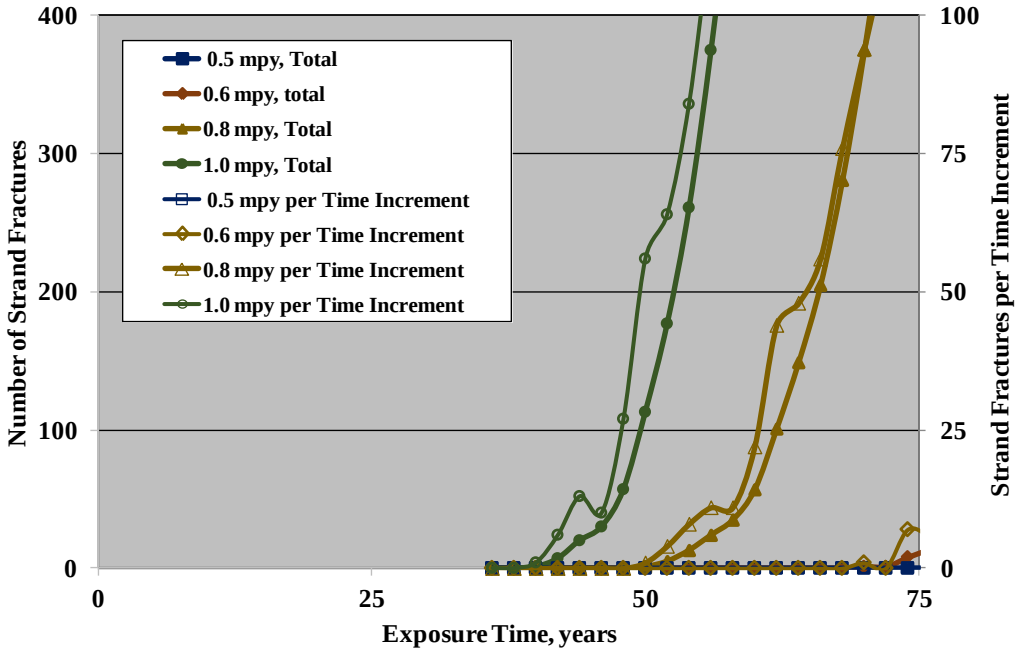

Source: FHWA.

Figure 105. Graph. Number of strand fractures and number per time increment versus time for $\mu(CRE)$ = 0.5, 0.6, 0.8, and 1.0 mpy and $\sigma(CRE)/\mu(CRE)$ = 0.5.

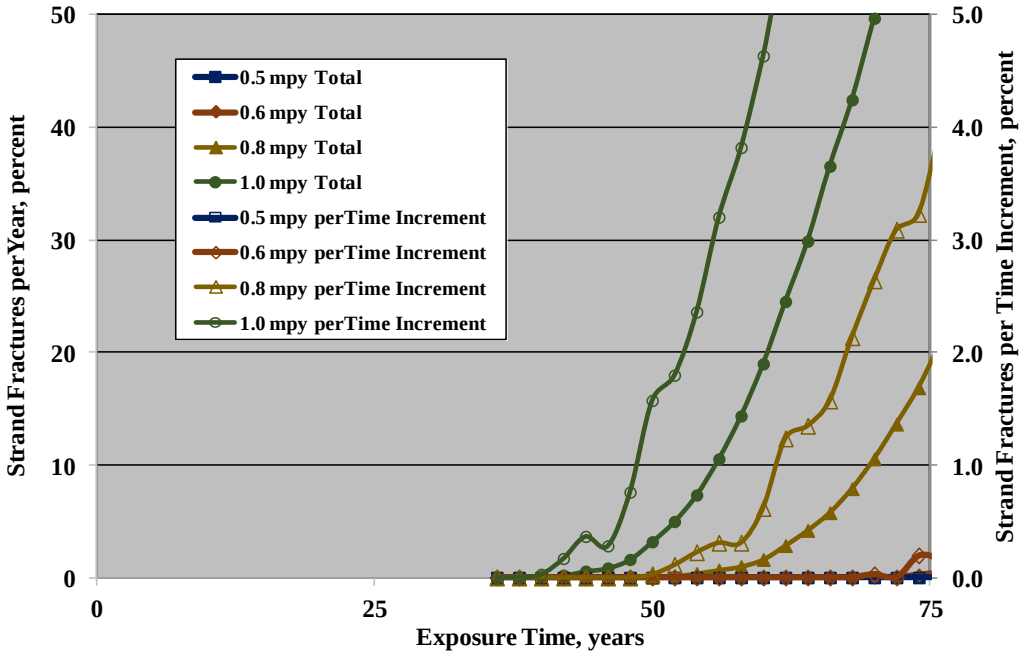

Source: FHWA.

Figure 106. Graph. Percent of strand fractures and percent per time increment versus time for $\mu(CRE)$ = 0.5, 0.6, 0.8, and 1.0 mpy and $\sigma(CRE)/\mu(CRE)$ = 0.5.

Table 85. Strand fractures versus time for $\mu(CRE)$ = 3.0, 4.0, and 5.0 mpy and $\sigma(CRE)/\mu(CRE)$ = 0.5.

Exposure Time (Year)	$\mu(CRE)$ = 3.0 mpy	$\mu(CRE)$ = 4.0 mpy	$\mu(CRE)$ = 5.0 mpy
0	0	0	0
1	0	0	0
2	0	0	0
3	0	0	0
4	0	0	0
5	0	0	0
6	0	0	0
7	0	0	0
8	0	0	1
9	0	0	24
10	0	1	115
11	0	20	314
12	0	58	681
13	0	179	1,189
14	7	379	1,784
15	24	681	2,321

Table 86. Strand fractures per time increment for $\mu(CRE)$ = 3.0, 4.0, and 5.0 mpy and $\sigma(CRE)/\mu(CRE)$ = 0.5.

Exposure Time (Year)	$\mu(CRE)$ = 3.0 mpy	$\mu(CRE)$ = 4.0 mpy	$\mu(CRE)$ = 5.0 mpy
0	0	0	0
1	0	0	0
2	0	0	0
3	0	0	0
4	0	0	0
5	0	0	0
6	0	0	0
7	0	0	0
8	0	0	1
9	0	0	23
10	0	1	91
11	0	19	199
12	0	38	367
13	0	121	—
14	7	200	—
15	17	302	—

—No information available.

Table 87. Percent of strand fractures versus time for $\mu(CRE)$ = 3.0, 4.0, and 5.0 mpy and $\sigma(CRE)/\mu(CRE)$ = 0.5.

Exposure Time (Year)	$\mu(CRE)$ = 3.0 mpy	$\mu(CRE)$ = 4.0 mpy	$\mu(CRE)$ = 5.0 mpy
0	0.0	0.0	0.0
1	0.0	0.0	0.0
2	0.0	0.0	0.0
3	0.0	0.0	0.0
4	0.0	0.0	0.0
5	0.0	0.0	0.0
6	0.0	0.0	0.0
7	0.0	0.0	0.0
8	0.0	0.0	0.0
9	0.0	0.0	0.7
10	0.0	0.0	3.2
11	0.0	0.6	8.8
12	0.0	1.6	19.1
13	0.0	5.0	33.4
14	0.2	10.6	50.1
15	0.7	19.1	65.1

Table 88. Percent of strand fractures per time increment for $\mu(CRE)$ = 3.0, 4.0, and 5.0 mpy and $\sigma(CRE)/\mu(CRE)$ = 0.5.

Exposure Time (Year)	$\mu(CRE)$ = 3.0 mpy	$\mu(CRE)$ = 4.0 mpy	$\mu(CRE)$ = 5.0 mpy
0	0.0	0.0	0.0
1	0.0	0.0	0.0
2	0.0	0.0	0.0
3	0.0	0.0	0.0
4	0.0	0.0	0.0
5	0.0	0.0	0.0
6	0.0	0.0	0.0
7	0.0	0.0	0.0
8	0.0	0.0	0.0
9	0.0	0.0	0.6
10	0.0	0.0	1.9
11	0.0	0.5	3.0
12	0.0	0.5	4.7
13	0.0	2.3	—
14	0.2	2.2	—
15	0.3	2.9	—

—No information available.

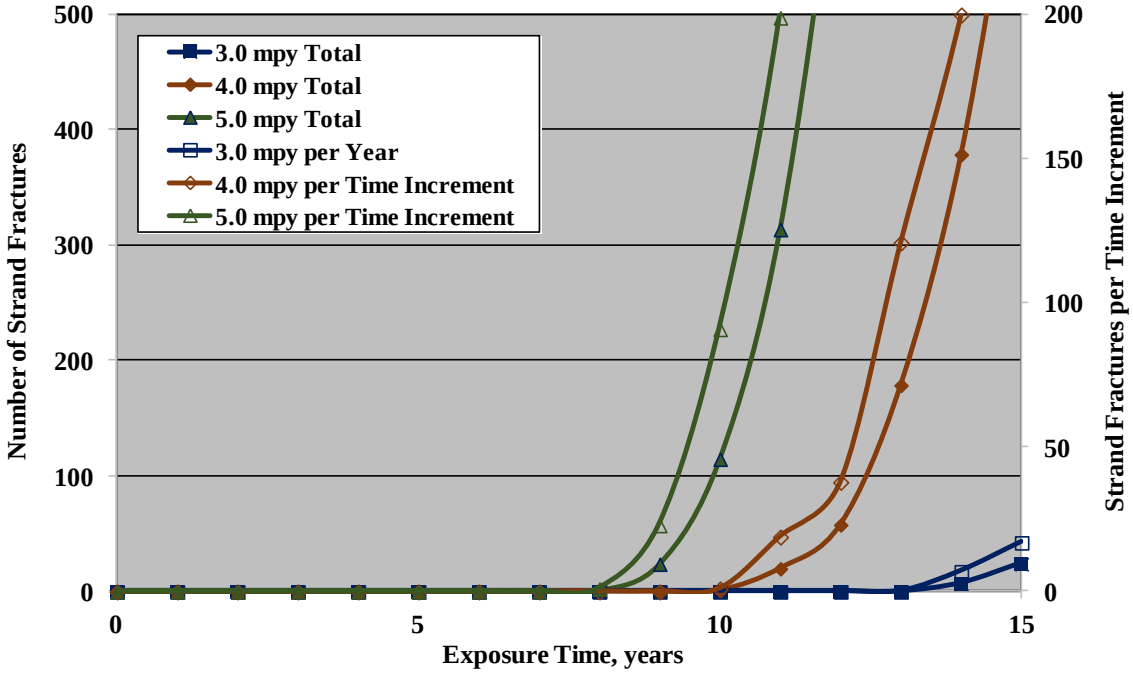

Source: FHWA.

Figure 107. Graph. Number of strand fractures and number per time increment versus time for $\mu(CRE)$ = 3.0, 4.0, and 5.0 mpy and $\sigma(CRE)/\mu(CRE)$ = 0.5.

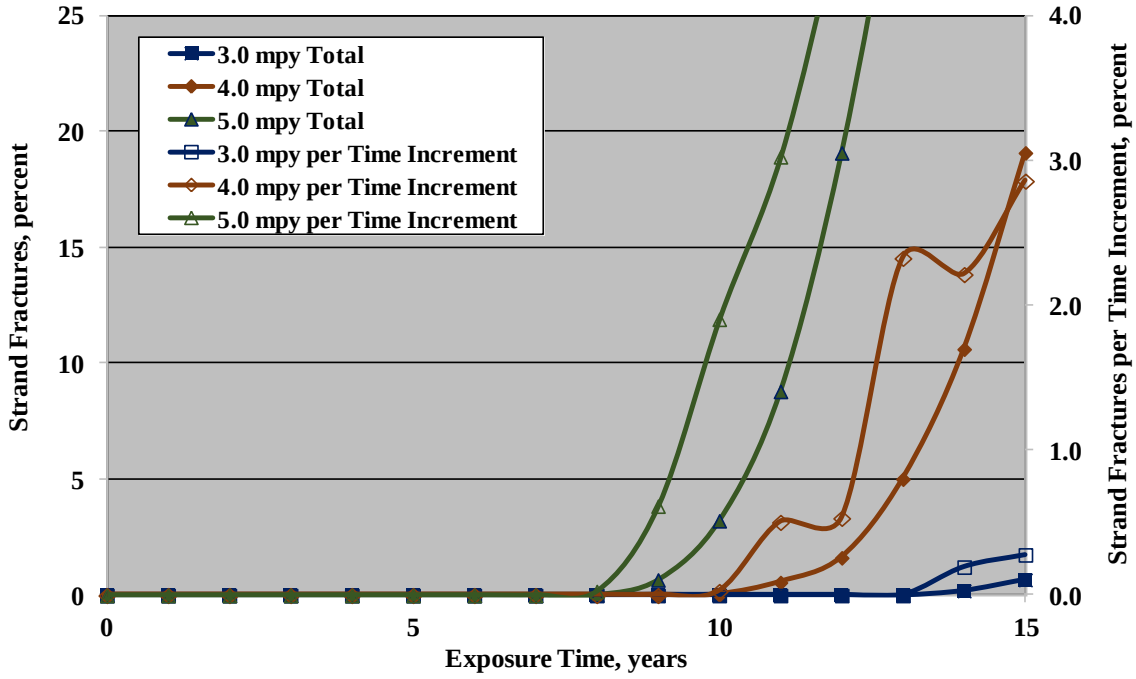

Source: FHWA.

Figure 108. Graph. Percent of strand fractures and percent per time increment versus time for $\mu(CRE)$ = 3.0, 4.0, and 5.0 mpy and $\sigma(CRE)/\mu(CRE)$ = 0.5.

Table 89. Strand fractures versus time for $\mu(CRE)$ = 3.0, 4.0, and 5.0 mpy and $\sigma(CRE)/\mu(CRE)$ = 0.5.

Exposure Time (Year)	$\mu(CRE)$ = 10.0 mpy	$\mu(CRE)$ = 20.0 mpy
0.00	0	0
0.25	0	0
0.50	0	0
0.75	0	0
1.00	0	0
1.25	0	0
1.50	0	0
1.75	0	0
2.00	0	0
2.25	0	0
2.50	0	13
2.75	0	76
3.00	0	299
3.25	0	776
3.50	0	1,530
3.75	0	2,295
4.00	1	2,882
4.25	11	—
4.50	24	—
4.75	48	—
5.00	117	—

—No information available.

Table 90. Strand fractures per time increment for $\mu(CRE)$ = 10.0 and 20.0 mpy and $\sigma(CRE)/\mu(CRE)$ = 0.5.

Exposure Time (Year)	$\mu(CRE)$ = 10.0 mpy	$\mu(CRE)$ = 20.0 mpy
0.00	0	0
0.25	0	0
0.50	0	0
0.75	0	0
1.00	0	0
1.25	0	0
1.50	0	0
1.75	0	0
2.00	0	0
2.25	0	0
2.50	0	13
2.75	0	63
3.00	0	223
3.25	0	477
3.50	0	754
3.75	0	765
4.00	1	587
4.25	10	—
4.50	13	—
4.75	24	—
5.00	69	—

—No information available.

Table 91. Percent of strand fractures versus time for $\mu(CRE)$ = 10.0 and 20.0 mpy and $\sigma(CRE)/\mu(CRE)$ = 0.5.

Exposure Time (Year)	$\mu(CRE)$ = 10.0 mpy	$\mu(CRE)$ = 20.0 mpy
0.00	0.0	0.0
0.25	0.0	0.0
0.50	0.0	0.0
0.75	0.0	0.0
1.00	0.0	0.0
1.25	0.0	0.0
1.50	0.0	0.0
1.75	0.0	0.0
2.00	0.0	0.0
2.25	0.0	0.0
2.50	0.0	0.4
2.75	0.0	2.1
3.00	0.0	8.4
3.25	0.0	21.8
3.50	0.0	42.9
3.75	0.0	64.4
4.00	0.0	80.9
4.25	0.3	—
4.50	0.7	—
4.75	1.3	—
5.00	3.3	—

—No information available.

Table 92. Percent of strand fractures per time increment for $\mu(CRE)$ = 10.0 and 20.0 mpy and $\sigma(CRE)/\mu(CRE)$ = 0.5.

Exposure Time (Year)	$\mu(CRE)$ = 10.0 mpy	$\mu(CRE)$ = 20.0 mpy
0.00	0	0
0.25	0	0
0.50	0	0
0.75	0	0
1.00	0	0
1.25	0	0
1.50	0	0
1.75	0	0
2.00	0	0
2.25	0	0
2.50	0	13
2.75	0	63
3.00	0	223
3.25	0	477
3.50	0	754
3.75	0	765
4.00	1	587
4.25	10	—
4.50	13	—
4.75	24	—
5.00	69	—

— No information available.

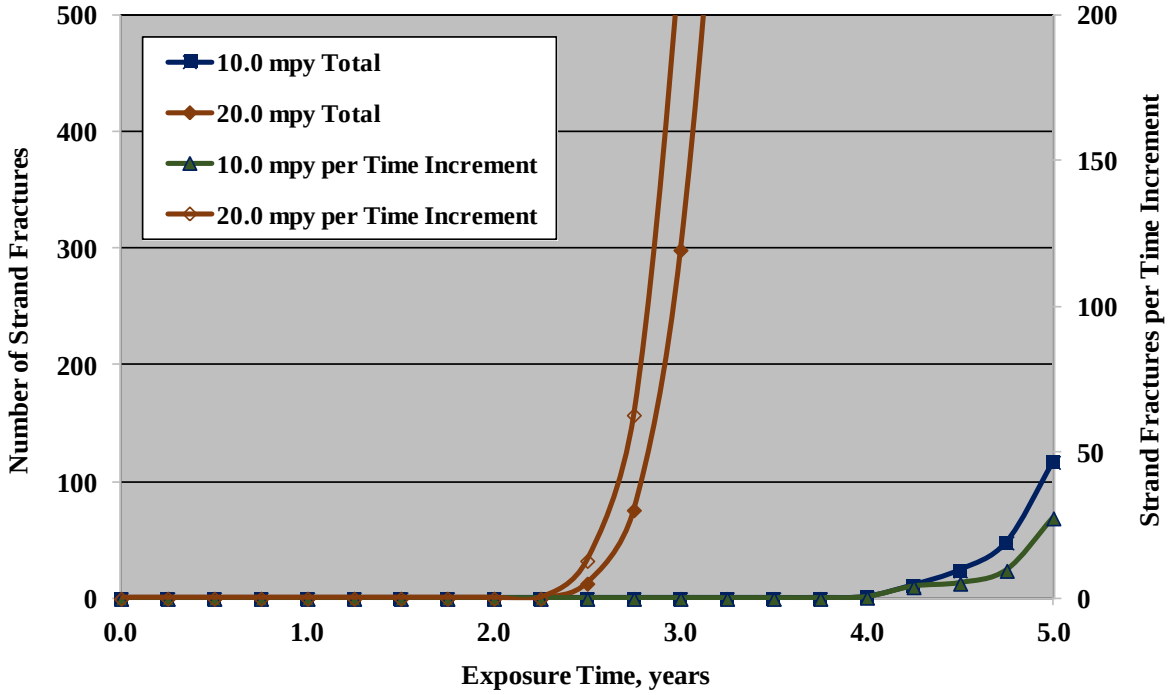

Source: FHWA.

Figure 109. Graph. Number of strand fractures and number per time increment versus time for $\mu(CRE)$ = 10 and 20 mpy and $\sigma(CRE)/\mu(CRE)$ = 0.5.

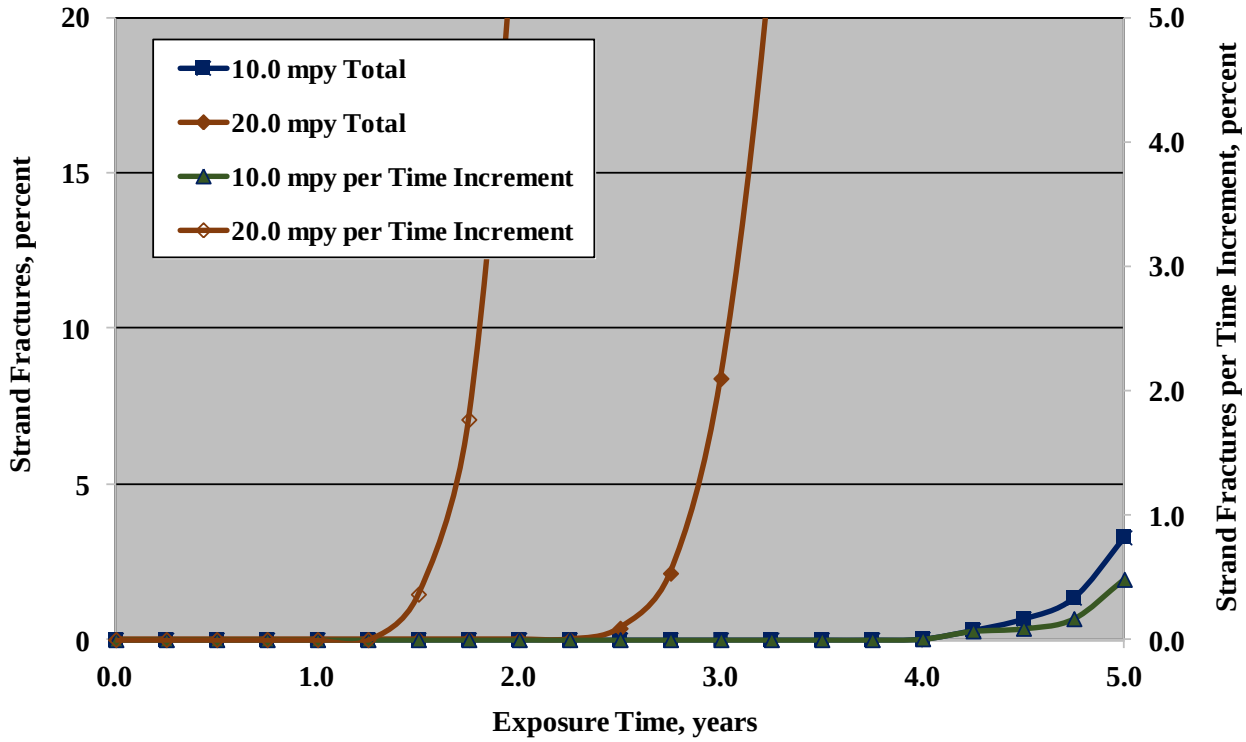

Source: FHWA.

Figure 110. Graph. Percent of strand fractures and percent per time increment versus time for $\mu(CRE)$ =10.0 and 20.0 mpy and $\sigma(CRE)/\mu(CRE)$ = 0.5.

Table 93. Number of tendon failures versus time for $\mu(CRE)$ = 0.5, 0.6, 0.8, and 1.0 mpy and $\sigma(CRE)/\mu(CRE)$ = 0.5.

Exposure Time (Year)	$\mu(CRE)$ = 0.5 mpy	$\mu(CRE)$ = 0.6 mpy	$\mu(CRE)$ = 0.8 mpy	$\mu(CRE)$ = 1.0 mpy
40	0	0	0	0
42	0	0	0	0
44	0	0	0	0
46	0	0	0	0
48	0	0	0	0
50	0	0	0	0
52	0	0	0	0
54	0	0	0	0
56	0	0	0	3
58	0	0	0	7
60	0	0	0	16
62	0	0	0	46
64	0	0	0	83
66	0	0	0	127
68	0	0	0	147
70	0	0	3	158
72	0	0	7	159
74	0	0	11	162
76	0	0	26	162

Table 94. Number of tendon failures per time increment for $\mu(CRE)$ = 0.5, 0.6, 0.8, and 1.0 mpy and $\sigma(CRE)/\mu(CRE)$ = 0.5.

Exposure Time (Year)	$\mu(CRE)$ = 0.5 mpy	$\mu(CRE)$ = 0.6 mpy	$\mu(CRE)$ = 0.8 mpy	$\mu(CRE)$ = 1.0 mpy
40	0	0	0	0
42	0	0	0	0
44	0	0	0	0
46	0	0	0	0
48	0	0	0	0
50	0	0	0	0
52	0	0	0	0
54	0	0	0	0
56	0	0	0	3
58	0	0	0	4
60	0	0	0	9
62	0	0	0	30
64	0	0	0	37
66	0	0	0	44
68	0	0	0	—
70	0	0	3	—
72	0	0	4	—
74	0	0	4	—
76	0	0	15	—

—No information available.

Table 95. Percent of tendon failures versus time for $\mu(CRE)$ = 0.5, 0.6, 0.8, and 1.0 mpy and $\sigma(CRE)/\mu(CRE)$ = 0.5.

Exposure Time (Year)	$\mu(CRE)$ = 0.5 mpy	$\mu(CRE)$ = 0.6 mpy	$\mu(CRE)$ = 0.8 mpy	$\mu(CRE)$ = 1.0 mpy
40	0.0	0.0	0.0	0.0
42	0.0	0.0	0.0	0.0
44	0.0	0.0	0.0	0.0
46	0.0	0.0	0.0	0.0
48	0.0	0.0	0.0	0.0
50	0.0	0.0	0.0	0.0
52	0.0	0.0	0.0	0.0
54	0.0	0.0	0.0	0.0
56	0.0	0.0	0.0	1.9
58	0.0	0.0	0.0	4.3
60	0.0	0.0	0.0	9.9
62	0.0	0.0	0.0	28.4
64	0.0	0.0	0.0	51.2
66	0.0	0.0	0.0	78.4
68	0.0	0.0	0.0	90.7
70	0.0	0.0	1.9	97.5
72	0.0	0.0	4.3	98.1
74	0.0	0.0	6.8	100.0
76	0.0	0.0	16.0	100.0

Table 96. Percent of tendon failures per unit time versus time for $\mu(CRE)$ = 0.5, 0.6, 0.8, and 1.0 mpy and $\sigma(CRE)/\mu(CRE)$ = 0.5.

Exposure Time (Year)	$\mu(CRE)$ = 0.5 mpy	$\mu(CRE)$ = 0.6 mpy	$\mu(CRE)$ = 0.8 mpy	$\mu(CRE)$ = 1.0 mpy
40	0.0	0.0	0.0	0.0
42	0.0	0.0	0.0	0.0
44	0.0	0.0	0.0	0.0
46	0.0	0.0	0.0	0.0
48	0.0	0.0	0.0	0.0
50	0.0	0.0	0.0	0.0
52	0.0	0.0	0.0	0.0
54	0.0	0.0	0.0	0.0
56	0.0	0.0	0.0	1.9
58	0.0	0.0	0.0	2.5
60	0.0	0.0	0.0	5.6
62	0.0	0.0	0.0	18.5
64	0.0	0.0	0.0	22.8
66	0.0	0.0	0.0	27.2
68	0.0	0.0	0.0	—
70	0.0	0.0	1.9	—
72	0.0	0.0	2.5	—
74	0.0	0.0	2.5	—
76	0.0	0.0	9.3	—

—No information available.

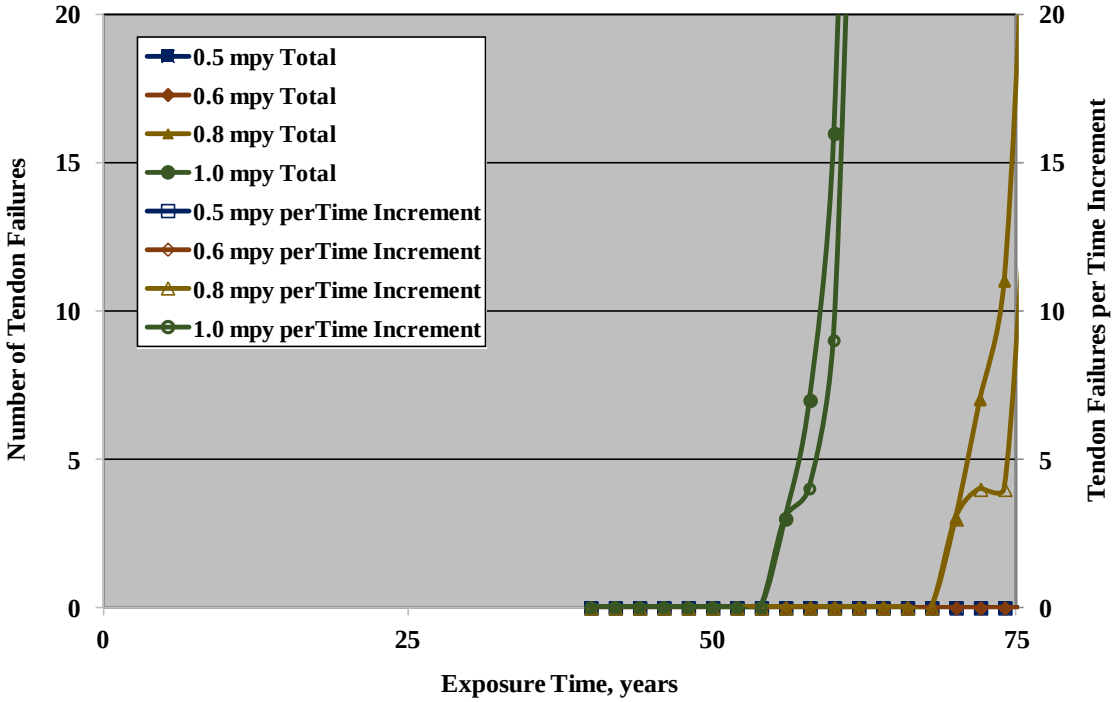

Source: FHWA.

Figure 111. Graph. Number of tendon failures and number per time increment versus time for $\mu(CRE)$ = 0.5, 0.6, 0.8, and 1.0 mpy and $\sigma(CRE)/\mu(CRE)$ = 0.5.

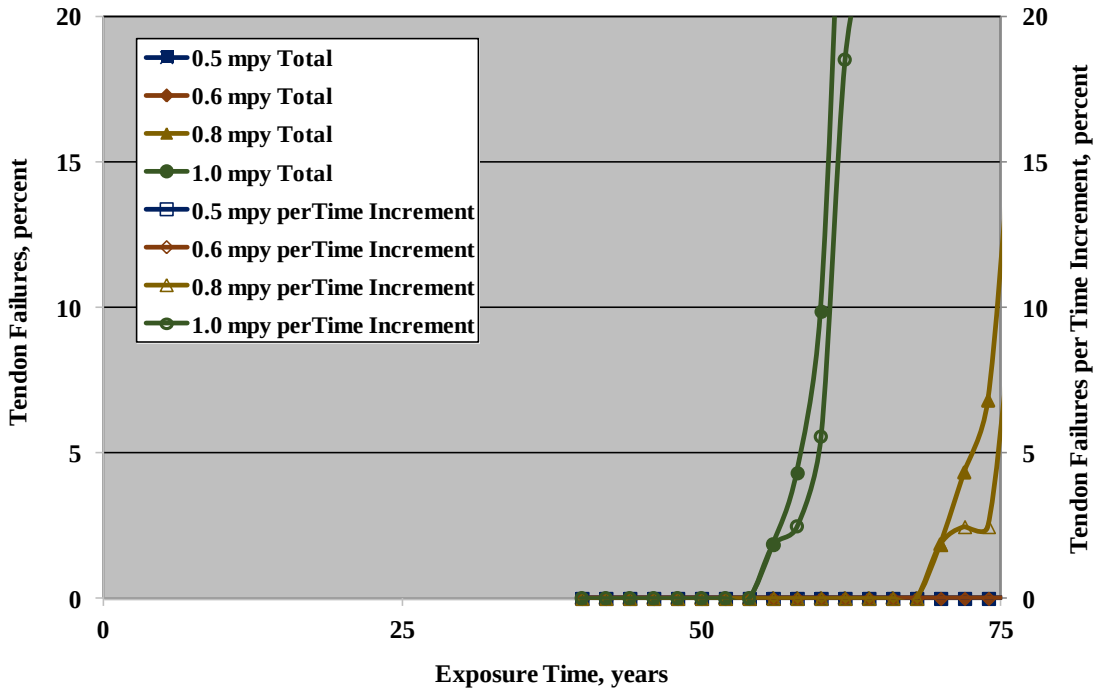

Source: FHWA.

Figure 112. Graph. Percent of tendon failures and percent per time increment versus time for $\mu(CRE)$ = 0.5, 0.6, 0.8, and 1.0 mpy and $\sigma(CRE)/\mu(CRE)$ = 0.5.

Table 97. Number of tendon failures versus time for $\mu(CRE)$ = 3.0, 4.0, and 5.0 mpy and $\sigma(CRE)/\mu(CRE)$ = 0.5.

Exposure Time (Year)	$\mu(CRE)$ = 3.0 mpy	$\mu(CRE)$ = 4.0 mpy	$\mu(CRE)$ = 5.0 mpy
0	0	0	0
1	0	0	0
2	0	0	0
3	0	0	0
4	0	0	0
5	0	0	0
6	0	0	0
7	0	0	0
8	0	0	0
9	0	0	0
10	0	0	0
11	0	0	0
12	0	0	17
13	0	0	101
14	0	3	160
15	0	17	162
16	0	84	—
17	0	152	—
18	0	161	—
19	6	162	—
20	19	162	—

—No information available.

Table 98. Number of tendon failures per time increment versus time for $\mu(CRE)$ = 3.0, 4.0, and 5.0 mpy and $\sigma(CRE)/\mu(CRE)$ = 0.5.

Exposure Time (Year)	$\mu(CRE)$ = 3.0 mpy	$\mu(CRE)$ = 4.0 mpy	$\mu(CRE)$ = 5.0 mpy
0	0	0	0
1	0	0	0
2	0	0	0
3	0	0	0
4	0	0	0
5	0	0	0
6	0	0	0
7	0	0	0
8	0	0	0
9	0	0	0
10	0	0	0
11	0	0	0
12	0	0	17
13	0	0	84
14	0	3	—
15	0	14	—
16	0	67	—
17	0	68	—
18	0	—	—
19	6	—	—
20	13	—	—

—No information available.

Table 99. Percent of tendon failures versus time for $\mu(CRE)$ = 3.0, 4.0, and 5.0 mpy and $\sigma(CRE)/\mu(CRE)$ = 0.5.

Exposure Time (Year)	$\mu(CRE)$ = 3.0 mpy	$\mu(CRE)$ = 4.0 mpy	$\mu(CRE)$ = 5.0 mpy
0	0.0	0.0	0.0
1	0.0	0.0	0.0
2	0.0	0.0	0.0
3	0.0	0.0	0.0
4	0.0	0.0	0.0
5	0.0	0.0	0.0
6	0.0	0.0	0.0
7	0.0	0.0	0.0
8	0.0	0.0	0.0
9	0.0	0.0	0.0
10	0.0	0.0	0.0
11	0.0	0.0	0.0
12	0.0	0.0	10.5
13	0.0	0.0	62.3
14	0.0	1.9	98.8
15	0.0	10.5	100.0
16	0.0	51.9	—
17	0.0	93.8	—
18	0.0	99.4	—
19	3.7	100.0	—
20	11.7	100.0	—

—No information available.

Table 100. Percent of tendon failures per time increment versus time for $\mu(CRE)$ = 3.0, 4.0, and 5.0 mpy and $\sigma(CRE)/\mu(CRE)$ = 0.5.

Exposure Time (Year)	$\mu(CRE)$ = 3.0 mpy	$\mu(CRE)$ = 4.0 mpy	$\mu(CRE)$ = 5.0 mpy
0	0.0	0.0	0.0
1	0.0	0.0	0.0
2	0.0	0.0	0.0
3	0.0	0.0	0.0
4	0.0	0.0	0.0
5	0.0	0.0	0.0
6	0.0	0.0	0.0
7	0.0	0.0	0.0
8	0.0	0.0	0.0
9	0.0	0.0	0.0
10	0.0	0.0	0.0
11	0.0	0.0	0.0
12	0.0	0.0	10.5
13	0.0	0.0	51.9
14	0.0	1.9	—
15	0.0	8.6	—
16	0.0	41.4	—
17	0.0	42.0	—
18	0.0	—	—
19	2.3	—	—
20	7.2	—	—

—No information available.

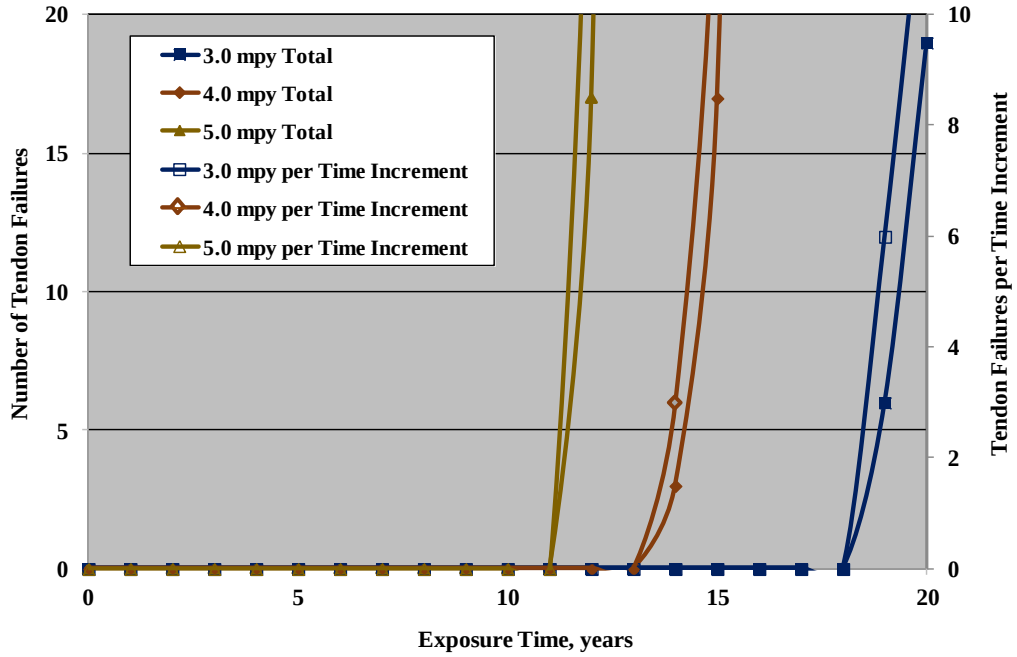

Source: FHWA.

Figure 113. Graph. Number of tendon failures and failures per time increment versus time for $\mu(CRE)$ = 3.0, 4.0, and 5.0 mpy and $\sigma(CRE)/\mu(CRE)$ = 0.5.

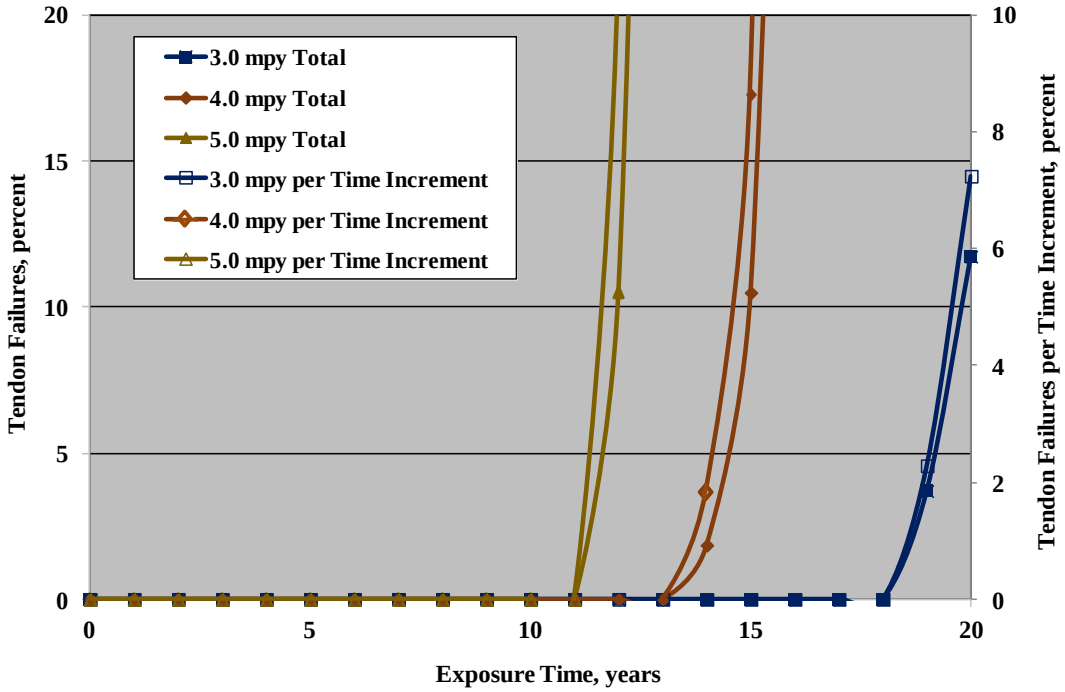

Source: FHWA.

Figure 114. Graph. Percent of tendon failures and percent per time increment versus time for $\mu(CRE)$ = 3.0, 4.0, and 5.0 mpy and $\sigma(CRE)/\mu(CRE)$ = 0.5.

Table 101. Number of tendon failures versus time for $\mu(CRE)$ = 10.0 and 20.0 mpy and $\sigma(CRE)/\mu(CRE)$ = 0.5.

Exposure Time (Year)	$\mu(CRE)$ = 10.0 mpy	$\mu(CRE)$ = 20.0 mpy
2.00	0	0
2.25	0	0
2.50	0	0
2.75	0	0
3.00	0	17
3.25	0	101
3.50	0	160
3.75	0	162
4.00	0	162
4.25	0	162
4.50	0	162
4.75	0	162
5.00	0	162
5.25	0	162
5.50	0	162
5.75	7	162
6.00	12	162
6.25	44	162
6.50	46	162
6.75	41	162
7.00	11	162

Table 102. Number of tendon failures per time increment versus time for $\mu(CRE)$ = 10.0 and 20.0 mpy and $\sigma(CRE)/\mu(CRE)$ = 0.5.

Exposure Time (Year)	$\mu(CRE)$ = 10.0 mpy	$\mu(CRE)$ = 20.0 mpy
2.00	0	0
2.25	0	0
2.50	0	0
2.75	0	0
3.00	0	17
3.25	0	84
3.50	0	59
3.75	0	2
4.00	0	—
4.25	0	—
4.50	0	—
4.75	0	—
5.00	0	—
5.25	0	—
5.50	0	—
5.75	7	—
6.00	5	—
6.25	32	—
6.50	2	—
6.75	—	—
7.00	—	—

—No information available.

Table 103. Percent of tendon failures versus time for $\mu(CRE)$ = 10.0 and 20.0 mpy and $\sigma(CRE)/\mu(CRE)$ = 0.5.

Exposure Time (Year)	$\mu(CRE)$ = 10.0 mpy	$\mu(CRE)$ = 20.0 mpy
2.00	0	0
2.25	0	0
2.50	0	0
2.75	0	0
3.00	0	10
3.25	0	62
3.50	0	99
3.75	0	100
4.00	0	100
4.25	0	100
4.50	0	100
4.75	0	100
5.00	0	100
5.25	0	100
5.50	0	100
5.75	4	100
6.00	7	100
6.25	27	100
6.50	28	100
6.75	25	100
7.00	7	100

—No information available.

Table 104. Percent of tendon failures per time increment versus time for $\mu(CRE)$ = 10.0 and 20.0 mpy and $\sigma(CRE)/\mu(CRE)$ = 0.5.

Exposure Time (Year)	$\mu(CRE)$ = 10.0 mpy	$\mu(CRE)$ = 20.0 mpy
2.00	0	0
2.25	0	0
2.50	0	0
2.75	0	0
3.00	0	10
3.25	0	52
3.50	0	36
3.75	0	—
4.00	0	—
4.25	0	—
4.50	0	—
4.75	0	—
5.00	0	—
5.25	0	—
5.50	0	—
5.75	4	—
6.00	3	—
6.25	20	—
6.50	—	—
6.75	—	—
7.00	—	—

—No information available.

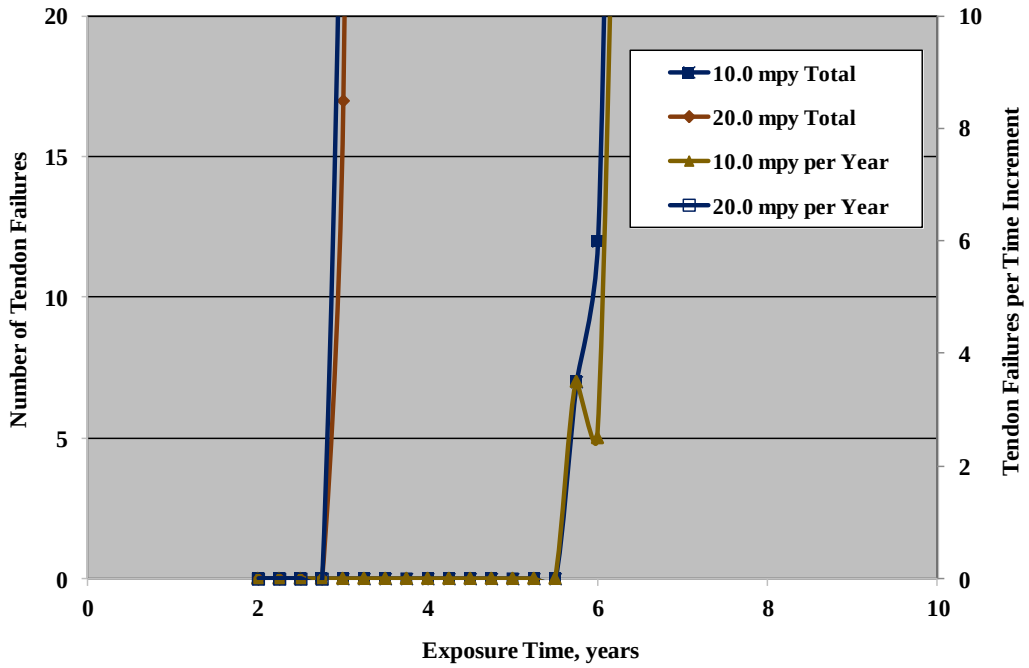

Source: FHWA.

Figure 115. Graph. Number of tendon failures and failures per time increment versus time for $\mu(CRE)$ = 10.0 and 20.0 mpy and $\sigma(CRE)/\mu(CRE)$ = 0.5.

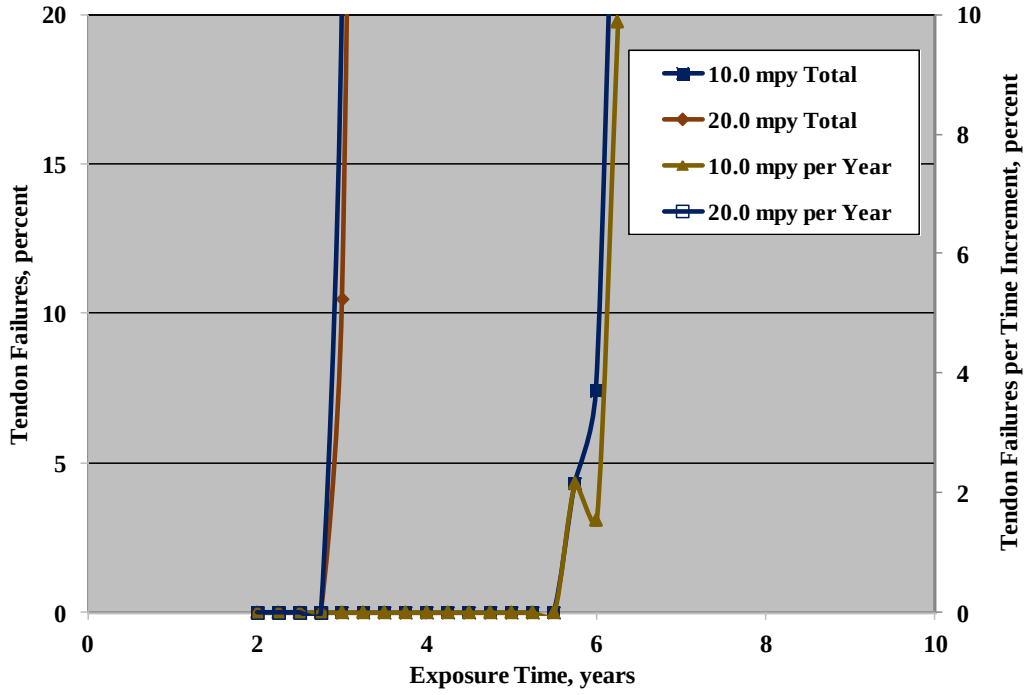

Source: FHWA.

Figure 116. Graph. Percent of tendon failures and percent per time increment versus time for $\mu(CRE)$ = 10.0 and 20.0 mpy and $\sigma(CRE)/\mu(CRE)$ = 0.5.

FURTHER CONSIDERATIONS

In addition, several aspects of the proposed fracture and failure projection methodology warrant further discussion. First, for a given $\mu(CRE)$, the above results indicate that fractures/failures just subsequent to T_f and prior to the inflection point are greatest for tendons and least for wires. This is a consequence of only 3 wires of a strand having to fracture for the latter to break and 7 strands of a 22-strand tendon to fracture for the latter to fail. Also, while no fractures/failures are projected to 75 yr for $\mu(CRE)$ = 0.5 mpy, at $\mu(CRE)$ = 1.0 mpy, almost 2 to near 6 percent of tendons are projected to fail per 2 yr between years 56 and 60 (see table 96). Table 105 summarizes this point where T_f for wires, strands, and tendons is listed for $\mu(CRE)$ = 1.0, 5.0, 10.0, 20.0, and 80.0 mpy, along with the subsequent time for 10 percent of wires and strands to fracture and tendons to fail. These results indicate that for even relatively modest corrosion rates such as 5 mpy, the rate of tendon failures, once initiated, is unmanageable, particularly within the context of detection via a biannual bridge inspection. The projections in table 105 pertain not to all tendons on a bridge but only to ones with a grout deficiency or deficiencies that result in the indicated corrosion rates. For these cases, tendon failure avoidance requires that, first, wires or perhaps strands (not tendons) be monitored for fractures and that, second, intervention takes place once one or both of these reach a defined threshold. Also, the fracture/failure rates projected above will be even more rapid if $\sigma(CRE)$ is less that the 0.5 value investigated above.

Table 105. Summary table for T_f and for a subsequent 10 percent of fractures/failures.

$\mu(CRE)$ (mpy)	Wires T_f (Year)	Strands T_f (Year)	Tendons T_f (Year)	Wires: Additional Time for 10 Percent Fractures/ Failures (Year)	Strands: Additional Time for 10 Percent Fractures/ Failures (Year)	Tendons: Additional Time for 10 Percent Fractures/ Failures (Year)
1	33	40	56	26	16	5
5	5	8	12	5	3	<1
10	2.3	4.0	5.8	2.3	1.4	0.2
20	1.2	2.0	2.9	1.3	0.8	0.1
40	0.65	1.20	1.51	0.65	0.31	0.05
80	0.32	0.60	0.75	0.36	0.16	0.04

While plots of wire fractures per unit time versus time follow a smooth trend of progressively increasing rates, for strands and tendons these are more irregular. This resulted because of randomness of number groupings (6 to represent each strand and 22 sets of 6 for tendons (see above)).

The above methodology might be employed in practice by considering that, if a failed tendon or tendons are disclosed, then projection of further occurrences could involve correlating this timing and the number of failures with the appropriate table/figure above that provides the best fit. Alternatively, a forensic analysis could estimate $\mu(CRE)$ and $\sigma(CRE)$ and then the same correlations established. However, the results would apply only to tendons with a comparable grout deficiency. Disclosure of a failed tendon or tendons is most likely to occur during a

biannual bridge inspection and identify such for external tendons only. However, this should then result in inspection of internal ones as well according to a previously proposed protocol.[1] Once this is done, rate of any future failures can be projected.

A follow-on issue pertains to probability that a limited number of contiguous tendon failures might occur with potentially catastrophic consequences. For example, a common box girder bridge design involves three external tendons on each side, and failure of two contiguous ones may place the section at or near the limit state. Thus, in the case of such a bridge with, for example, 30 box sections (180 tendons total), the probability of a second failure next to a first is very low (0.01). Although even this may be unacceptable, it is based on the assumption that tendons with deficient grout are randomly distributed, which may not be the case. For example, as noted above, two failed tendons were disclosed on the Ringling Causeway Bridge some 8 yr after construction.[10] Invasive inspection then identified 15 additional tendons with deficient grout and corrosion, and these were subsequently replaced. Because these tendons were in the same general vicinity, it is likely that issues associated with the grout quality or placement (or both) were responsible. Hence, randomness of deficiencies, corrosion, and failures cannot necessarily be assumed.

CHAPTER 5. APPLICATION TO POST-TENSIONED BRIDGES

GENERAL

For the above PT tendon failure projection methodology to be useful to bridge engineers, it must be applicable in practice and relate to actual structures. Two approaches are proposed depending on the situation at issue and the end objective. The first considers that focus is on a specific tendon that may be at risk with the objective of projecting the number of both past (if any) and future wire and strand fractures as a function of time, from which occurrence of tendon failures can be forecast. The second does the same but for tendons of either a representative portion of a bridge or an entire bridge. In either case, the extent of any grout deficiency or deficiencies must be defined, including the following:

- Concentration of chlorides in the grout.
- Presence of free sulfates.
- Presence, type, and extent of any physical deficiencies.
- Combinations of the above.

Different possibilities are discussed and evaluated below.

CHEMICALLY DEFICIENT GROUT

Grouts in this category are either chloride contaminated or exhibit free sulfates (or both) but are considered physically sound, meaning an absence of voids; free water; and soft, separated, chalky, or segregated material.[21] However, tendons with physically deficient grout can also exhibit elevated chlorides or sulfates (or both), which may further exacerbate the situation.

American Concrete Institute committee reports list chloride limits for prestressed concrete as 0.06 wt% cement for water-soluble chlorides and 0.08 wt% cement for acid-soluble chlorides.[22–24] Determination of chloride limits specific to PT tendons was addressed by the FHWA phase 1 study, where 0.40 wt% cement of chlorides was identified as a threshold limit for occurrence of rust spots with pits possibly initiating beneath these and 0.80 wt% cement of chlorides as a limit above which rapid corrosion progression can occur with structural integrity potentially being at risk in the near future. That the latter two values are greater than the committee limits probably reflects a factor of safety being incorporated for the former.

Application of the tendon failure projection methodology presented and evaluated above requires knowing, first, the concentration of chlorides, either for a single tendon if that is the focus (see above) or for multiple tendons and, second, the relationship between this concentration and corrosion rate. If the source of chlorides is from prepackaged SikaGrout® 300PT grout produced at the company's Marion, Ohio, facility from 2002 to 2010, then concentration is likely to vary depending on grout lot. In this case, construction records may be helpful in relating chloride contamination level to individual tendons. In addition or independently, chloride concentration should be determined by grout sampling and analysis according to a recommended procedure.[15] Chlorides in grout can also arise from marine exposure or deicing salts in conjunction with leakage at construction joints and tendon sheathing defects.

Given grout chloride concentration or concentration range in a specific tendon or set of tendons, findings from the FHWA phase 1 study can be employed to estimate the distribution of pit depths and associated corrosion rates, and from this, timing of wire and strand fractures and tendon failures can be projected. Thus, table 4 lists maximum pit depth for strands in sound grout with chloride concentration 0.80 wt% cement (Specimen Number 0.8%–F–S) as 5 mils with μ = 3.60 mils and σ = 1.52 mils (σ/μ = 0.42). Maximum pit depth for Specimen Number 2.0%–F–S (chloride concentration 2.00 wt% cement), on the other hand, was 12 mils with μ = 4.11 mils and σ = 2.01 mils (σ/μ = 0.49). Thus, while mean pit depth for each of the two chloride concentrations is not that different, the maximum is 2.4 times greater for strands exposed to the higher chloride grout. The greater number of pits in the higher chloride grout compared to the lower (35 versus 5; see table 4) may have been at least partly responsible for this difference.

Specimen Numbers 0.8%–F–S and 2.0%–F–S were exposed for 178 d, which assuming attack rate was constant over this time, corresponds to a corrosion rate for the deepest pits of 10.3 and 24.6 mpy, respectively. Such a determination may underestimate what results from a more prolonged exposure for several reasons. First, pitting is likely to involve an initiation period which, if this were known, should lead to a higher calculated corrosion rate because time of propagation would be less than 178 d. Second, some time subsequent to initiation may be required for acidification to fully develop with corrosion rate being less during this period. There is no way to address or compensate for either of these two issues; however, neither is thought to be a source of significant underestimation of corrosion rate. Lastly, there is the possible effect of tendon length, as discussed above; however, it was concluded that this factor need not be taken into account in projecting the onset of fractures and failures except, perhaps, for very short tendons, and even in this case, any projected T_f should be greater than for longer tendons. Thus, T_f projections for longer tendons applied to shorter ones should be conservative.

Projection of wire and strand fractures and tendon failures in chloride-contaminated, physically sound grout involves measurement of grout chloride concentration and, from this, determination of the mean and standard deviation of corrosion rate based on data from the phase 1 study. Thus, data for Specimen Numbers 0.8%–F–S and 2.0%–F–S indicate dependence of the mean and standard deviation of corrosion rate ($\mu(CRE)$ and $\sigma(CRE)$, respectively) on chloride concentration, [Cl^-], as conforming to the equations in figure 117 and figure 118, respectively (units on chloride concentration are wt% cement and for corrosion rate mpy). These apply to chloride concentrations greater than or equal to 0.80 wt% cement, this threshold being the lowest concentration for which measureable pitting was reported for strands in physically sound grout, and while there is certainly an upper limit for applicability, this is probably not reached for concentrations that are likely to be encountered for chloride-contaminated grout within tendons.[16] Given these data, an analysis can be performed according to the protocol proposed herein and T_f for wires, strands, and tendons determined, as well as subsequent rates of fracture/failure. Two qualifications must be recognized, however; first, the equations in figure 117 and figure 118 are based on data from only two specimens, and second, the experiments from which these relationships were developed involved the specific ambient, hot and humid, and freezing and drying exposure conditions, times, and sequences illustrated in figure 45 through figure 47. Other exposure histories may affect corrosion performance differently.

$$\mu(CRE) = 0.43 \cdot [Cl^-] + 3.26$$

Figure 117. Equation. Expression for mean corrosion rate as a function of chloride concentration in physically sound grout.

$$\sigma(CRE) = 0.025 \cdot [Cl^-]^2 + 0.348 \cdot [Cl^-] + 1.216$$

Figure 118. Equation. Expression for standard deviation of corrosion rate as a function of chloride concentration in physically sound grout.

Two alternatives, options 1 and 2, respectively, are proposed whereby bridge engineers can project T_f for wires, strands, and tendons. The first (option 1) involves depth measurement of pits on extracted wires and the subsequent determination of the mean and standard deviation. From these and knowing the exposure time, $\mu(CRE)$ and $\sigma(CRE)$ can be calculated. Obviously, this option is relatively involved in that the acquisition of such data and ensuring that it is representative may be difficult or impractical. Alternatively, option 2 considers that grout chloride concentration alone is known, from which $\mu(CRE)$ and $\sigma(CRE)$ can be calculated from the equations in figure 117 and figure 118. Table 106 lists T_f for wires, strands, and tendons determined using the protocol developed in chapter 2 for mean corrosion rates in the range of 0.5 to 10 mpy and standard deviations for each of 0.10, 0.30, 0.50, and 0.60. These rates extend to below the threshold for which the equations in figure 117 and figure 118 apply, considering the possibility that the rust spots reported in the phase 1 study for exposure to grout with 0.4 less than or equal to $[Cl^-]$ less than 0.8 might eventually develop into active pits. Likewise, figure 119 through figure 122 show plots of T_f for wires, strands, and tendons, respectively, as a function of mean corrosion rate for each of the four $\sigma(CRE)/\mu(CRE)$ ratios, and figure 123 through figure 134 show the best fit equation for each set of conditions according to a fourth polynomial curve fit ($R^2 > 0.99$ in each case).

Table 106. T_f for wires, strands, and tendons with $\mu(CRE)$ in the range of 0.5–10 mpy and $\sigma(CRE) = 0.10–0.60$.

$\mu(CRE)$ (mpy)	$\sigma(CRE)/\mu(CRE)$	Wire T_f (Year)	Strand T_f (Year)	Tendon T_f (Year)
0.50	0.10	61.2	>75	>75
0.50	0.30	52.3	>75	>75
0.50	0.50	43.3	>75	>75
0.50	0.60	39.7	>75	>75
1.00	0.10	30.6	54.0	66.0
1.00	0.30	26.1	50.0	63.6
1.00	0.50	21.6	40.0	55.3
1.00	0.60	19.8	38.0	53.0
2.00	0.10	15.0	27.6	33.7
2.00	0.30	13.8	24.0	31.5
2.00	0.50	10.8	20.5	27.6
2.00	0.60	09.9	19.0	26.8
3.00	0.10	10.1	18.0	21.9
3.00	0.30	09.1	16.0	20.8
3.00	0.50	7.1	13.8	18.5
3.00	0.60	6.4	12.7	17.8
4.00	0.10	8.1	14.0	16.9
4.00	0.30	6.9	12.0	15.8
4.00	0.50	5.2	10.1	13.9
4.00	0.60	4.9	9.7	13.8
5.00	0.10	5.1	9.0	11.0
5.00	0.30	4.3	8.0	10.4
5.00	0.50	3.7	6.7	9.2
5.00	0.60	3.3	6.3	8.7
6.00	0.10	3.8	6.9	8.3
6.00	0.30	3.2	6.0	7.6
6.00	0.50	2.6	5.0	7.0
6.00	0.60	2.4	4.8	6.9
7.00	0.10	3.0	5.5	6.7
7.00	0.30	2.6	4.7	6.3
7.00	0.50	2.1	4.0	5.6
7.00	0.60	2.0	3.8	5.9

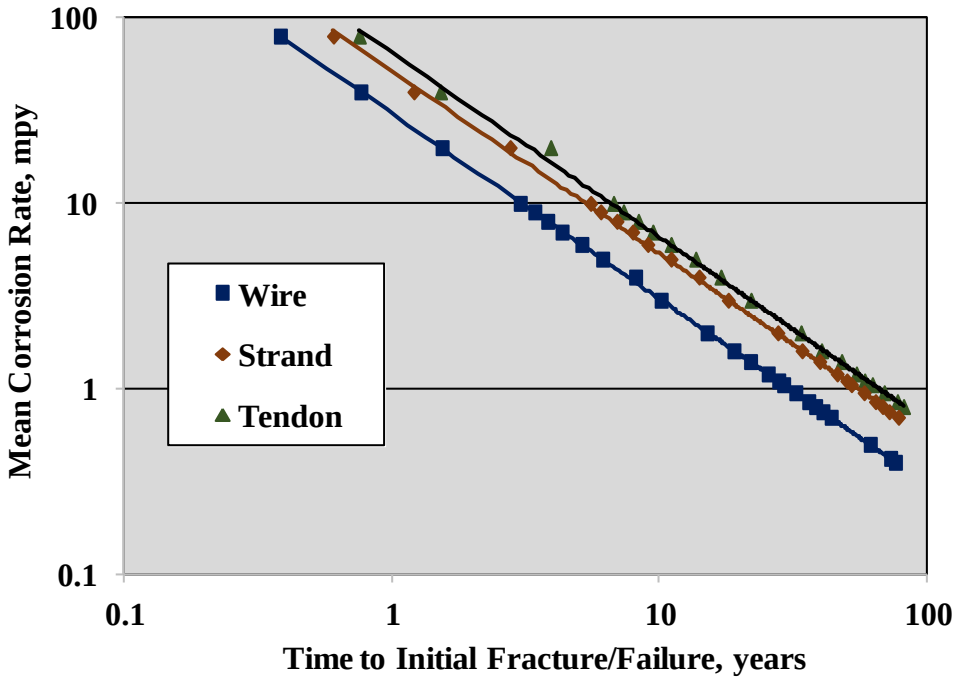

Source: FHWA.

Figure 119. Graph. Plot of T_f for wires, strands, and tendons as a function of corrosion rate for $\sigma(CRE)/\mu(CRE) = 0.10$.

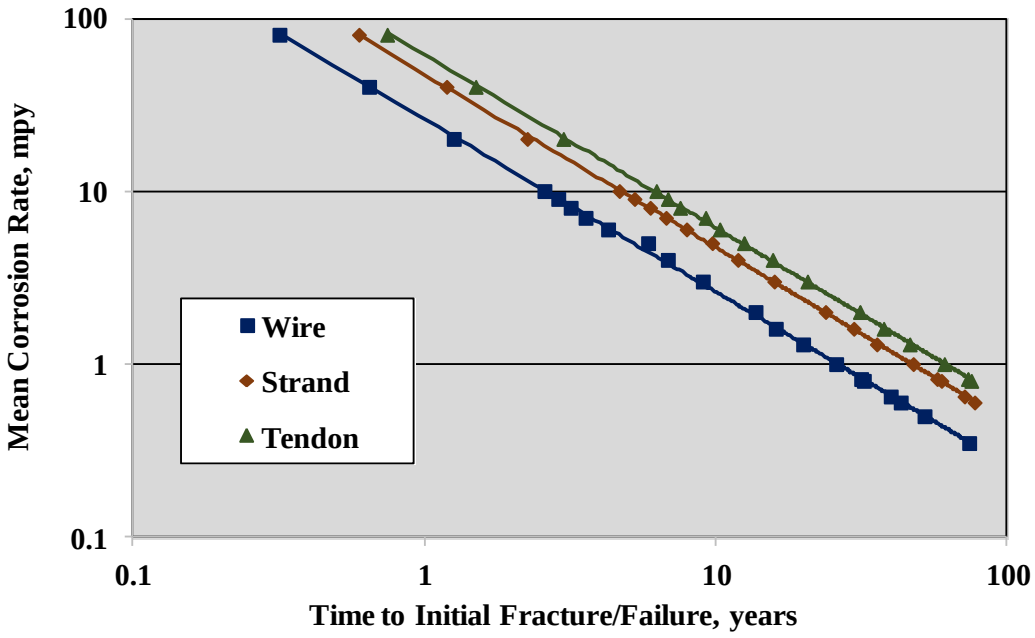

Source: FHWA.

Figure 120. Graph. Plot of T_f for wires, strands, and tendons as a function of corrosion rate for $\sigma(CRE)/\mu(CRE) = 0.30$.

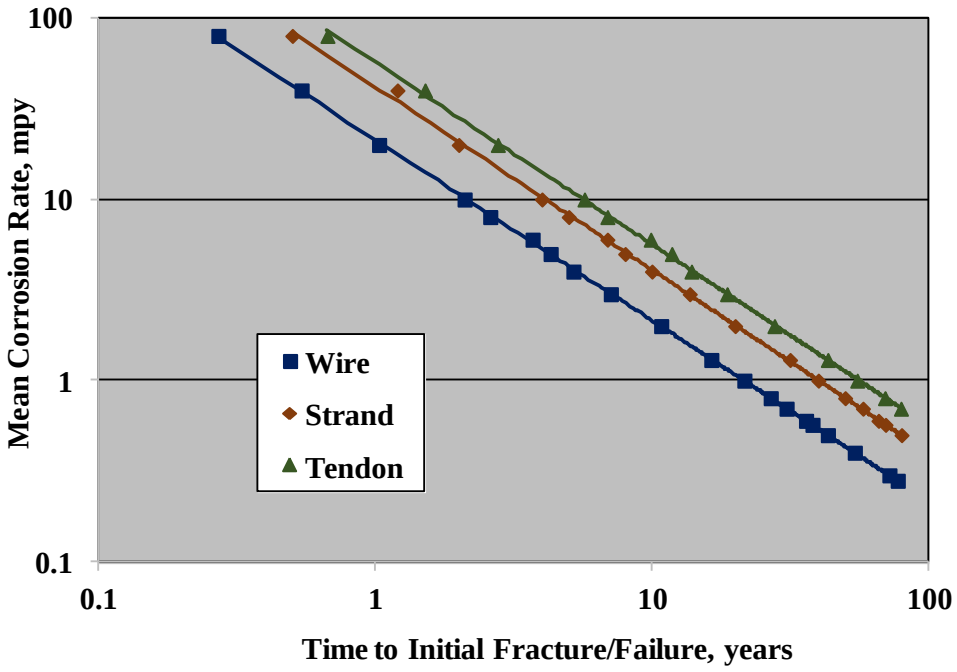

Source: FHWA.

Figure 121. Graph. Plot of T_f for wires, strands, and tendons as a function of corrosion rate for $\sigma(CRE)/\mu(CRE)$ = 0.50.

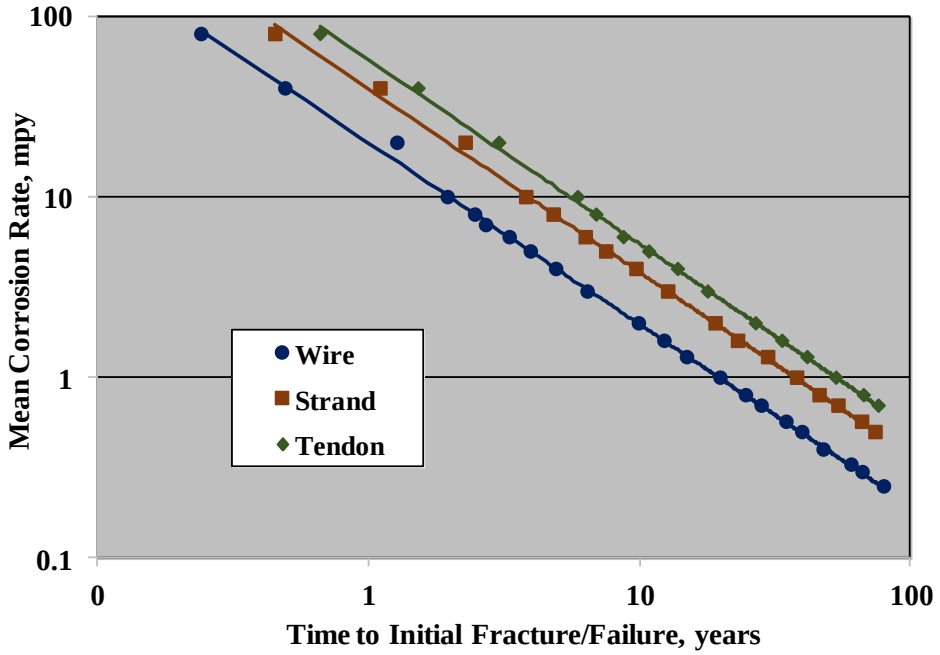

Source: FHWA.

Figure 122. Graph. Plot of T_f for wires, strands, and tendons as a function of corrosion rate for $\sigma(CRE)/\mu(CRE)$ = 0.60.

$$T_f = 30.54 \cdot \mu(CRE)^{-1.02}$$

Figure 123. Equation. Dependence of T_f for wires on $\mu(CRE)$ for $\sigma(CRE)/\mu(CRE)$ = 0.10.

$$T_f = 55.34 \cdot \mu(CRE)^{-1.02}$$

Figure 124. Equation. Dependence of T_f for strands on $\mu(CRE)$ for $\sigma(CRE)/\mu(CRE)$ = 0.10.

$$T_f = 66.22 \cdot \mu(CRE)^{-1.00}$$

Figure 125. Equation. Dependence of T_f for tendons on $\mu(CRE)$ for $\sigma(CRE)/\mu(CRE)$ = 0.10.

$$T_f = 26.09 \cdot \mu(CRE)^{-1.00}$$

Figure 126. Equation. Dependence of T_f for wires on $\mu(CRE)$ for $\sigma(CRE)/\mu(CRE)$ = 0.30.

$$T_f = 47.58 \cdot \mu(CRE)^{-1.00}$$

Figure 127. Equation. Dependence of T_f for strands on $\mu(CRE)$ for $\sigma(CRE)/\mu(CRE)$ = 0.30.

$$T_f = 61.92 \cdot \mu(CRE)^{-1.00}$$

Figure 128. Equation. Dependence of T_f for tendons on $\mu(CRE)$ for $\sigma(CRE)/\mu(CRE)$ = 0.30.

$$T_f = 21.25 \cdot \mu(CRE)^{-1.00}$$

Figure 129. Equation. Dependence of T_f for wires on $\mu(CRE)$ for $\sigma(CRE)/\mu(CRE)$ = 0.50.

$$T_f = 40.81 \cdot \mu(CRE)^{-1.00}$$

Figure 130. Equation. Dependence of T_f for strands on $\mu(CRE)$ for $\sigma(CRE)/\mu(CRE)$ = 0.50.

$$T_f = 56.78 \cdot \mu(CRE)^{-1.00}$$

Figure 131. Equation. Dependence of T_f for tendons on $\mu(CRE)$ for $\sigma(CRE)/\mu(CRE)$ = 0.50.

$$T_f = 19.72 \cdot \mu(CRE)^{-0.99}$$

Figure 132. Equation. Dependence of T_f for wires on $\mu(CRE)$ for $\sigma(CRE)/\mu(CRE)$ = 0.60.

$$T_f = 37.61 \cdot \mu(CRE)^{-0.98}$$

Figure 133. Equation. Dependence of T_f for strands on $\mu(CRE)$ for $\sigma(CRE)/\mu(CRE)$ = 0.60.

$$T_f = 53.38 \cdot \mu(CRE)^{-0.98}$$

Figure 134. Equation. Dependence of T_f for tendons on $\mu(CRE)$ for $\sigma(CRE)/\mu(CRE)$ = 0.60.

As an example of the proposed analysis, consider a tendon system for which average grout chloride concentration has been measured as 2.50 wt% cement. By the equations in figure 117 and figure 118, this translates to a mean corrosion rate of 4.34 mpy and standard deviation 2.24 ($\sigma(CRE)/\mu(CRE)$ = 0.52), respectively. Figure 135 shows a plot of wire, strand, and tendon fracture/failure progression for this case according to the chapter 2 protocol, and table 107 lists T_f for wires, strands, and tendons as determined from, first, the analysis that led to figure 135 (calculated) and, second, interpolation between results for $\mu(CRE)$ = 4.00 and 5.00 mpy with $\sigma(CRE)$ = 0.50 per the equations in figure 129 through figure 131, for which $\mu(CRE)$ bounds the value at hand, $\mu(CRE)$ = 4.34 mpy. The interpolated result is seen to be about 3 percent higher than what was calculated for tendon failure, and it is concluded that the method is an appropriate approach to projecting the onset of fractures and failures in cases where the mean grout chloride concentration is known.

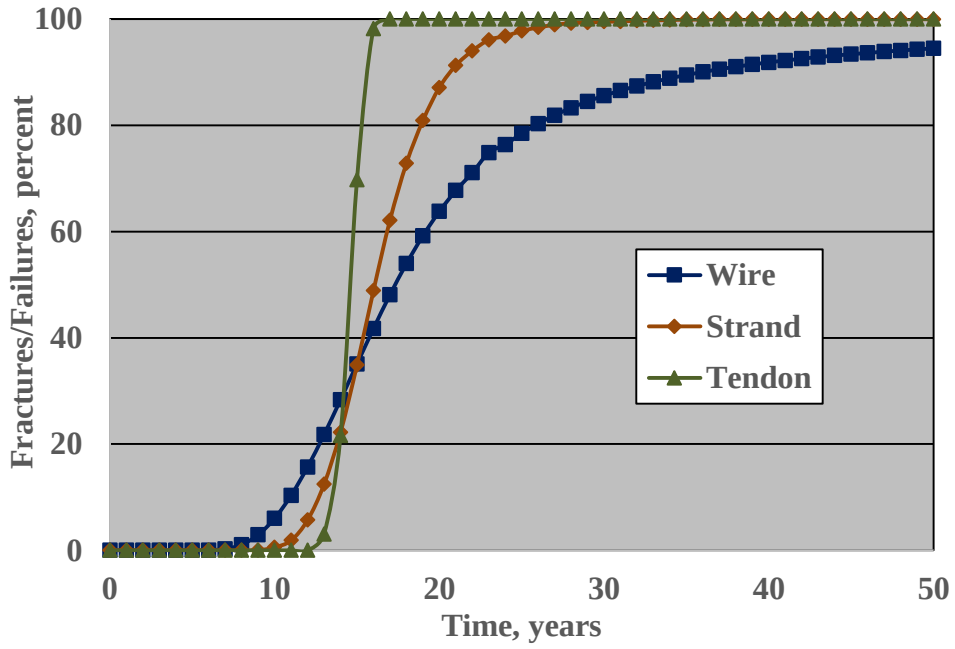

Source: FHWA.

Figure 135. Graph. Plot of projected wire and strand fractures and tendon failures as a function of time for a mean chloride concentration of 2.50 wt% cement and standard deviation 2.24.

Table 107. Calculated and interpolated T_f values for wires, strands, and tendons with $\mu(CRE)$ = 4.34 mpy and $\sigma(CRE)$ = 2.24.

$\mu(CRE)$ (mpy)	$\sigma(CRE)$ (mpy)	σ/μ	Wire T_f	Strand T_f	Tendon T_f
4.00	2.00	0.50	5.37	10.00	13.86
4.34*	2.24	0.52	4.79	9.00	12.87
4.34**	2.24	0.52	5.00	9.60	13.21
5.00	2.50	0.50	4.25	8.80	11.88

*Calculated (figure 130 analysis).
**Interpolated.

Projection of the rate of fractures/failures subsequent to T_f being reached can be made from the above and from tables and figures in the appendixes considering the appropriate $\mu(CRE)$ and $\sigma(CRE)$. However, doing this is considered fortuitous in the case of tendons because repairs, rehabilitations, or replacement (or a combination of these) must be performed prior to T_f for tendons being reached, since the subsequent failure rate quickly becomes unacceptably high for remaining tendons with a similar extent of deficiency, even when $\mu(CRE)$ is relatively low (see figure 111, for example).

PHYSICALLY DEFICIENT GROUT

Both field and laboratory experience have indicated that tendons with physically deficient grout can be subject to failure after a relatively short period of time (months to several years).[8,10,11] However, in at least some of these occurrences, elevated levels of free sulfates (a chemical deficiency) were also reported, and this probably contributed significantly to the failures. Consequently, disclosure of such situations requires immediate intervention (repair or replacement) with two possible exceptions. First, if air voids alone are present and the grout is otherwise physically sound and without free sulfates or water, then tendons so exposed can either be periodically inspected or have repairs made. Second, a physical deficiency or deficiencies may adversely affect or put at risk only a relatively small number of strands in a given tendon. In this regard, figure 136 shows a cross-section view of a failed tendon from the Ringling Causeway Bridge.[8] Thus, while more than 7 of the 22 strands are seen to be in physically deficient grout and fracture of these caused tendon failure, others were in hardened grout and presumably remained protected from corrosion. For cases where the number of strands exposed to physically deficient grout is relatively small and insufficient, if they fracture to cause tendon failure, then it may be acceptable first to remove and replace this grout to the extent that this can be done and second to establish a program for subsequent monitoring. The possibility should be considered, however, that other regions of tendons with such deficiency or deficiencies may have a greater number of strands at risk.

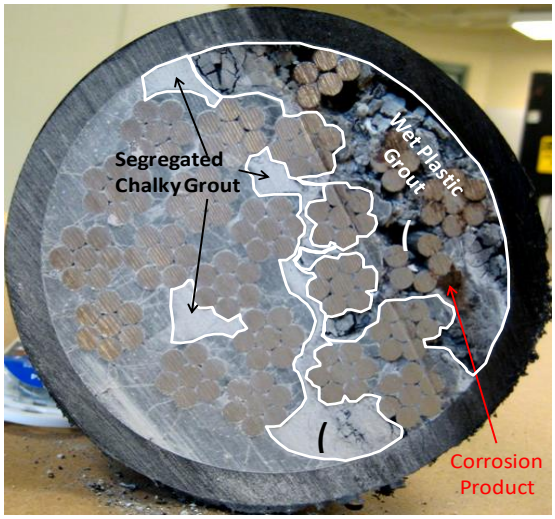

Source: Courtesy of the Florida Department of Transportation.

Figure 136. Photo. Cross-section view of a failed tendon from the Ringling Causeway Bridge

An additional possibility considers that, if wire or strand fractures are determined to have occurred and timing can be estimated, then it may be possible to relate these to the results in the applicable tables and figures above and from there estimate the rate of future occurrences for tendons with the same extent of grout deficiency.

FRACTURE/FAILURE PROJECTION BASED ON FIELD OR LABORATORY DATA

Based on the protocol proposed from the present study, T_f of wires, strands, and tendons can be forecast whether the issue is in laboratory results as in phases 1 and 2, or in field determinations based on measurements, as described above for the Ringling Causeway Bridge. Thus, given information regarding $\mu(CRE)$ and $\sigma(CRE)$, the appropriate selection from equations in figure 84 through figure 86 and figure 123 through figure 134 can be employed to project T_f of wires, strands, and tendons. These equations include $\mu(CRE)$ values to 80 mpy, which encompass what was encountered in the phase 1 and phase 2 studies and what has been experienced to date for actual structures. Once these values are known or are estimated, then comparison with the appropriate tables and figures (table 69 through table 104 and figure 99 through figure 116) facilitates projection of fracture/failure rate(s) once initiated.

CHAPTER 6. REPORTED TENDON FAILURES IN BRIDGES AND FIELD TESTING

GENERAL

Bridge tendon failures and occurrence of deficient grout have continued to be reported despite specification of thixotropic grout. Findings for two of these, the Ringling Causeway Bridge in Florida and the Carbon Plant Bridge in Texas, are reviewed below along with nondestructive testing (NDT) findings for the former. As noted above, failures on the Ringling Causeway were disclosed approximately 8 yr after construction. For the latter, deficient grout was found to be present shortly after construction; however, no tendon failures have been reported. Summarized also are NDT results for the Varina-Enon Bridge in Virginia for which a tendon failure was disclosed in 2007. This bridge was commissioned in 1990, and tendons in this case were fabricated using conventional neat cement grout containing cement, water, and admixtures mixed onsite. Testing programs that were performed on the Varina-Enon and Ringling Causeway Bridges are summarized.

VARINA-ENON BRIDGE (VIRGINIA)

As noted above, a failed tendon was disclosed on this bridge in 2007, some 17 yr after construction. Figure 137 shows a photograph of this tendon. In response to this, an NDE of selected tendons was performed using the permanent magnet-type magnetic main flux method (MMFM) for the purpose of identifying tendons containing corrosion damage. It was determined that this particular MMFM can detect as little as 1.5-percent section loss. Figure 138 shows the MMFM device mounted on a tendon, and figure 139 shows the MMFM testing on this bridge.

Source: FHWA.

Figure 137. Photo. Photograph of a failed tendon on the Varina-Enon Bridge.

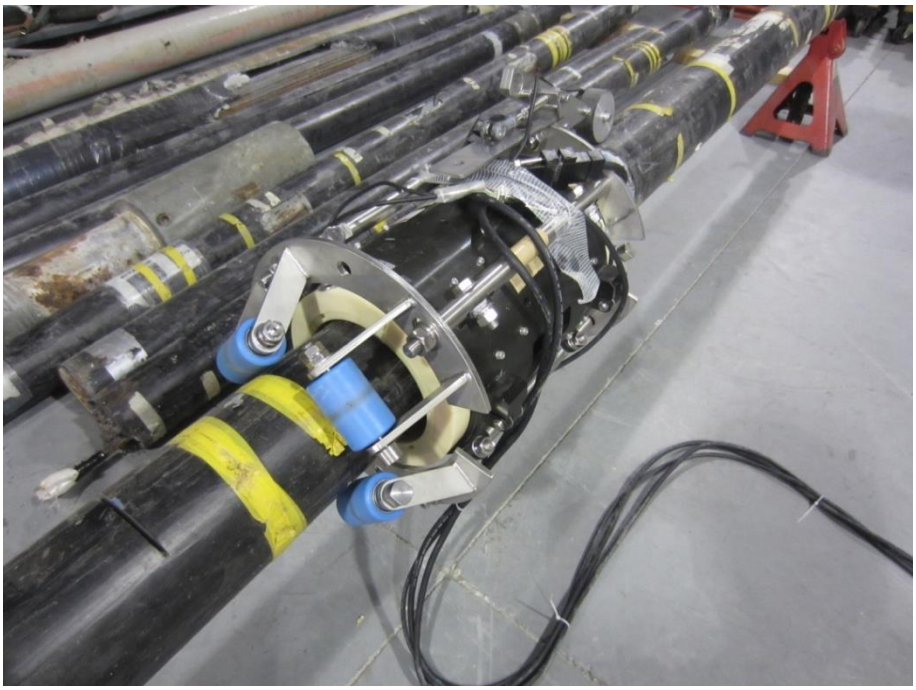

Source: FHWA.

Figure 138. Photo. Permanent magnet-type MMFM device.

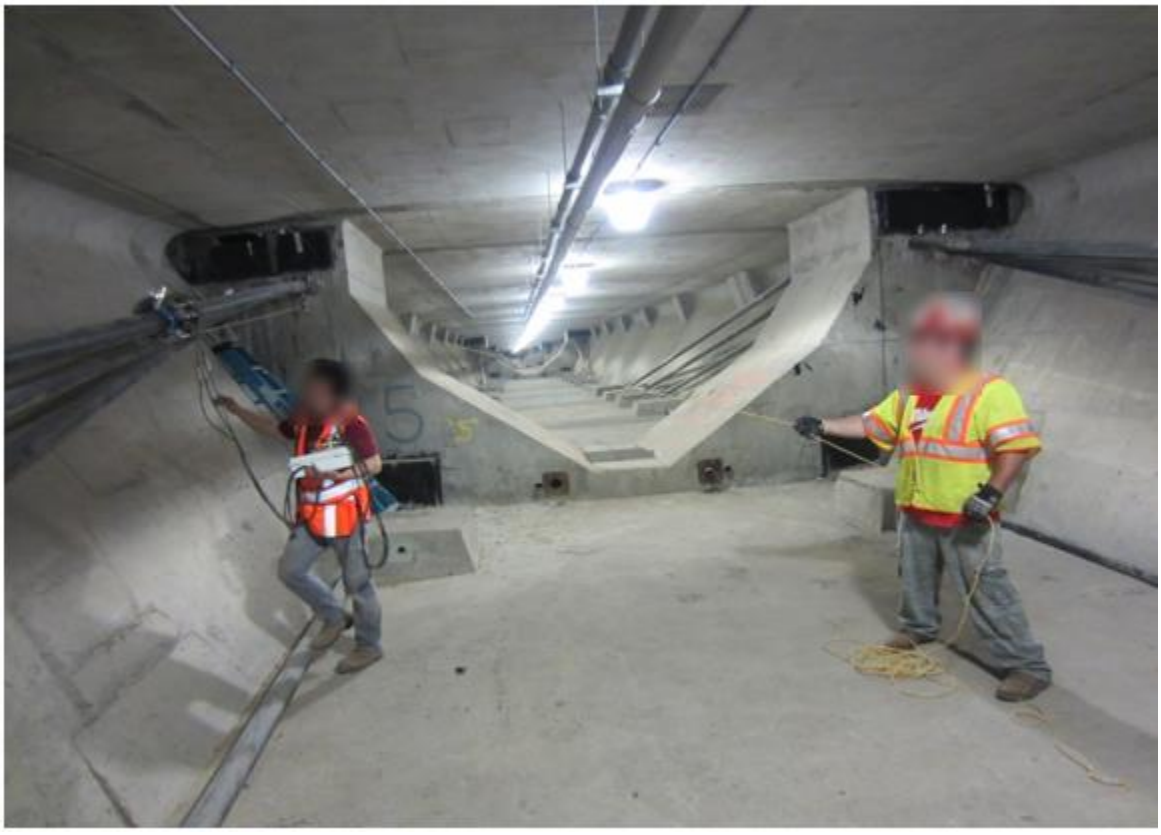

Source: FHWA.

Figure 139. Photo. MMFM field testing.

In May 2015, 22 tendons were scanned, and 6 sections, approximately 24-inches each, in 4 tendons, were excavated to compare actual conditions with the MMFM data. None of the examined tendons showed recognizable corrosion damage. Instead, large longitudinal grout voids were discovered in each case. Figure 140 shows a typical example of the grout condition for an opened tendon. As a result, field pit depth data could not be collected from this bridge.

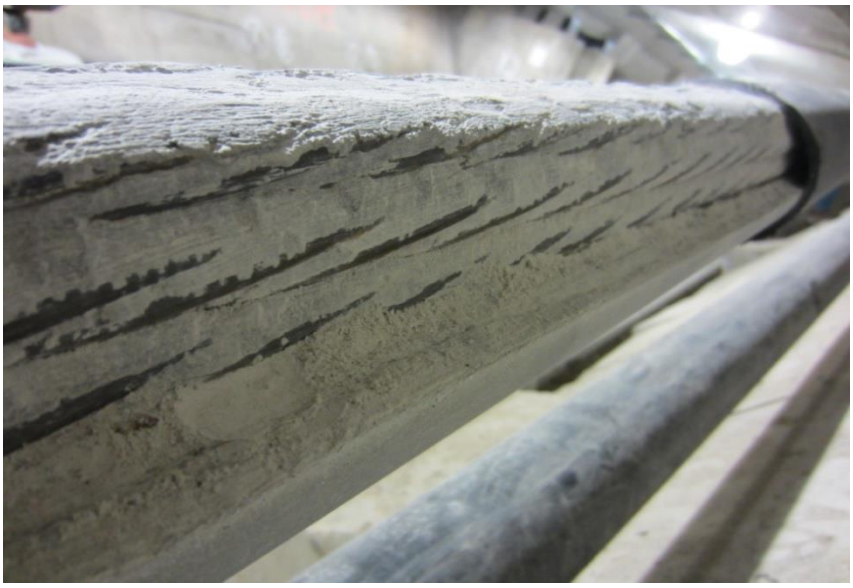

Source: FHWA.

Figure 140. Photo. Typical condition of the opened tendon.

RINGLING CAUSEWAY BRIDGE (FLORIDA)

As noted above, corrosion-induced failure of 2 external 22-strand tendons on this segmental bridge was discovered in 2011, some 8 yr post construction. Both failures occurred along an upslope adjacent to an upper deviation block. The attack was attributed to grout segregation and presence of free water with different regions being wet and plastic, white and chalky, separated, and sedimented (figure 136) with greater concentration of chlorides and sulfates at higher elevations than at lower ones. While the grout was SikaGrout® 300PT, it was not from the Marion, Ohio, company facility. Subsequent investigation revealed 15 other tendons with similar grout deficiencies and severe corrosion. Consequently, these tendons were replaced. Timing of the two failures was discussed previously in conjunction with verification of the T_f projection methodology.

When this study commenced, retrieved tendon segments were stored at the Florida Department of Transportation (FDOT) State Materials Office in Gainesville, Florida. Later, FDOT donated all tendon segments to the FHWA NDE laboratory for further research. Figure 141 shows some of these as they were received. Based on severity of corrosion damage, 4 strands, approximately 48 inches in length, representing different levels of corrosion damage from most severe to minor, were selected. Figure 142 shows these.

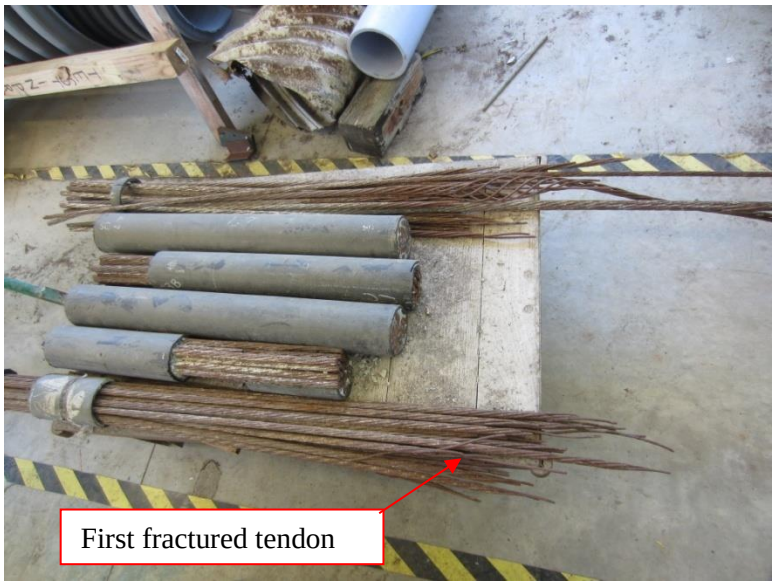

Source: FHWA.

Figure 141. Photo. Tendon sections retrieved from the Ringling Causeway Bridge.

Source: FHWA.

Figure 142. Photo. Selected strand samples.

A total of seven 10-inch strand pieces were cut: four from the fractured end and three from the opposite (saw-cut) end. The cut strand samples were untwisted, and 48 individual wires (1 wire was missing) were acid cleaned to remove corrosion products. Figure 143 shows the cleaned condition of the most severely corroded strand sample.

A total of 367 pit depth measurements were made on 48 wires. Table 108 summarizes statistics of the pit depth data. The diameter of the intact outer wires was 198 mils, and the measured deepest pit was 162.5 mils, which is equivalent to a corrosion rate of 21.5 mpy considering a 7.5-yr

exposure. Additional information regarding pit depths is provided in chapter 3 in conjunction with the model validation work.

Source: FHWA.

Figure 143. Photo. Cleaned strand sample exhibiting the worst corrosion damage.

Table 108. Pit depth statistics for the Ringling Causeway Bridge strand samples.

Factor	Measurment (mil)
Mean	34.5
Standard Deviation	33.6
Maximum	161.5

CARBON PLANT ROAD BRIDGE (TEXAS)

As a second example, figure 144 shows an opened anchorage on the recently constructed (2010) Carbon Plant Road Bridge over IH-37 in Texas, as reported by that State's DOT.[25] The upper portion of the grout labeled A was soft, segregated, and wet, and free water was stated to have flowed from this region on removal of the endcap. The lower portion of the grout (labeled B) was gray, hardened, and dry. Corrosion of strands in the A grout and air space was apparent. The grout was stated as being SikaGrout® 300PT from that company's Marion, Ohio, facility, and chloride concentrations for the in-place grout as high as 5.27 wt% grout[1] were reported, well in excess of the 0.08 wt% cement listed in specifications and guides. (See references 23, 24, 26, and 27). Considering this, an analysis was performed based on the protocol described in chapter 5 to project the time of initial fractures/failures for this tendon had not remedial measures been taken or the tendon replaced. The calculations necessarily assumed that the entire duct was filled with grout. Consequently, the findings probably apply best to other regions of the duct that may exhibit chemically deficient grout only (elevated chloride but no free water or type 1 grout).

[1]Approximately two-thirds of SikaGrout 300PT is cementitious material.

Assuming then that 67 percent of the grout in the duct is cement translates to a chloride concentration of 3.53 wt% cement. From the equations in figure 117 and figure 118, $\mu(CRE)$ = 4.78 mpy and $\sigma(CRE)$ = 2.76, respectively ($\sigma(CRE)/\mu(CRE)$ = 0.58). Based on these, T_f for wires, strands, and tendons was calculated as 3.8, 7.5, and 10.8 yr, respectively, using the equations in figure 132 through figure 134 for which $\sigma(CRE)/\mu(CRE)$ = 0.60. It should be noted that the reported chloride concentration of up to 5.27 wt% grout implies that concentration at other sampled sites was lower. However, this is not relevant since tendon failure should occur at the region of greatest chloride concentration, all other factors being the same. In other words, tendons fail according to the "weakest link" principle. Alternatively, it is possible, if not likely, that higher chloride concentrations were present elsewhere along the tendon, in which case the T_f values listed above are nonconservative.

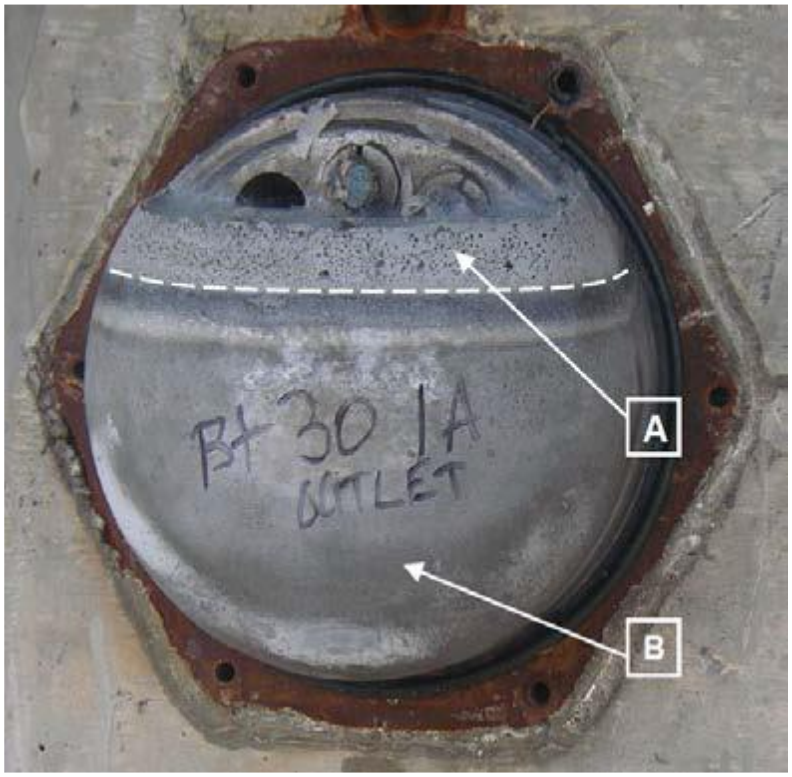

Source: Courtesy of Texas Department of Transportation.

Figure 144. Photo. Anchorage region of a tendon from the Carbon Plant Road Bridge subsequent to endcap removal. Part A was soft, segregated, and wet grout, and part B was gray, hardened, and dry grout.[(15)]

APPENDIX A. PROJECTED WIRE AND STRAND FRACTURE AND TENDON FAILURE RATES FOR $\sigma(CRE)/\mu(CRE) = 0.3$

Table 109. Number of wire fractures versus time for $\mu(CRE)$ in the range of 0.5–1.0 mpy and $\sigma(CRE)/\mu(CRE) = 0.3$.

Exposure Time (Year)	$\mu(CRE)$ = 0.5 mpy	$\mu(CRE)$ = 0.6 mpy	$\mu(CRE)$ = 0.8 mpy	$\mu(CRE)$ = 1.0 mpy
20	0	0	0	0
22	0	0	0	0
24	0	0	0	0
26	0	0	0	1
28	0	0	0	1
30	0	0	0	3
32	0	0	0	5
34	0	0	1	10
36	0	0	1	19
38	0	0	3	34
40	0	0	4	57
42	0	0	8	89
44	0	0	13	133
46	0	1	20	189
48	0	1	32	254
50	0	2	47	328
52	0	3	68	408
54	0	4	95	490
56	1	6	127	571
58	1	9	166	649
60	1	13	209	720
62	2	18	256	783
64	3	25	307	836
66	4	34	359	877
68	6	45	411	905
70	8	58	463	919
72	11	74	513	921
74	15	92	560	909
76	19	108	602	886

Table 110. Percent of wire fractures versus time for $\mu(CRE)$ in the range of 0.5–1.0 mpy and $\sigma(CRE)/\mu(CRE) = 0.3$.

Exposure Time (Year)	$\mu(CRE)$ = 0.5 mpy	$\mu(CRE)$ = 0.6 mpy	$\mu(CRE)$ = 0.8 mpy	$\mu(CRE)$ = 1.0 mpy
20	0.0	0.0	0.0	0.0
22	0.0	0.0	0.0	0.0
24	0.0	0.0	0.0	0.0
26	0.0	0.0	0.0	0.0
28	0.0	0.0	0.0	0.0
30	0.0	0.0	0.0	0.0
32	0.0	0.0	0.0	0.0
34	0.0	0.0	0.0	0.1
36	0.0	0.0	0.0	0.2
38	0.0	0.0	0.0	0.3
40	0.0	0.0	0.0	0.6
42	0.0	0.0	0.1	1.0
44	0.0	0.0	0.1	1.6
46	0.0	0.0	0.2	2.5
48	0.0	0.0	0.4	3.7
50	0.0	0.0	0.6	5.3
52	0.0	0.0	0.9	7.2
54	0.0	0.1	1.4	9.5
56	0.0	0.1	2.0	12.1
58	0.0	0.1	2.7	15.2
60	0.0	0.2	3.7	18.5
62	0.0	0.3	4.9	22.2
64	0.0	0.4	6.4	26.1
66	0.1	0.5	8.0	30.2
68	0.1	0.8	10.0	34.4
70	0.1	1.0	12.1	38.7
72	0.2	1.4	14.5	43.0
74	0.3	1.8	17.1	47.3
76	0.3	2.3	20.0	51.4

Table 111. Number of wire fractures per time increment for $\mu(CRE)$ in the range of 0.5–1.0 mpy and $\sigma(CRE)/\mu(CRE) = 0.3$.

Exposure Time (Year)	$\mu(CRE)$ = 0.5 mpy	$\mu(CRE)$ = 0.6 mpy	$\mu(CRE)$ = 0.8 mpy	$\mu(CRE)$ = 1.0 mpy
20	0	0	0	0
22	0	0	0	0
24	0	0	0	0
26	0	0	0	1
28	0	0	0	1
30	0	0	0	3
32	0	0	0	5
34	0	0	1	10
36	0	0	1	19
38	0	0	3	34
40	0	0	4	57
42	0	0	8	89
44	0	0	13	133
46	0	1	20	189
48	0	1	32	254
50	0	2	47	328
52	0	3	68	408
54	0	4	95	490
56	1	6	127	571
58	1	9	166	649
60	1	13	209	720
62	2	18	256	783
64	3	25	307	836
66	4	34	359	877
68	6	45	411	905
70	8	58	463	919
72	11	74	513	921
74	15	92	560	909
76	19	108	602	886

Table 112. Percent of wire fractures per time increment for $\mu(CRE)$ in the range of 0.5–1.0 mpy and $\sigma(CRE)/\mu(CRE) = 0.3$.

Exposure Time (Year)	$\mu(CRE)$ = 0.5 mpy	$\mu(CRE)$ = 0.6 mpy	$\mu(CRE)$ = 0.8 mpy	$\mu(CRE)$ = 1.0 mpy
20	0.0	0.0	0.0	0.0
22	0.0	0.0	0.0	0.0
24	0.0	0.0	0.0	0.0
26	0.0	0.0	0.0	0.0
28	0.0	0.0	0.0	0.0
30	0.0	0.0	0.0	0.0
32	0.0	0.0	0.0	0.0
34	0.0	0.0	0.0	0.0
36	0.0	0.0	0.0	0.1
38	0.0	0.0	0.0	0.2
40	0.0	0.0	0.0	0.3
42	0.0	0.0	0.0	0.4
44	0.0	0.0	0.1	0.6
46	0.0	0.0	0.1	0.9
48	0.0	0.0	0.1	1.2
50	0.0	0.0	0.2	1.5
52	0.0	0.0	0.3	1.9
54	0.0	0.0	0.4	2.3
56	0.0	0.0	0.6	2.7
58	0.0	0.0	0.8	3.0
60	0.0	0.1	1.0	3.4
62	0.0	0.1	1.2	3.7
64	0.0	0.1	1.4	3.9
66	0.0	0.2	1.7	4.1
68	0.0	0.2	1.9	4.2
70	0.0	0.3	2.2	4.3
72	0.1	0.3	2.4	4.3
74	0.1	0.4	2.6	4.3
76	0.1	0.5	2.8	4.1

Table 113. Number of wire fractures versus time for $\mu(CRE)$ in the range of 3.0–5.0 mpy and $\sigma(CRE)/\mu(CRE)$ = 0.3.

Exposure Time (Year)	$\mu(CRE)$ = 3.0 mpy	$\mu(CRE)$ = 4.0 mpy	$\mu(CRE)$ = 5.0 mpy
0	0	0	0
1	0	0	0
2	0	0	0
3	0	0	0
4	0	0	0
5	0	0	1
6	0	0	5
7	0	2	28
8	0	10	130
9	1	39	439
10	5	130	1,123
11	14	352	2,296
12	40	795	3,960
13	100	1,531	6,013
14	222	2,592	8,280
15	445	3,960	—

—No information available.

Table 114. Percent of wire fractures versus time for $\mu(CRE)$ in the range of 3.0–5.0 mpy and $\sigma(CRE)/\mu(CRE)$ = 0.3.

Exposure Time (Year)	$\mu(CRE)$ = 3.0 mpy	$\mu(CRE)$ = 4.0 mpy	$\mu(CRE)$ = 5.0 mpy
0	0	0	0
1	0	0	0
2	0	0	0
3	0	0	0
4	0	0	0
5	0	0	0
6	0	0	0
7	0	0	0.1
8	0	0	0.6
9	0	0.2	2.1
10	0	0.6	5.3
11	0.1	1.6	10.7
12	0.2	3.7	18.5
13	0.5	7.2	28.1
14	1.0	12.1	38.7
15	2.1	18.5	—

—No information available.

Table 115. Number of wire fractures per time increment versus time for $\mu(CRE)$ in the range of 3.0–5.0 mpy and $\sigma(CRE)/\mu(CRE) = 0.3$.

Exposure Time (Year)	$\mu(CRE)$ = 3.0 mpy	$\mu(CRE)$ = 4.0 mpy	$\mu(CRE)$ = 5.0 mpy
0	0	0	0
1	0	0	0
2	0	0	0
3	0	0	0
4	0	0	0
5	0	0	1
6	0	0	4
7	0	2	24
8	0	8	101
9	1	29	309
10	3	90	685
11	10	222	1,173
12	26	443	1,664
13	60	736	2,053
14	123	1,061	2,267
15	223	1,368	—

—No information available.

Table 116. Percent of wire fractures per time increment versus time for $\mu(CRE)$ in the range of 3.0–5.0 mpy and $\sigma(CRE)/\mu(CRE) = 0.3$.

Exposure Time (Year)	$\mu(CRE)$ = 3.0 mpy	$\mu(CRE)$ = 4.0 mpy	$\mu(CRE)$ = 5.0 mpy
0	0.0	0.0	0.0
1	0.0	0.0	0.0
2	0.0	0.0	0.0
3	0.0	0.0	0.0
4	0.0	0.0	0.0
5	0.0	0.0	0.0
6	0.0	0.0	0.0
7	0.0	0.0	0.1
8	0.0	0.0	0.5
9	0.0	0.1	1.4
10	0.0	0.4	3.2
11	0.0	1.0	5.5
12	0.1	2.1	7.8
13	0.3	3.4	9.6
14	0.6	5.0	10.6
15	1.0	6.4	—

—No information available.

Table 117. Number of wire fractures versus time for $\mu(CRE)$ = 10.0 and 20.0 mpy and $\sigma(CRE)/\mu(CRE)$ = 0.3.

Exposure Time (Year)	$\mu(CRE)$ = 10.0 mpy	$\mu(CRE)$ = 20.0 mpy
0.00	0	0
0.25	0	0
0.50	0	0
0.75	0	0
1.00	0	0
1.25	0	1
1.50	0	5
1.75	0	28
2.00	0	130
2.25	0	439
2.50	1	1,123
2.75	2	2,296
3.00	5	3,960
3.25	12	6,013
3.50	28	7,132
3.75	63	8,280
4.00	130	—
4.25	248	—
4.50	439	—
4.75	725	—
5.00	1,123	—

—No information available.

Table 118. Percent of wire fractures versus time for $\mu(CRE)$ = 10.0 and 20.0 mpy and $\sigma(CRE)/\mu(CRE)$ = 0.3.

Exposure Time (Year)	$\mu(CRE)$ = 10.0 mpy	$\mu(CRE)$ = 20.0 mpy
0.00	0.0	0.0
0.25	0.0	0.0
0.50	0.0	0.0
0.75	0.0	0.0
1.00	0.0	0.0
1.25	0.0	0.0
1.50	0.0	0.0
1.75	0.0	0.1
2.00	0.0	0.6
2.25	0.0	2.1
2.50	0.0	5.3
2.75	0.0	10.7
3.00	0.0	18.5
3.25	0.1	28.1
3.50	0.1	33.4
3.75	0.3	38.7
4.00	0.6	—
4.25	1.2	—
4.50	2.1	—
4.75	3.4	—
5.00	5.3	—

—No information available.

Table 119. Number of wire fractures per time increment versus time for $\mu(CRE)$ = 10.0 and 20.0 mpy and $\sigma(CRE)/\mu(CRE)$ = 0.3.

Exposure Time (Year)	$\mu(CRE)$ = 10.0 mpy	$\mu(CRE)$ = 20.0 mpy
0.00	0	0
0.25	0	0
0.50	0	0
0.75	0	0
1.00	0	0
1.25	0	1
1.50	0	4
1.75	0	24
2.00	0	101
2.25	0	309
2.50	0	685
2.75	1	1,173
3.00	3	1,664
3.25	7	2,053
3.50	16	1,119
3.75	35	1,148
4.00	67	—
4.25	118	—
4.50	191	—
4.75	286	—
5.00	399	—

—No information available.

Table 120. Percent of wire fractures per time increment versus time for $\mu(CRE)$ = 10.0 and 20.0 mpy and $\sigma(CRE)/\mu(CRE)$ = 0.3.

Exposure Time (Year)	$\mu(CRE)$ = 10.0 mpy	$\mu(CRE)$ = 20.0 mpy
0.00	0.0	0.0
0.25	0.0	0.0
0.50	0.0	0.0
0.75	0.0	0.0
1.00	0.0	0.0
1.25	0.0	0.0
1.50	0.0	0.0
1.75	0.0	0.1
2.00	0.0	0.5
2.25	0.0	1.4
2.50	0.0	3.2
2.75	0.0	5.5
3.00	0.0	7.8
3.25	0.0	9.6
3.50	0.1	5.2
3.75	0.2	5.4
4.00	0.3	—
4.25	0.6	—
4.50	0.9	—
4.75	1.3	—
5.00	1.9	—

—No information available.

Table 121. Number of strand fractures versus time for $\mu(CRE)$ in the range of 0.5–1.0 mpy and $\sigma(CRE)/\mu(CRE) = 0.3$.

Exposure Time (Year)	$\mu(CRE)$ = 0.5 mpy	$\mu(CRE)$ = 0.6 mpy	$\mu(CRE)$ = 0.8 mpy	$\mu(CRE)$ = 1.0 mpy
40	0	0	0	0
42	0	0	0	0
44	0	0	0	0
46	0	0	0	0
48	0	0	0	1
50	0	0	0	13
52	0	0	0	28
54	0	0	0	45
56	0	0	0	110
58	0	0	0	196
60	0	0	1	311
62	0	0	11	459
64	0	0	22	650
66	0	0	32	906
68	0	0	57	1,183
70	0	0	110	1,518
72	0	0	173	1,825
74	0	0	247	2,149
76	0	0	351	2,424

Table 122. Percent of strand fractures versus time for $\mu(CRE)$ in the range of 0.5–1.0 mpy and $\sigma(CRE)/\mu(CRE) = 0.3$.

Exposure Time (Year)	$\mu(CRE)$ = 0.5 mpy	$\mu(CRE)$ = 0.6 mpy	$\mu(CRE)$ = 0.8 mpy	$\mu(CRE)$ = 1.0 mpy
40	0.0	0.0	0.0	0.0
42	0.0	0.0	0.0	0.0
44	0.0	0.0	0.0	0.0
46	0.0	0.0	0.0	0.0
48	0.0	0.0	0.0	0.0
50	0.0	0.0	0.0	0.4
52	0.0	0.0	0.0	0.8
54	0.0	0.0	0.0	1.3
56	0.0	0.0	0.0	3.1
58	0.0	0.0	0.0	5.5
60	0.0	0.0	0.0	8.7
62	0.0	0.0	0.3	12.9
64	0.0	0.0	0.6	18.2
66	0.0	0.0	0.9	25.4
68	0.0	0.0	1.6	33.2
70	0.0	0.0	3.1	42.6
72	0.0	0.0	4.9	51.2
74	0.0	0.0	6.9	60.3
76	0.0	0.0	9.8	68.0

Table 123. Number of strand fractures per time increment versus time for $\mu(CRE)$ in the range of 0.5–1.0 mpy and $\sigma(CRE)/\mu(CRE) = 0.3$.

Exposure Time (Year)	$\mu(CRE)$ = 0.5 mpy	$\mu(CRE)$ = 0.6 mpy	$\mu(CRE)$ = 0.8 mpy	$\mu(CRE)$ = 1.0 mpy
40	0	0	0	0
42	0	0	0	0
44	0	0	0	0
46	0	0	0	0
48	0	0	0	1
50	0	0	0	12
52	0	0	0	15
54	0	0	0	17
56	0	0	0	65
58	0	0	0	86
60	0	0	1	115
62	0	0	10	148
64	0	0	11	191
66	0	0	10	256
68	0	0	25	—
70	0	0	53	—
72	0	0	63	—
74	0	0	74	—
76	0	0	104	—

—No information available.

Table 124. Percent of strand fractures per time increment versus time for $\mu(CRE)$ in the range of 0.5–1.0 mpy and $\sigma(CRE)/\mu(CRE) = 0.3$.

Exposure Time (Year)	$\mu(CRE)$ = 0.5 mpy	$\mu(CRE)$ = 0.6 mpy	$\mu(CRE)$ = 0.8 mpy	$\mu(CRE)$ = 1.0 mpy
40	0.0	0.0	0.0	0.0
42	0.0	0.0	0.0	0.0
44	0.0	0.0	0.0	0.0
46	0.0	0.0	0.0	0.0
48	0.0	0.0	0.0	0.0
50	0.0	0.0	0.0	0.3
52	0.0	0.0	0.0	0.1
54	0.0	0.0	0.0	0.1
56	0.0	0.0	0.0	1.3
58	0.0	0.0	0.0	0.6
60	0.0	0.0	0.0	0.8
62	0.0	0.0	0.3	0.9
64	0.0	0.0	0.0	1.2
66	0.0	0.0	0.0	1.8
68	0.0	0.0	0.4	—
70	0.0	0.0	0.8	—
72	0.0	0.0	0.3	—
74	0.0	0.0	0.3	—
76	0.0	0.0	0.8	—

—No information available.

Table 125. Number of strand fractures versus time for $\mu(CRE)$ in the range of 3.0–5.0 mpy and $\sigma(CRE)/\mu(CRE) = 0.3$.

Exposure Time (Year)	$\mu(CRE)$ = 3.0 mpy	$\mu(CRE)$ = 4.0 mpy	$\mu(CRE)$ = 5.0 mpy
5	0	0	0
6	0	0	0
7	0	0	0
8	0	0	0
9	0	0	0
10	0	0	13
11	0	0	76
12	0	1	299
13	0	28	776
14	7	112	1,530
15	24	299	2,295
16	64	655	—
17	151	1,193	—
18	275	1,840	—
19	468	2,443	—
20	705	2,883	—

—No information available.

Table 126. Percent of strand fractures versus time for $\mu(CRE)$ in the range of 3.0–5.0 mpy and $\sigma(CRE)/\mu(CRE) = 0.3$.

Exposure Time (Year)	$\mu(CRE)$ = 3.0 mpy	$\mu(CRE)$ = 4.0 mpy	$\mu(CRE)$ = 5.0 mpy
5	0.0	0.0	0.0
6	0.0	0.0	0.0
7	0.0	0.0	0.0
8	0.0	0.0	0.0
9	0.0	0.0	0.0
10	0.0	0.0	0.4
11	0.0	0.0	2.1
12	0.0	0.0	8.4
13	0.0	0.8	21.8
14	0.2	3.1	42.9
15	0.7	8.4	64.4
16	1.8	18.4	—
17	4.2	33.5	—
18	7.7	51.6	—
19	13.1	68.5	—
20	19.8	80.9	—

—No information available.

Table 127. Number of strand fractures per unit time versus time for $\mu(CRE)$ in the range of 3.0–5.0 mpy and $\sigma(CRE)/\mu(CRE) = 0.3$.

Exposure Time (Year)	$\mu(CRE)$ = 3.0 mpy	$\mu(CRE)$ = 4.0 mpy	$\mu(CRE)$ = 5.0 mpy
5	0	0	0
6	0	0	0
7	0	0	0
8	0	0	0
9	0	0	0
10	0	0	13
11	0	0	63
12	0	1	223
13	0	27	477
14	7	84	754
15	17	187	765
16	40	356	—
17	87	538	—
18	124	647	—
19	193	603	—
20	237	440	—

—No information available.

Table 128. Percent of strand fractures per time increment versus time for $\mu(CRE)$ in the range of 3.0–5.0 mpy and $\sigma(CRE)/\mu(CRE) = 0.3$.

Exposure Time (Year)	$\mu(CRE)$ = 3.0 mpy	$\mu(CRE)$ = 4.0 mpy	$\mu(CRE)$ = 5.0 mpy
5	0.0	0.0	0.0
6	0.0	0.0	0.0
7	0.0	0.0	0.0
8	0.0	0.0	0.0
9	0.0	0.0	0.0
10	0.0	0.0	0.4
11	0.0	0.0	1.8
12	0.0	0.0	6.3
13	0.0	0.8	13.4
14	0.2	2.4	21.2
15	0.5	5.2	21.5
16	1.1	10.0	—
17	2.4	15.1	—
18	3.5	18.2	—
19	5.4	16.9	—
20	6.6	12.3	—

— No information available.

Table 129. Number of strand fractures versus time for $\mu(CRE)$ = 10.0 and 20.0 mpy and $\sigma(CRE)/\mu(CRE)$ = 0.3.

Exposure Time (Year)	$\mu(CRE)$ = 10.0 mpy	$\mu(CRE)$ = 20.0 mpy
2.00	0	0
2.25	0	0
2.50	0	13
2.75	0	76
3.00	0	299
3.25	0	501
3.50	0	776
3.75	0	1,113
4.00	0	—
4.25	0	—
4.50	0	—
4.75	1	—
5.00	13	—
5.25	30	—
5.50	73	—
5.75	171	—
6.00	299	—

—No information available.

Table 130. Percent of strand fractures versus time for $\mu(CRE)$ = 10.0 and 20.0 mpy and $\sigma(CRE)/\mu(CRE)$ = 0.3.

Exposure Time (Year)	$\mu(CRE)$ = 10.0 mpy	$\mu(CRE)$ = 20.0 mpy
2.00	0.0	0.0
2.25	0.0	0.0
2.50	0.0	0.4
2.75	0.0	2.1
3.00	0.0	8.4
3.25	0.0	14.1
3.50	0.0	21.8
3.75	0.0	31.2
4.00	0.0	—
4.25	0.0	—
4.50	0.0	—
4.75	0.0	—
5.00	0.4	—
5.25	0.8	—
5.50	2.0	—
5.75	4.8	—
6.00	8.4	—

—No information available.

Table 131. Number of strand fractures per unit time versus time for $\mu(CRE)$ = 10.0 and 20.0 mpy and $\sigma(CRE)/\mu(CRE)$ = 0.3.

Exposure Time (Year)	$\mu(CRE)$ = 10.0 mpy	$\mu(CRE)$ = 20.0 mpy
2.00	0	0
2.25	0	0
2.50	0	13
2.75	0	63
3.00	0	223
3.25	0	202
3.50	0	275
3.75	0	337
4.00	0	—
4.25	0	—
4.50	0	—
4.75	1	—
5.00	12	—
5.25	17	—
5.50	43	—
5.75	98	—
6.00	128	—

—No information available.

Table 132. Percent of strand fractures per time increment versus time for $\mu(CRE)$ = 10.0 and 20.0 mpy and $\sigma(CRE)/\mu(CRE)$ = 0.3.

Exposure Time (Year)	$\mu(CRE)$ = 10.0 mpy	$\mu(CRE)$ = 20.0 mpy
2.00	0	0
2.25	0	0
2.50	0	0.4
2.75	0	2.1
3.00	0	8.4
3.25	0	14.1
3.50	0	21.8
3.75	0	31.2
4.00	0	—
4.25	0	—
4.50	0	—
4.75	0	—
5.00	0.4	—
5.25	0.8	—
5.50	2.0	—
5.75	4.8	—
6.00	8.4	—

—No information available.

Table 133. Number of tendon failures versus time for $\mu(CRE)$ in the range of 0.5–1.0 mpy and $\sigma(CRE)/\mu(CRE) = 0.3$.

Exposure Time (Year)	$\mu(CRE)$ = 0.5 mpy	$\mu(CRE)$ = 0.6 mpy	$\mu(CRE)$ = 0.8 mpy	$\mu(CRE)$ = 0.1 mpy
50	0	0	0	0
52	0	0	0	0
54	0	0	0	0
56	0	0	0	0
58	0	0	0	0
60	0	0	0	0
62	0	0	0	6
64	0	0	0	15
66	0	0	0	50
68	0	0	0	102
70	0	0	0	—
72	0	0	0	—
74	0	0	0	—
76	0	0	1	—

—No information available.

Table 134. Percent of tendon failures versus time for $\mu(CRE)$ in the range of 0.5–1.0 mpy and $\sigma(CRE)/\mu(CRE) = 0.3$.

Exposure Time (Year)	$\mu(CRE)$ = 0.5 mpy	$\mu(CRE)$ = 0.6 mpy	$\mu(CRE)$ = 0.8 mpy	$\mu(CRE)$ = 0.1 mpy
50	0.0	0.0	0.0	0.0
52	0.0	0.0	0.0	0.0
54	0.0	0.0	0.0	0.0
56	0.0	0.0	0.0	0.0
58	0.0	0.0	0.0	0.0
60	0.0	0.0	0.0	0.0
62	0.0	0.0	0.0	3.7
64	0.0	0.0	0.0	5.6
66	0.0	0.0	0.0	21.6
68	0.0	0.0	0.0	32.1
70	0.0	0.0	0.0	—
72	0.0	0.0	0.0	—
74	0.0	0.0	0.0	—
76	0.0	0.0	0.6	—

—No information available.

Table 135. Number of tendon failures per unit time versus time for $\mu(CRE)$ in the range of 0.5–1.0 mpy and $\sigma(CRE)/\mu(CRE) = 0.3$.

Exposure Time (Year)	$\mu(CRE)$ = 0.5 mpy	$\mu(CRE)$ = 0.6 mpy	$\mu(CRE)$ = 0.8 mpy	$\mu(CRE)$ = 0.1 mpy
50	0	0	0	0
52	0	0	0	0
54	0	0	0	0
56	0	0	0	0
58	0	0	0	0
60	0	0	0	0
62	0	0	0	6
64	0	0	0	9
66	0	0	0	35
68	0	0	0	52
70	0	0	0	—
72	0	0	0	—
74	0	0	0	—
76	0	0	1	—

—No information available.

Table 136. Percent of tendon failures per time increment versus time for $\mu(CRE)$ in the range of 0.5–1.0 mpy and $\sigma(CRE)/\mu(CRE) = 0.3$.

Exposure Time (Year)	$\mu(CRE)$ = 0.5 mpy	$\mu(CRE)$ = 0.6 mpy	$\mu(CRE)$ = 0.8 mpy	$\mu(CRE)$ = 0.1 mpy
50	0.0	0.0	0.0	0.0
52	0.0	0.0	0.0	0.0
54	0.0	0.0	0.0	0.0
56	0.0	0.0	0.0	0.0
58	0.0	0.0	0.0	0.0
60	0.0	0.0	0.0	0.0
62	0.0	0.0	0.0	3.7
64	0.0	0.0	0.0	5.6
66	0.0	0.0	0.0	21.6
68	0.0	0.0	0.0	32.1
70	0.0	0.0	0.0	—
72	0.0	0.0	0.0	—
74	0.0	0.0	0.0	—
76	0.0	0.0	0.6	—

—No information available.

Table 137. Number of tendon failures versus time for $\mu(CRE)$ in the range of 3.0–5.0 mpy and $\sigma(CRE)/\mu(CRE) = 0.3$.

Exposure Time (Year)	$\mu(CRE)$ = 3.0 mpy	$\mu(CRE)$ = 4.0 mpy	$\mu(CRE)$ = 5.0 mpy
10	0	0	0
11	0	0	0
12	0	0	0
13	0	0	35
14	0	0	150
15	0	0	162
16	0	16	162
17	0	103	—
18	0	161	—
19	6	162	—
20	19	—	—
21	71	—	—
22	137	—	—
23	157	—	—
24	161	—	—
25	162	—	—

—No information available.

Table 138. Percent of tendon failures versus time for $\mu(CRE)$ in the range of 3.0–5.0 mpy and $\sigma(CRE)/\mu(CRE) = 0.3$.

Exposure Time (Year)	$\mu(CRE)$ = 3.0 mpy	$\mu(CRE)$ = 4.0 mpy	$\mu(CRE)$ = 5.0 mpy
10	0.0	0.0	0.0
11	0.0	0.0	0.0
12	0.0	0.0	0.0
13	0.0	0.0	21.6
14	0.0	0.0	92.6
15	0.0	0.0	—
16	0.0	9.9	—
17	0.0	63.6	—
18	0.0	—	—
19	3.7	—	—
20	11.7	—	—
21	43.8	—	—
22	84.6	—	—
23	96.9	—	—
24	—	—	—
25	—	—	—

—No information available.

Table 139. Number of tendon failures per unit time versus time for $\mu(CRE)$ in the range of 3.0–5.0 mpy and $\sigma(CRE)/\mu(CRE) = 0.3$.

Exposure Time (Year)	$\mu(CRE)$ = 3.0 mpy	$\mu(CRE)$ = 4.0 mpy	$\mu(CRE)$ = 5.0 mpy
10	0	0	0
11	0	0	0
12	0	0	0
13	0	0	35
14	0	0	115
15	0	0	—
16	0	16	—
17	0	87	—
18	0	—	—
19	6	—	—
20	13	—	—
21	52	—	—
22	66	—	—
23	20	—	—
24	—	—	—
25	—	—	—

—No information available.

Table 140. Percent of tendon failures per time increment versus time for $\mu(CRE)$ in the range of 3.0–5.0 mpy and $\sigma(CRE)/\mu(CRE) = 0.3$.

Exposure Time (Year)	$\mu(CRE)$ = 3.0 mpy	$\mu(CRE)$ = 4.0 mpy	$\mu(CRE)$ = 5.0 mpy
10	0.0	0.0	0.0
11	0.0	0.0	0.0
12	0.0	0.0	0.0
13	0.0	0.0	21.6
14	0.0	0.0	71.0
15	0.0	0.0	—
16	0.0	9.9	—
17	0.0	53.7	—
18	0.0	—	—
19	3.7	—	—
20	8.0	—	—
21	32.1	—	—
22	40.7	—	—
23	12.3	—	—
24	—	—	—
25	—	—	—

—No information available.

Table 141. Number of tendon failures versus time for $\mu(CRE)$ = 10.0 and 20.0 mpy and $\sigma(CRE)/\mu(CRE)$ = 0.3.

Exposure Time (Year)	$\mu(CRE)$ = 10.0 mpy	$\mu(CRE)$ = 20.0 mpy
3.00	0	0
3.25	0	7
3.50	0	35
3.75	0	90
4.00	0	150
4.25	0	—
4.50	0	—
4.75	0	—
5.00	0	—
5.25	0	—
5.50	0	—
5.75	0	—
6.00	0	—
6.25	7	—
6.50	35	—
6.75	90	—
7.00	150	—

—No information available.

Table 142. Percent of tendon failures versus time for $\mu(CRE)$ = 10.0 and 20.0 mpy and $\sigma(CRE)/\mu(CRE)$ = 0.3.

Exposure Time (Year)	$\mu(CRE)$ = 10.0 mpy	$\mu(CRE)$ = 20.0 mpy
3.00	0.0	0.0
3.25	0.0	4.3
3.50	0.0	21.6
3.75	0.0	55.6
4.00	0.0	92.6
4.25	0.0	—
4.50	0.0	—
4.75	0.0	—
5.00	0.0	—
5.25	0.0	—
5.50	0.0	—
5.75	0.0	—
6.00	0.0	—
6.25	4.3	—
6.50	21.6	—
6.75	55.6	—
7.00	92.6	—

—No information available.

Table 143. Number of tendon failures per unit time versus time for $\mu(CRE)$ = 10.0 and 20.0 mpy and $\sigma(CRE)/\mu(CRE)$ = 0.3.

Exposure Time (Year)	$\mu(CRE)$ = 10.0 mpy	$\mu(CRE)$ = 20.0 mpy
3.00	0	0
3.25	0	7
3.50	0	28
3.75	0	—
4.00	0	—
4.25	0	—
4.50	0	—
4.75	0	—
5.00	0	—
5.25	0	—
5.50	0	—
5.75	0	—
6.00	0	—
6.25	7	—
6.50	28	—
6.75	55	—
7.00	60	—

—No information available.

Table 144. Percent of tendon failures per time increment versus time for $\mu(CRE)$ = 10.0 and 20.0 mpy and $\sigma(CRE)/\mu(CRE)$ = 0.3.

Exposure Time (Year)	$\mu(CRE)$ = 10.0 mpy	$\mu(CRE)$ = 20.0 mpy
3.00	0	0
3.25	0	4
3.50	0	17
3.75	0	—
4.00	0	—
4.25	0	—
4.50	0	—
4.75	0	—
5.00	0	—
5.25	0	—
5.50	0	—
5.75	0	—
6.00	0	—
6.25	4	—
6.50	17	—
6.75	34	—
7.00	37	—

—No information available.

APPENDIX B. PROJECTED WIRE AND STRAND FRACTURE AND TENDON FAILURE RATES FOR $\sigma(CRE)/\mu(CRE) = 0.6$

Table 145. Number of wire fractures versus time for $\mu(CRE)$ in the range of 0.5–1.0 mpy and $\sigma(CRE)/\mu(CRE) = 0.6$.

Exposure Time (Year)	$\mu(CRE)$ = 0.5 mpy	$\mu(CRE)$ = 0.6 mpy	$\mu(CRE)$ = 0.8 mpy	$\mu(CRE)$ = 1.0 mpy
18	0	0	0	0
20	0	0	0	1
22	0	0	0	3
24	0	0	1	9
26	0	0	2	22
28	0	0	4	51
30	0	0	9	106
32	0	1	19	198
34	0	1	38	337
36	0	3	70	531
38	1	5	123	782
40	1	9	201	1,089
42	2	16	310	1,450
44	3	27	453	1,859
46	5	44	634	2,313
48	9	70	851	2,806
50	14	107	1,105	3,332
52	23	158	1,394	3,885
54	35	225	1,715	4,460
56	52	310	2,067	5,051
58	76	414	2,445	5,653
60	107	539	2,849	6,262
62	149	685	3,273	6,872
64	201	851	3,716	7,481
66	265	1,039	4,175	8,083
68	342	1,245	4,646	8,677
70	433	1,471	5,127	9,257
72	539	1,715	5,616	9,821
74	659	1,976	6,109	10,366
76	794	2,253	6,604	10,890

Table 146. Percent of wire fractures versus time for $\mu(CRE)$ in the range of 0.5–1.0 mpy and $\sigma(CRE)/\mu(CRE) = 0.6$.

Exposure Time (Year)	$\mu(CRE)$ = 0.5 mpy	$\mu(CRE)$ = 0.6 mpy	$\mu(CRE)$ = 0.8 mpy	$\mu(CRE)$ = 1.0 mpy
18	0.0	0.0	0.0	0.0
20	0.0	0.0	0.0	0.0
22	0.0	0.0	0.0	0.0
24	0.0	0.0	0.0	0.0
26	0.0	0.0	0.0	0.1
28	0.0	0.0	0.0	0.2
30	0.0	0.0	0.0	0.5
32	0.0	0.0	0.1	0.9
34	0.0	0.0	0.2	1.6
36	0.0	0.0	0.3	2.5
38	0.0	0.0	0.6	3.7
40	0.0	0.0	0.9	5.1
42	0.0	0.1	1.4	6.8
44	0.0	0.1	2.1	8.7
46	0.0	0.2	3.0	10.8
48	0.0	0.3	4.0	13.1
50	0.1	0.5	5.2	15.6
52	0.1	0.7	6.5	18.2
54	0.2	1.1	8.0	20.9
56	0.2	1.4	9.7	23.6
58	0.4	1.9	11.4	26.4
60	0.5	2.5	13.3	29.3
62	0.7	3.2	15.3	32.1
64	0.9	4.0	17.4	35.0
66	1.2	4.9	19.5	37.8
68	1.6	5.8	21.7	40.6
70	2.0	6.9	24.0	43.3
72	2.5	8.0	26.3	45.9
74	3.1	9.2	28.6	48.5
76	3.7	10.5	30.9	50.9

Table 147. Number of wire fractures per time increment versus time for $\mu(CRE)$ in the range of 0.5–1.0 mpy and $\sigma(CRE)/\mu(CRE) = 0.6$.

Exposure Time (Year)	$\mu(CRE)$ = 0.5 mpy	$\mu(CRE)$ = 0.6 mpy	$\mu(CRE)$ = 0.8 mpy	$\mu(CRE)$ = 1.0 mpy
18	0	0	0	0
20	0	0	0	1
22	0	0	0	2
24	0	0	0	6
26	0	0	1	14
28	0	0	2	29
30	0	0	5	55
32	0	0	10	92
34	0	1	19	139
36	0	1	33	194
38	0	2	52	251
40	0	4	78	307
42	1	7	109	361
44	1	11	144	410
46	2	17	180	454
48	4	26	218	493
50	5	37	254	526
52	8	51	289	553
54	12	67	321	575
56	17	85	351	591
58	24	104	379	602
60	32	125	403	609
62	41	146	425	611
64	52	167	443	608
66	64	187	459	603
68	77	207	471	593
70	91	226	481	580
72	106	244	488	564
74	120	261	493	545
76	135	277	495	524

Table 148. Percent of wire fractures per time increment versus time for $\mu(CRE)$ in the range of 0.5–1.0 mpy and $\sigma(CRE)/\mu(CRE) = 0.6$.

Exposure Time (Year)	$\mu(CRE)$ = 0.5 mpy	$\mu(CRE)$ = 0.6 mpy	$\mu(CRE)$ = 0.8 mpy	$\mu(CRE)$ = 1.0 mpy
18	0.0	0.0	0.0	0.0
20	0.0	0.0	0.0	0.0
22	0.0	0.0	0.0	0.0
24	0.0	0.0	0.0	0.0
26	0.0	0.0	0.0	0.1
28	0.0	0.0	0.0	0.1
30	0.0	0.0	0.0	0.3
32	0.0	0.0	0.0	0.4
34	0.0	0.0	0.1	0.7
36	0.0	0.0	0.2	0.9
38	0.0	0.0	0.2	1.2
40	0.0	0.0	0.4	1.4
42	0.0	0.0	0.5	1.7
44	0.0	0.1	0.7	1.9
46	0.0	0.1	0.8	2.1
48	0.0	0.1	1.0	2.3
50	0.0	0.2	1.2	2.5
52	0.0	0.2	1.4	2.6
54	0.1	0.3	1.5	2.7
56	0.1	0.4	1.6	2.8
58	0.1	0.5	1.8	2.8
60	0.1	0.6	1.9	2.8
62	0.2	0.7	2.0	2.9
64	0.2	0.8	2.1	2.8
66	0.3	0.9	2.1	2.8
68	0.4	1.0	2.2	2.8
70	0.4	1.1	2.2	2.7
72	0.5	1.1	2.3	2.6
74	0.6	1.2	2.3	2.6
76	0.6	1.3	2.3	2.5

Table 149. Number of wire fractures versus time for $\mu(CRE)$ in the range of 3.0–5.0 mpy and $\sigma(CRE)/\mu(CRE) = 0.6$.

Exposure Time (Year)	$\mu(CRE)$ = 3.0 mpy	$\mu(CRE)$ = 4.0 mpy	$\mu(CRE)$ = 5.0 mpy
0	0	0	0
1	0	0	0
2	0	0	0
3	0	0	0
4	0	0	1
5	0	1	13
6	0	8	28
7	2	43	188
8	7	149	493
9	26	338	846
10	73	566	1,812
11	157	782	1,443
12	274	961	1,531
13	404	1,095	1,544
14	529	1,183	1,496
15	641	1,229	1,395
16	736	1,237	—
17	811	1,214	—
18	867	—	—
19	904	—	—
20	924	—	—

—No information available.

Table 150. Percent of wire fractures versus time for $\mu(CRE)$ in the range of 3.0–5.0 mpy and $\sigma(CRE)/\mu(CRE) = 0.6$.

Exposure Time (Year)	$\mu(CRE)$ = 3.0 mpy	$\mu(CRE)$ = 4.0 mpy	$\mu(CRE)$ = 5.0 mpy
0	0.0	0.0	0.0
1	0.0	0.0	0.0
2	0.0	0.0	0.0
3	0.0	0.0	0.0
4	0.0	0.0	0.0
5	0.0	0.0	0.1
6	0.0	0.0	0.1
7	0.0	0.2	0.9
8	0.0	0.7	2.3
9	0.1	1.6	4.0
10	0.3	2.6	8.5
11	0.7	3.7	6.7
12	1.3	4.5	7.2
13	1.9	5.1	7.2
14	2.5	5.5	7.0
15	3.0	5.7	6.5
16	3.4	5.8	—
17	3.8	5.7	—
18	4.1	—	—
19	4.2	—	—
20	4.3	—	—

—No information available.

Table 151. Number of wire fractures per time increment versus time for $\mu(CRE)$ in the range of 3.0–5.0 mpy and $\sigma(CRE)/\mu(CRE) = 0.6$.

Exposure Time (Year)	$\mu(CRE)$ = 3.0 mpy	$\mu(CRE)$ = 4.0 mpy	$\mu(CRE)$ = 5.0 mpy
0	0	0	0
1	0	0	0
2	0	0	0
3	0	0	0
4	0	0	1
5	0	1	13
6	0	8	28
7	2	43	188
8	7	149	493
9	26	338	846
10	73	566	1,812
11	157	782	1,443
12	274	961	1,531
13	404	1,095	1,544
14	529	1,183	1,496
15	641	1,229	1,395
16	736	1,237	—
17	811	1,214	—
18	867	—	—
19	904	—	—
20	924	—	—

—No information available.

Table 152. Percent of wire fractures per time increment versus time for $\mu(CRE)$ in the range of 3.0–5.0 mpy and $\sigma(CRE)/\mu(CRE) = 0.6$.

Exposure Time (Year)	$\mu(CRE)$ = 3.0 mpy	$\mu(CRE)$ = 4.0 mpy	$\mu(CRE)$ = 5.0 mpy
0	0.0	0.0	0.0
1	0.0	0.0	0.0
2	0.0	0.0	0.0
3	0.0	0.0	0.0
4	0.0	0.0	0.0
5	0.0	0.0	0.1
6	0.0	0.0	0.1
7	0.0	0.2	0.7
8	0.0	0.5	1.4
9	0.1	0.9	1.7
10	0.2	1.1	4.5
11	0.4	1.0	—
12	0.5	—	—
13	0.6	—	—
14	0.6	—	—
15	0.5	—	—
16	0.4	—	—
17	0.4	—	—
18	0.3	—	—
19	0.2	—	—
20	0.1	—	—

—No information available.

Table 153. Number of wire fractures versus time for $\mu(CRE)$ = 10.0 and 20.0 mpy and $\sigma(CRE)/\mu(CRE)$ = 0.6.

Exposure Time (Year)	$\mu(CRE)$ = 10.0 mpy	$\mu(CRE)$ = 20.0 mpy
0.00	0	0
0.25	0	0
0.50	0	0
0.75	0	0
1.00	0	1
1.25	0	14
1.50	0	107
1.75	0	433
2.00	1	1,105
2.25	4	2,113
2.50	14	3,383
2.75	43	4,826
3.00	107	6,356
3.25	231	7,901
3.50	433	9,396
3.75	724	—
4.00	1,105	—
4.25	1,571	—
4.50	2,113	—
4.75	2,720	—
5.00	3,383	—

—No information available.

Table 154. Percent of wire fractures versus time for $\mu(CRE)$ = 10.0 and 20.0 mpy and $\sigma(CRE)/\mu(CRE)$ = 0.6.

Exposure Time (Year)	$\mu(CRE)$ = 10.0 mpy	$\mu(CRE)$ = 20.0 mpy
0.00	0.0	0.0
0.25	0.0	0.0
0.50	0.0	0.0
0.75	0.0	0.0
1.00	0.0	0.0
1.25	0.0	0.1
1.50	0.0	0.5
1.75	0.0	2.0
2.00	0.0	5.2
2.25	0.0	9.9
2.50	0.1	15.8
2.75	0.2	22.6
3.00	0.5	29.7
3.25	1.1	36.9
3.50	2.0	43.9
3.75	3.4	—
4.00	5.2	—
4.25	7.3	—
4.50	9.9	—
4.75	12.7	—

—No information available.

Table 155. Number of wire fractures per time increment versus time for $\mu(CRE)$ =10.0 and 20.0 mpy and $\sigma(CRE)/\mu(CRE)$ = 0.6.

Exposure Time (Year)	$\mu(CRE)$ = 10.0 mpy	$\mu(CRE)$ = 20.0 mpy
0.00	0	0
0.25	0	0
0.50	0	0
0.75	0	0
1.00	0	1
1.25	0	13
1.50	0	93
1.75	0	326
2.00	1	672
2.25	3	1,007
2.50	10	1,270
2.75	28	1,443
3.00	65	1,531
3.25	124	1,544
3.50	202	1,496
3.75	291	—
4.00	381	—
4.25	466	—
4.50	542	—
4.75	608	—
5.00	662	—

—No information available.

Table 156. Percent of wire fractures per time increment versus time for $\mu(CRE)$ = 10.0 and 20.0 mpy and $\sigma(CRE)/\mu(CRE)$ = 0.6.

Exposure Time (Year)	$\mu(CRE)$ = 10.0 mpy	$\mu(CRE)$ = 20.0 mpy
0.00	0.0	0.0
0.25	0.0	0.0
0.50	0.0	0.0
0.75	0.0	0.0
1.00	0.0	0.0
1.25	0.0	0.1
1.50	0.0	0.4
1.75	0.0	1.5
2.00	0.0	3.1
2.25	0.0	4.7
2.50	0.0	5.9
2.75	0.1	6.7
3.00	0.3	7.2
3.25	0.6	7.2
3.50	0.9	7.0
3.75	1.4	—
4.00	1.8	—
4.25	2.2	—
4.50	2.5	—
4.75	2.8	—

—No information available.

Table 157. Number of strand fractures versus time for $\mu(CRE)$ in the range of 0.5–1.0 mpy and $\sigma(CRE)/\mu(CRE) = 0.6$.

Exposure Time (Year)	$\mu(CRE)$ = 0.5 mpy	$\mu(CRE)$ = 0.6 mpy	$\mu(CRE)$ = 0.8 mpy	$\mu(CRE)$ = 1.0 mpy
30	0	0	0	0
32	0	0	0	0
34	0	0	0	0
36	0	0	0	0
38	0	0	0	1
40	0	0	0	13
42	0	0	0	24
44	0	0	0	36
46	0	0	1	77
48	0	0	2	129
50	0	0	13	194
52	0	0	23	283
54	0	0	32	394
56	0	0	49	517
58	0	0	91	672
60	0	0	137	847
62	0	1	185	1,027
64	0	2	256	1,224
66	0	11	332	1,454
68	0	19	436	1,646
70	0	24	544	1,853
72	0	32	664	2,049
74	1	44	801	2,221
76	1	70	952	2,400

Table 158. Percent of strand fractures versus time for $\mu(CRE)$ in the range of 0.5–1.0 mpy and $\sigma(CRE)/\mu(CRE) = 0.6$.

Exposure Time (Year)	$\mu(CRE)$ = 0.5 mpy	$\mu(CRE)$ = 0.6 mpy	$\mu(CRE)$ = 0.8 mpy	$\mu(CRE)$ = 1.0 mpy
30	0.0	0.0	0.0	0.0
32	0.0	0.0	0.0	0.0
34	0.0	0.0	0.0	0.0
36	0.0	0.0	0.0	0.0
38	0.0	0.0	0.0	0.0
40	0.0	0.0	0.0	0.4
42	0.0	0.0	0.0	0.7
44	0.0	0.0	0.0	1.0
46	0.0	0.0	0.0	2.2
48	0.0	0.0	0.1	3.6
50	0.0	0.0	0.4	5.4
52	0.0	0.0	0.6	7.9
54	0.0	0.0	0.9	11.1
56	0.0	0.0	1.4	14.5
58	0.0	0.0	2.6	18.9
60	0.0	0.0	3.8	23.8
62	0.0	0.0	5.2	28.8
64	0.0	0.1	7.2	34.3
66	0.0	0.3	9.3	40.8
68	0.0	0.5	12.2	46.2
70	0.0	0.7	15.3	52.0
72	0.0	0.9	18.6	57.5
74	0.0	1.2	22.5	62.3
76	0.0	2.0	26.7	67.3

Table 159. Number of strand fractures per time increment versus time for $\mu(CRE)$ in the range of 0.5–1.0 mpy and $\sigma(CRE)/\mu(CRE) = 0.6$.

Exposure Time (Year)	$\mu(CRE)$ = 0.5 mpy	$\mu(CRE)$ = 0.6 mpy	$\mu(CRE)$ = 0.8 mpy	$\mu(CRE)$ = 1.0 mpy
30	0	0	0	0
32	0	0	0	0
34	0	0	0	0
36	0	0	0	0
38	0	0	0	1
40	0	0	0	12
42	0	0	0	11
44	0	0	0	12
46	0	0	1	41
48	0	0	1	52
50	0	0	11	65
52	0	0	10	89
54	0	0	9	111
56	0	0	17	123
58	0	0	42	155
60	0	0	46	175
62	0	1	48	180
64	0	1	71	197
66	0	9	76	230
68	0	8	104	192
70	0	5	108	207
72	0	8	120	196
74	1	12	137	172
76	0	26	151	179

Table 160. Percent of strand fractures per time increment versus time for $\mu(CRE)$ in the range of 0.5–1.0 mpy and $\sigma(CRE)/\mu(CRE) = 0.6$.

Exposure Time (Year)	$\mu(CRE)$ = 0.5 mpy	$\mu(CRE)$ = 0.6 mpy	$\mu(CRE)$ = 0.8 mpy	$\mu(CRE)$ = 1.0 mpy
30	0.0	0.0	0.0	0.0
32	0.0	0.0	0.0	0.0
34	0.0	0.0	0.0	0.0
36	0.0	0.0	0.0	0.0
38	0.0	0.0	0.0	0.0
40	0.0	0.0	0.0	0.3
42	0.0	0.0	0.0	0.3
44	0.0	0.0	0.0	0.3
46	0.0	0.0	0.0	1.2
48	0.0	0.0	0.0	1.5
50	0.0	0.0	0.3	1.8
52	0.0	0.0	0.3	2.5
54	0.0	0.0	0.3	3.1
56	0.0	0.0	0.5	3.5
58	0.0	0.0	1.2	4.3
60	0.0	0.0	1.3	4.9
62	0.0	0.0	1.3	5.1
64	0.0	0.0	2.0	5.5
66	0.0	0.3	2.1	6.5
68	0.0	0.2	2.9	5.4
70	0.0	0.1	3.0	5.8
72	0.0	0.2	3.4	5.5
74	0.0	0.3	3.8	4.8
76	0.0	0.7	4.2	5.0

Table 161. Number of strand fractures versus time for $\mu(CRE)$ in the range of 3.0–5.0 mpy and $\sigma(CRE)/\mu(CRE) = 0.6$.

Exposure Time (Year)	$\mu(CRE)$ = 3.0 mpy	$\mu(CRE)$ = 4.0 mpy	$\mu(CRE)$ = 5.0 mpy
0	0	0	0
1	0	0	0
2	0	0	0
3	0	0	0
4	0	0	0
5	0	0	0
6	0	0	0
7	0	0	0
8	0	0	13
9	0	0	57
10	0	13	208
11	0	39	477
12	0	139	884
13	7	297	1,395
14	24	547	1,914
15	57	884	2,377
16	139	1,272	2,736
17	250	1,705	3,003
18	415	2,116	3,186
19	614	2,462	3,298
20	884	2,736	3,376

Table 162. Percent of strand fractures versus time for $\mu(CRE)$ in the range of 3.0–5.0 mpy and $\sigma(CRE)/\mu(CRE) = 0.6$.

Exposure Time (Year)	$\mu(CRE)$ = 3.0 mpy	$\mu(CRE)$ = 4.0 mpy	$\mu(CRE)$ = 5.0 mpy
0	0.0	0.0	0.0
1	0.0	0.0	0.0
2	0.0	0.0	0.0
3	0.0	0.0	0.0
4	0.0	0.0	0.0
5	0.0	0.0	0.0
6	0.0	0.0	0.0
7	0.0	0.0	0.0
8	0.0	0.0	0.4
9	0.0	0.0	1.6
10	0.0	0.4	5.8
11	0.0	1.1	13.4
12	0.0	3.9	24.8
13	0.2	8.3	39.1
14	0.7	15.3	53.7
15	1.6	24.8	66.7
16	3.9	35.7	76.8
17	7.0	47.8	84.3
18	11.6	59.4	89.4
19	17.2	69.1	92.5
20	24.8	76.8	94.7

Table 163. Number of strand fractures per time increment versus time for $\mu(CRE)$ in the range of 3.0–5.0 mpy and $\sigma(CRE)/\mu(CRE) = 0.6$.

Exposure Time (Year)	$\mu(CRE)$ = 3.0 mpy	$\mu(CRE)$ = 4.0 mpy	$\mu(CRE)$ = 5.0 mpy
0	0	0	0
1	0	0	0
2	0	0	0
3	0	0	0
4	0	0	0
5	0	0	0
6	0	0	0
7	0	0	0
8	0	0	13
9	0	0	44
10	0	13	151
11	0	26	269
12	0	100	407
13	7	158	511
14	17	250	519
15	33	337	463
16	82	388	—
17	111	433	—
18	165	411	—
19	199	346	—
20	270	274	—

—No information available.

Table 164. Percent of strand fractures per time increment versus time for $\mu(CRE)$ in the range of 3.0–5.0 mpy and $\sigma(CRE)/\mu(CRE) = 0.6$.

Exposure Time (Year)	$\mu(CRE)$ = 3.0 mpy	$\mu(CRE)$ = 4.0 mpy	$\mu(CRE)$ = 5.0 mpy
0	0.0	0.0	0.0
1	0.0	0.0	0.0
2	0.0	0.0	0.0
3	0.0	0.0	0.0
4	0.0	0.0	0.0
5	0.0	0.0	0.0
6	0.0	0.0	0.0
7	0.0	0.0	0.0
8	0.0	0.0	0.4
9	0.0	0.0	1.2
10	0.0	0.4	4.2
11	0.0	0.7	7.5
12	0.0	2.8	11.4
13	0.2	4.4	14.3
14	0.5	7.0	14.6
15	0.9	9.5	13.0
16	2.3	10.9	—
17	3.1	12.1	—
18	4.6	11.5	—
19	5.6	9.7	—
20	7.6	7.7	—

—No information available.

Table 165. Number of strand fractures versus time for $\mu(CRE)$ = 10.0 and 20.0 mpy and $\sigma(CRE)/\mu(CRE)$ = 0.6.

Exposure Time (Year)	$\mu(CRE)$ = 10.0 mpy	$\mu(CRE)$ = 20.0 mpy
0.00	0	0
0.25	0	0
0.50	0	0
0.75	0	0
1.00	0	0
1.25	0	0
1.50	0	0
1.75	0	0
2.00	0	13
2.25	0	57
2.50	0	208
2.75	0	477
3.00	0	884
3.25	0	1,395
3.50	0	1,914
3.75	1	2,377
4.00	13	2,736
4.25	29	3,003
4.50	57	3,186
4.75	123	3,298
5.00	208	3,376

Table 166. Percent of strand fractures versus time for $\mu(CRE)$ = 10.0 and 20.0 mpy and $\sigma(CRE)/\mu(CRE)$ = 0.6.

Exposure Time (Year)	$\mu(CRE)$ = 10.0 mpy	$\mu(CRE)$ = 20.0 mpy
0.00	0.0	0.0
0.25	0.0	0.0
0.50	0.0	0.0
0.75	0.0	0.0
1.00	0.0	0.0
1.25	0.0	0.0
1.50	0.0	0.0
1.75	0.0	0.0
2.00	0.0	0.4
2.25	0.0	1.6
2.50	0.0	5.8
2.75	0.0	13.4
3.00	0.0	24.8
3.25	0.0	39.1
3.50	0.0	53.7
3.75	0.0	66.7
4.00	0.4	76.8
4.25	0.8	84.3
4.50	1.6	89.4
4.75	3.5	92.5
5.00	5.8	94.7

Table 167. Number of strand fractures per time increment versus time for $\mu(CRE)$ = 10.0 and 20.0 mpy and $\sigma(CRE)/\mu(CRE)$ = 0.6.

Exposure Time (Year)	$\mu(CRE)$ = 10.0 mpy	$\mu(CRE)$ = 20.0 mpy
0.00	0	0
0.25	0	0
0.50	0	0
0.75	0	0
1.00	0	0
1.25	0	0
1.50	0	0
1.75	0	0
2.00	0	13
2.25	0	44
2.50	0	151
2.75	0	269
3.00	0	407
3.25	0	511
3.50	0	519
3.75	1	463
4.00	12	—
4.25	16	—
4.50	28	—
4.75	66	—
5.00	85	—

Table 168. Percent of strand fractures per time increment versus time for $\mu(CRE)$ = 10.0 and 20.0 mpy and $\sigma(CRE)/\mu(CRE)$ = 0.6.

Exposure Time (Year)	$\mu(CRE)$ = 10.0 mpy	$\mu(CRE)$ = 20.0 mpy
0.00	0.0	0.0
0.25	0.0	0.0
0.50	0.0	0.0
0.75	0.0	0.0
1.00	0.0	0.0
1.25	0.0	0.0
1.50	0.0	0.0
1.75	0.0	0.0
2.00	0.0	0.4
2.25	0.0	1.2
2.50	0.0	4.2
2.75	0.0	7.5
3.00	0.0	11.4
3.25	0.0	14.3
3.50	0.0	14.6
3.75	0.0	13.0
4.00	0.3	—
4.25	0.4	—
4.50	0.8	—
4.75	1.9	—
5.00	2.4	—

Table 169. Number of tendon failures versus time for $\mu(CRE)$ in the range of 0.5–1.0 mpy and $\sigma(CRE)/\mu(CRE) = 0.6$.

Exposure Time (Year)	$\mu(CRE)$ = 0.5 mpy	$\mu(CRE)$ = 0.6 mpy	$\mu(CRE)$ = 0.8 mpy	$\mu(CRE)$ = 1.0 mpy
40	0	0	0	0
42	0	0	0	0
44	0	0	0	0
46	0	0	0	0
48	0	0	0	0
50	0	0	0	0
52	0	0	0	0
54	0	0	0	3
56	0	0	0	9
58	0	0	0	16
60	0	0	0	45
62	0	0	0	76
64	0	0	0	111
66	0	0	0	143
68	0	0	5	153
70	0	0	9	159
72	0	0	16	159
74	0	0	36	162
76	0	0	62	162

Table 170. Percent of tendon failures versus time for $\mu(CRE)$ in the range of 0.5–1.0 mpy and $\sigma(CRE)/\mu(CRE) = 0.6$.

Exposure Time (Year)	$\mu(CRE)$ = 0.5 mpy	$\mu(CRE)$ = 0.6 mpy	$\mu(CRE)$ = 0.8 mpy	$\mu(CRE)$ = 1.0 mpy
40	0.0	0.0	0.0	0.0
42	0.0	0.0	0.0	0.0
44	0.0	0.0	0.0	0.0
46	0.0	0.0	0.0	0.0
48	0.0	0.0	0.0	0.0
50	0.0	0.0	0.0	0.0
52	0.0	0.0	0.0	0.0
54	0.0	0.0	0.0	1.9
56	0.0	0.0	0.0	5.6
58	0.0	0.0	0.0	9.9
60	0.0	0.0	0.0	27.8
62	0.0	0.0	0.0	46.9
64	0.0	0.0	0.0	68.5
66	0.0	0.0	0.0	88.3
68	0.0	0.0	3.1	94.4
70	0.0	0.0	5.6	98.1
72	0.0	0.0	9.9	98.1
74	0.0	0.0	22.2	100.0
76	0.0	0.0	38.3	100.0

Table 171. Number of tendon failures per time increment versus time for $\mu(CRE)$ in the range of 0.5–1.0 mpy and $\sigma(CRE)/\mu(CRE) = 0.6$.

Exposure Time (Year)	$\mu(CRE)$ = 0.5 mpy	$\mu(CRE)$ = 0.6 mpy	$\mu(CRE)$ = 0.8 mpy	$\mu(CRE)$ = 1.0 mpy
40	0	0	0	0
42	0	0	0	0
44	0	0	0	0
46	0	0	0	0
48	0	0	0	0
50	0	0	0	0
52	0	0	0	0
54	0	0	0	3
56	0	0	0	6
58	0	0	0	7
60	0	0	0	29
62	0	0	0	31
64	0	0	0	35
66	0	0	0	32
68	0	0	5	—
70	0	0	4	—
72	0	0	7	—
74	0	0	20	—
76	0	0	26	—

—No information available.

Table 172. Percent of tendon failures per time increment versus time for $\mu(CRE)$ in the range of 0.5–1.0 mpy and $\sigma(CRE)/\mu(CRE) = 0.6$.

Exposure Time (Year)	$\mu(CRE)$ = 0.5 mpy	$\mu(CRE)$ = 0.6 mpy	$\mu(CRE)$ = 0.8 mpy	$\mu(CRE)$ = 1.0 mpy
40	0.0	0.0	0.0	0.0
42	0.0	0.0	0.0	0.0
44	0.0	0.0	0.0	0.0
46	0.0	0.0	0.0	0.0
48	0.0	0.0	0.0	0.0
50	0.0	0.0	0.0	0.0
52	0.0	0.0	0.0	0.0
54	0.0	0.0	0.0	1.9
56	0.0	0.0	0.0	3.7
58	0.0	0.0	0.0	4.3
60	0.0	0.0	0.0	17.9
62	0.0	0.0	0.0	19.1
64	0.0	0.0	0.0	21.6
66	0.0	0.0	0.0	19.8
68	0.0	0.0	3.1	—
70	0.0	0.0	2.5	—
72	0.0	0.0	4.3	—
74	0.0	0.0	12.3	—
76	0.0	0.0	16.0	—

—No information available.

Table 173. Number of tendon failures versus time for $\mu(CRE)$ in the range of 3.0–5.0 mpy and $\sigma(CRE)/\mu(CRE) = 0.6$.

Exposure Time (Year)	$\mu(CRE)$ = 3.0 mpy	$\mu(CRE)$ = 4.0 mpy	$\mu(CRE)$ = 5.0 mpy
0	0	0	0
1	0	0	0
2	0	0	0
3	0	0	0
4	0	0	0
5	0	0	0
6	0	0	0
7	0	0	0
8	0	0	0
9	0	0	0
10	0	0	0
11	0	0	6
12	0	0	47
13	0	0	139
14	0	9	161
15	0	47	162
16	0	120	162
17	0	157	—
18	3	162	—
19	11	162	—
20	47	—	—

—No information available.

Table 174. Percent of tendon failures versus time for $\mu(CRE)$ in the range of 3.0–5.0 mpy and $\sigma(CRE)/\mu(CRE) = 0.6$.

Exposure Time (Year)	$\mu(CRE)$ = 3.0 mpy	$\mu(CRE)$ = 4.0 mpy	$\mu(CRE)$ = 5.0 mpy
0	0.0	0.0	0.0
1	0.0	0.0	0.0
2	0.0	0.0	0.0
3	0.0	0.0	0.0
4	0.0	0.0	0.0
5	0.0	0.0	0.0
6	0.0	0.0	0.0
7	0.0	0.0	0.0
8	0.0	0.0	0.0
9	0.0	0.0	0.0
10	0.0	0.0	0.0
11	0.0	0.0	3.7
12	0.0	0.0	29.0
13	0.0	0.0	85.8
14	0.0	5.6	99.4
15	0.0	29.0	—
16	0.0	74.1	—
17	0.0	96.9	—
18	1.9	—	—
19	6.8	—	—
20	29.0	—	—

—No information available.

Table 175. Number of tendon failures per time increment versus time for $\mu(CRE)$ in the range of 3.0–5.0 mpy and $\sigma(CRE)/\mu(CRE)$ = 0.6.

Exposure Time (Year)	$\mu(CRE)$ = 3.0 mpy	$\mu(CRE)$ = 4.0 mpy	$\mu(CRE)$ = 5.0 mpy
0	0	0	0
1	0	0	0
2	0	0	0
3	0	0	0
4	0	0	0
5	0	0	0
6	0	0	0
7	0	0	0
8	0	0	0
9	0	0	0
10	0	0	0
11	0	0	6
12	0	0	41
13	0	0	92
14	0	9	22
15	0	38	—
16	0	73	—
17	0	37	—
18	3	—	—
19	8	—	—
20	36	—	—

—No information available.

Table 176. Percent of tendon failures per time increment versus time for $\mu(CRE)$ in the range of 3.0–5.0 mpy and $\sigma(CRE)/\mu(CRE) = 0.6$.

Exposure Time (Year)	$\mu(CRE)$ = 3.0 mpy	$\mu(CRE)$ = 4.0 mpy	$\mu(CRE)$ = 5.0 mpy
0	0.0	0.0	0.0
1	0.0	0.0	0.0
2	0.0	0.0	0.0
3	0.0	0.0	0.0
4	0.0	0.0	0.0
5	0.0	0.0	0.0
6	0.0	0.0	0.0
7	0.0	0.0	0.0
8	0.0	0.0	0.0
9	0.0	0.0	0.0
10	0.0	0.0	0.0
11	0.0	0.0	3.7
12	0.0	0.0	25.3
13	0.0	0.0	56.8
14	0.0	5.6	13.6
15	0.0	23.5	—
16	0.0	45.1	—
17	0.0	22.8	—
18	1.9	—	—
19	4.9	—	—
20	22.2	—	—

—No information available.

Table 177. Number of tendon failures versus time for $\mu(CRE)$ = 10.0 and 20.0 mpy and $\sigma(CRE)/\mu(CRE)$ = 0.6.

Exposure Time (Year)	$\mu(CRE)$ = 10.0 mpy	$\mu(CRE)$ = 20.0 mpy
1.00	0	0
1.25	0	0
1.50	0	0
1.75	0	0
2.00	0	0
2.25	0	0
2.50	0	0
2.75	0	6
3.00	0	47
3.25	0	139
3.50	0	161
3.75	0	162
4.00	0	162
4.25	0	—
4.50	0	—
4.75	0	—
5.00	0	—
5.25	0	—
5.50	6	—
5.75	17	—
6.00	47	—
6.25	90	—
6.50	139	—
6.75	155	—
7.00	161	—

—No information available.

Table 178. Percent of tendon failures versus time for $\mu(CRE)$ = 10.0 and 20.0 mpy and $\sigma(CRE)/\mu(CRE)$ = 0.6.

Exposure Time (Year)	$\mu(CRE)$ = 10.0 mpy	$\mu(CRE)$ = 20.0 mpy
1.00	0.0	0.0
1.25	0.0	0.0
1.50	0.0	0.0
1.75	0.0	0.0
2.00	0.0	0.0
2.25	0.0	0.0
2.50	0.0	0.0
2.75	0.0	3.7
3.00	0.0	29.0
3.25	0.0	85.8
3.50	0.0	99.4
3.75	0.0	100.0
4.00	0.0	100.0
4.25	0.0	—
4.50	0.0	—
4.75	0.0	—
5.00	0.0	—
5.25	0.0	—
5.50	3.7	—
5.75	10.5	—
6.00	29.0	—
6.25	55.6	—
6.50	85.8	—
6.75	95.7	—
7.00	99.4	—

—No information available.

Table 179. Number of tendon failures per time increment versus time for $\mu(CRE)$ = 10.0 and 20.0 mpy and $\sigma(CRE)/\mu(CRE)$ = 0.6.

Exposure Time (Year)	$\mu(CRE)$ = 10.0 mpy	$\mu(CRE)$ = 20.0 mpy
1.00	0	0
1.25	0	0
1.50	0	0
1.75	0	0
2.00	0	0
2.25	0	0
2.50	0	0
2.75	0	6
3.00	0	41
3.25	0	92
3.50	0	22
3.75	0	—
4.00	0	—
4.25	0	—
4.50	0	—
4.75	0	—
5.00	0	—
5.25	0	—
5.50	6	—
5.75	11	—
6.00	30	—
6.25	43	—
6.50	49	—
6.75	16	—
7.00	—	—

—No information available.

Table 180. Percent of tendon failures per time increment versus time for $\mu(CRE)$ = 10.0 and 20.0 mpy and $\sigma(CRE)/\mu(CRE)$ = 0.6.

Exposure Time (Year)	$\mu(CRE)$ = 10.0 mpy	$\mu(CRE)$ = 20.0 mpy
1.00	0.0	0.0
1.25	0.0	0.0
1.50	0.0	0.0
1.75	0.0	0.0
2.00	0.0	0.0
2.25	0.0	0.0
2.50	0.0	0.0
2.75	0.0	3.7
3.00	0.0	25.3
3.25	0.0	56.8
3.50	0.0	13.6
3.75	0.0	—
4.00	0.0	—
4.25	0.0	—
4.50	0.0	—
4.75	0.0	—
5.00	0.0	—
5.25	0.0	—
5.50	3.7	—
5.75	6.8	—
6.00	18.5	—
6.25	26.5	—
6.50	30.2	—
6.75	9.9	—
7.00	—	—

—No information available.

REFERENCES

1. Lee, S-K. and Zielske, J. (2014). *An FHWA Special Study: Post-Tensioning Tendon Grout Chloride Thresholds*, Report No. FHWA-HRT-14-039, Federal Highway Administration, Washington, DC.

2. ASTM A416/A416M-12a. (2012). Standard Specification for Steel Strand, Uncoated Seven-Wire for Prestressed Concrete, ASTM International, West Conshohocken, PA.

3. Powers, R.G., Sagues, A.A., and Virmani, Y.P. (2002). *Corrosion of Post-Tensioned Tendons in Florida Bridges*, Technical Memorandum No. 3843, pp. 579–594, Public Works Research Institute, Tsukuba, Japan.

4. Parsons Brinckerhoff and Quade & Douglas, Inc. (2002). *Sunshine Skyway Bridge Post-Tensioned Tendons Investigation*, Final Report to Florida Department of Transportation District Seven, Tallahassee, FL.

5. Corven Engineering, Inc. (2001). *Mid-Bay Bridge Post-Tensioning Evaluation*, Final Report to Florida Department of Transportation District Three, Tallahassee, FL.

6. Hartt, W.H. and Venugopalan, S. (2002). *Corrosion Evaluation of Post-Tensioned Tendons on the Mid Bay Bridge in Destin, Florida*, Final Report to Florida Department of Transportation, Tallahassee, FL.

7. FIGG Bridge Engineers, Inc. (2010). *I-295 Varina-Enon Bridge Tendon Replacement*, Final Report to Virginia Department of Transportation, Richmond, VA.

8. Lau, K., Lasa, I., and Parades, M. (2011). *Corrosion Development of PT Tendons with Deficient Grout: Corrosion Failure in Ringling Causeway Bridge*, Draft Report, Florida Department of Transportation State Materials Office, Gainesville, FL.

9. Lau, K., Parades, M., Lasa, I., and Radols, J. (2013). "*Laboratory Corrosion Assessment of Post-Tensioned Tendons Repaired with Dissimilar Grout*," Paper No. C2013-0002602, Presented at CORROSION/13, NACE, Houston, TX.

10. Lau, K., Lasa, I., and Parades, M. (2013). "Bridge Tendon Failures in the Presence of Deficient Grout." *Materials Performance*, November, p. 64, National Association of Corrosion Engineers (NACE) International, Houston, TX.

11. Bertolini, L. and Carsana, M. (2011). "High pH Corrosion of Prestressing Steel in Segregated Grout," *Modeling of Corroding Concrete Structures*, [eds.] C. Andrade and G. Mancini, RILEM Series 5, Cedex, France.

12. FHWA Memorandum. (2011). *ACTION: Elevated Chloride Levels in SikaGrout® 300 PT Cementitious Grout*, Memorandum, Federal Highway Administration, Washington, DC.

13. Lee, S-K. (2012). *Literature Review of Chloride Threshold Values for Grouted Post-Tensioned Tendons*, Report No. FHWA-HRT-12-067, Federal Highway Administration, Washington, DC.

14. FHWA Technical Advisory. (2013). "*Recommendations for Assessing and Managing Long-Term Performance of Post-Tensioned Bridges Having Tendons Installed with Grout Containing Elevated Levels of Chloride*." Federal Highway Administration, Washington, DC.

15. Theryo, T.S., Hartt, W.H., and Paczkowski, P. (2013). *Guidelines for Sampling, Assessing, and Restoring Defective Grout in Prestressed Concrete Post-Tensioning Ducts*, Report No. FHWA-HRT-13-028, Federal Highway Administration, Washington, DC.

16. Hartt, W.H., Poeydomenge, A., Stauder, A-L., and Scannell, W.T. (1998). *Long-Term Effects of Cathodic Protection on Prestressed Concrete Bridge Components*, Report No. FHWA-RD-98-075, Federal Highway Administration, Washington, DC.

17. Stauder, A-L. and Hartt, W.H. (1998). "*Cathodic Protection of Pre-Tensioned Concrete: Part I—Brittle Fracture Propensity of Corrosion Damaged Prestressing Tendon Wire*," Paper No. 635k, Presented at CORROSION/98, NACE, Houston, TX.

18. MacDougall, C. and Barlett, F. M. (2003). "Tests on Unbonded Seven-Wire Tendons with Broken Outer Wires," *ACI Structural Journal*, Post-Tensioning Institute, Farmington Hills, Michigan, Sept.–Oct., p. 581.

19. MacDougall, C. and Li, S. (2007). "Determining Broken Wires in Unbonded Seven-Wire Strands Using Penetration Tests," *PCI Journal*, Post-Tensioning Institute, Farmington Hills, Michigan, Sept.–Oct., p. 96.

20. Miller, R.L., Hartt, W.H., and Brown, R.P. (1976). "Stray Current and Galvanic Corrosion of Reinforcing Steel in Concrete." *Materials Performance*, *15*(5), p. 20, National Association of Corrosion Engineers (NACE) International, Houston, TX.

21. Lau, K., Lasa, I., Permanbar, S., and Krishnamurthy, K.V.K. (2016). "Anodic Behavior of Steel in Enhanced Sulfate Solutions," Paper No. C2016-7712, Presented at CORROSION/16, NACE, Houston, TX.

22. American Concrete Institute. (2011). *Building Code Requirements for Structural Concrete and Commentary*. Report by ACI Committee 318, ACI 318M-11, Farmington Hills, MI.

23. American Concrete Institute. (2008). *Guide to Durable Concrete*, Report by ACI Committee 201, ACI 201.2R-08, Farmington Hills, MI.

24. American Concrete Institute. (2010). *Protection of Metals in Concrete Against Corrosion*, Report by ACI Committee 222, ACI 222R-01, Farmington Hills, MI.

25. Merrill, B.D. (September 14, 2010). *Grout Testing and Analysis*, Memorandum, Texas Department of Transportation, Austin, TX.

26. AASHTO. (2010). *AASHTO LRFD Bridge Construction Specifications*, Third Edition, AASHTO, Washington, DC.

27. Post-Tensioning Institute. (2011). *Specifications for Grouting of Post-Tensioned Structures*, PTI M55.01-03, Farmington Hills, MI.

HRDI-20/05-18(WEB)E